COMPUTATIONAL STUDIES OF MATERIALS UNDER CYCLIC PLASTICITY.

by

VINCENT OLAYINKA ADEKUNLE OLOYEDE.
B.Sc (Hons.), M.Sc.

A Thesis submitted for the degree of Doctor of philosophy of the Faculty of engineering, University of London and the Diploma of Imperial College.

Department of mechanical Engineering,
Imperial College of Science and Technology,
University of London.

June 1986.

ABSTRACT.

Cyclic stress-strain curves are derived on the computer through the use of plasticity theory in which a mathematical theory of hardening is combined with experimentally observed material properties, such as the monotonic stress-strain curve and the Bauschinger effect. Experimental and computed monotonic and cyclic stress-strain curves for aluminium, H-18, and titanium alloys are presented in appendix F.

A second section deals with the use of the J-integral and Crack opening displacement (COD) in fatigue and fracture mechanics analyses involving notched specimens undergoing cyclic plastic loading. Extensive investigations are carried out in order to understand the behavioural patterns of these parameters under certain imposed loading conditions. These loading conditions are dictated by the intention of simulating on the computer the response to loading of a laboratory type notched specimen with a crack in the notch root plastic zone using the finite-element method. This study shows why the J-integral or COD can be used as macroparameters in the study of crack behaviour from the incipient stages of crack growth (i.e. crack nucleation and initiation), to short crack and the long crack growth stage.

Finally, it is argued that these studies offer a way of using monotonic and cyclic numerical analyses to explain crack arrest in some notched specimens.

ACKNOWLEDGEMENTS.

My deep appreciation goes to Prof. C.E. Turner for supervising this work. His remarkable readiness to meet and discuss even at short notices and when not easily convenient, coupled with the immense interest he showed in the work have contributed to the successful completion of the work.

I also want to express sincere gratitude to Mr. Hugh Macgillivray for being cooperative during the period I carried out experiments in the heavy testing laboratory, Mr. C. Noad and Dr. M.H. Bleackley for helping out in introducing me to the computational ingredients of my work and Dr. Etemad for the helpful discussions we had during the course of this thesis.. Yomi, for typing this thesis, Miss. D. Somefun for being such a good and helpful friend and for proof-reading parts of the thesis in conjunction with Mr. Dave Alleyne. Many thanks also to Mr. K. Martins and family and Mr. W. Ogundiran for their moral support and brotherly friendship.

My heart felt gratitude also goes to 'molade for showing a tremendous sense of purpose, self-denial and understanding, and also for shouldering singly those responsibilities which would normally call for dual involvement. A lot of thanks to our parents for their moral and financial support and for their invaluable hospitality to you and Oyinkan.

Lastly, I wish to thank the federal government of Nigeria for placing a trust and spending tax payers money on me by way of a schorlarship in respect of this research. I remain ever grateful to the people of Nigeria for giving me this opportunity even in these difficult times.

Thank you all once again. May happiness come over the motherland again!

'Kunle Oloyede.

CONTENTS.

	Page no
Abstract	1
Acknowledgement	2
CHAPTER 1: INTRODUCTION	19
CHAPTER 2: NUMERICAL COMPUTATION OF CYCLIC STRESS-STRAIN CURVE.	23
2.1: Linear Elastic Stress-strain Relationship	24
2.2: Plastic Stress-strain Relationship - (Levy - Mises Relationship)	25
2.3: Prandtl - Reuss Equations	26
2.4: The Flow Rule and Deformation Theory	28
2.5: Measures of Work-hardening and Strain-hardening	31
2.5.1: Work Hardening Hypothesis	31
2.5.2: Measurement of Plastic Strain	32
2.5.3: The Strain-hardening Hypothesis	33
2.6: Yield Criteria	34
2.6.1: Tresca's Yield Criterion	34
2.6.2: von-Mises Yield Criterion	35
2.6.2.1: Unloading	37
2.6.2.2: Tangency Condition	37

page no

2.6.2.3: Consistent Loading Condition 38

2.7: Response of Engineering Materials to Loading 38

2.8: Interpretation of the Illustrated Paths of Fig (2.1) 40

2.9: Yield Loci and Yield Models. 43

2.10: Relationship Between the Isotropic and Kinematic Hardening Models 52

2.11: The Mroz Model 54

2.12: Mechanical Sublayer Model 54

2.13: Anisotropic-yielding and Hardening Rules 55

2.14: Applicability of Hardening Rules to the Prediction of Material's Behaviour 55

2.15: Investigation of Yield Surface Behaviour 57

2.16: Summary of Anisotropic Hardening Functions and Interaction with the Bauschinger Effect 71

2.17: Quatitative Analysis of the Bauschinger Effect 72

2.18: Summary for Chapter Two. 78

CHAPTER 3: COMPUTER DERIVATION OF CYCLIC STRESS-STRAIN CURVE 80

Introduction 80

3.1: The Combined Hardening Rules 80

3.2 : Computation of Elastic-Plastic Theory (A Literature Survey) 83

3.3: The Generalized Elasto-Plasticity Model (Appendix A) 86

3.4: The Flow Rules 88

3.5: Movement of the Yield Surface 90

		page no
3.6:	Determination of Parameters for Computation	92
3.7:	Numerical Computation of the Generalized Elasto-Plasticity Theory	99
3.8:	Running Computer Program "Oyin"	103
3.9:	Material Response to Cyclic Loading	104
3.10:	The Monotonic and Cyclic Stress-strain Curves	107
3.11:	Derivation of the Cyclic Stress-strain Curve	109
3.12:	Experimental Analysis	116
3.13:	Using the Testing Machine	120
3.14:	Machine Control Modes	122
3.15:	Other Accessories	122
3.16:	Data Simulation	124
3.17:	Specimen Preparation	126
3.18:	Test Procedure	128
3.19:	Analysis of Experimental Data	129
3.20:	Convergence Problem	133
3.21:	Prolonged Running of Program	134
CHAPTER 4; FATIGUE OF NOTCHED SPECIMENS		135
4.1:	Introduction	135
4.2:	The Short Crack Problem	136
4.3:	Size of a Short Crack, a_o	138
4.4:	Macromechanics Parameters and the Short Crack	140
4.5:	The Stress Intensity Factor, K	142
4.6:	K_1 and Stress Distribution Ahead of a Notch	143
4.7:	K, ΔK and Fatigue Analysis	146
4.8:	Cracks Within Notch Plastic Field	152

		page no
4.9:	Strain Intensity Factor	153
4.10:	The Neuber's Rule	155
4.11:	Total Shear Deformation, ϕ Total	157
4.12	J Based Correlation of Fatigue Crack Growth Rate Data	159
4.13:	Application of the J-Integral	164
4.14:	The R-Curve Concept to Fatigue Crack	174
4.15:	Uniqueness Problem of the J-Integral	178
4.16:	The COD as a Characterizing Parameter	182
4.17:	Application of COD to Fatigue Crack Growth	184
4.18:	Plasticity Condition	185
4.19:	Notches and Crack Arrest	193
4.20:	Blunt and Sharp Notch Behaviour	193
4.21:	Blunt Notches	193
4.22:	Sharp Notches	195
4.23:	Crack Arrest	197
4.24:	Summary on Notch Fatigue Analyses	199

CHAPTER 5: THE INFLUENCE OF CYCLIC PLASTICITY ON THE PARAMETERS J-INTEGRAL AND THE CRACK OPENING DISPLACEMENT (COD) 202

5.1:	Introduction	202
5.2:	The Residual Stress Field and Cyclic Plasticity	203
5.3:	The Finite Element "Experimental" Specimen (Mesh)	204
5.4:	The Computer Program	205
5.5:	Path Independence of the J-Integral for Homogeneous Specimens	205
5.6:	The Bifurcated Specimen	206

		page no
5.7:	The Plastic J-Integral	210
5.8:	Rationalized Non-Dimensional Analysis for the J-Integral	211
5.9:	Procedure for Determining J_{cgc}	212
5.10:	The Crack Opening Displacement	213
5.11:	Determination of δ_{cgc}	214
5.12:	The Origin of Constant C or C_1	216
5.13:	Observations	218
5.14:	The Crack Opening Displacement Curves.	222
CHAPTER 6: CORRELATION OF FATIGUE CRACK GROWTH DATA		258
6.1:	Introduction	258
6.2:	Theoretical Basis for Crack Growth Correlation Parameter.	260
6.3:	Correlation of Crack Growth Data	264
6.4:	Determination of Strength Parameters for Analysis	265
6.5:	The Geometry Correction Factor, Y	266
6.6:	Observations	267
CHAPTER 7: DISCUSSIONS AND CONCLUSION		291
REFERENCES		**313**
APPENDIX A: Generalized Combined-hardening Theory		328
APPENDIX B: User Manual		341
APPENDIX C: Computer Data Files		352
APPENDIX D: Initial Strain Cycling and Single Cycle Loops		353
APPENDIX E: Prestrain Cyclic Curves		361
APPENDIX F: β Versus ε_p Curves and Stress-strain Curves		368

LIST OF FIGURES.

		Page No
Fig 2. 1	Theories of Reversed Loading	40
Fig 2. 2	Prager's Kinematic-hardening Model	43
Fig 2. 3	Ziegler's Modified Kinematic-hardening Model	46
Fig 2. 4	The Isotropic-hardening Model	47
Fig 2. 5	Slip Theory Model	48
Fig 2. 6	Piecewise Linear Plasticity Theory	50
Fig 2. 7	Isotropic and Kinematic-hardening Theories for a given Loading Path	52
Fig 2. 8	Comparison of the Various Hardening Rules	56
Fig 2. 9a	Loading Path and Stress-strain Curves for Determination of Initial and Subsequent Yield Points of a Typical Specimen in the First Quadrant	58
Fig 2. 9b	Loading Path and Stress-strain Curves for Determination of Initial and Subsequent Yield Points of a Typical Specimen in the Fourth Quadrant	59
Fig 2.10	Initial and Subsequent Yield Surfaces	60
Fig 2.11a	Stress Ratio Obtained for Alternative Pre-stress Direction	62
Fig 2.11b	Yield Surface Behaviour of 2 1/4 Cr $1M_o$ With Pre-stress in Axial Compression	62
Fig 2.11c	Yield Surface Behaviour of 2 1/4 Cr $1M_o$ With Pre-stress in Axial Tension	62
Fig 2.11d	Yield Surface Behaviour of Stainless Steel Type 304 - Showing Behavioural Pattern Under Different Initial Pre-strain Condition	62
Fig 2.12a	Determination of the Initial Flow Stress for Shear Strain	65

		Page No
Fig 2.12b	Determination of the Initial Flow Stress for Axial Strain	65
Fig 2.13	Effect of Tensile Pre-strain on the Direction of Plastic - Strain Increment Vectors	65
Fig 2.14	Backward Extrapolation for the Determination of Initial Flow Stress Using the Creep Curve	65
Fig 2.15	Further Illustrations of the Determination of the Initial Flow Stress	66
Fig 2.16	Yield Surface Behaviour Under Cyclic Loading	69
Fig 3. 1	Strain-hardening Theories Under Cyclic Loading	83
Fig 3. 2	A Physical Concept on the Kinematic Translation Parameter, β in Relation to Cyclic Hysteresis Loops	91
Fig 3. 3	Schematic Representation of the Stress Criterion	96
Fig 3. 4	Schematic Representation of the Energy Criterion	97
Fig 3. 5	Schematic Representation of the Strain-hardening Criterion	98
Fig 3. 6	Characteristics of a Settled Cyclic Hysteresis Loop	105
Fig 3. 7	Reserved Loading and the Behaviour of the Yield Surface	106
Fig 3. 8	Illustration of the Multiple Test Method	110
Fig 3. 9	Loading Sequence for the Incremental Test	111
Fig 3.10	Straining Program as a Function of Time	111
Fig 3.11	Cyclic Stress-strain Curves for the Incremental Step Tests	112
Fig 3.12	Illustration of the Monotonic Tension After Cyclic Straining Method	114

		Page No
Fig 3.13	Illustration of the Morrow Method	115
Fig 3.14	The Hour Glass Specimen	118
Fig 3.15	End-fittings of Hour Glass Specimen With Specimen Seated in Position	119
Fig 3.16	The Diametral Extensometer Mounted on Specimen Neck	123
Fig 3.17	Calibration of the Displacement Axis	127
Fig 4. 1	Crack Tip Co-ordinate and Stress System	142
Fig 4. 2	Crack Tip Plastic Zone and Stress Distribution	144
Fig 4. 3	Crack Tip Plastic Zone and the Effect of Irwin's Correlation	145
Fig 4. 4	Graphical Representation of Neuber's Rule	156
Fig 4. 5	Flat Surfaced U-notch in a Two-dimensional Field	161
Fig 4. 6	Non-linear Elasticity - Potential Energy Difference Analysis for J	162
Fig 4. 7a	Estimation of Small Crack ΔJ From Stress-strain Hysteresis Loops (78)	165
Fig 4. 7b	Three Types of Idealized Stress-Strain Behaviour	165
Fig 4. 8a	Fatigue Crack Growth Rate Versus ΔJ for Small Cracks Under Plastic Deformation (78)	166
Fig 4. 8b	Fatigue Crack Growth Rate Versus ΔJ for Various Geometrics (78)	166
Fig 4. 9	Comparison of Small Crack Data With Scatterband From Test Results for Ordinary and Large-sized Specimens (78)	169

		Page No
Fig 4.10a	Illustration of Yield Zone Around Notch Root for a Short Crack (80)	170
Fig 4.10b	Illustration of Yield Zone Around Notch Root for a Long Crack (80)	170
Fig 4.11	Fatigue Crack Growth Rates as a Function of ΔJ for G50.11 Steel (80)	171
Fig 4.12	Fatigue Crack Growth Rates as a Function of ΔJ for 1015 Steel (80)	171
Fig 4.13	da/dN versus J for ASTM A-36 steel.	174
Fig 4.14	Representation of Wide Range Crack Growth Resistance	175
Fig 4.15	Fatigue Crack Growth Resistance of Two Thicknesses of 2024 - T3 Aluminium	175
Fig 4.16	Low Cycle Fatigue Crack Growth Resistance Data for 2024 - T3 Aluminium	176
Fig 4.17	Concept of Near Field J in Applications to Variable Amplitude Cyclic Histories (85)	177
Fig 4.18	J-integral Versus Distance From Notch Tip (Finite Element Analysis) to Show Path Dependence of the J-integral (87)	179
Fig 4.19	Model for the Determination of COD	182
Fig 4.20	Idealization of the Crack Opening Displacement (COD)	186
Fig 4.21	Results of COD Cycling Results for 1/2 in Thick Mild Steel (105)	191
Fig 4.22	Hysteresis Loops: a - Initial Loop; b - Loop After Several Cycles Causing Crack Extension (105)	191

		Page No
Fig 4.23a	Results of COD Cycling Results of 1/4 in Thick Mild Steel (105)	192
Fig 4.23b	Results for Combined COD Cycling Results for 1/4 and 1/2 in Mild Steel (105)	192
Fig 4.24	Summary of Crack Behaviour Under Completely Reversed Tension - Compression Loading	196
Fig 4.25	Stress Intensity Factor Histories for Crack Arrest Experiments	196
Fig 4.26	Crack Extension Histories for Crack Arrest Experiments	198
Fig 5. 1	Homogeneous Finite-element Mesh	225
Fig 5. 2	Bifurcated Finite-element Mesh	225
Fig 5. 3	J-Integral for Different Paths in a Homogeneous Specimen.	226
Fig 5. 4	Influence of Size of Notch Plastic Field on J_{FF} (NFCS = 1.5 σ_O)	227
Fig 5. 5	Influence of Size of Notch Plastic Field on J_{FF} (NFCS = 2σ_O)	228
Fig 5. 6a	Comparison of J_{NF} and J_{FF} for (sNPF = 30 Elements) and (NFCS = 2σ_O)	229
Fig 5. 6b	Comparison of J_{NF} and J_{FF} (sNPF = 40 Elements)	230
Fig 5. 7	Comparison of J_{FF} for Different NFCS Values (sNPF = 40 Elements)	231
Fig 5. 8	Comparison of J_{NF} for Different NFCS Values (sNPF = 40 Elements)	232

		Page No
Fig 5. 9	Comparison of J_{NF} for Different NFCS Values (sNPF = 30 Elements)	233
Fig 5.10	Elastic Curves for J_{NF} and J_{FF} for Different sNPF (NFCS = $2\sigma_O$)	234
Fig 5.11	Contained Yield Values for J_{NF} and J_{FF} (sNPF = 16 Elements), (NFCS = $1.2\sigma_O$)	235
Fig 5.12	Contained Yield Values for J_{NF} and J_{FF} (sNPF = 16 Elements), (NFCS = $1.5\sigma_O$)	236
Fig 5.13	Contained Yield Values of J_{NF} and J_{FF} (sNPF = 40 Elements), (NFCS = $1.5\sigma_O$)	237
Fig 5.14	Contained Yield Values for J_{NF} and J^{FF} (sNPF = 75 Elements), (NFCS = $1.5\sigma_O$)	238
Fig 5.15	Contained Yield Values for J_{NF} and J_{FF} (sNPF = 16 Elements), (NFCS = $2\sigma_O$)	239
Fig 5.16	Contained Yield Values for J_{NF} and J_{FF} (sNPF = 40 Elements), (NFCS = $2\sigma_O$)	240
Fig 5.17	Contained Yield Values for J_{NF} and J_{FF} (sNPF = 75 Elements), (NFCS = $2\sigma_O$)	241
Fig 5.18	Plastic and Rationalized Non-dimensional Values of J_{NF} and J_{FF} (sNPF = 40 Elements, NFCS = $1.5\sigma_O$)	242

		Page No
Fig 5.19	Plastic and Rationalized Non-dimensional Values of J_{NF} and J_{FF} (sNPF = 75 Elements, NFCS = $1.5\sigma_O$)	243
Fig 5.20	Plastic and Rationalized Non-dimensional Values of J_{NF} and J_{FF} (sNPF = 40 Elements, NFCS = $2\sigma_O$)	244
Fig 5.21	Plastic and Rationalized Non-dimensional Values of J_{NF} and J_{FF} (sNPF = 75 Elements, NFCS = $2\sigma_O$)	245
Fig 5.22	Influence of sNPF on the COD (NFCS = $1.2\sigma_O$)	246
Fig 5.23	Influence of sNPF on the COD (NFCS = $1.5\sigma_O$)	247
Fig 5.24	Influence of sNPF on the COD (NFCS = $2\sigma_O$)	248
Fig 5.25	Comparison of the Effect Different NFCS on COD, (sNPF = 30 Elements)	249
Fig 5.26	Contained Yield Values of COD (NFCS = $1.5\sigma_O$)	250
Fig 5.27	Contained Yield Values of COD, (NFCS = $2\sigma_O$)	251
Fig 5.28	Plastic and Rationalized Non-dimensional Values of COD (NFCS = $1.5\sigma_O$), sNPF = 30 Elements	252
Fig 5.29	Plastic and Rationalized Non-dimensional Values of COD (NFCS = $1.5\sigma_O$, sNPF = 40 Elements)	253
Fig 5.30	Plastic and Rationalized Non-dimensional Values of COD (NFCS = $2\sigma_O$, sNPF = 30 Elements)	254

		Page No
Fig 5.31	Plastic and Rationalized Non-dimensional Values of COD (NFCS = $2\sigma_O$), sNPF = 40 Elements	255
Fig 5.32	Plastic and Rationalized Non-dimensional Values of COD (NFCS = $2\sigma_O$, sNPF = 75 Elements)	256
Fig 5.33	The EnJ design curve (based on local yielding).	257
Fig 6. 1	Finite-element mesh for strain distribution studies.	273
Fig 6. 2	Strain Distribution Ahead of a Notch (SCF = 2)	274
Fig 6. 3	Strain Distribution Ahead of a Notch (SCF = 3)	275
Fig 6. 4	Strain Distribution Ahead of a Notch (SCF = 5)	276
Fig 6. 5	Comparison of Strain Distribution Ahead of a Notch for Monotonic and Cyclic Loading (SCF = 5)	277
Fig 6. 6	Strain Distribution Ahead of a Sharp Crack (a/w = 0.05)	278
Fig 6. 7	Monotonic and Fatigue Crack Growth Correlation Using J_{cgc}, SCF = 2	283
Fig 6. 8	Monotonic and Fatigue Crack Growth Correlation Using J_{cgc}, SCF = 3	284
Fig 6. 9	Monotonic and Fatigue Crack Growth Correlation Using J_{cgc}, SCF = 5	285
Fig 6.10	Monotonic and Fatigue Crack Growth Correlation Using J_{cgc}, Sharp Crack a/w = 0.05	286
Fig 6.11	Monotonic and Fatigue Crack Growth Correlation Using δ_{cgc}, SCF = 2	287
Fig 6.12	Monotonic and Fatigue Crack Growth Correlation Using δ_{cgc}, SCF = 3	288

		Page No
Fig 6.13	Monotonic and Fatigue Crack Growth Correlation Using δ_{cgc}, SCF = 5	289
Fig 6.14	Monotonic and Fatigue Crack Growth Correlation Using δ_{cgc}, Sharp crack, a/w = 0.05	290
Fig.D.1a	Experimental cyclic hysteresis loops for aluminium (Displacement amplitude = 8.8%).	354
Fig.D.1b	Experimental monotonic loop for aluminium (Displacement amplitude = 8.8%).	354
Fig.D.2a	Experimental monotonic loop for aluminium (Displacement amplitude = 12%).	354
Fig.D.2b	Experimental cyclic hysteresis loops for aluminium (Displacement amplitude = 12%).	354
Fig.D.3a	Experimental monotonic loop for aluminium (Displacement amplitude = 14.5%).	355
Fig.D.3b	Experimental cyclic hysteresis loops for aluminium (Displacement amplitude = 14.5%).	355
Fig.D.4a	Experimental monotonic loop for aluminium (Displacement amplitude = 16%).	356
Fig.D.4b	Experimental cyclic hysteresis loops for aluminium (Displacement amplitude = 16%).	356
Fig.D.5a	Experimental monotonic loop for Titanium (Displacement amplitude = 13%).	357
Fig.D.5b	Experimental cyclic hysteresis loops for Titanium (Displacement amplitude = 13%).	357
Fig.D.6a	Experimental monotonic loop for Titanium (Displacement amplitude = 16%).	358
Fig.D.6b	Experimental cyclic hysteresis loops for Titanium (Displacement amplitude = 16%).	358

		Page no
Fig.D.7a	Experimental monotonic loop for stainless steel (Displacement amplitude = 15%).	359
Fig.D.7b	Experimental cyclic hysteresis loops for stainless steel (Displacement amplitude = 15%).	359
Fig.D.8a	Experimental monotonic loop for stainless steel (Displacement amplitude = 18.8%).	360
Fig.D.8b	Experimental cyclic hysteresis loops for stainless steel (Displacement amplitude = 18.8%).	360
Fig.E.1	Experimental prestrain and cyclic hysteresis loops for aluminium (20% prestrain, cyclic ampl.= 10.5%).	362
Fig.E.2	Experimental prestrain and cyclic hysteresis loops for aluminium (25.2% prestrain, cyclic ampl.= 10.5%).	362
Fig.E.3	Experimental prestrain and cyclic hysteresis loops for Titanium (31.5% prestrain, cyclic ampl.= 10.5%).	363
Fig.E.4	Experimental prestrain and cyclic hysteresis loops for Titanium (42% prestrain, cyclic ampl.= 10.5%).	363
Fig.E.5	Experimental prestrain and cyclic hysteresis loops for stainless steel (20.8% prestrain, cyclic ampl.=10.5%).	364
Fig.E.6	Experimental prestrain and cyclic hysteresis loops for stainless steel (31.5% prestrain, cyclic ampl.= 10.5%).	365
Fig.E.7	Experimental prestrain and cyclic hysteresis loops for stainless steel (42% prestrain, cyclic ampl.= 10.5%).	366
Fig.E.8	Experimental prestrain and cyclic hysteresis loops for stainless steel (52.5% prestrain, cyclic ampl.=10.5%).	367
Fig F 1	Variation of the Kinematic Translation Parameter with Initial Plastic Strain for Aluminium H18	369
Fig F 2	Variation of the Kinematic Translation Parameter with Initial Plastic Strain for Titanium (Ti-6211)	370

		Page no
Fig F 3	Variation of the Kinematic Translation Parameter with Initial Plastic Strain for Stainless Steel	371
Fig F 4	Comparison of the Variation of β with ε_p to Show Material Dependence of β	372
Fig F 5	Experimental and Computer Monotonic and Cyclic Stress-strain Curves for Aluminium H18	373
Fig F 6	Experimental and Computed Monotonic and Cyclic Stress-strain Curves for Titanium (Ti-6211)	374
Fig F 7	Variation of the Kinematic Translation Parameter with Initial Plastic Pre-strain for Aluminium H18	375
Fig F 8	Variation of the Kinematic Translation Parameter with Initial Plastic Pre-strain for Titanium (Ti-6211)	376
Fig F 9	Variation of the Kinematic Translation Parameter with Initial Plastic Pre-strain for Stainless Steel	377
Fig F10	Comparison of the Variation of β with Plastic Pre-Strain to Show Material Dependence of β	378
Fig F11	Computed Cyclic Hysteresis Loops for A1 - H18	379

LIST OF TABLES.

Table 1	Values of Jcgc, Jcgc, δcgc and δcgc for SCF=2	279
Table 2	Values of Jcgc, Jcgc, δcgc and δcgc for SCF=3	280
Table 3	Values of Jcgc, Jcgc, δcgc and δcgc for SCF=5	281
Table 4	Values of Jcgc, Jcgc, δcgc and δcgc for a small sharp crack, a/w 0.05.	282

CHAPTER ONE

INTRODUCTION

In recent times, the study of fracture mechanics has been extended beyond the linear-elastic fracture mechanics (LEFM) domain to include post yield fracture mechanics (PYFM). Under PYFM, efforts are usually concentrated on analyses related to elastic-plastic fracture mechanics (EPFM). In EPFM, the relatively large zone of plastic yielding and consequent material property change in the region at close proximity to a crack or notch tip plays a very important role in the determination of the macromechanical parameters that are used for quantifying crack behaviour during crack initiation, possible arrest, and probable propagation to failure. The inter-relationship between assumptions in EPFM, fatigue behaviour and the behaviour of the notch or crack root under cyclic loading is of primary importance in this thesis.

Some parameters like the cyclic yield stress-strain curve constitute an important factor in fatigue analysis. Normally, these parameters are determined through direct laboratory experiments on cyclic behaviour, but it is arguable that computation via numerical methods could be much faster and far more convenient. A new way of determining such parameters using the computer and certain simple data for a given material is examined and presented. Discussions on this method will be presented fully in a later chapter.

For a computer analysis, an adaptable theoretical model (in the numercial sense) is required. Consequently, efforts have been made to develop one and this is presented in appendix A. The data that will be necessary for running the program that has been developed are mainly obtainable through experiment, hence all effort must be geared towards formulating a theory for which the requirements will be less demanding as regards laboratory experimentation than the normal cyclic testing. The suggested theory recommends parameters which can be determined through a single cycle load-displacement experiment. The state values of these parameters can be varied experimentally to allow for adequate simulation of real material behaviour. Further discussions will be made in a later chapter.

The fatigue behaivour of short cracks is often associated with local high stress and plastic strain. The relationship to the variations in the values of these engineering parameters at the crack or notch tip can be found by finite-element method and is of interest in this thesis. Consequently, in the second section, these parameters and some suggested alternatives (e.g. by way of normalization) are studied with a view to describing and quantifying the processes at a short crack which is defined as one whose dimensions are of the order of a few grain size. The J-integral, crack opening displacement (COD) and probably, the plastic work are candidates for analyses. This study involves numerical computation and several "experiments" are carried out on the computer on a "standard notch specimen" (in the form of a finite-element mesh) containing a reasonably small crack in the engineering sense. This study is carried out in chapter five.

For notched specimens, the fatigue and fracture behaviour is usually related to their associated stress and strain concentration factors, The strain concentration factor is particularly important in cases of significant plasticity. In fact, these concentration factors do not only classify the particular notch in question through the stresses and strains obtainable at regions close to the notch tip, but also affect the values of the J-integral and COD as will be discussed later (57).

Most previous studies e.g. (117) have concentrated on determining engineering/fracture parameters for different notch configurations and in particular how they affect the threshold value for crack growth once a crack has initiated. In the work done here these parameters are not only calculated but the variation of some of these terms from regions just ahead of a crack tip to positions quite remote from it is also studied. This variation will then be used to describe whether an already initiated fatigue crack will propogate, slow down or completely arrest. This type of study is expected to lead to the modification of the Paris law which is well known not to describe the behaviour of a crack at the incipient stages of its growth (i.e. when it is still a very short or small crack in the engineering sense).

Furthermore, the concept of combining monotonically and cyclically determined data in fatigue study of notched specimens is introduced. This priniciple is expressed in chapter six and will be discussed fully in that part of the thesis.

Finally, the aims can be summarized as follows:

a) To represent the monotonic stress-strain curve and then to determine the cyclic stress-strain curves on the computer within limits of numerical accuracy.

b) To model the notch or crack tip in order to obtain the strain distribution ahead of blunt and sharp notch tips.

c) To use the values obtained in (a) and (b) to model the fatigue behaviour of notched specimens.

d) To modify the Paris law or make a simple suggestion on how such modification might be done in the light of the understanding gained on the behavioural pattern of the macromechanics parameters at the crack tip and regions remote to the tip.

CHAPTER TWO

NUMERICAL COMPUTATION OF CYCLIC STRESS-STRAIN CURVES.

INTRODUCTION

The emergence of the computer has considerably widened the scope of engineering analysis. The work in this section attempts to exploit this facility for the determination of cyclic stress-strain curves.

Numerical algorithmic models are used on the computer to solve defined problems. These models should be made as simple as possible in order to achieve ease of implementation, economize cost and time. Since the work here deals with the use of plasticity theory leading to numerical determination of cyclic stress-strain curve, relevant aspects of plasticity will be examined. Emphasis will be placed on the relationship between plasticity and the behaviour of a cyclically loaded material. A summary of the literature available on previous work will be provided and the relevance of such investigations to the thesis will be highlighted.

MATHEMATICAL THEORY OF PLASTICITY

Essentially, the mathematical theory of plasticity means the quantitative

representation of the relationship between stresses and strains under different loading modes and severity.

The plasticity relationship which will be used for developing the theory cited in appendix A and consequently the computer program are summarized and analysed here. This study is expected to lead to the choice of a specific yield criterion as well as a viable flow rule. In an attempt to describe plastic behaviour through mathematics, Ziegler (1) suggested that,

a) An initial yield condition must be established, so as to be able to define the elastic limit of the material in question.

b) Choice of a flow rule must be made, to relate the plastic strain increment to the stress and stress increments.

c) A hardening rule must be assumed for establishing condition of subsequent yield in the plastic state.

2.1: LINEAR ELASTIC STRESS-STRAIN RELATIONSHIP

Generally, the Hooke's Law relationship can be expressed as

$$\sigma_{ij} = C_{ijkl}\,\varepsilon_{kl} \qquad (2.1)$$

Where,

σ_{ij} are two-dimensional stress components.

ε_{ij} are two-dimensional strain components.

C_{ijkl} is tensor of elastic constants which can be written for isotropic

material as,

$$C_{ijkl} = \lambda\delta_{ij}\delta_{kl} + \lambda\delta_{ik}\delta_{jl} + \mu\delta_{il}\delta_{jk} \qquad (2.2)$$

Where λ and μ are the Lamé constants and δ_{ij} is the kronecker delta.

The kronecker delta itself is defined as follows:

$$\delta_{ij} = \begin{cases} 1 & i=j \\ 0 & i\neq j \end{cases} \quad \text{if}$$

2.2. PLASTIC STRESS-STRAIN RELATIONSHIP -(LEVY-MISES RELATIONSHIP)

Levy (1871) and Von Mises (1913) independently arrived at a set of equations for expressing the relationship between the increments of total strain and stress deviatorics. These equations are known as the Levy-Mises equations and are written as follows:

$$d\varepsilon_x/S_x = d\varepsilon_y/S_y = d\varepsilon_z/S_z = d\varepsilon_{yz}/\tau_{yz} = d\varepsilon_{zx}/\tau_{zx} = d\varepsilon_{xy}/\tau_{xy} = d\lambda \qquad (2.3)$$

or simply,

$$d\varepsilon_{ij} = S_{ij}d\lambda \qquad (2.4)$$

where,

δ_{ij} is the stress deviator tensor

$d\lambda$ is a nonnegative constant which may vary throughout the loading history.

In these equations the total strain increments are assumed to be equal to the plastic strain increments, the elastic strains being ignored. Thus these equations can only be applied to problems of large plastic flow and cannot be used in the elastic-plastic range which is normally of interest.

2.3. PRANDTL -REUSS EQUATIONS

Prandtl and Reuss particularized these equations (2.4) to express only the plastic components of strain and the modified equations are now known as the Prandtl -Reuss equations and are expressed as follows:

$$d\varepsilon^{p}_{ij} = S_{ij}d\lambda \qquad (2.5)$$

where,

Sij are the deviatoric stress components.

Equations (2.5) state that the increments of plastic strain depend on the current values of the deviatoric stress state, and not on the stress increment required to reach this plastic state. Also it is assumed that the principal axes of stress and of plastic strain increment tensors coincide. Furthermore, the equations give a relationship between the ratios of plastic strain increments in different directions and a yield criterion will be required in order to be able to determine the actual magnitudes of plastic strain increments.

As against this suggestion, analysis using the octahedral shear stress criterion and the Mohr stress circle show that,

$$d\lambda = d\gamma_o^p / \tau_{oct}$$

or

$$d\lambda = \sqrt{3/2}\, d\gamma_o^p / \sqrt{J_2} \qquad (2.6)$$

where,

γ_o is the octahedral shear strain

τ_{oct} is the octahedral shear stress component.

J_2 is the second invariant of the stress deviator tensor.

If equivalent or effective stress (σ_e) and plastic strain ($d\varepsilon_p$) are defined, a more convenient expression can be written as,

$$d\lambda = 3/2\, d\varepsilon_p / \sigma_e \qquad (2.7)$$

The relevance of this equation will be seen in appendix A.

Equation (2.5) allows for loading from one plastic state to another or from one loading surface to another, thereby guaranteeing consistent plastic deformation. Whenever contained plasticity is involved in stress analysis, a flow law will be needed to fully account for the phenomenon of deformation.

2.4. THE FLOW RULE AND DEFORMATION THEORY

The yield and loading conditions serve to establish criteria for yielding from some elastic or plastic state respectively. Additional information in the form of a constitutive relation between increments of plastic strain, stress and stress increments, is required to describe the plastic behaviour of a material. This constitutive relation called the flow rule, is based on the Drucker's postulate (2) for work-hardening materials.

This rule states that the total work done by an external agent during a complete cycle of loading and unloading must be positive. For this statement to be true, the following two assumptions must be satisfied;

a) The yield and loading surfaces must be convex with respect to the origin in stress space.

b) The plastic strain increment vector must lie on the outward normal to the loading surface at the instantaneous stress state.

The convexity condition in Prager's model (3) is satisfied by the ellipsoidal relationship which defines the Von Mises yield surface.

Requirement (b) provides a means of obtaining a constitutive relationship between the plastic strain increment, stresses and stress increment. This condition leads to the formation of the flow rule and the rule (4) in its complete state is written as follows,

$$d\varepsilon_{ij} = d\lambda \partial f (\sigma_{ij} , \alpha_{ij}) / d\sigma_{ij} \qquad (2.8)$$

where α_{ij} are the components of the amount of translation of the initial yield surface and $d\varepsilon_{ij}$ are the increments of plastic strain and $d\lambda$ is a positive scalar quantity referred to in texts as the plastic multiplier.

The flow rule leads to an incremental or flow theory of plasticity in which path dependence of the final state of stress and strain as attained from some previous state is manifested. Flow theory, in general, is distinct from the deformation theory of plasticity, in which the total plastic strains are related to the final stress state.

In deformation theory, a relationship exists only between the final states of stress and strain for a given loading process with unloading being specified by a separate law.

For proportional loading where the stress vector remains fixed in direction, flow and deformation theories coincide. Budiansky (5), showed that deformation theory can be consistent with the postulate cited here in the proportional loading regime.

Drucker's postulate will be used to develop the theory that constitutes the plasticity numerical model used for determining cyclic stress-strain relationship (appendix A).

At this juncture, it should be mentioned that there are at least two odds against the deformation theory which constitute themselves as follows;

a) The omission of the unloading phenomenon.
b) The non-representation of a general loading path.

For these reasons the deformation theory is ignored and the flow theory is adopted for the purpose of this thesis.

In order to be able to fully study the behaviour of an engineering material, these last two sections will need to be complemented by a hardening criterion, a viable yield surface etc. The next few sections therefore address these necessities.

2.5. MEASURES OF WORK-HARDENING AND STRAIN -HARDENING

Two work-hardening hypotheses are available for measuring the extent of the effect of plastic flow on a body that has been loaded beyond yield. They are called the work-hardening and strain-hardening hypotheses.

2.5.1 WORK-HARDENING HYPOTHESIS

Here it is assumed that the amount of hardening depends only on the total plastic work and is independent of the strain path (6). This therefore implies that the resistance to further yielding depends only on the amount of work done on a given material. This amount of work is measured by the yield criterion.

In the isotropic case,

$$F(\sigma_{ij}) = K \qquad (2.9)$$

where σ_{ij} are the two dimensional stress components and

K is allowed to change as the material work-hardens and the isotropic hardening function $F(\sigma_{ij})$ remains the same. In accordance with the requirement of this hypothesis,K, will be a function of the plastic work done per unit volume and then,

$$F(\sigma_{ij}) = f(WP) \qquad (2.10)$$

where

$$WP = \int \sigma_{ij}\, d\varepsilon^{p}_{ij}$$

Assuming an equivalent stress, σ_e in uniaxial tension, to represent the yield function,

$$\sigma_e = f(W^p) \qquad (2.11)$$

2.5.2. MEASUREMENT OF PLASTIC STRAIN

If the total work done, dW, in a loaded body per unit volume is assumed to be,

$$dW = \sigma_{ij}\, d\varepsilon_{ij} \qquad (2.12)$$

$$= \sigma_{ij} (d\varepsilon^e_{ij} + d\varepsilon^p_{ij})$$

$$= \sigma_{ij}\, d\varepsilon^e_{ij} + \sigma_{ij}\, d\varepsilon^p_{ij}$$

or

$$dW = dW^e + dW^p \qquad (2.13)$$

dW^e = recoverable elastic energy

dW^p = plastic work causing permanent deformation.

The plastic component of the work done can be expressed further as follows:

$$dW^p = S_{ij}\, d\varepsilon^p_{ij} \qquad (2.14)$$

Equation (2.12), has earlier (7) been shown to be

$$dW^p = \sigma_e d\varepsilon_p \qquad (2.15)$$

This allows the Prandtl-Reuss relations to be written as,

$$d\varepsilon^p_{ij} = 3/2\, dW^p / \sigma_e^2\, S_{ij} \qquad (2.16)$$

The functional relationship between the yield function and the plastic work can be obtained experimentally and the plastic strain increment can then be evaluated using equation (2.16).

2.5.3. THE STRAIN-HARDENING HYPOTHESIS

This uses equivalent plastic strain. It is assumed that the degree of plastic deformation is measurable by this quantity. In effect.

$$\varepsilon^p = \int d\varepsilon_p \qquad (2.17)$$

and the yield function is expressed as a function of ε_p as,

$$F(\sigma_{ij}) = H(\varepsilon_p) \qquad (2.18)$$

This functional relationship can be determined and it has been shown to be reliable for experimental data analysis. Using the equivalent stress once again,

$$\sigma_e = H(\varepsilon_p) \qquad (2.19)$$

Equations (2.11) and (2.19), can be shown to be equivalent under strict isotropic condition.

However, both of them become more complicated and they cease to be equivalent when anisotropic and Bauschinger effects characterize the behaviour of a material. The anisotropic relationships for all functions discussed above are evaluated in appendix A. They are simplified by assuming only two-dimensional effects and are derived as simple extensions of the isotropic functions.

These two hypotheses are cited at relevant points in appendix A. However, the strain hardening hypothesis is favoured in developing the elastic-plastic theory in this same text. This is because of its relative simplicity.

2.6. YIELD CRITERIA

2.6.1. TRESCA'S YIELD CRITERION

The simplest form of yield condition is the Tresca's yield criterion. This condition is based on the assumption that a material yields whenever the maximum shear stress reaches a critical value. Mathematically, it can be expressed as;

$$(\sigma_1 - \sigma_2) = K \qquad (2.20)$$

where σ_1 and σ_2 are the maximum and minimum principal stresses in the body and K is the numerical yield stress in tension .

Geometrically, the Tresca yield condition is represented as a piecewise linear surface.

2.6.2. VON MISES YIELD CRITERION

A relatively simple and easily applied yield criterion. Mathematically, the implication is that yielding occurs whenever the second invariant of deviatoric stress tensor, J_2', equals some critical value. The yield condition also leads to the following inferences:

1) That yielding begins whenever the internal energy of distortion exceeds a certain value.

2) That yielding begins whenever the shear stress on an octahedral plane exceeds a certain limit, the octahedral plane being referred to the principal stress directions.

Experimental revelations have brought about a lot of controversy on the study of the effect of plasticity on yield surface behaviour. Some investigators argue the existence of smooth surfaced yield loci while others noticed the existence of corners on the yield surfaces. Nevertheless, there is sufficient experimental evidence to support a smooth surface (25, 26, 27, 28, 38 39). The acceptance of smooth surface representation then, should lead to the choice of the Von Mises yield ellipse.

In simple plane stress mathematical formulation, this surface can be represented as follows,

$$f(\sigma_{ij}) = \sigma_x^2 - \sigma_x \sigma_y + \sigma_y^2 + 3\tau_{xy} - \sigma_o^2 \qquad (2.21)$$

since for plane stress,

$$(\sigma_z = \tau_{xz} = \tau_{yz} = 0),$$

where σ_o is the tensile yield stress, and all the other terms take their usual meanings as in stress analysis and as defined in the table of constants.

When initial plasticity is assumed or when the definition of a flow stress for the "elastic limit" is applicable in analyses, the subsequent yield or loading function can be represented as

$$f(\sigma_{ij}, \alpha_{ij}) = 0 \qquad (2.22)$$

where α_{ij} is a measure of the degree of work-hardening or isotropic movement of the yield surface in a given direction.

Equation (2.22) is capable of specifying conditions for loading and unloading from a plastic state in an isotropic situation. For incremental plasticity consideration, the total differential of this function is given by:

$$df = \partial f / \partial \sigma_{ij} \cdot d\sigma_{ij} + \partial f / \partial \alpha_{ij} \cdot d\alpha_{ij} \qquad (2.23)$$

This equation is very important and significantly useful in all its ramifications. The various parts, as described below, are used for computer formulaton with f=O representing a plastic state and f<O representing an

elastic state and f>O being defined only for subsequent loading regimes.Unloading from a plastic state to an elastic state will result in df<O.

2.6.2.1 UNLOADING

The unloading process is elastic in nature. This means that $d\alpha_{ij}$ =O. From equation (2.23), this case can be mathematically represented as,

$$\partial f / \partial \sigma_{ij} \, d\sigma_{ij} < 0 \qquad (2.24)$$

2.6.2.2. TANGENCY CONDITION

On the surface of an initial yield ellipse (where relevant a subsequent yield surface), the outward normal or vector of plastic strain drawn on the surface is perpendicular to the tangent drawn at the stress point. The mathematical expression for this situation is also derived from equation (2.23) by putting $d\alpha_{ij} = 0$, once again and is written as follows:

$$\partial f / \partial \sigma_{ij} \, d\sigma_{ij} = 0 \qquad (2.25)$$

This condition is one of perfect plasticity. The underlying assumptions relate to those of an elastic perfectly plastic material, hence the idealization of material behaviour. Because of this, some error is incurred in calculation as engineering materials rarely behave in the manner of the assumptions made.

2.6.2.3. CONSISTENT LOADING CONDITION

Prager's (3) consistent loading condition which allows for analysis to be done on subsequent yield surfaces with ease can be deduced from equation 2.23 as well.

It is expressed as,

$$\partial f / \partial \sigma_{ij} \; d\sigma_{ij} > 0 \qquad (2.26)$$

This expression is only relevant to the kinematic hardening case.

2.7 RESPONSE OF ENGINEERING MATERIALS TO LOADING.

First, loading, as used here refers to the loading and unloading sequence. The various phenomena that result when a material is subjected to a load-unloading history are cited below. These will be discussed in relation to the formation of yield theories from the reversed yielding curve, the behavioural pattern of the yield surface under plastic loading (followed by elastic unloading) and the mathematical representation of such behaviour under the same loading sequence.

2.7.1 ASPECTS OF REVERSED LOADING

The terminology reversed yielding is explicit and self-explanatory. It can be

quickly demonstrated in the laboratory by simply loading a specimen in tension to a regime beyond the elastic yield point and then unloading it into compression until it re-yields. This exercise produces different responses from different materials. The most important of the exhibited characteristics in the Bauschinger effect. Fig (2.1) shows a schematic representation of reversed loading with an illustration of the Bauschinger effect.

2.7.2 THE BAUSHINGER EFFECT

This is the phenomenon which occurs in several materials when loaded e.g. in tension to the same plastic stress $\sigma_1 > \sigma_0$, (where σ_0 is the uniaxial yield stress of the specific material in tension), and on unloading they exhibit different re-yield stresses.

This effect is material dependent and very sensitive to the state of loading and strain changes in a material. Several theories can be derived from the interesting revelations under reversed loading as shown in fig 2.1.

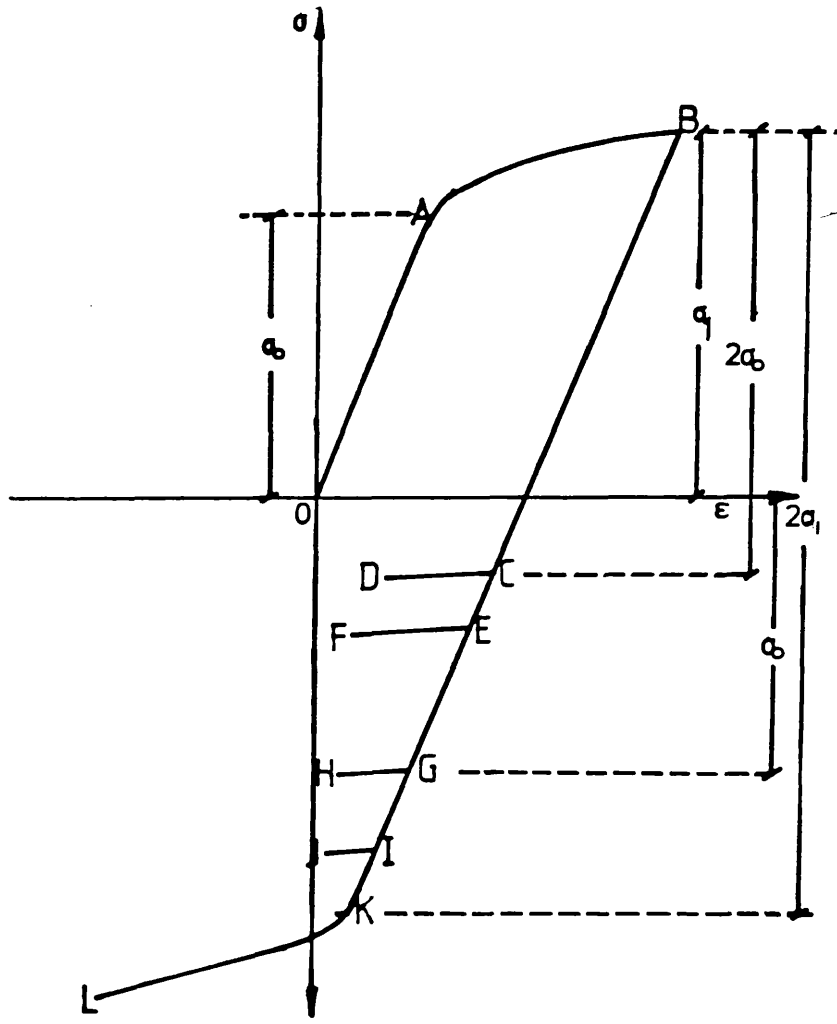


Fig. 2.1. THEORIES OF REVERSED LOADING.

2.8 INTERPRETATION OF THE ILLUSTRATED PATHS ON FIG (2.1)

2.8.1 PATH OABCD

At one end, the elastic unloading range will be approximately double the material's initial yield stress, so that the material will yield in compression

when,

$$\sigma_c = \sigma_1 - 2\sigma_0 \qquad (2.27)$$

where,

σ_c is the compressive yield stress and carries a negative sign;

σ_1 is the plastic stress in tension and

σ_0 is the yield stress in tension.

Equation (2.27) is represented by path OABCD on the diagram. This model states that the total elastic range of a relevant material remains constant whilst the actual compressive yield stress is reduced in magnitude due to previous tensile yielding. This theory can therefore be considered as a strict expression of the Bausclinger effect.

2.8.2 PATH OABCKL

Observations at the other extreme suggest another model. This is generally referred to as the isotropic hardening model. This theory stipulates that the hardening mechanism acts equally in tension and compression even though the yielding is in tension. Therefore compressive yielding will start when.

$$\sigma = -\sigma_1 \qquad (2.28)$$

This is represented by path OABKL. Under this theory, the compressive stress and the elastic range are both numerically increased by the hardening. This may be highly unrealistic for most materials.

2.8.3 PATH OABGH

A possible theory can be developed half-way between the two stated above. Here the compressive yield stress is independent of the tensile yield stress and the compressive yield strength remains fixed at,

$$\sigma = -\sigma_0 \qquad (2.29)$$

This case is represented by path OABGH.

2.8.4 PATHS OABEF AND OABIJ.

A fourth theory can make use of either path OABEF or OABIJ.
Any theory formed by using either of these paths or path OABGH (mentioned earlier) will be expressing a combined hardening phenomenon. Consequently, a theory formed by using any of the above last mentioned three paths will be germane to the behaviour of real materials and will be general.

Moreover, a general theory of this sort would adequately incorporate 2.7.2.1 and 2.7.2.2, each theory being obtainable as a particular case of the general theory.

2.9 YIELD LOCI AND YIELD MODELS.

2.9.1 THE KINEMATIC - HARDENING MODEL

The kinematic hardening model assumes work hardening where the initial yield surface retains its size, shape and orientation whilst being free to translate as a rigid body. Fig (2.2) illustrates this phenomenon. The direction of translation of the yield suface is that of the exterior normal at the stress point.

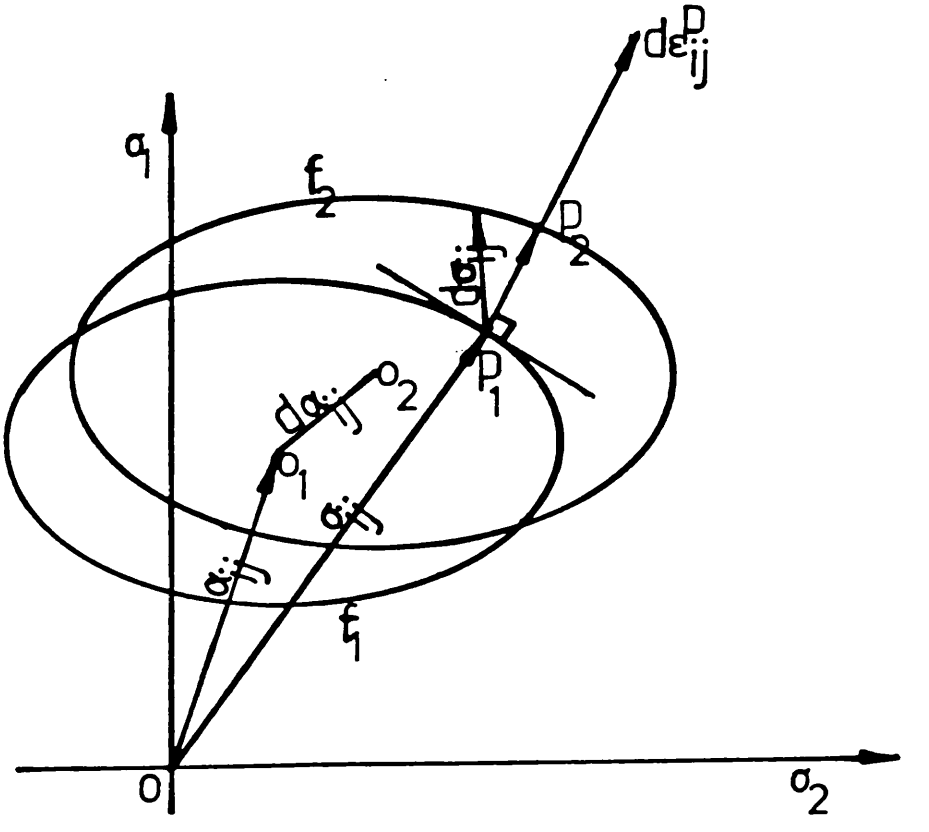


Fig. (2.2) Prager's Kinematic - hardening model. (3)

Prager (3) stated that if a current stess tensor, σ_{ij}, is achieved through an infinitesimal stress change, $d\sigma_{ij}$, as in fig (2.2), the corresponding infinitesimal translation of the centre O_1 to O_2 is $d\alpha_{ij}$.

Since the plastic strain increment vector $d\varepsilon^p_{ij}$ lies on the exterior normal to the yield surface f_1 at the stress point P_1, the flow rule for kinematic hardening rule for full dimensional stress space can be expressed mathematically as,

$$d\alpha_{ij} = c\, d\varepsilon^p_{ij} \qquad (2.30)$$

where c is a material constant and probably state dependent. most experiments involving aluminium and its alloys seem to lend credence to this model.

Shield and Ziegler (8) pointed out that distortion of the yield surface is likely if Prager's hardening rule were applied to different subspaces of the full stress space. In more explicit terms if the yield surface in 9-space, σ_{ik}, moves in the direction of the exterior normal at the stress point, the two-dimensional (original) yield locus does not do the same and may even deform in some circumstances. To overcome this difficulty, Ziegler(1) suggested a modification which was later observed to be reasonably accurate by other investigators e.g Rees(9). Fig (2.3) shows the basic concept of the improved model.

It is found that for an infinitesimal stress change, $d\sigma_{ij}$, caused by a translation of $d\alpha ij$, in a current stress tensor, σ_{ij}, the yield surface f_1 translates rigidly to f_2 in the direction of the vector connecting O_1 to the

stress point P_1. Hence P_1 translates to P_2 and the centre o_1 of f_1 translates to the center O_2 of f_2 in parallel directions. Because of this parallel transformation the loading and unloading processes follow paths O_1 to P_2 and P_2 to O_2 respectively. This assumption which leads to the formulation,

$$d\alpha_{ij} = (\sigma_{ij} - \alpha_{ij}) d\mu \qquad (2.31)$$

where α_{ij} and $d\alpha_{ij}$ are total and incremental stress translators and $d\mu$ is a scalar multiplier, is the Ziegler's modified relation for the infinitesimal translation $d\alpha_{ij}$.

A defect of this modified kinematic-hardening theory is that the path of the centre does not, in general, represent the strain path. However the loading path is readily obtainable by laying the incremental plastic strain vector $d\varepsilon^p_{ij}$ end to end. This procedure can be considerably simplified when the ends of vectors $cd\varepsilon^p_{ij}$ are made to terminate on the new yield surface as shown on fig (2.3).

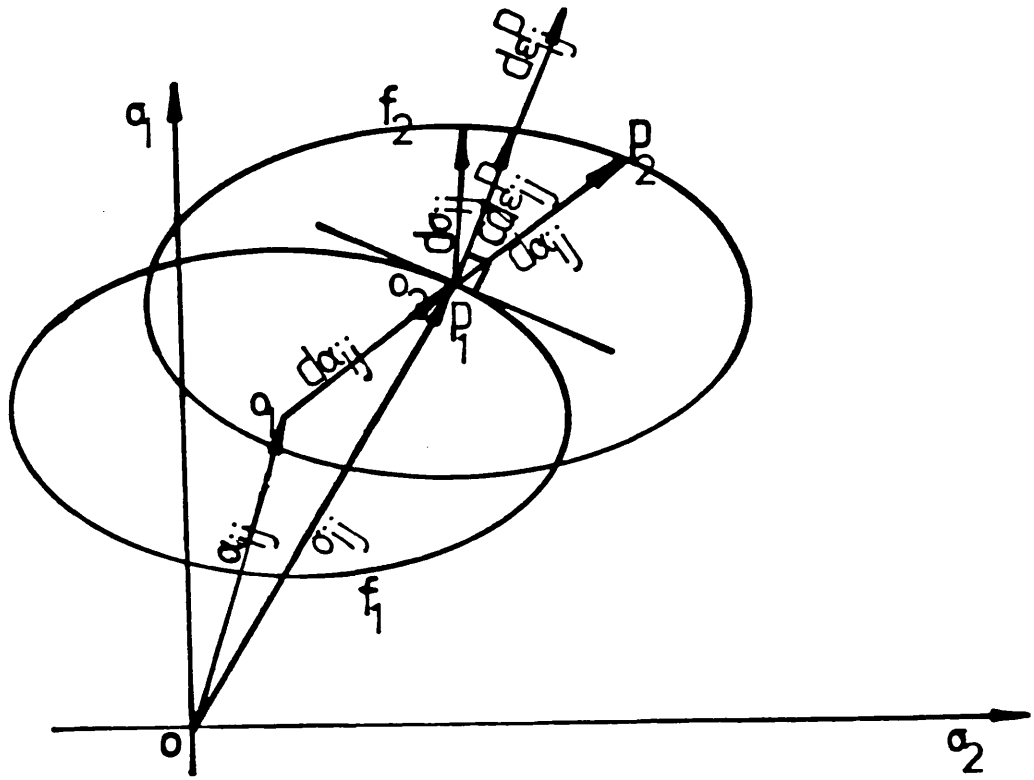


Fig.(2.3) Ziegler's modified kinematic-hardening model.(8)

2.9.2 ISOTROPIC HARDENING

This theory assumes that during plastic flow the yield surface maintains its shape, centre and orientation whilst expanding uniformly about the origin in a stress subspace. Fig(2.4) illustrates a two-dimensional plot of the yield and loading surfaces as the stress state changes from point a to b. Unloading and subsequent reloading in the reverse direction will result in yielding or the stress state represented by point c. The path b-c will be elastic and o-b is

equal to o-c . Unfortunately this model's representation of work hardening does not account for the Bauschinger effect which is exhibited by most real materials. Characteristically this theory suggests that due to work-hardening a material will exhibit an increase of the same magnitude in the yield stress in the tensile and compressive loading directions. Since anisotropy prevails during plastic deformation, a theory which predicts strict isotropy in the plastic loading regime will be unrepresentative of real behaviour and will consequently be expected to produce inaccurate results. This situation will aggravate when complex loading paths, involving changes in direction of the stress vector in a stres space are considered. Experimental results provide in(10,11,12,13) substantiate this conclusion.

Mathematical simplicty is an attractive property of this model and it would have been far more convenient to implement it numerically on its own on the computer. However, it may have to be part of a union of models in order to be able to formulate a more realistic model for representing the behaviour of structural materials.

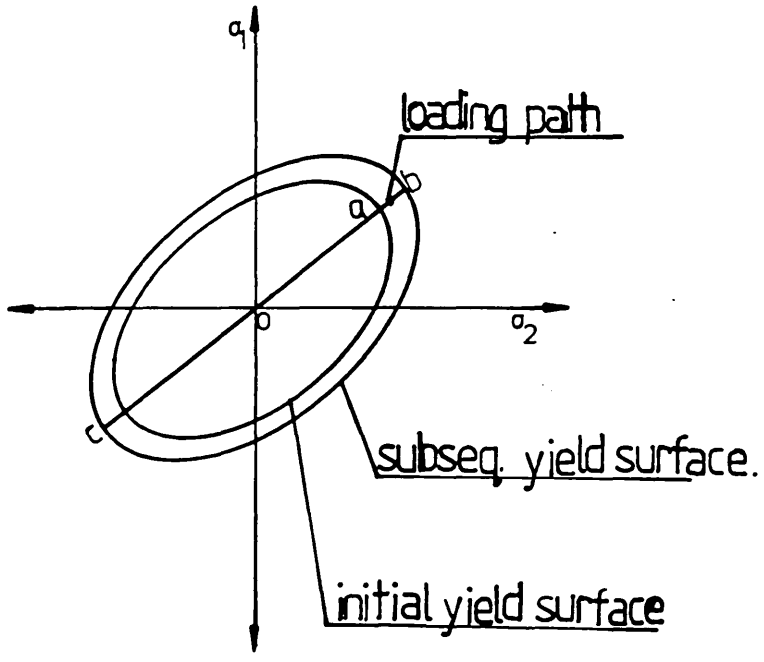


Fig. 2.4. The Isotropic - hardening Model.

2.9.3 SLIP THEORY MODEL

Bartdorf and Budiansky(14) based their argument on the slip surface in crystals and developed a theory which allows for a distortion of the loading surface relative to the yield surface and previous loading surfaces. This theory predicts the formation of corners of the instantaneous stress state on the loading surface during plastic deformation. Fig(2.5) shows the response of the yield function as it is taken from a stress state at the origin,0, to final state at point c. The shaded regions,I ,II,III, show the loading stages from the first loaded point 1 to point c. The yield surface is the unshaded ellipse. The constitutive relationship between stresses and strains can be very complicated since the stress state is usually in a corner (point of singularity).

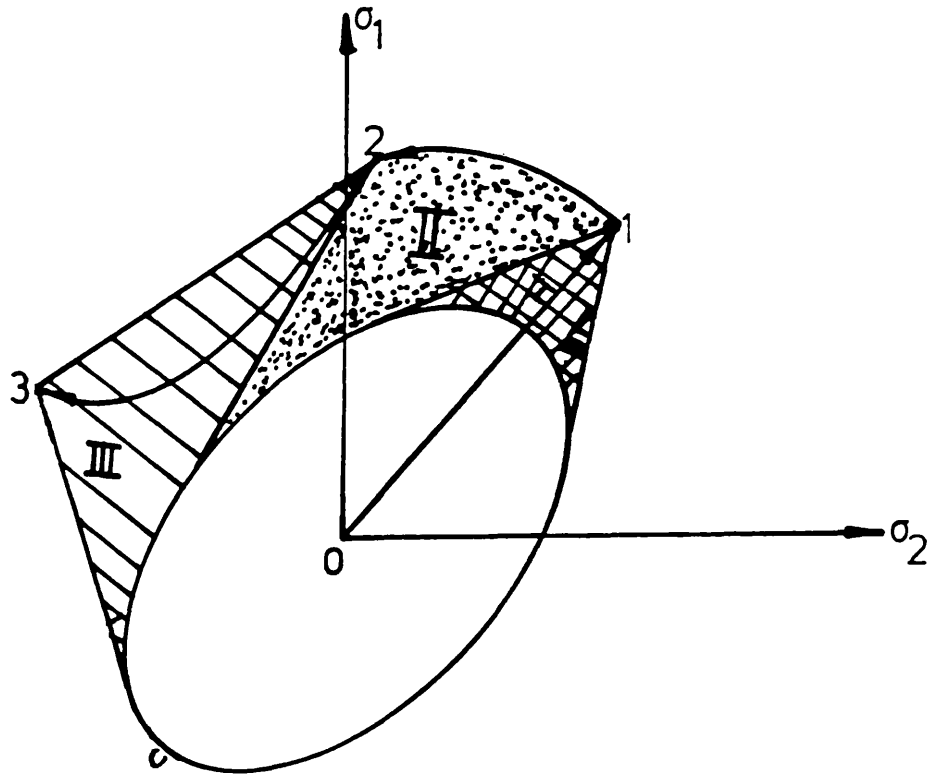


Fig 2. 5 Slip Theory Model (14)

Experimental data provided by (11,12,15,25) indicate the formation of corners and distortion of the loading surface, but careful examination will reveal that they are not particularly representative of the slip theory predictions. The theory also fails to incorporate the Baushinger effect. This theory has to be rejected because of its unmanageable complexity and omission of the Bauschinger effect.

2.9.4 PEICEWISE LINEAR PLASTICITY THEORY.

Fig (2.6) Shows the representation of this theory for a loading sequence from o-c.

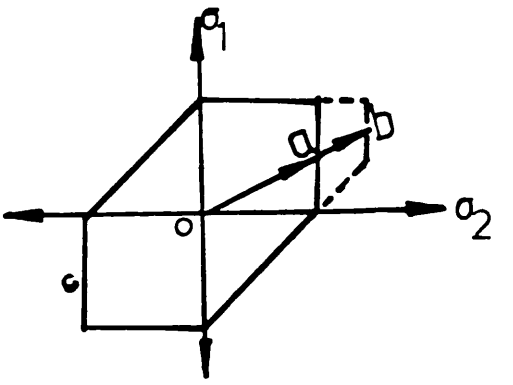
In this representation, the yield surface is described by a finite number of plane surfaces, whose intersections constitute points of singularity or corners. The Tresca criterion is quite germane to this type of phenomenon. The loading surface is also assumed to consist of plane surfaces and the subsequent hardening behaviour can be classified as follows:

A) The hardening rule of independent plane loading surface:

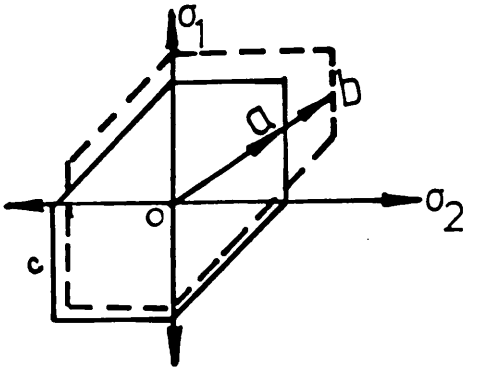
Sanders' (16) work is a typical representation of this loading system. As shown in fig 2.6a, the non-zero stress components are σ_1 and σ_2 and a loading path, o - b, in any quadrant of the stress plane does not affect the loading surface in the remaining quadrants. Consequently this rule omits the Bauschinger effect and can be disregarded immediately.

B) The hardening rule of interdependent loading surfaces (17)

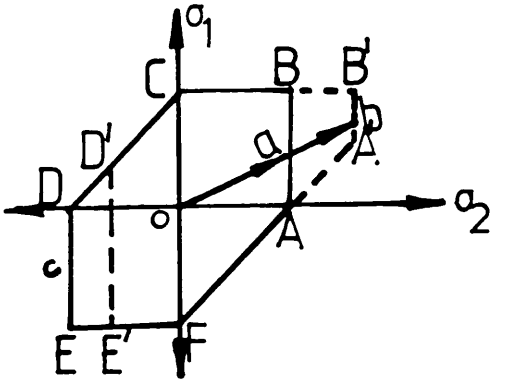
This rule is a generalization of rule (a) By allowing for dependence between the planes that comprise the loading surface, a loading path intersecting any



a.



b.



c.

$$|B'B| = |EE'|$$

Fig 2. 6 Piecewise Linear Plasticity Theory

one plane of this surface may effect changes in each of the remaining planes. Fig (2.6b) shows that this hardening rule can be used to specify any piece wise linear loading surface and is capable of accounting for the Bauschinger effect.

Stricklin (18) in his work argued that plastic straining is due to slipping along three independent slip planes, along any one of which the shear is a maximum. In considering this special case of interdependent loading surfaces the piecewise linear stress-strain relationships are written in terms of coefficients representing the hardening behaviour of a material. These coefficients are functions of stress and are dependent upon a linear strain - hardening rule as applied in the cited text. By specifying the correspondence between various segments of yield surface and the slip planes, total plastic strains for any loading are considered as the sum of contributions from the three independent sets of slip planes. A further assumption is the maintenance of a constant elastic range from tensile to compressive yielding. Fig (2.6.c) is a schematic representation of this special case. This diagram clearly shows the Bauschinger effect.

It will be a very onerous task implementing this interdependent loading surfaces criterion on the computer because of its inherent singularity points at the corners of the suggested surface hence, this model will not be used despite its capability to monitor the Bauschinger effect.

2.10 RELATIONSHIP BETWEEN THE ISOTROPIC AND KINEMATIC HARDENING MODELS.

Fig. (2.7). summarizes the relationship between the predictions of the isotropic and kinematic hardening loading surfaces.

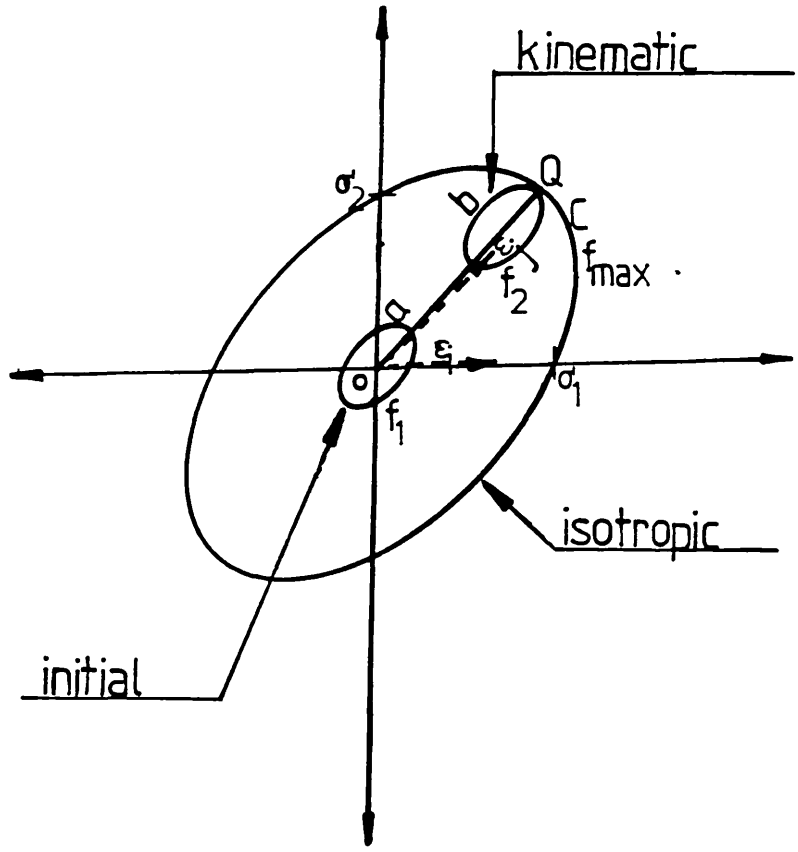


Fig.(2.7) Isotropic and Kinematic-hardening theories for same loading path,OQ

Consider a loading path OQ as shown in diagram.

ε_i and ε_j are strain components. This diagram manifests the difference in behaviour of the loading surfaces namely b and c and also the difference in the

strain values represented by ε_i and ε_j surfaces b and c are kinematically hardened and the isotropically hardened surfaces respectively.

If f is a yield function the initial yield function may be repesented by f_1, the kinematic surface by f_2 and the isotropic one by f_{max}, the loading surface or subsequent yield surface or current yield surface can be non-dimensionally represented as follows:

Put $f = 1$

then for the diagram shown:

the plastic cases can be represented by,

$$f = f_{max}, \quad f \geqslant 1 \quad \text{and} \quad \dot{f} > 0$$

the elastic case will be either,

$$f < f_{max} \quad \text{or} \quad f < 1 \quad \text{or} \quad \dot{f} \leqslant 0 \qquad (2.32)$$

at the surface f_{max} and for the loading path OQ,

$$f_1 = f_2 = f_{max} \qquad (2.33)$$

Also at the stress point i.e. at Q, there exists a unique normal and the plastic strain vector assumes the same direction as this normal.
This functional analysis is particularly useful for computation and surface behaviour on the computer.

2.11 THE MROZ MODEL.

The Mroz model (19,20), is a combined-hardening rule. It employs the concept of a field of surfaces of constant work-hardening moduli. Each nodal stress value in a piecewise linear uniaxial stress-strain curve is represented in stress space by a surface geometrically similar to the initial yield surface, but of different size. The yield surface is assumed to translate and expand within this field, contacting and then pushing each surface along with it as each is encountered. Each surface is associated with a value of the work-hardening modulus characteristic of the piecewise linear segment immediately following the represented nodal stress value.
The governing work-hardening modulus at any point in an arbitrary loading history is that modulus associated with the largest surface in contact with the stress state prior to an increment of plastic deformation.
This model has been found adequate for studying cyclic strain-hardening and cyclic softening (23).

2.12 MECHANICAL SUBLAYER MODEL.

It is also referred to as the Besseling-White model. It uses an arrangement of elastic-plastic elements in parallel to represent material behaviour. First proposed by Duwez(21) and then modified by White(22), the elemental properties are determined from a piecewise linearization of a tensile stress-strain curve. This model predicts a rigid body translation of the yield surface during plastic deformation. It was tested on the computer in (23) and found to be applicable to cyclic analyses.

2.13. ANISOTROPIC - YIELDING AND - HARDENING RULES.

In ordinary metallurgical terminology, a material which exhibits variation of property in different direction is said to be in a state of anisotropy. Anisotropy manifests itself either as anisotropic yielding or anisotropic hardening. When a material is anisotropic only in its tensile and compressive yield strengths only, the kinematic-hardening theory on its own is adequate for representing its behaviour. However, when the rates of hardening in the forward and reversed plastic curves are different anisotropic hardening has to be included in theory. Hence, the consideration of anisotropic hardening allows for a more generalization of the reversed loading behaviour of materials.

They either occur together or independently to reflect the behaviour of a relevant material during loading. The combination of the kinematic and isotropic hardening models offers a mathematical similarity to the concept of anisotropic yielding and the Bauschinger effect phenomenon. It is now believed that a full representation of material behaviour could be achieved by forming a union between the rules of kinematic-hardening, isotropic hardening and anisotropic yielding and hardening rules. This combination will be discussed later.

2.14. APPLICABILITY OF HARDENING RULES TO THE PREDICTION OF MATERIAL'S BEHAVIOUR

Hunsaker, Vaughan and Stricklin (23) investigated the suitability of either of isotropic hardening or anisotropic hardening rules like the Prager-Ziegler kinematic hardening, Mroz model(19) or the mechanical sublayer model(21,22)

for the prediction of the plastic behaviour of a material under uniaxial and biaxial loading conditions. The computer studies carried out led them to conclude that under reversed loading, the Mroz model (close to the combined-hardening model and the mechanical sublayer models) give significantly better results than either the isotropic or kinematic hardening models.

The mechanical sublayer model illustrated in figure (2.8) is recommended for computer studies under the aforementioned loading condition because it requires less computer storage than the Mroz model (23). It was also observed that the isotropic hardening rule is well suited to simple monotonic loading behaviour whilst the kinematic hardening model is suitable for the more complicated bilinear uniaxial loading. This speculation was later confirmed by Liu (24). This study confirms that the combined-hardening model is most suited to cyclic studies. It was shown earlier (34) that the general behaviour of the yield surface under this type of loading follows the combined-hardening sequence and it can now be seen that even the specific aspect of hardening is best described via the combined-hardening theory and this line of argument is followed in the present work.

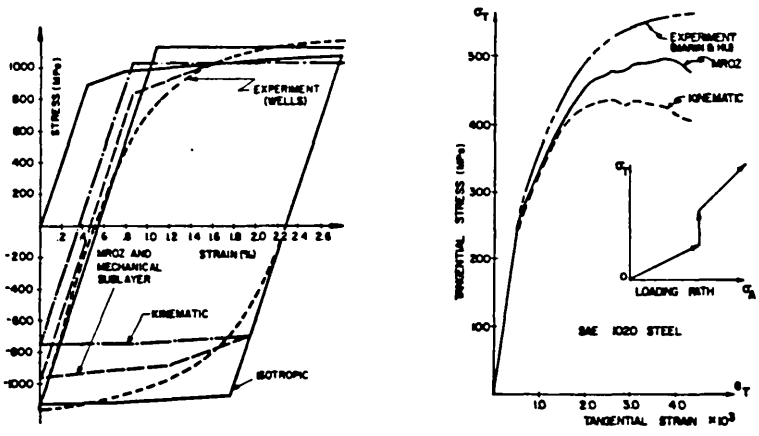


Fig. 2.8 Comparison of the various hardening rules.(23)

2.15. INVESTIGATION OF YIELD SURFACE BEHAVIOUR
- EXPERIMENTAL -

2.15.1. NAGHDI et al (25)

The pioneering Naghdi et al work on the investigation of yield surface behaviour is very important in that it set up one of the best methods for doing this type of study. The experiments were done on tubular 24S-T-4 aluminium alloy under a tension-torsion-reversed tension loading sequence and the procedure is schematically presented in figs (2-9a) and (2.9b). The sequence of events regarding the experimental procedure diagramatized in these figures is fully explained in the cited paper (16). The outcome of the experiments carried out is presented in fig (2.10).

It was observed that the yield surface did move and translate to a subsequent one. Also the initial as well as the subsequent yield surfaces were found to be convex. There was a prominent display of the Bauschinger effect. It was argued that the initial yield surface could be well fitted by applying an isotropic theory of plasticity as explained earlier, but an anisotropic strain-hardening theory has to be employed in fitting the experimentally derived initial and subsequent yield surface in the same stress subspace which in this case is the $\tau_{\theta z}$ - σ_z coordinate axes as shown in fig(2.10). Finally, it was confirmed that the experimentally derived yield surface agrees very well with the Von-Mises yield condition within limits of experimental accuracy. The experimental procedure used in the present work derives from the pattern of these authors' work, even though the actual experiment was carried out in a σ_x - σ_y coordinate axes.

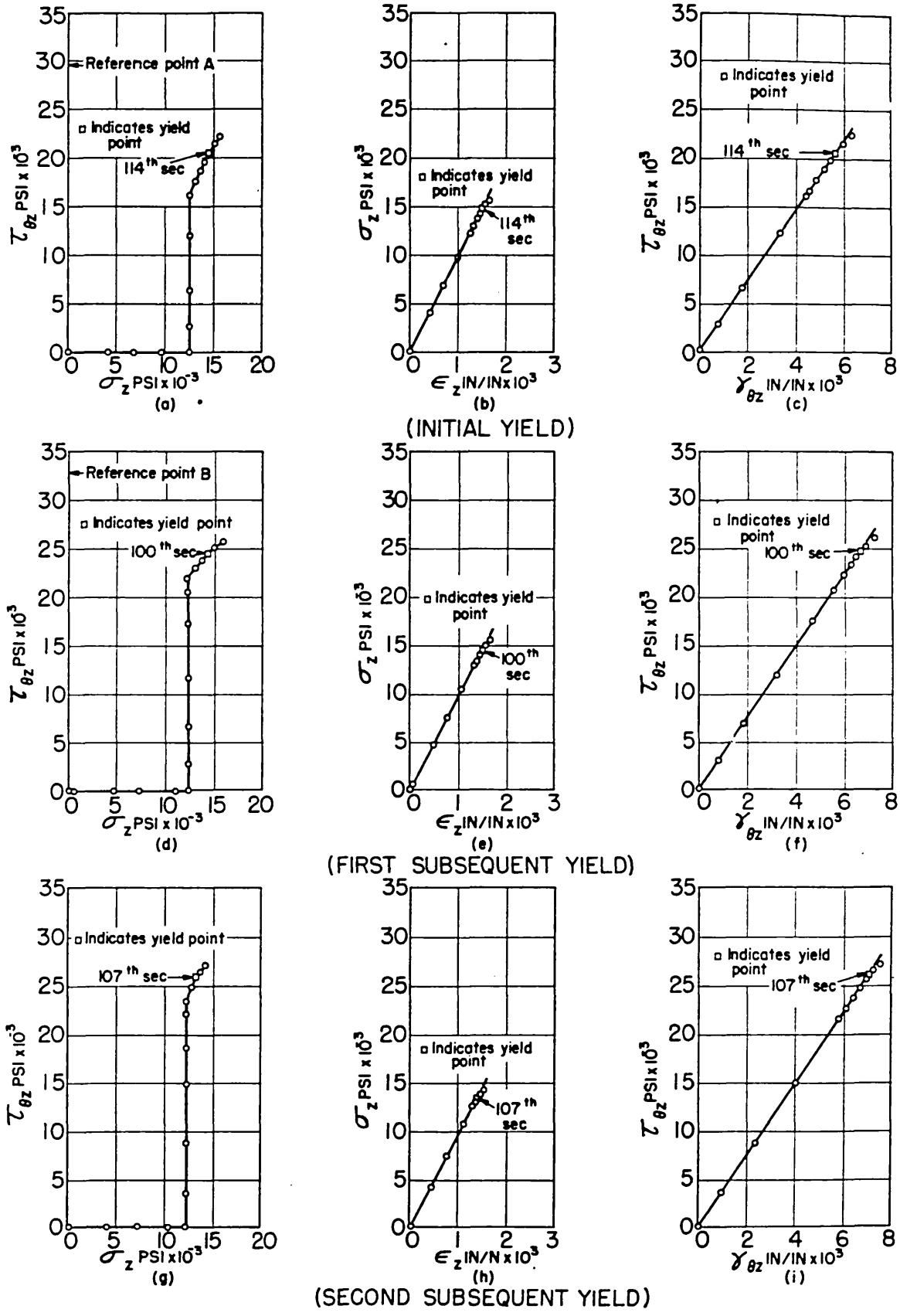


Fig 2. 9a Loading path and stress-strain curves for determination of initial and subsequent yield points of a typical specimen in the first quadrant (25)

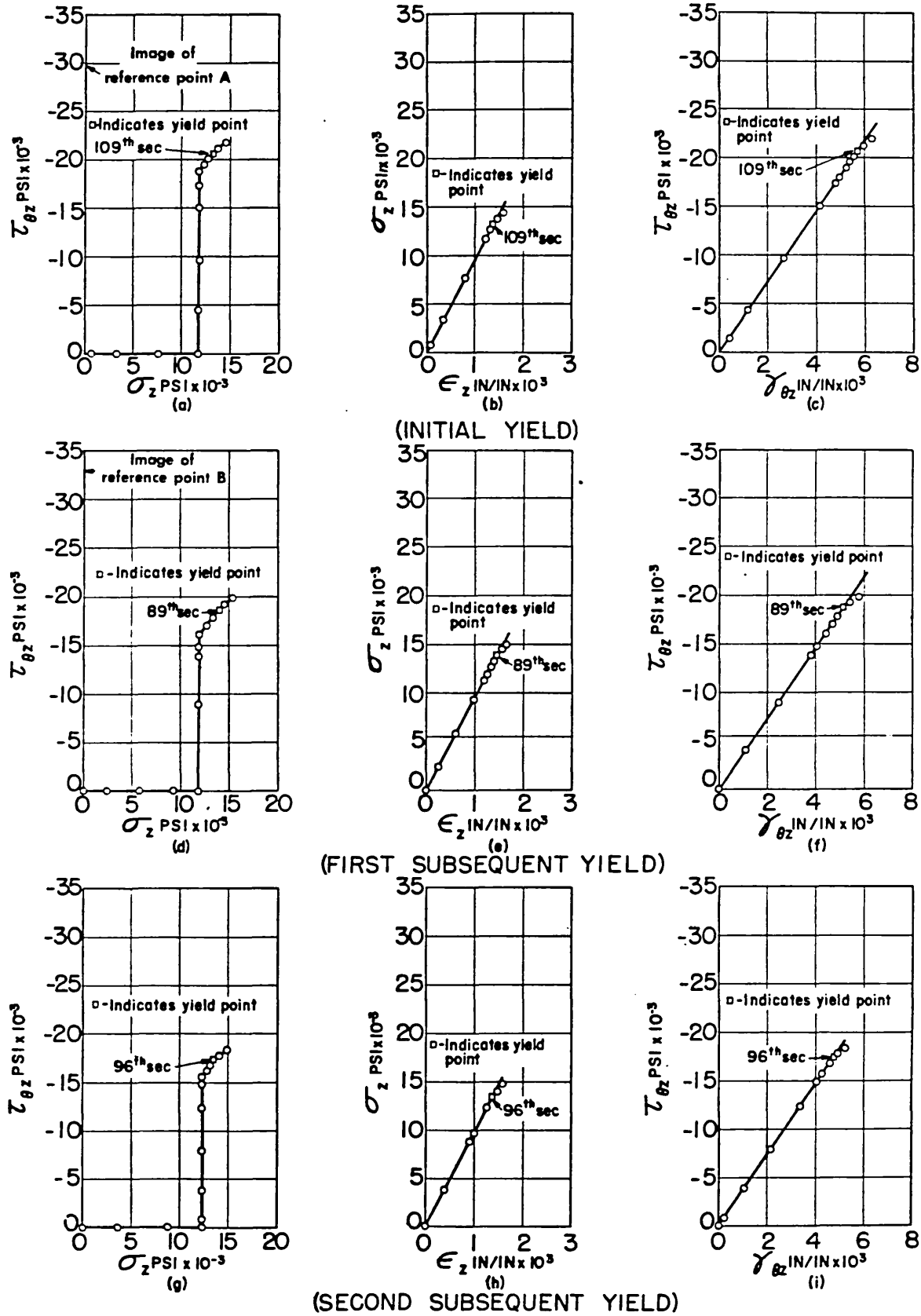


Fig 2. 9b Loading path and stress-strain curves for determination of initial and subsequent yield points of a typical specimen in the fourth quadrant (25)

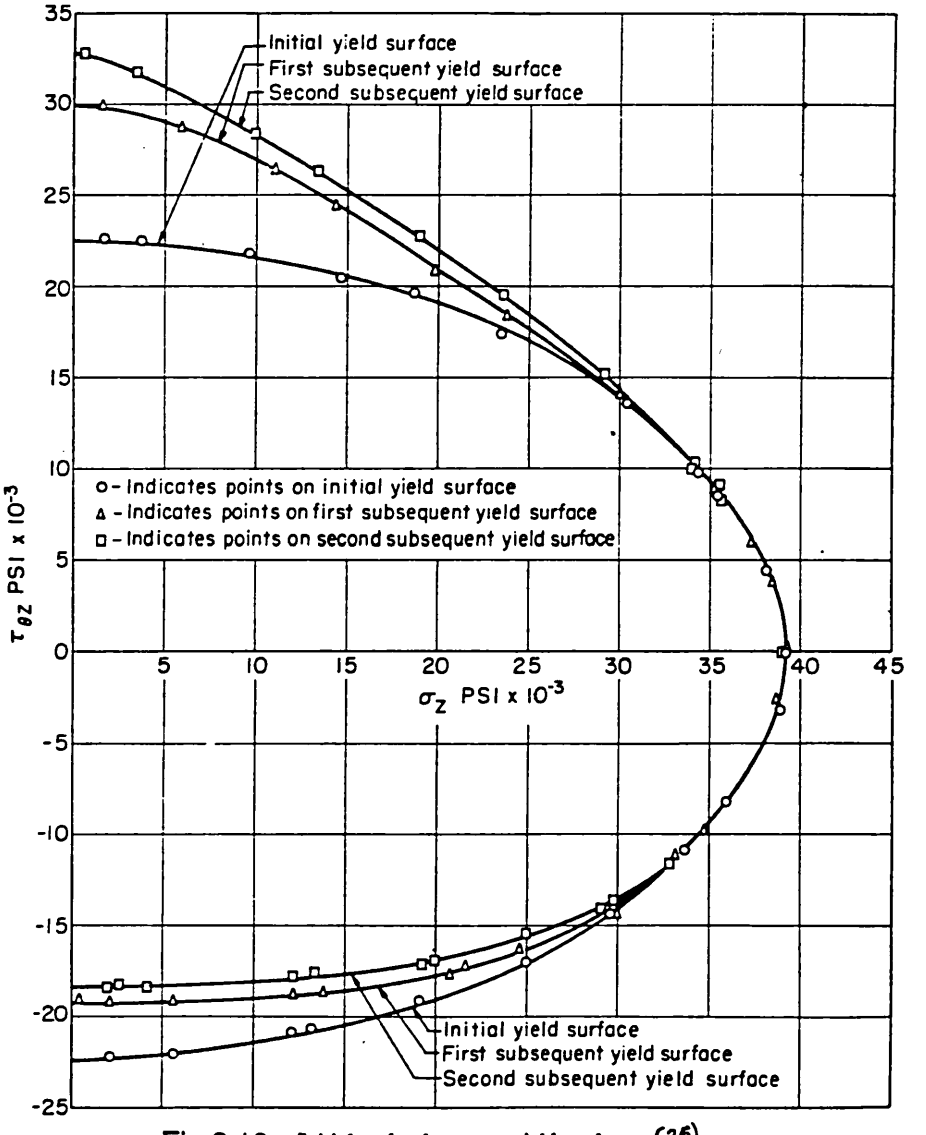


Fig 2.10 **Initial and subsequent yield surfaces** (25)

2.15.2 MORETON et al

Moreton et al (26), experimenting on pressure vessel steels loaded biaxially, concluded that the movement of the yield surface into the subsequent positions identifies closely with the kinematic-hardening rule. They also used a computer program to verify that the post-yield stress path was a linear projection of the elastic path. This finding lends credence to Prager's original assumption which suggests that the direction of translation of the virgin yield surface is coincident with the direction of the exterior normal to the stress point as chosen on the same yield locus. In the case of an initially prestressed specimen, these experiments also confirm that the direction of movement of the yield surface is in the direcion of the prestress vector. This observation therefore, shows that the dynamic behaviour of the yield surface is more sensitive on the condition of prestress or prestrain than the state of biaxial loading. These experiments also reveal that rotations are negligible during movement of the yield surface in a stress-subspace, therefore the effect of rotation may be safely ignored when developing a theoretical model for describing the yield surface. Figs (2.11a,b,c,d) summarize the finding of these authors. Figs 2.11b and c are of particular relevance to the type of experiments carried out by the author in order to derive cyclic stress-strain curves so as to enable comparison between the computed and experimentally derived curves.

2.15.3. SHELTON et al.

These workers (27,28) observed that prestressing a material causes its yield surface to differ in size from that of a virgin material. For example, if the

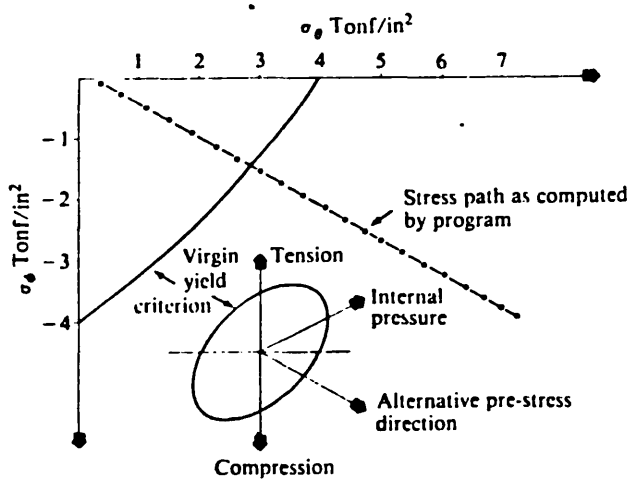
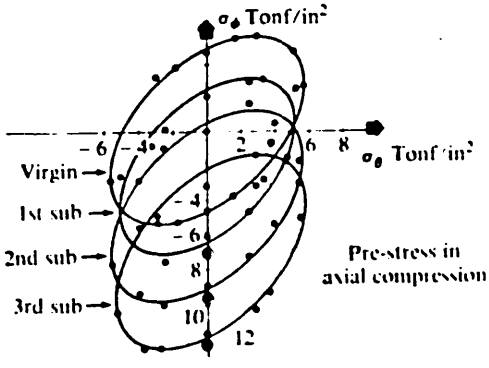


Fig 2.11a Stress ratio obtained for alternative pre-stress direction (26)



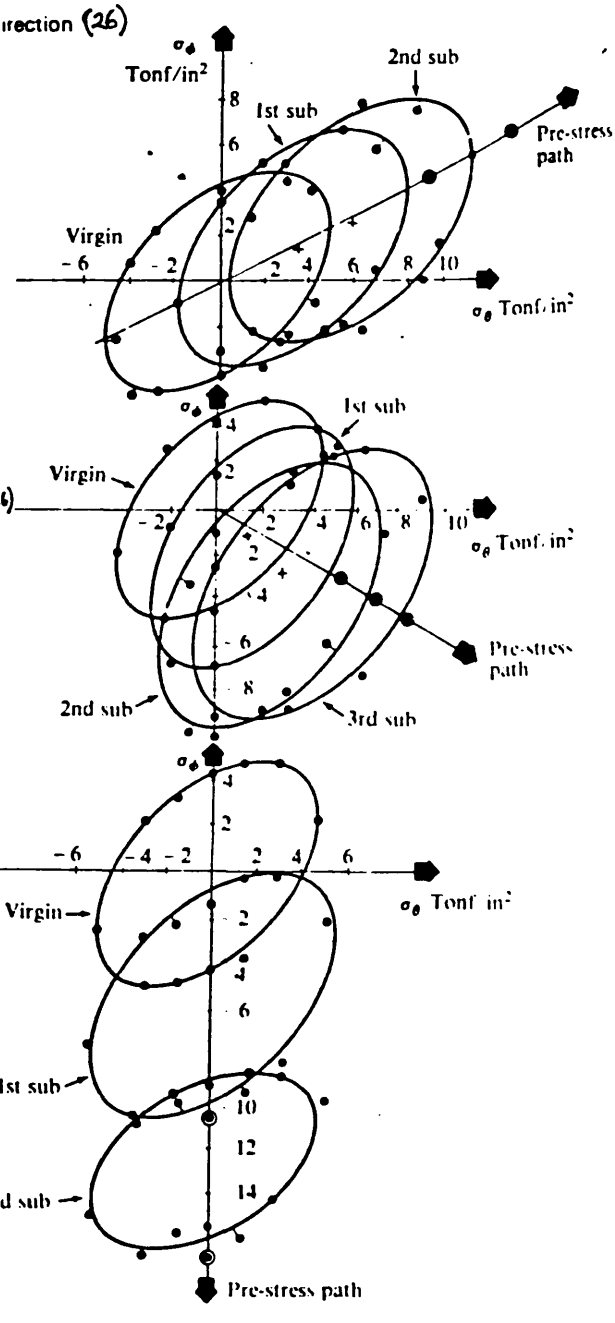


Fig 2.11b Yield surface behaviour of 2¼Cr. 1Mo (26)

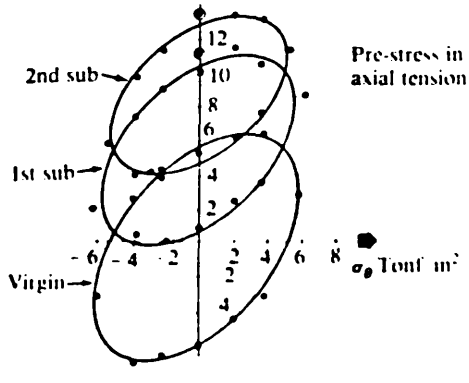


Fig 2.11c Yield surface behaviour of 2¼Cr. 1Mo (26)

Fig 2.11d Yield surface behaviour of stainless steel type 304 (26)

material hardens, the yield locus behaves in a manner attributable to combined-hardening in the stress space in the direction of the prestress vector. In a similar work, Rogan and Shelton (29), suggested that an effective yield stress should be defined when dealing with pre-stress or pre-strain situation and that its magnitude should be at the point of intersection of the projected elastic line and the tangent to the plastic stress-strain curve. Fig (2.12 a and b) illustrate this concept. They based their investigation on Hill's (30) equation which states that,

$$2f = A(\sigma_\theta - \sigma_z)^2 + B(\sigma_z - \sigma_r)^2 + C(\sigma_r - \sigma_\theta)^2 + 2D\tau_{\theta z}^2 + 2E\tau_{zr}^2 + 2F\tau_{r\theta}^2 = 1 \qquad (2.34)$$

where, A,B,C,D,E,F are parameters characteristic of the current state of anisotropy or subsequent flow loci. Note that the applicability of this equation is limited to situations where the reference axes are coincident with the principal axes of anisotropy, and,

Edelman and Drucker's (31),

$$f = 1/2\, C_{ijkl}(\sigma_{ij}' - m\,\varepsilon^p_{ij})(\sigma_{kl}' - m\,\varepsilon^p_{kl}) = \text{Const.} \qquad (2.35)$$

where σ_{ij}' are the deviatoric stresses, ε^p_{ij} are the pre-strain and m is a constant to allow for the Bauschinger effect.

Appreciable agreement was found between the experimental data and the prediction of these two equation and in particular their work on pre-strained

En 24 steel confirmed that equation (2.35) was capable of describing all their yield loci in mathematical terms. They also confirmed that the condition of anisotropy and the Bauschinger effect should be considered in terms of the prior plastic strain history or deformation path and not as being independent of the final geometical configuration of a specimen. This particular observation is very useful and bears particular relevance to the present work. Its manifestation will be seen in chapter three. Fig 2.13 shows how subsequent flow stresses hence flow loci at various pre-stress values are determined. The construction described here is seen to follow the Prager - Ziegler models, except that the yield surface increased in size. The test was carried out in a tensile - shear - stress space. The short line at the bottom of each vector is drawn normal to it and thus will be tangential to any flow locus. Three conditions will have to be met in order to map adequately the particular flow locus which describes the onset of plastic flow. These are :

a) The backward extrapolation from the curves relating εt to σ and γt to τ, which are independent of time , see fig 2.14

b) Backward extrapolation from the 'long time' curves relating σ to ε and τ to γ see fig 2.15 and

c) The resulting flow locus must be normal to the plastic - strain increment vectors for each particular σ/τ ratio at the $|\sigma|$ and $|\tau|$ of the flow stress. i.e it must accord strongly to the Prager- Ziegler model and pass though the stress space normally to all the plastic strain increment vectors which it encounters.

This text substantiates strongly the validity of the plastic flow theories already cited. Furthermore the methods of analysis, especially as regards the determination of plastic flow stress though the extrapolation methods presented, are extremely valuable and of help in this thesis.

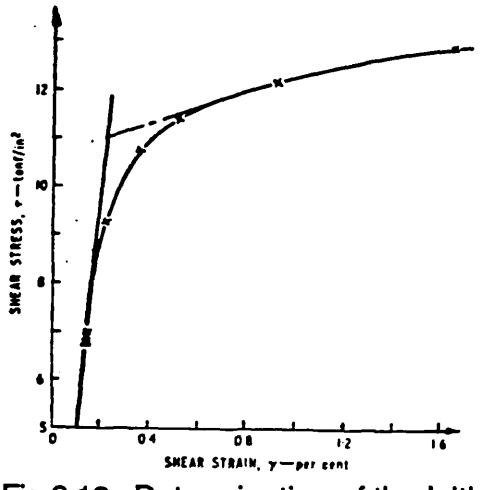


Fig 2.12a Determination of the Initial Flow Stress for Shear Strain (29)

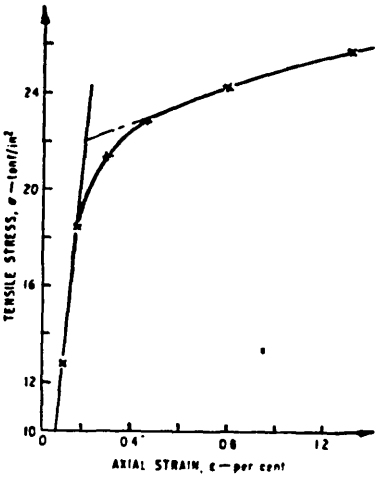


Fig 2.12b Determination of the Initial Flow Stress for Axial Strain (29)

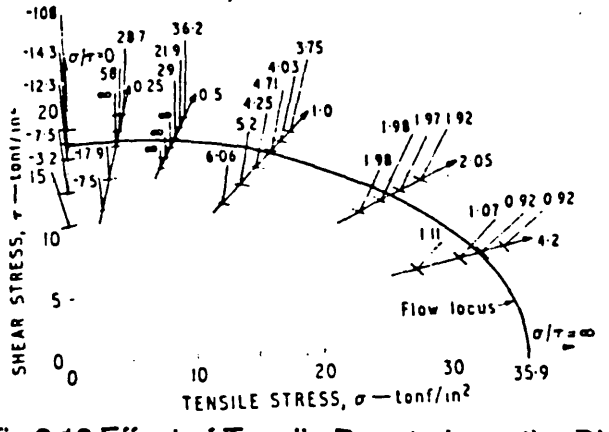


Fig 2.13 Effect of Tensile Pre-strain on the Direction of Plastic - Strain Increment Vectors (29)

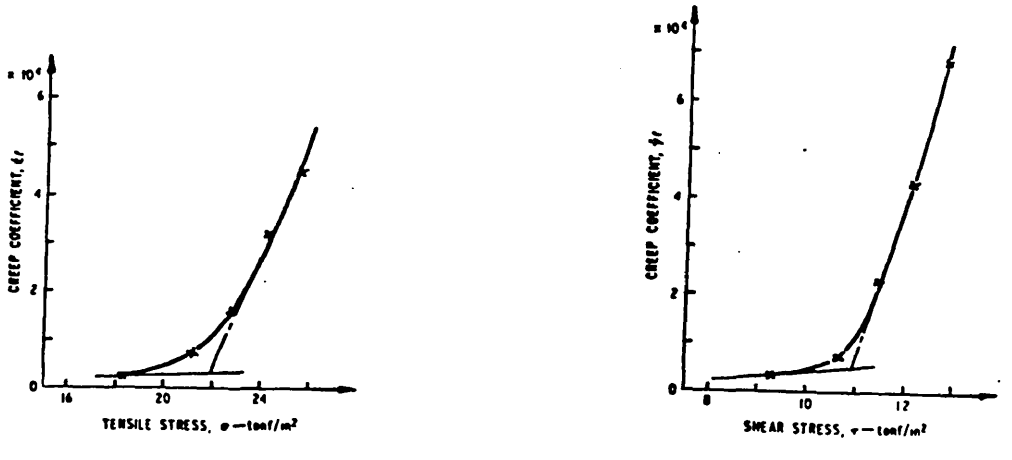


Fig 2.14 Backward Extrapolation for the Determination of Initial Flow Stress Using the Creep Curve (29)

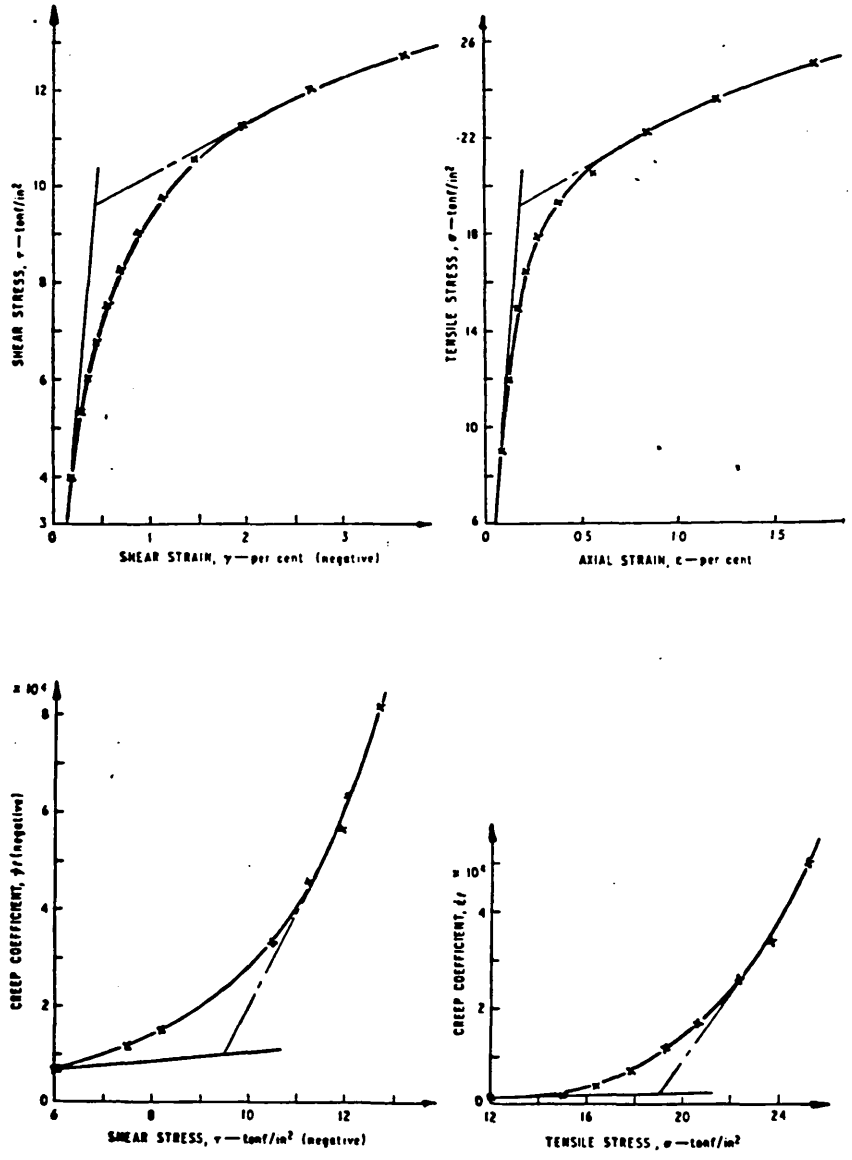


Fig 2.15 Further Illustrations of the Determination of the Initial Flow Stress (29)

2.15.4

Holloway and Shelton (32), worked successfully with the assumptions that for the yield stress in flow situations,it is adequate to use the point of intersection of the projected elastic line and the backward extrapolated tangent of the plastic curve - It is suggested that this definition when used in conjunction with the normality rule provides a useful means of studying subsequent yield loci. It is worth noting however, that most of the assumptions here and in so many works of the kind are based on the fact that most metals yield at points ahead of the elastic limit. It was observed that all of their experimental yield loci were smooth and continuous and the behaviour is essentially kinematic, they finally concluded that the theory of Edelman and Drucker(31) agreed very much with their experimental data.

2.15.5

Williams and Svenson (33), confirmed that the plastic stress-strain increment vector is perpendicular to the yield locus. They also noted that following a tensile prestrain,the subsequent yield loci did not undergo any rotation, within limits of experimental error. The same conclusion can be drawn about the subsequent yield surfaces after a torsional pre-strain (34). It was speculated in this text that there may be some rotation under a combined prestress but a later work (26) has shown that only negligible rotation occurred under combined-stress prestrain situation and that a model that discards rotation can be considered reasonably adequate. These authors (35) have used a statistical approach to develop a model based upon an aggre gate of work-hardening inclusions embedded in a matrix of elastic-plastic material. The suggested yield function can be written as follows;

$$f = (I_{ijkl} + A_o \varepsilon_{ij}^p \varepsilon_{kl}^p)\,(\sigma_{ij} + \alpha_{ij})\,(\sigma_{ij} + \alpha_{kl}) = K^2 \qquad (2.36)$$

where

$$I_{ijkl} = \delta_{ik}\,\delta_{jl} - 1/3\,\delta_{ij}\,\delta_{kl}$$

$$\alpha_{ij} = \varepsilon_{ij}^{p}\,(\,L_{pqrs}\,\sigma_{pq}\,\sigma_{rs} - m'\,)$$

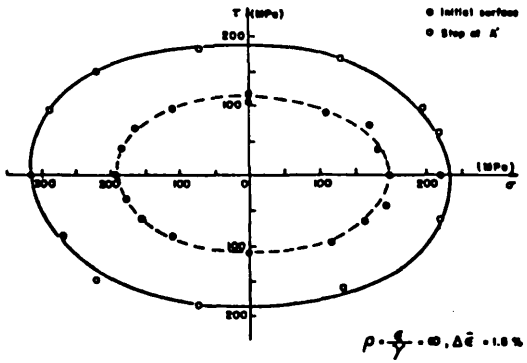
m' has been shown by Rees (9) to be the Bauschinger effect parameter.

2.15.6

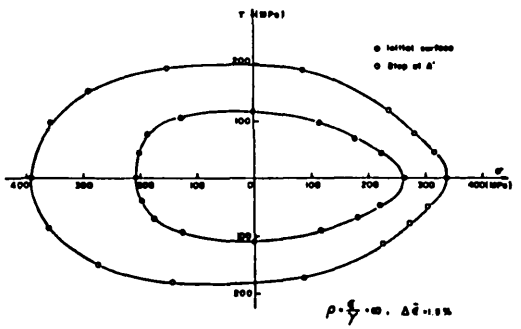
Hancell and Harvey (36), observed that the simple kinematic hardening model does not accurately predict the modes of deformation in problems of plastic collapse. It is adequate for the incorporation of the Bauschinger effect but the range of elastic unloading predicted by this theory is questionable since that observed in experiments is different. However, it is suggested that in the absence of sustained stress and with the yield surface allowed to expand or contract as it translates, the cyclic stress-strain hysteresis curves can be developed with reasonable accuracy. This work is suggestive of the relevance of a combined-hardening approach to representing material behaviour.

2.15.7

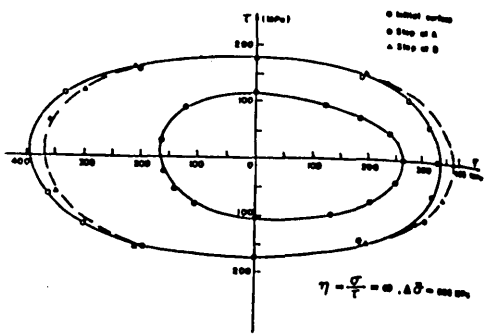
Ellyin and Neale (37), observed that a uniform expansion of the initial yield surface (or isotropic-hardening type of behaviour) occurs at steady-state under reversed axial strains see fig 2.16a, Fig. 2.16.b indicated an initially anisotropic specimen which retains its condition of anisotropy whilst also expanding after about 200 cycles of reversed axial straining. Further cycling of the same specimen reveals a subsequent yield surface which shows an eradication of this initial anisotropy as shown in fig. 2.16c.



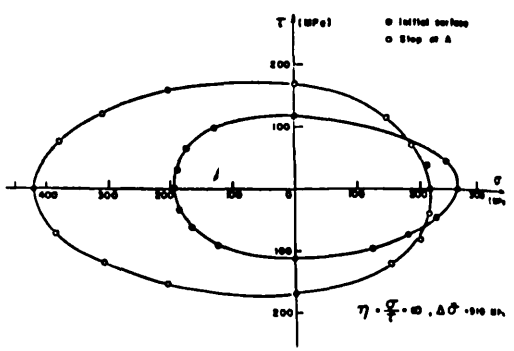
a



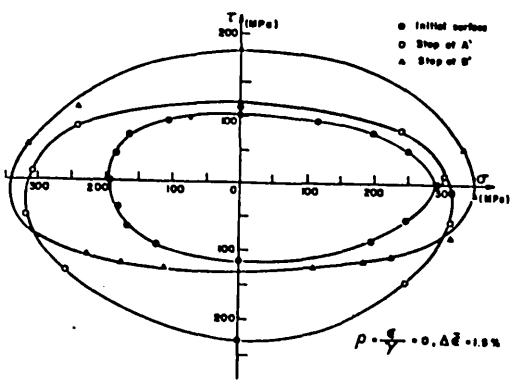
b



c



d



e

Fig 2.16 Yield Surface Behaviour Under Cyclic Loading (37)

This figure also shows that the yield surface expanded and translated along the loading direction or σ- axis. Fig. 2.16d shows that at steady-state the amount of translation increases with stress amplitude ($\Delta\sigma$) and that, despite an overall hardening, it was still possible for the subsequent yield point to be less than the initial yield point. It can thus be concluded from this work, that for aluminium alloys undergoing cyclic or repeated loading, the initial yield surface expands or work-hardens and translates, whilst initial anisotropy disappears once steady-state is reached. Finally, under load-controlled cycling, the behaviour of the initial yield surface is dependent on the cyclic stress amptitude range ($\Delta\sigma$) and independent of the stress ratio. This work makes an important revelation as regards the work done by the present author in that it shows that it is possible to investigate the behaviour of the yield surface under repeated loading by carrying out a uniaxial experiment. It also shows that the behavioural pattern under the stipulated condition is in agreement with the use of the combined-hardening theory fig. 2.16e thus lending credence to the theoretical background of the computational work done in this thesis.

2.15.8

Parker and Bassett (38), concluded that the initial loading behaviour of α-brass specimens can be explained in terms of a yield criterion $f=2\,\sigma_R^2$ (similar to the von Mises yield criterion) for a material which possesses one degree of anisotropy in the radial direction. They noticed that:

a) There is no existence of a nested set of yield surfaces

b) There is no evidence of corners on the subsequent yield surfaces.

c) There is a strong positive cross effect.

d) A Bauschinger effect acts over the whole quadrant of stress space representing reversed loading to the initial surface.

e) The subsequent yield surfaces show rotation with respect to the initial yield locus.

f) The isotropic model can be applied in the case of this particular material.

Observations b, d and e are important since they give some information on the behaviour of the subsequent yield surface.

2.16 SUMMARY OF ANISOTROPIC HARDENING FUNCTIONS AND INTERACTION WITH THE BAUSCHINGER EFFECT

The leading models of anisotropic hardening are presented here. They all expect the kinematic hardening model to serve as the basic theory which would then be modified to formulate a more realistic model. The first section compiles the models whilst the second section deals with the anaylsis of these models with respect to the Bauschinger effect.

2.16.1 Prager and Zieglers models (3), (1)

The initial loading surface is given by

$$f_0 (\sigma_{ij}) = 0 \qquad (2.37)$$

and the subsequent ones by

$$f (\sigma_{ij} , \alpha_{ij}) = fo (\sigma_{ij} - \alpha_{ij}) = 0 \qquad (2.38)$$

where α_{ij} is the translation tensor and is expressed in the flow rule as

$$d\alpha_{ij} = c\, d\varepsilon^{p}_{ij} \qquad (2.39)$$

and

C is a constant called the tangent modulus.

Applying the usual flow law (1), equation (2.39) can be rewritten as

$$d\alpha_{ij} = c\, d\varepsilon^{p}_{ij} = d\sigma\, n_{ij} \qquad (2.40)$$

where n_{ij} is a unit outward normal to the loading surface

Ziegler modified this model for consistency along the loading path and suggested that equation (2.39) is better written as

$$d\sigma_{ij} = d\mu\,(\sigma_{ij} - \alpha_{ij}) \qquad (2.41)$$

where $d\mu$ is a scalar multiplier.

2.16.2 Edelman and Drucker (31)

Ths suggested function is based on the interaction of prestrain and yield stress components. It is written in deviatoric stress state as follows:

$$f = 1/2\, C_{ijkl}\,(\sigma_{ij} - m\,\varepsilon^{p}_{ij})\,(\sigma'_{kl} - m\,\varepsilon^{p}_{kl}) = K^2 \qquad (2.42)$$

where

m and C_{ijKl} are emperical constants.

2.16.3 Williams and Svensson (33)

This is a statistical model of yielding based on aggregate of work hardened inclusions embedded in a matrix of elastic-plastic material. They proposed that when subjected to an arbitary plastic strain history, the behaviour of the subsequent yield surface obtained for an aggregate is governed by the inclusion which suffered the least amount of local plastic strain.
The yield function then is as follows:

$$f = (I_{ijkl} + A_o \varepsilon^p_{ij} \varepsilon^p_{kl}) (\sigma_{ij} + \alpha_{ij}) (\sigma_{kl} + \alpha_{kl}) = K^2 \qquad (2.43)$$

where,

$$I_{ijkl} = \delta_{ik} \delta_{jl} - 1/3 \, \delta_{ij} \delta_{kl}$$

and

$$\alpha_{ij} = \varepsilon^p_{ij} (L_{pqrs} \sigma_{pq} \sigma_{rs} - m')$$

2.16.4 Yoshimura (40)

This is written in full dimensional form as

$$f = 1/2 \, C_{ijkl} \sigma'_{ij} \sigma'_{kl} - B \varepsilon^p_{ij} \sigma'_{ij} = K^2 \qquad (2.44)$$

where B is a positive scalar in an invariant term which represents the Bauschinger effect through a translation of the surface and a change in its size.

The tensor C_{ijkl} is expreseed as follows:

$$C_{ijkl} = \delta_{ijkl} + AL_{ijkl} + A^2M_{ijkl}$$

$$C_{ijkl} = \delta_{ijkl} + A_1M_{ijkl}$$

where,

$$\delta_{ijkl} = 1/2 \, (\delta_{ik} \, \delta_{jl} + \delta_{il} \, \delta_{jk})$$

$$L_{ijkl} = 1/2 \, (\delta_{ik} \, \varepsilon^p_{jl} + \delta_{jl} \, \varepsilon^p_{ik} + \delta_{il} \, \varepsilon^p_{jk} + \delta_{jk} \, \varepsilon^p_{il})$$

$$M_{ijkl} = 1/2 \, (\varepsilon^p_{ik} \, \varepsilon^p_{jl} + \varepsilon^p_{il} \, \varepsilon^p_{jk})$$

2.16.5 Baltov and Sawczuk model (41)

An anisotropic hardening rule was developed through the use of the kinematic hardening rule. The final solution allows the initial yield surface to translate, expand and rotate is stress space. In full non-dimensional deviatoric stress space the surface is expressed as follows:

$$(I_{ijkl} + A\alpha_{ij} \alpha_{kl}) (\sigma'_{ij} - \alpha'_{ij}) (\sigma'_{kl} - \alpha_{kl}) = 2f = 1 \qquad (2.45)$$

where I_{ijkl} is the isotropic tensor and is written as

$$I_{ijkl} = 0.5 \, (\delta_{ik} \, \delta_{jl} + \delta_{il} \, \delta_{jk} - 2/3 \, \delta_{ij} \, \delta_{kl}) \qquad (2.46)$$

and A is the hardening constant.

σ and α differ from their physical equivalents by a factor, $(1/\sqrt{2})\,k$.

Consider a rigid plastic thin walled tube subjected to axial extension in a σ-τ stress space, and whose state of deformation can be expressed as,

$$\varepsilon_{11} \neq 0, \quad \varepsilon_{12} \neq 0, \quad \varepsilon_{22} = \varepsilon_{33} = -1/2\,\varepsilon_{11}, \quad \varepsilon_{23} = \varepsilon_{31} = 0 \qquad (2.47)$$

if $\alpha_{11} = \alpha_1$ and $\alpha_{12} = \alpha_2$, the proposed yield surface equation (2.46) reduces to,

$$\{(2/3 + A\alpha_1^2)(\sigma - 3/2\,\alpha_1)^2 + 4\alpha_1\alpha_2(\sigma - 3/2\,\alpha_1)(\tau - \alpha_2) + 4(1/2 + A\alpha_2^2)(\tau - \alpha_2)^2\} - 1 = 0 \qquad (2.48)$$

for axial extension alone, $\alpha_1 \neq 0$, $\alpha_2 = 0$, so that,

$$\{(2/3 + A\alpha_1^2)(\sigma - 3/2\,\alpha_1^2)\} + 2\tau = 1 \qquad (2.49)$$

gives the pattern of behaviour of the yield surface. Note that this model carefully excludes rotation of the yield surface and as cited earlier (26) the effect of rotation may actually be negligible in some materials.

2.17 QUANTITATIVE ANALYSIS OF THE BAUSCHINGER EFFECT.

As highlighted in the previous section, both experimental and theoretical studies have been carried out in order to understand the behaviourof the initial yield surface. However, most of the models arrived at do not specifically quantify the Bauschinger effect despite the fact that many of them incorporate this effect. Rees(9), therefore re-analysed these models in terms of the Bauschinger effect. He argued that the size of a modified yield surface and the translation coordinates of its centre (0,b) are dependent on the chosen definition. Furthermore, the yield point is assumed to be the only

point on a stress- strain curve with an exact definition and all other points are considered as mere gross indications of yielding with direct usefulness in design whenever small or large amounts of permanent set is involved

2.17.1 PRAGER AND ZIEGLER

For a translation of the yield surface happening in a σ - τ stress subspace, the shear stress translation parameter, β, was found to be,

$$\beta = (\tau_f + \tau_r) / 2 = C \gamma_f^p \qquad (2.50)$$

where C is a material constant. τ_f and τ_r are the forward and reversed yield shear stresses (in all cases in the section) and γ_f^p, is the plastic component of the shear strain. This translation parameter, β, regarded here as the measure of the exhibited Bauschinger effect in a metal.

2.17.2 Baltov and Sawczuk

For this model the associated Bauschinger effect is estimated as,

$$\beta = \tau_r /k = \tau_f/k(\sqrt{\{ (\tau_f/k - 1)^2 + A(\tau_f/k - 1)^4\} - 1})/(\sqrt{\{(\tau_f/k - 1)^2 + A(\tau_f/k - 1)^4\} + 1)) \qquad (2.51)$$

where k is the yield stress in torsion and A is the hardening constant.
When H=0, kinematic hardening results.

2.17.3 Edelman and Drucker

Here a constant m is used to quantify the Bauschinger effect in the reduced relationship,

$$\tau_r = - (\tau_f - m\gamma_f^p) \qquad (2.52)$$

which is arrived at after using a translation

$$\beta = m \gamma_f^p / 2 \qquad (2.53)$$

on the initial yield locus.

2.17.4 Yoshimura

The Bauschinger effect for this model was found to be controlled by two scalar quantities expressed in the following relationship:

$$\tau_r = - \{ \tau_f - B \gamma_f^p / (1 + (A \gamma_f^p)2 /4) \} \qquad (2.54)$$

A and B are then the two scalar parameters that control the Bauschinger effect.

2.17.5. Williams and Svensson.

Finally, the Bauschinger effect for this model is of the form seen in

$$\tau_r = - (\tau_f - m' \gamma_f^p) \qquad (2.55)$$

m' being the controlling parameter for the Baushinger effect. This relationship is actually similar to that given in equation (2.52). However, m in (2.52) is a constant whilst m' is not.

Of these quantitative representation of the Bauschinger effect the Edelman and Drucker, and the Williams and Svensson (where the Bauschinger effect is not constant) are found to agree more with experimental results obtained by this investigator. This finding will be investigated further in this thesis in order to be able to choose the more relevant solution out of the two. Rees also suggested that for torsional loading, Bauschinger effect parameter is a scalar coefficient of plastic pre-strain. This finding offers a useful background to the recent work and there will be concerted effort to establish the actual variation of the Bauschinger effect parameter in a tensile-compression loading path and under plastic straining.

2.18. Summary for chapter two.

1). The mathematical theory of plasticity can be modified and used to study the behaviour of materials under reversed or repeated loading condition.
2). The Von Mises yield surface is relevant and easier to work with on the computer.
3). The combined hardening theory is better at representing material behaviour under repeated loading.

4). The particular adaptation of Drucker's flow rule by Prager i.e,

$d\alpha_{ij} = c\, d\varepsilon^{p}_{ij}$ is applicable.

5). The Bauschinger effect parameter may be material and state dependent. This will be investigated for confirmation in the next chapter.

6). The yield surface can expand, translate, rotate in some instances and /or deform during plastic loading.

CHAPTER THREE

COMPUTER DERIVATION OF CYCLIC STRESS-STRAIN CURVE

Introduction

To derive cyclic stress-strain curves on the computer, a suitable elastic-plastic model must be developed. Most of the requirements for developing a model of this type have been studied in chapter two. It was also pointed out that none of these models previously discussed can adequately describe material behaviour on its own. As mentioned earlier Hunsaker et al (23) have studied most of the available hardening models numerically and came out with the suggestion that only a combination of two or more of the individual models can offer good grounds for studying cyclic material behaviour. Some of the available combined-hardening theories are studied in subsequent sections.

3.1. THE COMBINED-HARDENING RULES

3.1.1 Hodge (42) first argued that available rules e.g. the isotropic-hardening and kinematic-hardening, would have to be modified in order to get more representative behavioural models. It was then postulated that a yield surface will translate and expand during plastic deformation. He also argued that if the amount of expansion and hardening are both functions of the same scalar, e.g. the total plastic strain or total work (as mentioned earlier), then a uniaxial test of cyclic loading between fixed strain values would be sufficient to determine the required hardening rule

parameters.

The hardening parameters suggested by this author are of the traditional forms like the tangent or plastic moduli and the hardening index(n).

3.1.2 Krieg (43) introduced the concept of two surfaces in which a smaller one (the virgin yield surface), translates and expand inside a bigger one called the "limit surface" which is also allowed to translate and expand independently of the former. Here the hardening modulus is assumed to be a function of the distance between the surface at the loading point. The specialized form of this general theory recommends two experimental tests to be carried out in order to determine all appropriate hardening parameters. These two tests are: a). uniaxial tensile one at moderate strains, and b). uniaxial loading, unloading or reversed loading test.

The other combined hardening rules of relevance were cited in section 2.11 and 2.12 of chapter two. These are the Mroz(19,20) and mechanical sublayer(21,22) models.
Like in the previous text by Hodge, if it is assumed that the amount of expansion of each of the surfaces of constant workhardening moduli and the rate of strain-hardening are both functions of some scalar parameter such as the equivalent uniaxial plastic strain or total plastic work, then a uniaxial test of cyclic loading between fixed strain values would be sufficient to determine the required hardening rule parameters.
The other pertinent work on the combined-hardening model was that of Ellyin et al(37).
In accordance with evidence from these texts, the next few sections will be devoted to the development and implementation of an improved

combined-hardening theory.

3.1.3 LOGIC OF THE IMPROVED COMBINED-HARDENING MODEL.

Basically, the combined hardening theory is a simple combination of the isotropic-hardening and kinematic-hardening rules. The improved model presented in this thesis goes a step further. The first half of the theory deals with the combination of the two hardening theories mentioned whilst the improvement comes in the form of the inclusion of the anisotropic hardening phenomenon. Anisotropic hardening as mentioned in chapter two expresses the possibility of different hardening rates along the tensile and compressive paths of the forward and reversed plastic stress-strain curve. This behaviour is observable in many structural materials.

Consequently, the combined-hardening theory will now be defined as the combination of the isotropic-hardening, kinematic-hardening and anisotropic hardening theories. This conceptual approach to combined-hardening was used in the theory presented in appendix A. Fig. 3.1. gives a physical representation of the isotropic-hardening, kinematic-hardening and combined-hardening rules as consequences of reversed-loading. Repeated reversed loading is what is carried out when a material is cycled, since this is true combined-hardening rule will then not only be an adequate representation of material behaviour for a single cycle loading sequence but will also represent material behaviour of the "new materials" as steady state is approached. The relationship between points on a load-unloading stress-strain curve and the yield locus will be presented in the next section.

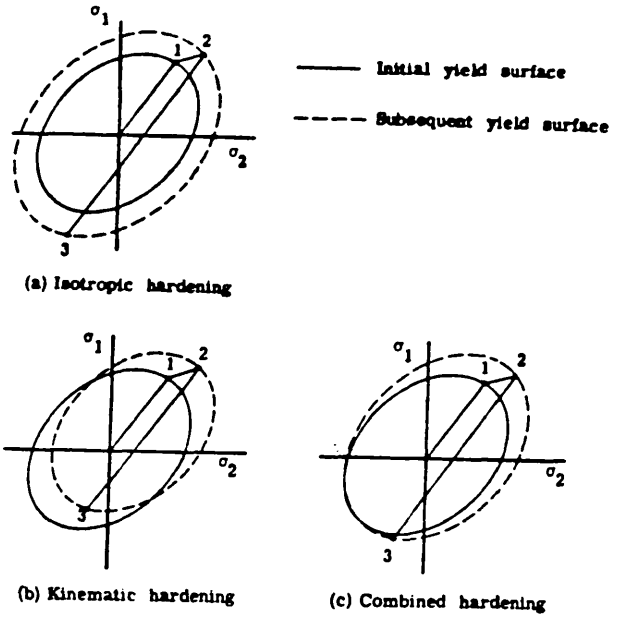


Fig.3.1. Strain-hardening Theories Under Cyclic Loading

3.2. COMPUTATION OF ELASTIC-PLASTIC THEORY (A LITERATURE SURVEY)

Some earlier computational work was done by Newman (44). He adapted Hodge's (42) combined-hardening theory - which originally used the Tresca's yield surface- to the Von Mises yield surface. The choice of a smooth Mises surface made it possible to avoid problems of singularities posed by the corners on the Tresca's yield surface. He interpolated linearly between the formula by Zienkiewicz et al (45) which express the shift in the yield

surfaces as,

$$d\bar{\sigma} = \{\partial\phi/\partial\sigma\}^T \{d\sigma\} \qquad (3.1)$$

for a purely isotropic situation when ($d\alpha=0$), and that of Isakson et al (4) who suggested that for a purely kinematic-hardening situation or $d\sigma = 0$, the shift in the yield surface is expressed as,

$$\{d\alpha\} = \{\partial\phi/\partial\sigma\} (\{\partial\phi/\partial\sigma\}^T \{d\sigma\} / \{\partial\phi/\partial\sigma\}^T \{\partial\phi/\partial\sigma\}) \qquad (3.2)$$

He then came up with the relationship,

$$d\sigma = (1-\beta) \{\partial\phi/\partial\sigma\}^T \{d\sigma\} \qquad (3.3)$$

or

$$\{d\alpha\} = \beta \{\partial\phi/\partial\sigma\} [\{\partial\phi/\partial\sigma\}^T \{d\sigma\} / \{\partial\phi/\partial\sigma\}^T \{\partial\phi/\partial\sigma\} \qquad (3.4)$$

where $\{\ \}^T$ is transpose of a matrix

$d\phi$ is the change in the current stress state

$d\sigma$ is the change in the original stress state

$d\alpha$ is the translation of the centre of the yield

β is the kinematic-hardening coefficient.

It was then deduced that when $\beta=0$, the behaviour of the yield surface is purely isotropic and the shift in the yield surface is entirely in σ with $\{d\alpha\}=0$. $\beta=1$, is deemed representative of purely kinematic behaviour, and the

shift in the yield surface is entirely in $\{\alpha\}$ with $d\sigma=0$. Furthermore, he reckoned that if $0 < \beta < 1$, the yield surface both expands and translates normal to the yield surface for small incremental changes in the stress state.

This form of combined-hardening theory obtained through the stated linear interpolation was used for computational studies of fatigue crack growth. However, the author did not derive any cyclic stress-strain curves, hence it is unknown if this method of direct interpolation is adequate for constructing the said curve. This omission will now be addressed. Furthermore, this work poses some important questions which are summarized below:

1) Is this parameter β a material property? if it is what material property will give the value of β?

2) What method can be employed in order to study this material property, hence the derivation ofβ?

3) What is its relationship to external parameters like for example, the plastic strain when a material is being deformed?

4) Can an emperical formula be developed to represent its variation?

5) Does this parameter only vary between 0 and 1? What exactly does a particular value of it mean in terms of material response to cyclic loading?

These questions will now be answered in subsequent sections.

3.3 THE GENERALISED ELASTO-PLASTICITY MODEL (APPENDIX A)

3.3.1. TECHNICAL FEATURES.

This model is an improved combined hardening theory comprising the isotropic-hardening, kinematic-hardening and anisotropic hardening theories Because of its components, it is able to allow for uniform expansion, translation and possible disparity in the tensile and compressive hardening behaviour of a material.

The Bauschinger effect is monitored through the kinematic-hardening rule and the incremental theory of plasticity is used in theory. Furthermore, the von Mises yield surface is assumed for initial and subsequent loading.

3.3.2 THE ISOTROPIC COMPONENT:

The yield surface is represented by,

$$F(\sigma_{ij}, k) = 0 \qquad (3.5)$$

or

$$f(\sigma_{ij}) - Y(k) = 0 \qquad (3.6)$$

where,

$f(\sigma_{ij})$ is the yield function which can be written as,

$$\sqrt{3/2\ \sigma'_{ij}\ \sigma'_{ij}} - \bar{\sigma} = 0 \qquad (3.7)$$

where,

$$\sigma'_{ij} = \sigma_{ij} - 1/3\ \delta_{ij}\ \sigma_{ij} \qquad (3.8)$$

$\tilde{\sigma}$ is the equivalent stress,

δ_{ij} is the kronecker delta and defined according to the Einstein tensor summation as in chapter two.

σ'_{ij} are the deviatoric stress components.

k is the hardening parameter and Y(k) is the hardening criterion.

3.3.3 THE KINEMATIC HARDENING COMPONENT

Under this condition the yield surface is represented as,

$$f(X_{ij}) - Y(k) = 0 \qquad (3.9)$$

where,

$X_{ij} = \sigma_{ij} - \alpha_{ij}$. (this is considered an anisotropic yield function)

In the x-y plane, the yield surface can be written as,

$$f(X_{ij}) = [(\sigma_x-\alpha_x)^2 + (\sigma_y-\alpha_y)^2 + (\sigma_x-\alpha_x)(\sigma_y-\alpha_y) + 3(\tau_{xy}-\alpha_{xy})^2]^{1/2} - \tilde{\sigma} \qquad (3.10)$$

where α_{ij} is a translation parameter for the movement of the centre of the yield surface.

σ is the current yield stress.

In the simple tensile case equation (3.10) reduces to,

$$\sqrt{3/2\ (\sigma'_{ij} - \alpha_{ij})\ (\sigma'_{ij} - \alpha_{ij})} \ - \ Y(k) \ = \ 0 \qquad (3.11)$$

on the deviatoric plane.

3.4 THE FLOW RULES

3.4.1. ISOTROPIC FLOW RULE

The assumed flow rule in this case is similar to the Prandtl-Reuss equations and is written as,

$$d\varepsilon^{p}_{ij} \ = \ d\lambda\, \sigma'_{ij} \qquad (3.12)$$

This leads to a stress-strain relationship written as follows:

$$d\varepsilon_{ij} \ = \ D^{-1}\, d\sigma_{ij} + d\lambda\, \sigma'_{ij} \qquad (3.13)$$

so that

$$d\lambda = \sigma'_{ij}\, D\, d\varepsilon_{ij} / A \ + \ \sigma'_{ij}\, D\, \sigma'_{ij} \qquad (3.14)$$

and,

$$A=H'= d\sigma / d\varepsilon_p \qquad (3.15)$$

where,

D is the elasticity modulus

and H' is the slope of the uniaxial plastic stress-strain curve. (indication of the assumption a constant hardening index).

3.4.2 KINEMATIC FLOW RULE

The rule applied here is a reduced or special form of the Drucker's incremental plasticity flow laws. The relationship is,

$$d\varepsilon^p_{ij} = d\lambda \partial f/\partial X_{ij} = d\lambda S_{ij} \qquad (3.16)$$

Using this rule (3.16), (3.13) can be modified to be more representative of material behaviour by re-writing it as,

$$d\varepsilon_{ij} = D^{-1}\, d\sigma_{ij} + d\lambda S_{ij} \qquad (3.17)$$

The deviatoric stress components σ'_{ij} are measured on the initial yield locus or on the surface of an isotropically expanded subsequent yield surface whilst the components S_{ij} are referred to the translated subsequent yield surface.

3.5. MOVEMENT OF THE YIELD SURFACE

Under the kinematic-hardening assumption, the translation of the yield surface α_{ij}, is expressed in differential form as,

$$d\alpha_{ij} = cd\varepsilon^{p}_{ij} \qquad (3.18)$$

In using equation(3.18), Prager's(3) model has been assumed. C is a material constant which is taken as the tangent or plastic modulus of rigidity in most texts.

Equation (3.18) is written in the present text as,

$$d\alpha_{ij} = \beta d\varepsilon^{p}_{ij} \qquad (3.19)$$

where β is named kinematic translation parameter. It is linked with the exhibited Bauschinger effect in a material. It is assumed to be characteristic of a material undergoing plastic loading and it is a positive scalar function of external parameters like stress and strain. In this wise the relationship can be written as $\beta = \beta(\sigma,\varepsilon)$.
If equation (3.19) is re-arranged as,

$$\beta = d\alpha_{ij} / d\varepsilon^{p}_{ij} \qquad (3.20)$$

then for an amount of translation $d\alpha$, or shift in the position of the original yield surface, β is seen to be an elliptical variable with the incremental plastic strain. On a physical perspective, if the stress-strain curve is made up of equal segments along the plastic part (fig. 3.2) and each subsequent point from 0 to D identifies with a point on a current yield surface, the amount of translation is equal from one point to the other (equal lengths of segments, each segment representing a translation), then the plastic strain will change as well as the current value of the kinematic translation parameter β(re β_1, β_2 etc).

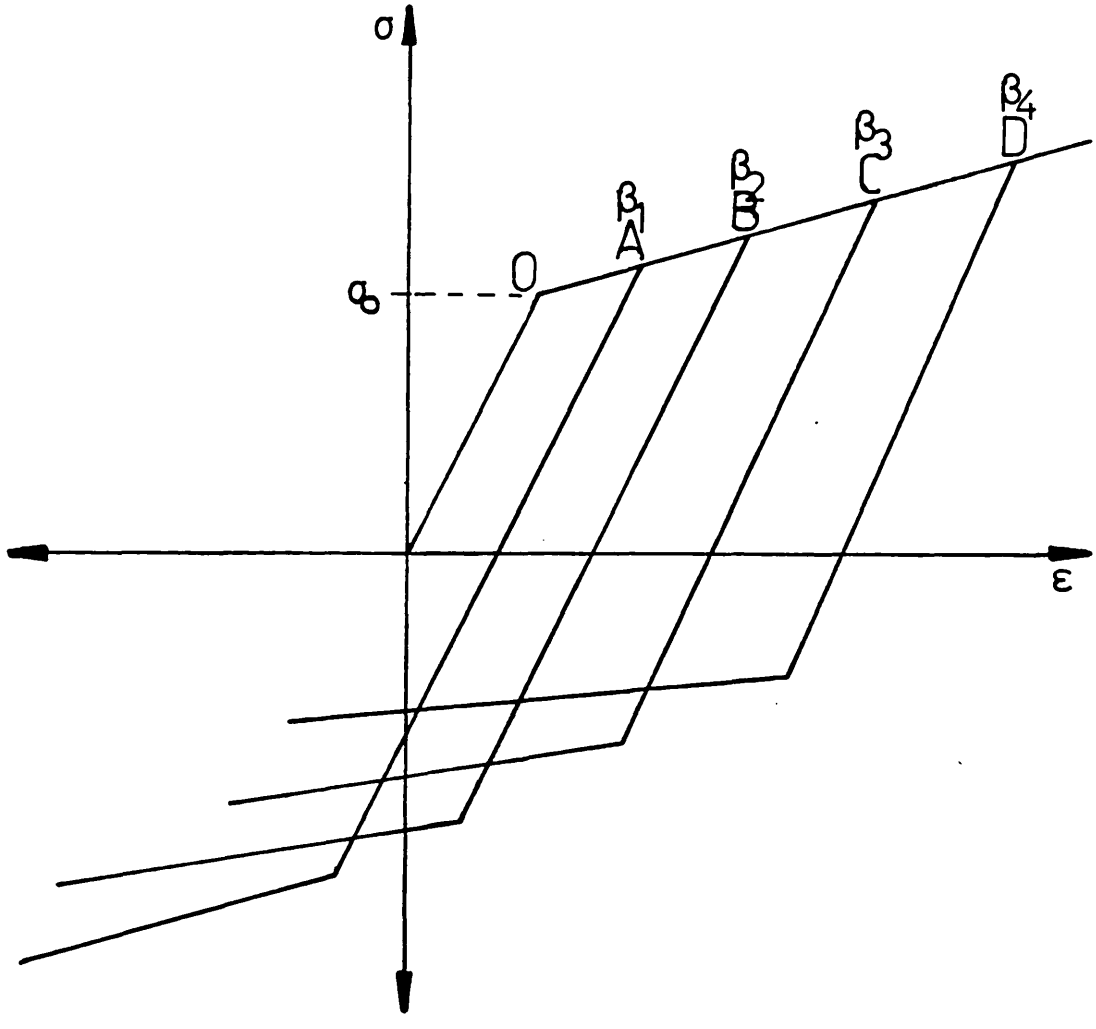


Fig.3.2 A Physical Concept on the Kinematic Translation

When the transition of the yield surface is defined as in equation (3.19), the elastic-plastic relationship can be modified as follows;

(the plastic scalar multiplier $d\lambda$ becomes),

$$d\lambda = S_{ij} D d\varepsilon_{ij} / A_* + S_{kl}\beta S_{kl} + S_{kl} D S_{kl} \qquad (3.21)$$

and

$$d\sigma_{ij} = [D - (DS_{kl}S_{kl}D / A_* + S_{mn}\beta S_{mn} + S_{mn}DS_{mn})] d\varepsilon_{ij} \qquad (3.22)$$

where

$$A_* = df(X_{ij}) / d\varepsilon_p = H' \qquad (3.23)$$

and is termed the anisotropic hardening parameter. The function A is discussed later.

Equations (3.21), (3.22) and (3.23) are the important aspects of the computational work reported in this section of the thesis.

3.6 DETERMINATION 0F PARAMETERS FOR COMPUTATION

3.6.1 THE HARDENING FUNCTION. H'

There are two noteworthy aspects of hardening in most real material. One is that most materials exhibit anisotropic hardening or unequal hardening under tensile and compressive loading. Secondly, the hardening index as measured along the plastic stress-strain curve is not constant but a function of the stresses and strains measurable along this curve. Assuming the Ramberg-Osgood relationship,

$$\sigma / \sigma_0 = \alpha_c (\varepsilon/\varepsilon_0)^n \qquad (3.24)$$

where σ_0 and ε_0 are the uniaxial tensile yield stress and strain respectively and σ and ε are current states of stress and strain. n is the constant hardening index.

If, (46) $$H' = EE_T / E-E_T \qquad (3.25)$$

where,

E is the Young's modulus.

$E_T = d\sigma / d\varepsilon$ is the tangent modulus.

then, differentiating equation (3.24) and using equation (3.25) will give,

$$H' = (E(\varepsilon/\varepsilon_0)^n)/((E/\alpha_c(\varepsilon/\sigma_0)) - n(\varepsilon/\varepsilon_0)^n) \qquad (3.26)$$

The function H' (equation 3.26) is implemented in a subroutine of the finite-element program and this subroutine returns an instantaneous value of H' to replace A_X in the incremental plastic stress-strain routine.

α_c is constant and also accounts for material response in the plastic state.

3.6.2 EXPERIMENTS

3.6.2.1 MONOTONIC EXPERIMENTS

Under this programme, a single cycle load-displacement loop was obtained. The monotonic stress-strain curve can be constructed from the part of the

loop in the first quadrant. Furthermore, the parameters β, n, α_c were also determined from the same curves. These values are then used in computational analysis.

3.6.2.2 CYCLIC INVESTIGATION.

Two types of laboratory cyclic experiments were carried out in order to be able to compare data and establish the viability of the developed computer program.

The first one consists of prestraining the specimen to an "initial" value of strain. It is then unloaded and cycled at a strain amplitude equal to the value of that "initial" prestrain. The loops in appendices D and E illustrate this exercise.

The second type allows for prestraining a specimen and then cycling the same specimen at a value of strain amplitude less than the initial prestrain value. Appendix F2 contains the loops obtained via this method. This experiment was particularly done in order to calculate the values of β and then compare them with those calculated using the initial strain data as in the above paragraph.

The final type of cyclic investigation involved the use of the finite-element program to obtain settled cyclic hysteresis loops from which the settled cyclic stress-strain curves were constructed. Appendix F presents the computed settled cyclic hysteresis loops for aluminium alloy H18.

3.6.3 DETERMINATION OF α_c AND n

For a set of monotonic stress-strain data,

α_c and n can be determined by taking the logarithms of equation (3.24) i.e,

$$\log (\sigma/\sigma_0) = \log (\alpha_c) + n\log (\varepsilon/\varepsilon_0) \qquad (3.27)$$

so that in a plot of $\log(\sigma/\sigma_o)$ against $\log (\varepsilon/\varepsilon_0)$, α_c is determined by taking the intercept and n is the slope of the curve.

3.6.4 METHODS FOR DETERMINING THE KINEMATIC TRANSLATION PARAMETER, β.

There are three established methods for determining the kinematic translation or Bauschinger effect related parameter, β. These are:

a) The stress criterion.
b) The energy criterion.
c) The strain-hardening criterion.

3.6.4.1 The stress criterion.

Consider a specimen that was initially prestrained to a point F as shown in fig(3.3) and then cycled for only one loop (the monotonic load-unloading displacement curve) at a strain amplitude less than or equal to the value of

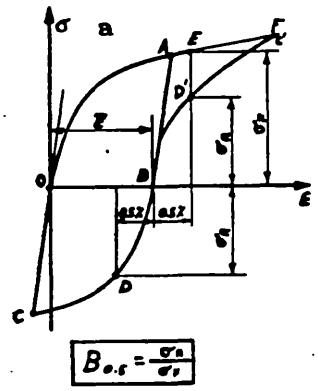


Fig.3.3 Schematic representation of the stress criterion.

initial prestrain. The values of the forward flow stress, σ_f, and the reversed yield stress, σ_R, are obtained as shown on diagram. In this respect, β is expressed as a function of the σ_f and σ_R. The applicable relationship is derived in the text presented (see appendix A).

3.6.4.2 The energy criterion.

Fig(3.4) presents a graphical construction for the use of the energy criterion. This criterion is based on the evaluation of the energy per unit volume savec in performing an amount of deformation in reversed loading, as compared to energy E_p required to reach the maximum stress in forward deformation. The value of β is expressed as a ratio E_s' / E_p.

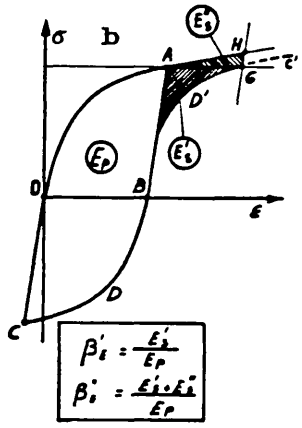


Fig (3.4) Schematic representation of the energy criterion.

Some authors have modified this definition to include energy calculated as a result of area E_S" shown on plot, instead of E_S'. Under this assumptions, the expression is one of

$$\beta'_E = E_S' / E_p \qquad (3.28)$$

and

$$\beta''_E = (E'_S + E''_S)/E_p$$

3.6.4.3 The strain-hardening criterion.

This allows the parameter β to be measured by considering the change in the slope of the stress-strain curve in the plastic zone in reversed loading at a determined pre-strain value. Fig.(3.5) illustrates this method. Under this type of assumption the required parameter is defined as the difference between the forword and reverse slopes at the same strain value.

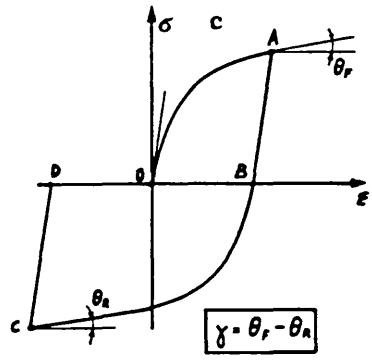


Fig.3.5 Schematic representation of the strain-hardening criterion.

All of these methods have been tested using numerical computational methods(47) and have been found to compare very well. The stress criterion has been adopted for analysing the experimental data of the present work.

3.7. NUMERICAL COMPUTATION OF THE GENERALIZED ELASTO-PLASTICITY THEORY

In attempting to computerize this theory, the important parameters and equations are put in matrix form as shown in appendix A. The framework on which this program is built is the elastic-plastic (loading) computer program provided by Owen and Hinton (46). The computer program compiled has as many as over thiry-five subroutines dealing with the matrix analyses of variables, plastic flow equations and calculation of cyclic data to plot hysteresis loops.

The program is a two dimensional finite-element one and is displacement controlled. It is called "OYIN". Some of the important subroutines and functions are discussed here.

3.7.1. SUBROUTINE STRESS

This subroutine does the final calculation of stress for every guass point in a mesh by using values returned from the Jacobian matrix, STRAIN and PLAST routines. Residual forces on each element are also calculated here.

3.7.2. SUBROUTINE PLAST

Here yielding is taken into account and incremental plasticity is used to derive the incremental stress values which are then used to modify the elastic stress to their elastic-plastic values. The Von Mises yield criterion and surface are incorporated into the program here and the yield surface is

allowed to change its size and translate. The components of the vector $d\alpha_{ij}$ from the centre of the yield ellipse are calculated and stored as SALFA and ALFYD. SALFA is the component of this motion for the movement of the centre of the orignal yield surface to the centre of the first of the subsequent yield surfaces. ALFYD is used to represent the same vector as translation proceeds from the first subsequent yield surface to the second and so on in a logical progression.

The original yield stress (note that for most materials, the point of deviation from the elastic line may not be well defined and extrapolation may have to be made on the elastic and plastic curves and their point of intersection taken as the yield point of material) of a material is input as one of the initally supplied data, but having established the magnitude of the displacements along the translation path of the orignal yield surface, the current or subsequent yield surfaces or the value of stress due to work-hardening or work-softening can then be calculated. The plasticity relationship equation (3.22), which calculates the incremental flow stress is implemented as statement 265 in this subroutine. This statement is written to incorporate the hardening function AH.

Some other useful calculations done in this subroutine are those of the deviatoric stress components (DFS), total strain, the slope of the elastic-plastic stress-strain curve, the reversed yield stress, plastic zone area, the elastic energy and nodal forces (used for the calculation of the residual load).

3.7.3. SUBROUTINE PFLOW

Deals specifically with analysing the difference between the elastic and

elastic-plastic stress ($d\sigma_{ij}$). It uses the input value of the kinematic translation parameter, the numerically derived deviatoric stresses , strains and some other material properties to calculate the equivalent plastic incremental stress multiplier ($d\lambda$) or DLAM as it is called in this subroutine. DLAM is then used to evaluate the required elastic-plastic incremental stress, which is then transferred for use in subroutine PLAST.

3.7.4 SUBROUTINE DMAT

The data input concerning material properties are coordinated and put in initialized forms in this subroutine. The moduli of rigidity for the plane strain and plane stress conditions are also determined here.

3.7.5 SUBROUTINE RELOAD

This subroutine provides a way of controlling the loading and unloading sequence through imposed displacement factors. This sequence can be used for the production of full areas or half areas of cyclic hysterersis loops. The pattern of displacement loading and unloading is flexible and allows for matching a specific value of strain amplitude with corresponding kinematic translation parameter (β). The format of block RELOAD is given in appendix C where a typical data file is presented.

3.7.6. SUBROUTINE STRAIN.

This subroutine calculates and returns values of strain and elastic stress

from prescribed displacement. The three components of strain are calculated according to the imposed condition of plane strain or plane stress The values calculated here are also used in subroutine PLAST.

3.7.7 SUBROUTINE JACOB

Here a Jacobian matrix is evaluated. Each element is fully defined through the use of its input corner nodes to calculate the mid-side nodes. This ensures the establishment of all the eight nodes needed to represent an isoparametric element. the Jacobian matrix is set up after these nodes have been calculated and then used to establish the shape function and differential of same, which are necessary for calculating the strain in subroutine STRAIN.

3.7.8. SUBROUTINES STORE AND INTAPE 9

The program developed consumes a lot of computer time,hence units. Because of this it would be necessary to do cycling in stages. Arrangements were made to store any previously calculated data in tape 9 by using subroutine STORE for use whenever cycling is to be continued e.g. 5 cycles may be carried out at a go and the evaluated values stored and then retrieved through the use of subroutine intape 9. The file so retrieved will then constitute the starting data for the next batch of cycles to be carried out.

From time to time the numbers of records stored on Tape 9 will be output on Tape 6. A code number is used to inform the computer of what data to retrieve and where to retrieve them. Usually, a statement,

"N RECORDS WRITTEN ON TAPE 9" is written at the foot of a set of output numbers. In which case "N" would be the number of the set of data that the computer will need to start cycling from. A code number of one is input as control parameter (restart code) when cycling does not start from the zeroth one.

Whenever there is no initial data to retrieve, this code number will be input as ZERO (see appendix B - User manual).

3.7.9. FUNCTION HHH

This function constitutes the numerical expression for the slope of the plastic part of the stress-strain curve, hence plastic or anisotropic hardening rule. Equation (3.26) is implemented here. The values calculated are returned for used in Subroutine PLAST.

3.7.10 FUNCTION WDE AND SUBROUTINE DFDS

Function WDE calculate the elastic strain energy density whilst subroutine DFDS evalutes the differential of the yield surface function with respect to the related deviatoric stress components and the equivalent stress.

3.8 RUNNING COMPUTER PROGRAM "OYIN"

A user manual is produced and presented in appendix B and representative data files, one for the monotonic case and one for the cyclic case are provided in appendix C. Whereas available cyclic programs (44,48) require

that the monotonic stress-strain curve be divided into several points and that the plastic stresses and strains that define these points be input into the program as a basic data in order to be able to compute the cyclic stress-strain curve, the program that is presently developed does not require a complete monotonic stress-strain curve to be input but parameters extracted from some monotonic loading-unloading experiments. These parameters have been discussed.

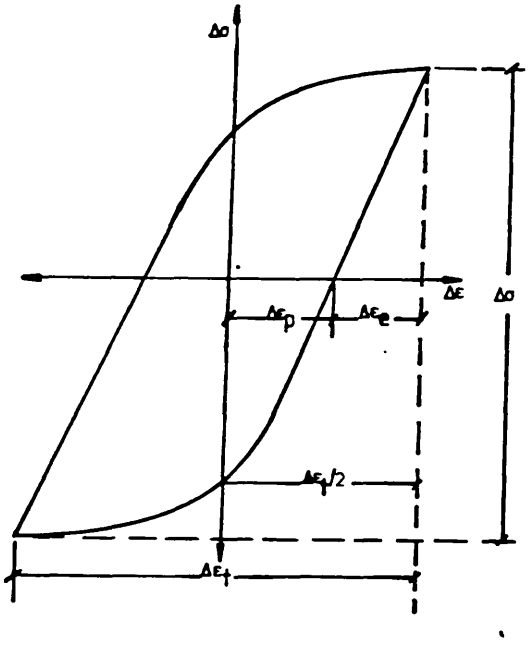
Two files named FILE1 and DATAN are required for running the program. FILE1 contains a full description of the geometry of a finite-element mesh to be used for computation, the total number of elements and nodes etc are contained in this file. The DATAN file is as set up in appendix C. This data file contains nine material properties including the magnitude of kinematic translation parameter, β. When cycling is simulated, the value of β and corresponding strain amplitude are chosen from an experimental curve and this value of strain is achieved through the imposed displacements input in block RELOAD. Full explanation is given in appendix C·

3.9 MATERIAL RESPONSE TO CYCLIC LOADING

When a material is being cycled, a "new material" is produced per cycle due to the plastic deformation caused in the original material. By the time cycling is completed, a series of materials would have been produced, culminating in the production of a cyclically saturated material.
The yield point of the material then ceases to be that obtained during the first or intermediate cycles due to plasticity and plastic strain incremental memory effect, but that at steady state. These "new materials", in

accordance with the reversed loading phenomenon will have their associated Bauschinger effect, flow stress in tension and reverse yield point. The reverse yield point will be between the kinematic-hardening and isotropic-hardening points (see fig 3.1). Consequently different values of the Bauschinger effect parameter results and each of this values will identify strongly with the degree of plasticity attained in tension in each cycle. This reasoning enhances understanding of cyclic behaviour and its relationship with plasticity and makes a combined hardening theory very reasonable.

During cycling continuous loops are formed until saturation. These loops are called hysteresis loops. Each of the loops will represent a "new material", hence a new yield surface. The area of each loop is a measure of the plastic work causing changes in the material per cycle. The basic characteristics of a loop are shown in fig (3.6).



Fig(3.6) Characteristics of a settled cyclic hysteresis loop.

A settled hysteresis loop can therefore be considered to be a summary of the relationship between plasticity, work or strain-hardening, reversed loading and fatigue behaviour when cyclic stress-strain analyses are carried out. Normally, cyclic stress-strain curves are produced from steady hysteresis loops as will be seen in later sections. Fig. 3.7 shows how points on a single reversed loading stress-strain curve can be projected to simulated the motion of the initial yield surface.

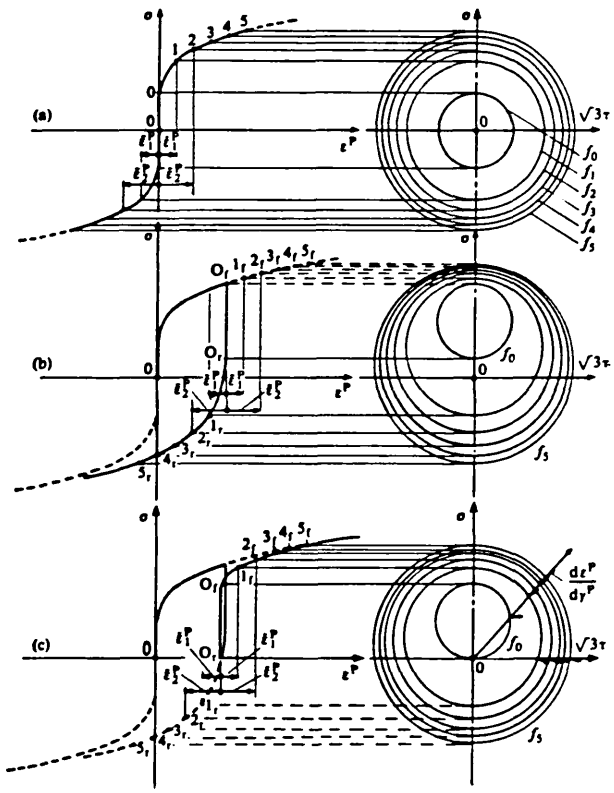


Fig 3. 7 Reversed Loading and the Behaviour of the Yield Surface

3.10 THE MONOTONIC ANC CYCLIC STRESS-STRAIN CURVES

In a macroscopic analysis, a stress-strain curve is regarded as a simple and comprehensive approach for summarizing the mechanical response of a material to loading. There are two types of such a curve namely, monotonic and cyclic.

3.10.1 THE MONOTONIC STRESS-STRAIN CURVE

The monotonic stress-strain curve can be derived from a load-displacement curve. The load-displacement curve itself is obtainable on e.g. an X-Y plotter as a feedback from a testing machine such as the Maye s testing machine. For completeness, the load-displacement curve will be defined as the most authentic representation of the macroscopic physical variations in the mechanical properties of a material as loading or straining is carried out. For the monotonic case the load must be non-reversing all the time.

For sometime now this curve has been regarded as adequate for the provision of data for design purposes and in some cases has been used as the basis for numerical computational cyclic studies in different models (to be discussed later). Normally, service materials are subjected to varying loading, even when they have been used to construct structures which are meant to experience strict monotonic conditions in service, hence it has become imperative to attach importance to the provision of cyclic stress-strain curves for design and general engineering purposes.

3.10.2. THE CYCLIC STRESS-STRAIN CURVE

The cyclic stress-strain curve is the complementary curve that expresses

a similar form of mechanical variation under reversible or ever varying loading. It is defined as the relationship between the saturated amplitudes of stress and strain. The steady state cyclic deformation resistance of a material is usually different from the monotonic stress-strain response.

During cyclic loading structural changes occur very fast. These changes are both metallurgical and mechanical. It is the mechanical aspect of the changes that shall be dealt with in this text. At the begining of cycling the changes are very intensive, with the intensity decreasing as the number of cycles increases or as steady state is approached. After a relatively small number of cycles (small in comparison to the number of cycles to fracture), the measured quantity usually reaches a saturated value (49). In accordance with this observation, a lot of separate hysteresis loops are produced at the begining of cycling reaching saturation after a few cycles depending on the degree of imposed plasticity (through the plastic strain) and the intrinsic properties of the material itself. When saturation is reached during an experiment, the tracing pen on the X-Y plotter continues to trace the same loop for several cycles. the cyclic stress-strain curve itself is derived from the saturated or settled hysteresis loop (s).

Each hysteresis loop can be considered as representing a particular material and yield locus (see fig 3.7). Since normally the area of a hysteresis loop is a measure of the instantaneous plastic work, it can be concluded that the magnitude of plastic work per cycle can be useful for ascertaining steadiness in cyclic behaviour. Steadiness will then be assumed when the value of the plastic work remains constant for several cycles. This criterion is used particularly for confirming steadiness in the computational cyclic analysis.

In comparison to the monotonic situation, engineering materials either harden or soften after cyclic loading.

Hardening and softening can also be confirmed through continuous measurement of the size of the hysteresis loops. However, care must be taken in the use of the hysteresis loop area change criterion for this purpose since the change varies according to the type of test.

For instance, fatigue hardening in stress-controlled tests manifests itself by decrease in the strain amplitude and increase in the area of loop, whilst the same process for strain controlled tets shows an increase in stress amplitude and a decrease in area. It is also important to note that fatigue hardening is common to annealed metals while fatigue softening is typical for materials that were initially strengthened before cycling is carried out.

In order to have complete data to represent material behavioural pattern, monotonic and cyclic stress-strain curves have to be provided. The possibility of using the computer for this job without recourse to experiments is an important step forward.

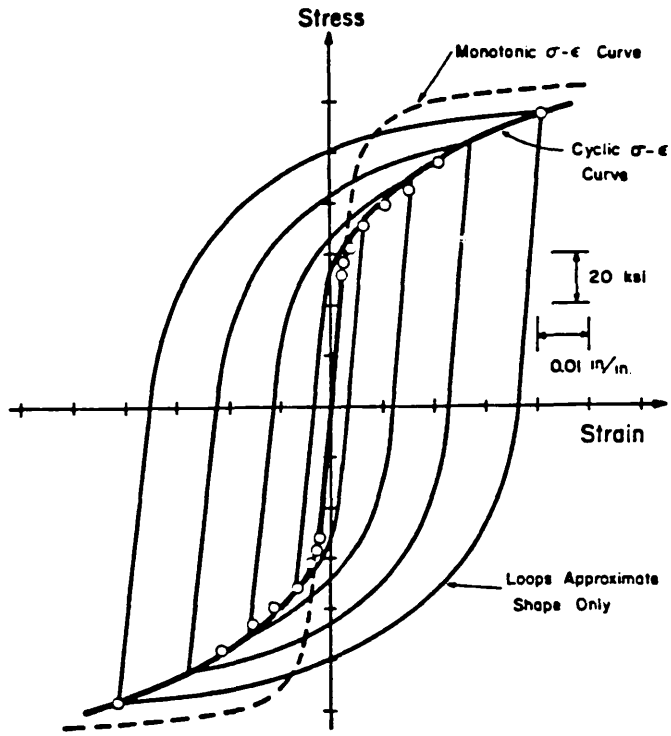
3.11 DERIVATION OF THE CYCLIC STRESS-STRAIN CURVE.

Established experiments are designed such that the load or strain level employed during cycling can be increased in steps and the locus of the tips of corresponding settled hysteresis loops traced out to form the cyclic stress-strain curve. In effect, the cyclic stress-strain curve can be redefined as the locus of the tips of the stable hysteresis loops from several comparison tests at different completely reversed constant amplitudes (50). It should be noted that the definition is not unique as it is just in accordance

with one established method out of a group of employable methods. Four methods of deriving the cyclic stress-strain curve are cited as follows:

3.11.1 MULTIPLE STEP TESTS

Bairstow (51) and Dugdale (52) cited that cyclic hysteresis loops rapidly become stable or steady due to sudden changes in cyclic strain amplitude. Their work thus makes it possible to obtain several points on the cyclic stress-strain curve from a single specimen by cycling at varying or stepwise amplitudes.



Fig(3.8) Illustration of the multiple test method. (53)

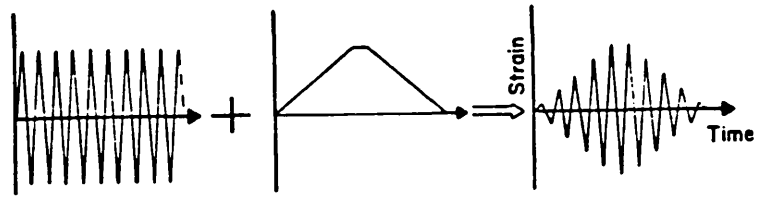
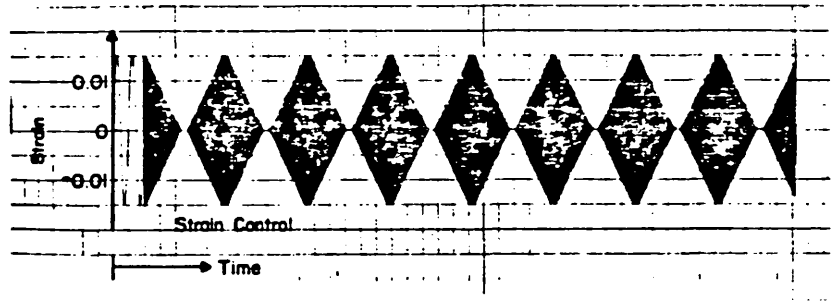
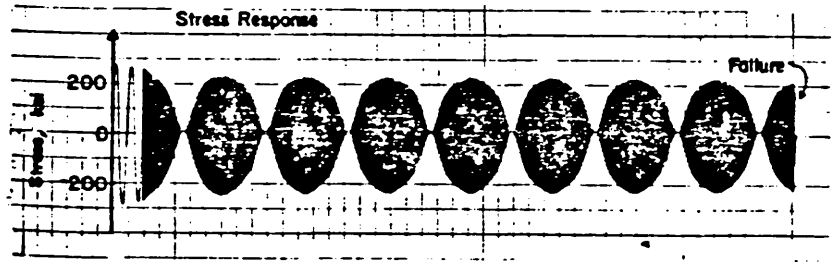


Fig 3. 9 Loading Sequence for the Incremental Test (53)



a



b

Fig 3.10 Straining Program as a Function of Time (53)

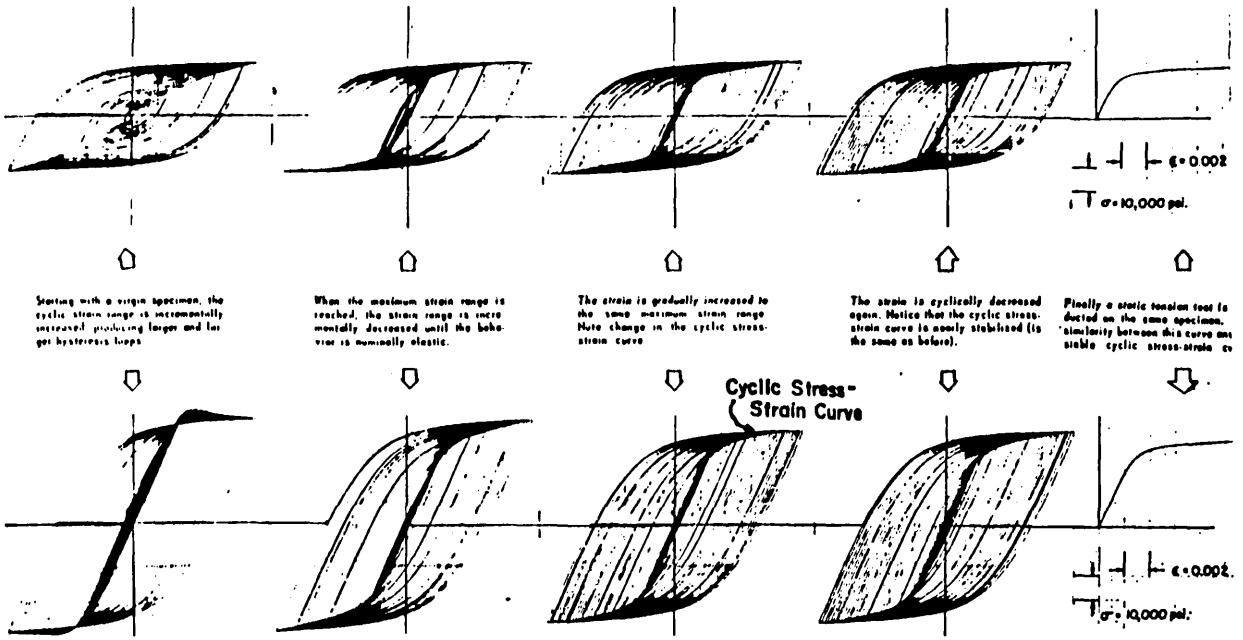


Fig 3.11 Cyclic Stress-strain Curves for the Incremental (53)

Cycling is carried out for each stress amplitude until steady state is reached or for a chosen strain until steadiness is attained. Whichever method is
employed, subsequent amplitudes are chosen after a previous steady-state has been reached. This type of test can be affected by the order of the straining sequence.
In the light of this a high-to-low strain sequence is generally preferable. Mean stress effect is important and this can be eliminated or minimized by decreasing the strain amplitude incrementally to zero stress and strain between blocks. (fig. 3.8) shows settled hysteresis loops, monotonic and cyclic stress-strain curves for SAE4340 Steel (53) using this method.

3.11.2 INCREMENTAL STEP TESTS.

This is the method when a specimen is subjected to blocks of gradually increasing and then decreasing strain amplitudes as shown in fig (3.9). This offers a quick method for determining the cyclic stress-strain curve. After a few blocks, the material cyclically stabilizes. A continuous plot of the hysteresis loops throughout a block results in a series of superimposed loops with a clearly defined locus of the tips corresponding to the cyclic stress-strain curve. A typical test record of controlled strain amplitude blocks and the stress response of the specimen to this straining program as functions of time are shown in fig (310) (3.11). The stress-strain curves of the first three loading blocks for a quenched and tempered steel are shown in fig (3.11). Softening is obvious here.

3.11.3. MONOTONIC TENSION AFTER CYCLIC STRAINING

This method can be complementary to either of the methods mentioned above. It consists simply of pulling the specimen to fracture in tension after it has been cyclically stabilized through either multiple or incremental step tests.

An application of this technique is presented in fig (3.12) for an aluminium alloy after going through incremental step cycling. It can be observed that the resulting monotonic tension curve is almost coincident with the locus of the loop tips.

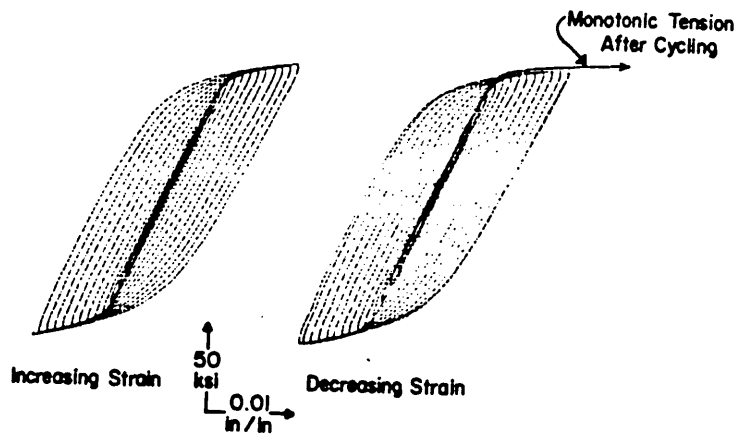


Fig.(3.12) Illustration of the monotonic tension after cyclic straining method. (53)

3.11.4. INDIVIDUAL HYSTERESIS LOOPS METHOD

This method concerns itself with the use of only one stable hysteresis loop. Suggested by Morrow (54), the outer trace of a single stable hysteresis loop may be superimposed on the cyclic stress-strain curve if the stress and strain measured from the loop tip are divided by a factor of 2. This method is presented in fig (3.13).

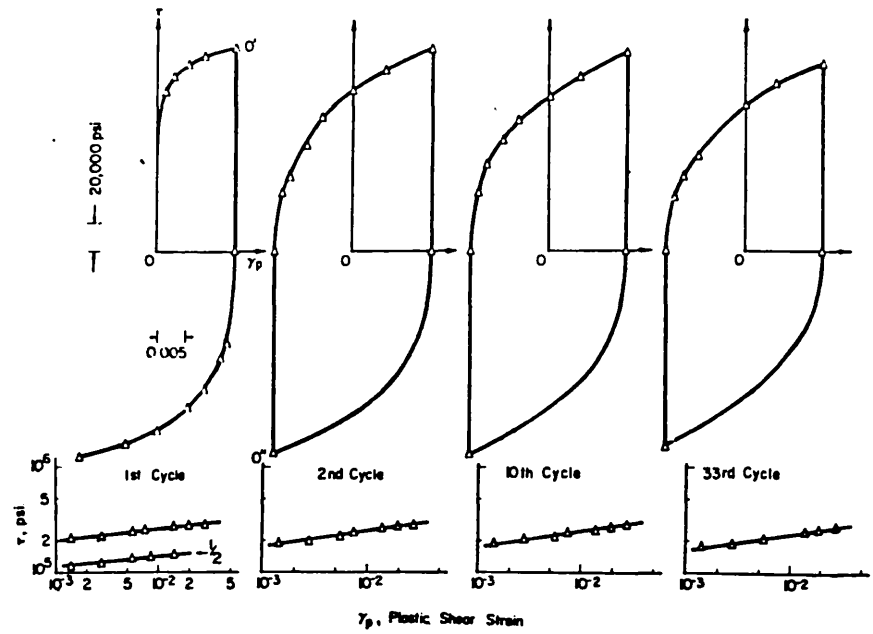


Fig.(3.13) Illustration of the Morrow method. (53)

Of these cited methods, the two methods presented in 3.11.1 and 3.11.4 will be applied for analysing the data obtained from our experiments. The Morrow method is particularly attractive in terms of the economics of producing cyclic stress-strain curves on the computer since it affords the opportunity of cycling a specimen at a high strain amplitude until steady state is reached and then using the loop obtained to predict the stress and strain at the tip of loops corresponding to lower strain amplitudes. Once these intermediate points are obtained the cyclic stress-strain curve can be conveniently plotted. The method will be tested for experimental and computational analysis and compared with the multiple step test method curve.

3.12 EXPERIMENTAL ANALYSES

INTRODUCTION

The break down of experiments are as follows:

1. a) Determination of single cyclic hysteresis loops at different values of chosen plastic strain amplitude.

b) Cycling of specimen to steady-state at a value of plastic strain amplitude.

c) Derivation of experimental monotonic and cyclic stress-strain curves, the monotonic strain-hardening index and where applicable the Ramberg-Osgood constant α_c as it appears in,

$$\sigma/\sigma_0 = \alpha_c (\varepsilon/\varepsilon_0)^n$$

d) Determination of the Bauschinger effect, hence, kinematic translation parameter (β).

2. Introduction of pre-strain to strengthen an already annealed material before cycling it at a lower strain amplitude. This is necessary in order to study the variation of the kinematic translation parameter (β) with plastic pre strain.

3.12.1 SPECIMEN CONFIGURATION

The shape of specimen is governed principally by plasticity considerations. The type of experiments demand the use of rounded specimens. Since the onset of plasticity is normally characterized by necking, a specimen with an initial neck was chosen so that local plasticity at region occupied by the neck is achieved quickly and at less "intense" machine crosshead displacement. Due to these considerations, an hour glass configuration fig (3.14) was opted for. This type of specimen is round and carries an initial neck. The specimen ends are of the button type to ensure square sitting inside machine grips. Earlier experimenters adopted the use of hollow cylindrical specimens tested in tension for reasons of avoiding barrelling of a test piece under tensile/compressive conditions. The hour glass specimen is a much improved specimen and can be tested under tensile-compressive condition without the risk of barrelling or buckling. Some of the assets of the hour glass specimen are as follows:

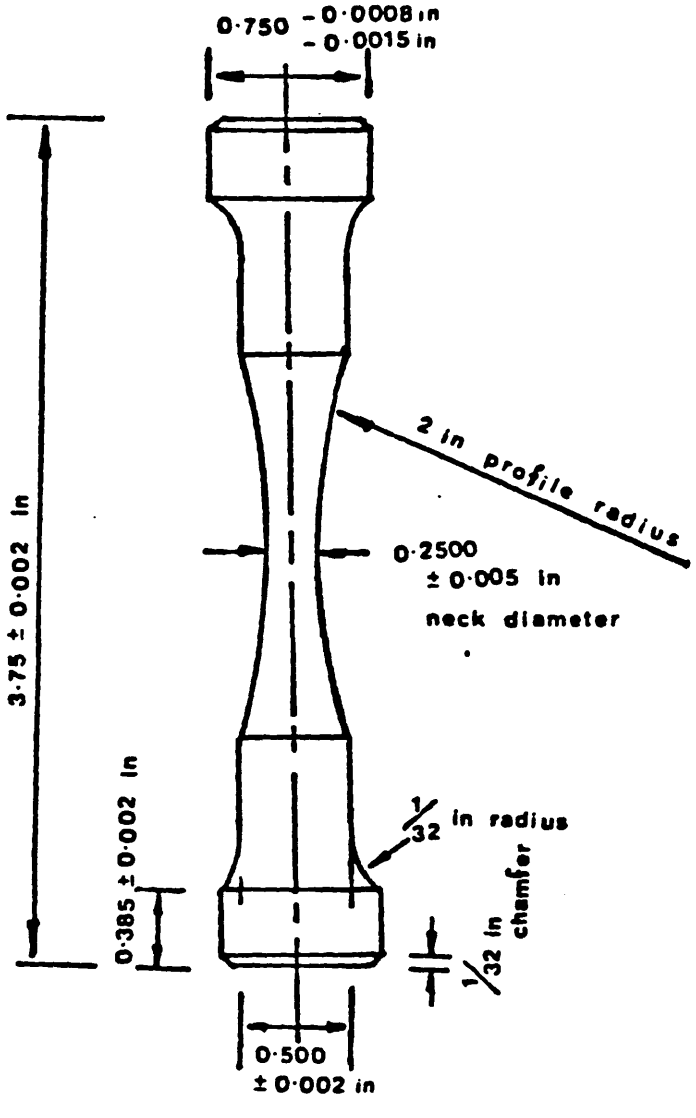


Fig 3.14 The Hour Glass Specimen

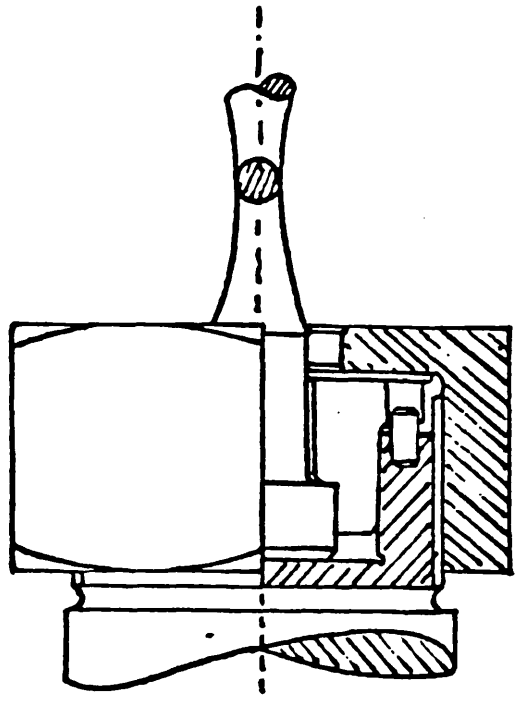


Fig 3.15 End-fittings of Hour Glass Specimen
With Specimen Seated in Position

1) Inflicted strains can be controlled and measured at the neck of the specimen where fracture is expected to occur.
2) Relatively high magnitudes of compressive strains can be attained in the specimen without the risk of buckling it.
3) The 'neck' is suitable for carrying a diametral extensometer.
4) Internal and surface flaws are less likely to affect the experimental result since most of the strain is localized at the neck - This concentrates data generation to a comparatively small region at the imposed 'neck'.

However, a problem with the hour glass specimen is that the diametral changes measurable are considerably smaller compared with the axial changes that can be measured in a normal cylindrical specimen.

Consequently, strain measurement using the chosen type of test piece can be very laborious and requires some precision.

3.13. USING THE TESTING MACHINE

Detailed description of the Maye s machine is given elsewhere (55,56). However, mention is made here of those parts of the testing machine which were directly useful in the tests carried out.

3.13.1 SPECIMEN GRIPPING

Fig (3.15) shows the end-fittings with the specimen seated in position. A split collet is used to locate the button end laterally. A nut is used to force the collet against the button end of the specimen, consequently, pressing the

end of the specimen against the face of the end-fitting. The upper end-fitting screws on to the load cell while the lower end has a flange which is bolted to the upper face of the moving ram which protrudes upwards from the bottom part of the machine.
The load cell spindle is designed to have a fairly large resistance to lateral or angular deflection which ensures negligible lateral or angular movement of the specimen once properly mounted. This gripping method helps resistance to buckling. Finally, care must be taken to ensure that the two ends of the specimen are tightened so that sideways movement of the specimen is eliminated, since failure to do this will cause distortion of the experimental hysteresis loops plotted on the X-Y plotter.

3.13.2 ADJUSTMENT OF THE LOADING FRAME

The loading frame consists of an upper crosshead linked by two hard chrome plated columns to the base unit. The base unit carries the main hydraulic actuator equipped with a manifold mounted Moo g Servo valve and a Linear Variable Displacement Transducer (LVDT) (which is a position feed-back mechanism), microfilter and control valves. The hydraulic actuators are positioned or moved by adjusting the oil pressure of the base column that support them.

In order to fit a specimen between the upper crosshead and bottom part of the testing machine, the upper crosshead is moved down (by reducing oil pressure) and then tightened up to maintain it in the required position. The tightening is done by a torque wrench.

3.14 MACHINE CONTROL MODES

One of four different control modes can be chosen at a time during an experiment. The four possible modes are:

1) Position control
2 Load control
3) Strain control
4) Clip gauge control (strain bridge)

Any of these control modes can be used to achieve a desired loading condition in a specimen. After a choice of machine control mode, a command signal is activated and this becomes the dominant input function to the machine as experiment is carried out. In general, a command signal is usually a composite signal which has an associated static level on which one or more dynamic function can be superimposed.

Tranducers such as the strain gauge load cells (used for load detection), LVDT tranducers (for extension work) used in monitoring specimen conditions have associated electronic modules whose function is to provide adequate signal output levels for control and instrumentation on the machine. Static command adjustment is dependent on the particular feedback module selected e.g. load, strain or position while dynamic signals are usually derived from the same generator type regardless of the selected control mode. For the particular experiments carried out, specimens were mounted in machine position control mode while the actual curves production was done in strain control mode.

3.15 OTHER ACCESSORIES

A diametral extensometer mounted in a casing fig. (3.16) was used to

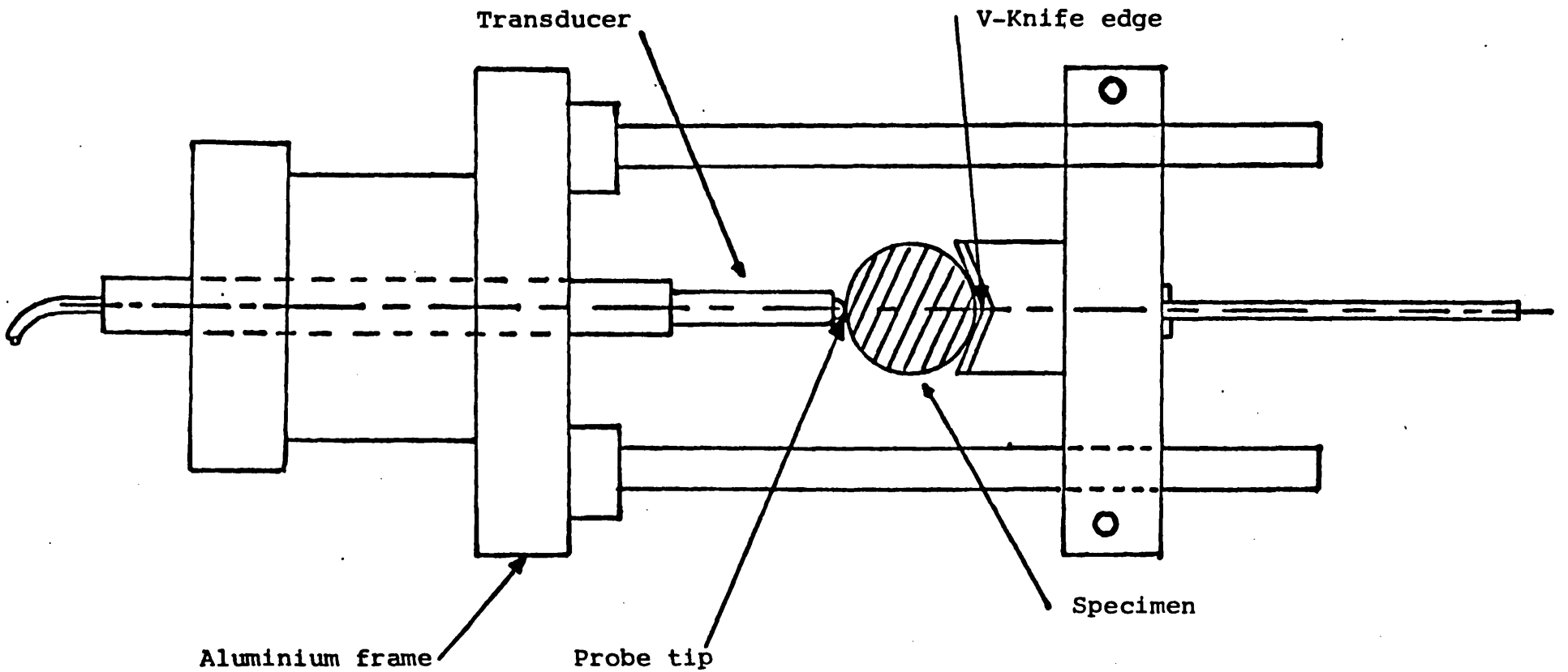


Fig 3.16 The Diametral Extensometer Mounted on Specimen Neck

obtain signals form the neck of the specimen.

The mounted unit consists of the LVDT and a knife edge. the LVDT was used to monitor any diametral changes in the specimen. Signals from the LVDT were transferred through the transducer module which is provided on the testing machine to the X-Y plotter.

The knife -edge completes a 'circular gauge' arrangement around the neck of the specimen. It makes contact with an arc at the neck while the LVDT presses on the other side of specimen opposite the knife-edge.

Rubber bands were used to hold the frame in a horizontal position. A lot of careful adjustment must be made in order to get the frame to an exactly horizontal position so that readings were accurate and dependable within experimental limits. It was observed that the hysteresis loops obtainable will be distorted if the specimen does not sit properly in the grips, the ends are not firmly fixed or if the extensiometer arrangement is eccentric to the horizontal axis. The use of rubber bands enhanced easier readjustment of the diametral extensometer as the specimen changes its dimension at the neck during cycling. Furthermore, flexibility of the bands provided room for adjusting the extensometer frame to the highly necessary horizontal position in "quick" time.

3.16 DATA SIMULATION

3.16.1 CALIBRATION OF AXES

This section refers to the grading of the X- and Y- axes. The basic principle involves relating feedback signals from the machine to distances on the X-Y plotter's log sheet. X- is the displacement axis while the Y-axis is used for

recording load variations.

3.16.2. DISPLACEMENT OR STRAIN SCALE

Displacements read from the LVDT are used to calculate the axial strains. Whereas the strain scale was calibrated in terms of axial displacement, the experimental results were in terms of diametral displacement. It was therefore necessary to convert these diametral displacements to their axial equivalents. Because each specimen was deformed to the plastic state, a no change in volume was assumed. The plastic axial strain was found to be twice the diametral one. The diametral plastic strain was obtained directly from experiments. The error incurred through this method of analysis is about 5%.

A solid cylindrical specimen with button-type ends was used for scale calibration. It was mounted in the same way as described for the hour-glass specimen. The machine was then set into position control mode, the diametral extensometer was put in place and then the machine's displacement transducer was set on the 0.1mm range. The strain readings were then percentages of the 0.1mm value.

The X-axis was marked for every 10% axial displacements, consequently enabling correlation between machine feedback and recorder logging. This calibration enables intermediate reading to be extracted from an experimental curve, since it was only possible to record the number corresponding to the maximum and minimum points on an experimentally logged curve.

After the above chart calibration was completed, the LVDT was removed and placed in a travelling micrometer. A step calibration was then carried out in order to verify the linearity of the relationship between the strain and the chart displacement; and also to ascertain if backlash or friction effects occurred.

This exercise is summarized in Fig. 3.17. It can be concluded that linearity occurred around its zero position which is halfway through its maximum stroke. Consequently, the displacement setting during the experiments were made to lie within the linearity limit so that appreciable accurracy could be achieved.

3.16.3 STRESS SCALING

The Y-axis is the load or stress axis. The load cell is designed to cause movement on the vertical axis of the X-Y plotter. A full scale deflection was read for a selected load range of 50kN. It was noted that 1mm of movement along the Y-axis corresponded to a load value of 0.19685kN. This calibration enabled direct reading of applied load from the X-Y plotter graphs. It must be noted that all load feedback are percentages of the selected load range.

3.17 SPECIMEN PREPARATION

Six hour-glass specimens from each of four different materials namely, titanium, mild steel, stainless steel and aluminium alloy H18 were made to specification, fig (3.14). The specimens were annealed according to established heat-treatment recommendation in the standards to relieve

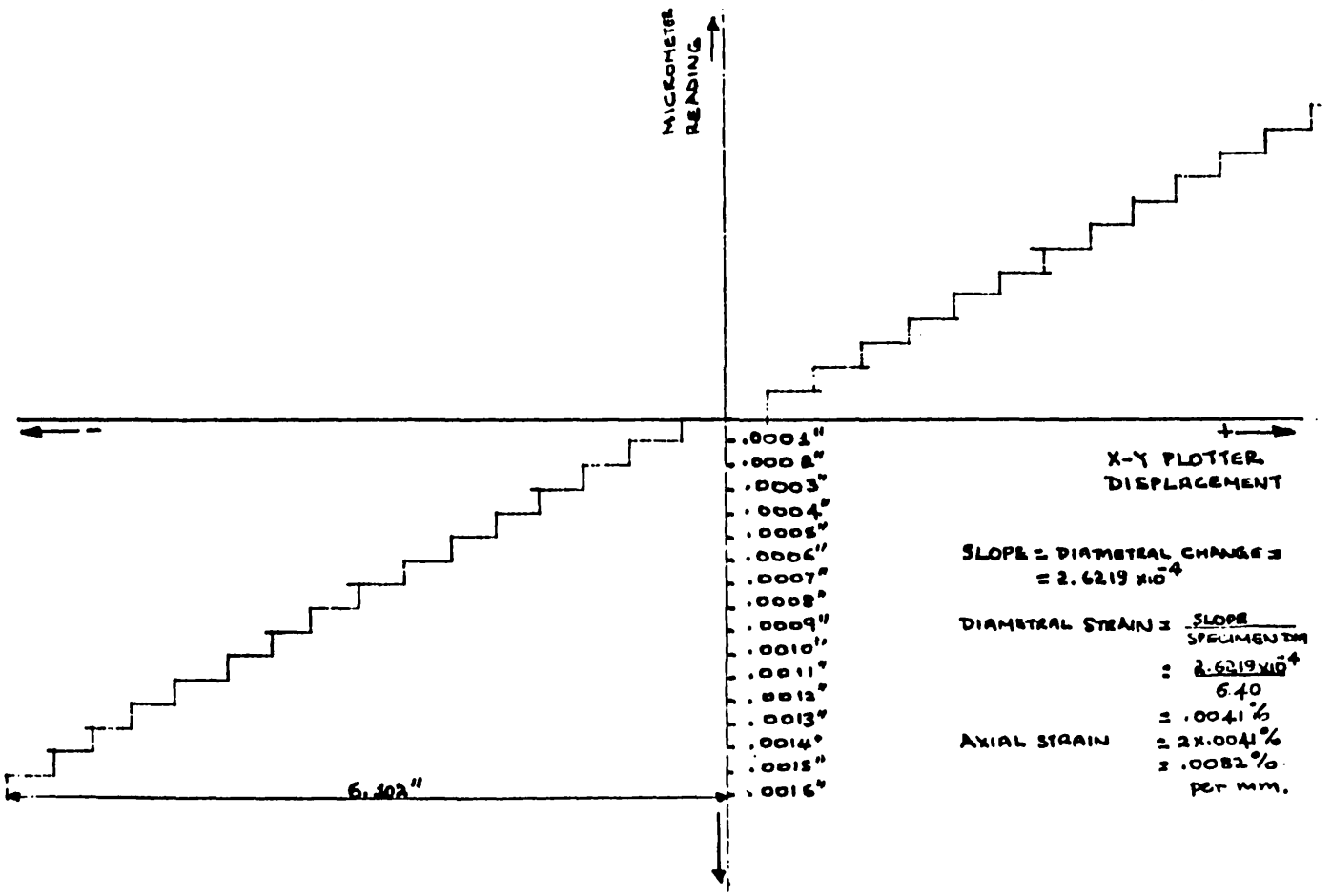


Fig 3.17 Calibration of the Displacement Axis

them of any residual stresses. Consequently, they become reasonably "isotropic" and are ready for the intended experiments.

With this material condition, the point of departure from linearity on the X-Y plotter can be reasonably assumed to lie on the virgin yield locus.

3.18 TEST PROCEDURE

Five specimens from each material were employed for the first set of experiments.

Each specimen was mounted between the machine grips, the LVDT housing was attached to the neck of the specimen through the use of four flexible rubber bands. Three points are noteworthy namely:

1) The LVDT housing must be placed completely horizontal. Any eccentricity causes severe distortion of the hysteresis loops (especially around the origin), consequently, causing problems in the derivation of cyclic stress-strain curves.
2) The LVDT, in its horizontal position was then adjusted to its zero position to enable reading from zero. When the LVDT is at zero, the strain gauge on the machine reads zero.
3) Also the machine would not go into strain control mode if the initial LVDT position is not zero.

Once these were ensured the strain control mode was chosen, a strain amplitude imposed and the cyclic frequency trip was activated.

The frequency is made very low when tracing the first cycle loop or the monotonic load-unloading curve. This is necessary in order to be able to have effective control on the machine and stop it at appropriate point which in the first instance was after this first loop had been traced. After obtaining this curve, the strain amplitude was noted and the specimen unloaded to zero load. The amount of strain is hereby referred to as INITIAL STRAIN.Afterwards, the sine wave signal was chosen, and then the cyclic trip unit was set on. Cycling was then carried out until steady-state was reached.

Steady-state was assumed after the tracing pen had traced the same loop for at least ten consecutive times or cycles.

The second type of experiment involved prestraining the specimens. The set up of the specimen and the LVDT unit was as previously described. To prestrain, a specimen was loaded to a specific high plastic strain value.

The plastic prestrain amplitude was different for each specimen. After prestraining, the specimen was then cycled at a much lower but constant strain amplitude. Steady-state was judged as earlier defined.

3.19 ANALYSIS OF EXPERIMENTAL DATA

3.19.1 MONOTONIC STRESS-STRAIN CURVES

These curves were derived from the first cycle load-unloading - displacement curves presented in appendix F). The curves refer to the

tensile part of the experimental load-displacement curve. The exercise is simply a "curve fitting" one in which the experimental load-displacement curve was converted point for point into its stress-strain equivalent.

3.19.2. DETERMINATION OF α_c AND HARDENING INDEX (n)

After obtaining the monotonic stress-strain data, the values of stresses and strains were normalized by dividing with the monotonic yield stress and the monotonic yield strain respectively. After this the logarithms of the normalized data were taken and then plotted. The hardening index (n) for any material studied was obtained from the slope of the curve whilst $\alpha_{c,}$ was obtained from the intercept of the same curve on the vertical axis. These values provide part of the material data for the computer program.

3.19.3 DETERMINATION OF THE KINEMATIC TRANSLATION PARAMETER, β

The stress criterion was used for deriving β in accordance with the suggestion in the elastic-plastic theory. The single loop curve is used in all cases of the determination through the exhibited Bauschinger effect of a tested specimen. β-values were calculated for the initial and prestrain experiments and the curves of β against appropriate strain and comparative curves are presented in appendix F.

In one-dimensional analysis,

$$\beta = d\alpha / d\varepsilon_p$$

For plasticity situation only, the condition on the original yield surface is such that,

$$\alpha_0 = 0$$

so that $\beta = d\alpha_1/d\varepsilon_p$

$$\alpha_1 = (H_1 - H_2)/2$$

In non-dimensinalized form,

$$\alpha_{1_{ND}} = [(H_1 - H_2)/H_0]/2$$

hence, $\beta = [(H_1 - H_2)/H_0]/2 \cdot \varepsilon_p$

where,

H_1 is the plastic stress in tension reached before unloading,

H_2 is the reverse yield stress,

and H_o is the yield stress in tension (used for non-dimensionalizing).

3.19.4 EXPERIMENTAL CYCLIC STRESS-STRAIN CURVES

These curves were derived for aluminium and titanium using multiple step and the single settled hysteresis loop method suggested by Morrow. These two methods were chosen because they represent the extremes of the available methods of analyses, hence since the former uses several settled hysteresis loops while the latter uses a single hysteresis loop.

3.19.5 COMPUTED MONOTONIC AND CYCLIC STRESS-STRAIN CURVES.

After obtaining the values of the yield stress (σ_o), the yield strain (ε_o), hence Young's modulus, the plastic state curve fitting factor, α_c, the hardening index(n) (which is used in the evaluation of function HHH or H' in program) and the value of β, the stage becomes set for computational analysis.

To determine the monotonic curve, all material property parameters were set out as in the user manual (appendix B). The value of the kinematic translation parameter, β, should be set to zero for this test.

For the cyclic stress-strain curve, all material properties including a curveof β vs ε_p are needed. A value of plastic strain amplitude at which the material was to be cycled was chosen , then a line was drawn from the corresponding strain value on the strain axis to meet the β-axis where the value of β is then chosen. The loading sequence (input to RELOAD subroutine) is constructed so that cycling was done to plus-minus this strain. For these values of β and ε_p then, a hysteresis loop is derived. Many settled hysteresis loops can be constructed for different values of β and ε_p combination if the multistep method is used. In the case of a choice of the Morrow method, a large plastic strain value is chosen with corresponding value of β. Using these values , a large settled cyclic hysteresis loop is produced, from which the cyclic stress-strain curve is then constructed.

The monotonic and cyclic stress-strain curves obtained from both

experimental and computational analysis are presented in appendix F.

3.20 CONVERGENCE PROBLEM

From (46), the convergence criterion for the monotonic situation is given as,

$$C_1 = |R|/|F| \qquad (3.31)$$

where |R| is the modulus of the residual load

and

|F| is the modulus of the total applied load.

When considering the cyclic case unloading exercise can cause some problems because it is quite possible that C_1 becomes an infinite number as |F| becomes ZERO. This problem was avoided by assuming an incremental modulus for this parameter and equation (3.31) is re-written as:

$$C_{1cy} = |R|/|\Delta F| \qquad (3.32)$$

and $|\Delta F|$ is the incremental modulus of load and C_{1cy} is the cyclic convergence criterion.

Equation (3.31) and (3.32) are unified to produce a more representative criterion as follows:

$$C = |R| / (k_1|F| + k_2|\Delta F|) \qquad (3.33)$$

and $K_1 = K_2 = 0.5$

Equation (3.33) is implemented as the convergence criterion in the program.

Convergence is achieved when $C > C^{n+1}$ where C^n and C^{n+1} are the values of criterion in n and n+1 iterations respectively.
In some cases, the output contains a message about the divergence of iterations. This should not be of much concern to the user since the message only reflects the sensitivity of the program to situations when the restraint forces are much bigger than IFI. In retrospect, this can be considered as a false divergence alarm.

3.21 PROLONGED RUNNING OF PROGRAM

During cycling, economic considerations demand that program running be truncated.

There is a start and restart facility built into the program. This allows the user to start from any load increment provided previous data are accessible. Consequently, previously computed are stored on Tapes 3,4 and 9. For continuous run, the data file remains the same with LINE 3 of the input file modified. See appendix C for format of the data file.

CHAPTER FOUR

FATIGUE OF NOTCHED SPECIMENS

4.1 INTRODUCTION

In a remotely loaded notched body, the notch constitutes a stress concentration and has the effect of raising the magnitude of the strains and stresses at the local or notch tip region (57). In fatigue cases, the region around the notch tip can be divided into two (58), namely the notch plastic and the notch elastic fields. The notch plastic zone is directly influenced by the notch and it usually contains enormous values of strains and stresses which may not be realistic for real materials without notches and this field is called the "fracture process zone". The interaction between fatigue loading and the microprocesses in this local region culminates in the nucleation and initiation of a crack. The crack formed here grows into the next region which is the notch elastic field. Here the crack encounters moderately high stresses and strains and it is treatable under modified macroscopic LEFM assumptions e.g by considering the extent of plastic zone ahead of a growing crack. The third region is that which is completely remote from the notch and for the sake of analysis here will be termed the "proper LEFM region". This region dominates from a finite distance away from the notch tip to the end of a specimen's ligament.

Several authors have used some macroscopic monotonic parameters modified into their incremental forms for fatigue purpose (eg ΔJ) to

correlate crack growth from the most local of the regions i.e, the notch plastic zone to the "proper LEFM region". When a crack is still in the notch plastic zone and its length is below a certain value (discussed later), it is usually referred to as a short crack. It is now well documented that short cracks are anomalous in behaviour when compared to long cracks which obey standard LEFM assumptions. Therefore, the question arises on whether it is physically plausible to analyse short and long cracks with the same type of macromechanics parameters as has been done by some investigators cited below!

Furthermore, a fatigued notched laboratory specimen is usually seen to exhibit at least two distinct sections of material along the crack face when the specimen is broken into two along the crack line. In the light of this evidence, it becomes questionable if uniform macroparameters as used in fracture mechanics are actually adequate for analysing the behaviour of a crack that may be travelling across these regions!!

In order to be able to answer these questions computer studies are carried out on the effect of separate regions of material properties on established fracture mechanics parameters like the J-integral and the crack opening displacement (COD). Before carrying out this study, small cracks will be examined and so will some other relevant fracture parameters.

4.2 THE SHORT CRACK PROBLEM

A short crack can be defined as the linkage between the initiation stage

and the long crack stage (59). The problem of short crack growth at notches is important because most fatigue failures originate at some kind of stress concentration and the period of crack growth through the notch plastic field may represent a major part of the total life. When this happens, a proper description of short crack growth is essential to accurate prediction of the fatigue life. Incidentally, incipient growth takes place inside the notch plastic field and efforts must be geared towards obtaining a parameter that is capable of correlating data in this situation.

Five categories of short crack problems have been identified in the work of Smith (59). These are summarised below:

a) The intrusion, extrusion mechanism of initiation in surface grain.

b) The cracks that are found to be present just below or at a stress level equal to the plain fatigue limit.

c) Non-propagating cracks found in notched specimens.

d) Slower than LEFM predictions for micro cracks in plain specimen.

e) Faster than LEFM predictions for micro cracks in plain specimens and macro cracks in notched geometries.

Statement (a) deals with the metallurgical aspect of this problem whilst (b) attempts to quantify the appropriate size of a short crack. The fourth problem (d) was observed by experimentalists like Lankford et al 60) and Morris (61).

Lankford et al (60), observed lower than LEFM growth in some Ni-based super alloys with grain size of the order of 3 to 5mm. Also, they argued

that the occurence of initially high growth rates in newly initiated cracks was due to specimen artifact.

Schijve (62) and Truyens (63) also suggested that slower crack growth could be caused by irregular crack surfaces and interaction of multiple initiation sites respectively. This phenomenon concerns itself with microscopic effects operative at a length of the order of a grain size and it seems at this stage that application of global macroparameters to the solution of this problem is inconceivable. However, the present work will not necessarily have to investigate crack behaviour in this metallurgical sense.

Despite the importance of the problems highlighted in statements (a), (b) and (d) above, the present work will only concern itself with just the problems defined in (c) and (e) and this Chapter will particularly search for a way of using macromechanics parameters in explaining and correlating crack growth at all stages.

4.3 SIZE OF A SHORT CRACK, a_o

Kitagawa et al (64), first argued that however small a crack might be,it will grow when the plain fatigue limit is exceeded. They also suggested that the intersection of the plain fatigue limit and the stress component of the long crack threshold should define a limiting crack size a_o below which usual LEFM assumptions will cease to apply.

Smith (59), also attempted an estimation of this limiting crack size by considering the minimum amount of material which might yield as loading is carried out. It was observed that K_{TH} (the fatigue crack threshold stress intensity factor) decreased when measured for small cracks using LEFM assumptions. The limiting size was finally fixed to a very small fraction of the visible crack length.

Lankford's (60) experimental data support the dependence of the limiting crack size a_0 on the type of material. For instance, it was observed that the limiting crack size in mild steel (which is about 1mm) is some two orders of magnitude larger than the limiting crack size in hard 4240 steel (about 10μm). Further evidence of material dependence of the parameter a_0 can be found in the literature compiled by Tanaka et al (65) and Elsender et al (66).

A useful conclusion of Tanaka et al (65) of probably metallurgical significance is the idea of the influence of grain boundaries on the behaviour of short cracks. Several other workers have since argued along this line e.g Miller (67) in their attempts to explain the unusual or anomalous behaviour of short cracks.

The point of engineering significance in all the above is the possibility of estimating the limiting crack size or the crack length a_0 to which LEFM can be reasonably applied as follows:

$$1.12\Delta\sigma_0\sqrt{\pi a_0} \leq \Delta K_{TH}. \qquad (4.1)$$

or

$$a_0 \leq 0.25\,[\Delta K_{TH}/\Delta\sigma_0]^2 \qquad (4.2)$$

where ΔK_{TH} is the threshold stress intensity factor.

a_0 is the limiting crack size below which LEFM does not apply.

$\Delta\sigma_0$ is the plain fatigue limit of a material.

Having established a feel for the size of a short crack, attempts will now be made to study fracture macroparameters that may be relevant to data correlation at this crack size.

4.4 MACROMECHANICS PARAMETERS AND THE SHORT CRACK

Smith (59), concluded that the "smallness" of a fatigue crack depends on material and stress level. Hence, no single length value can be suggested in order to define this occurence. Microstructural features like grain boundaries or inclusions and their interaction with cracks and their tip plastic zones and excessive plasticity causing the plastic zone to be larger than those allowable under LEFM assumptions are likely to be primary causes of the difference between short and long crack behaviours, he argued.

He went further to suggest that the effect of short cracks on the fatigue limits of plain and notched components can be adequately described by a combination of the engineering macroparameters of plain fatigue limit, threshold stress intensity factors and stress concentration factors. It can be said that this approach will possibly be the case if the situation was that of moderate plasticity at the notch local region.

In his paper on initiation and short fatigue cracks, K.J Miller (67)

concluded that during cycling:

i Fatigue cracks initiate immediately.

ii Fatigue limits are associated with non-propagating cracks rather than with the inability of a material to initiate a crack.

iii Crack growth rate in a surface grain decreases as the crack grows unless additional plasticity can be generated beyond the surface grain.

iv Effects such as grain size, periodic surface removal, grain

texture, non-propagating cracks, accelerated fatigue tests and surface finish can all be rationalised from fracture mechanics analysis of crack growth in a surface grain.

This present work shall not, however, concern itself with the intricacies of the initiation stages of crack growth, but it will be noted for the purposes of analysis that macroengineering parameters are capable of correlating data at the initial stages of crack growth.

4.5 THE STRESS INTENSITY FACTOR, K

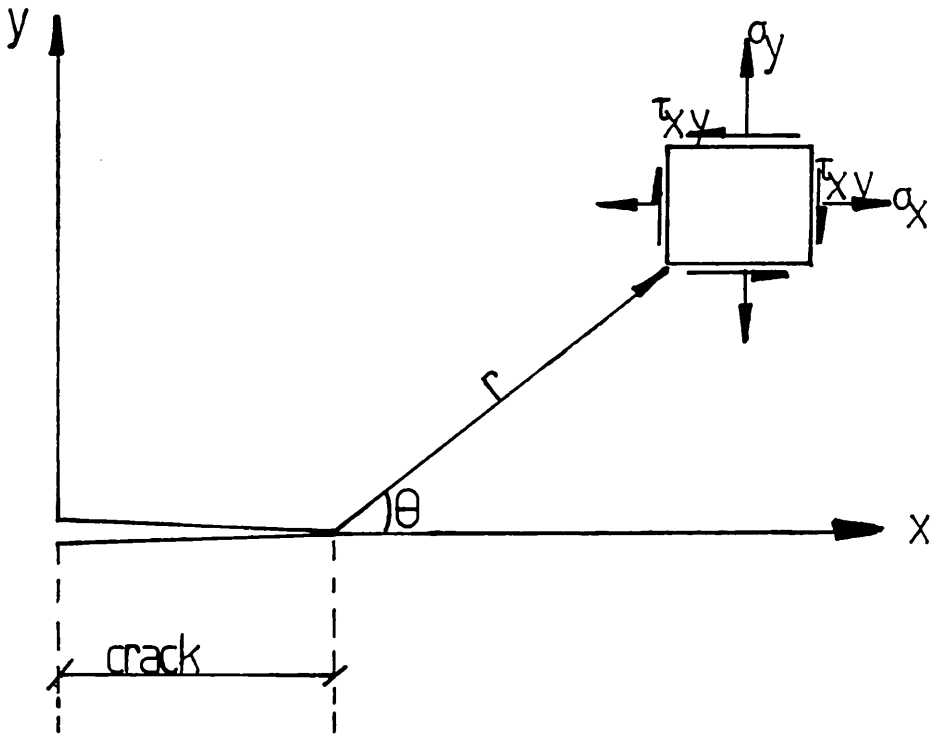


Figure 4.1: Crack tip coordinate and stress system

Consider a crack system constituted as shown above. In the vicinity of the crack tip, Sneddon (68) showed that:

$\sigma_x = K_1/(2\pi r)^{1/2} \text{Cos}\ (\theta/2)\ \{1 - \text{Sin}\ (\theta/2)\ \text{Sin}\ (3\theta/2)] + \text{non singular terms}$

$\sigma_y = K_1/(2\pi r)^{1/2} \text{Cos}\ (\theta/2)\ [1 + \text{Sin}\ (\theta/2)\ \text{Sin}\ (3\theta/2)] + \text{non singular terms}$

$\tau_{xy} = K_1/(2\pi r)^{1/2} \text{Cos}\ (\theta/2)\ \text{Sin}\ (\theta/2)\ \text{Cos}\ (3\theta/2) + \text{non singular terms}$

where (r,θ) are polar co ordinates based on the right hand crack tip and

σ_x, σ_y and τ_{xy} are the stresses acting on the element so located (Fig 4.1).

In simple terms K_1 is given by:

$$K_1 = \sigma\sqrt{\pi a} \qquad (4.2)$$

K_1 is known as the stress intensity factor and it gives the magnitude of the crack tip stress field singularity.

In terms of the energy release rate, G, from the Griffith-Irwin solution;

for plane stress,

$$K_1 = (GE)^{1/2} \qquad 4.3$$

for plane strain,

$$K_1 = (GE/(1 - \upsilon^2))^{1/2} \qquad 4.4$$

4.6 K_1 AND STRESS DISTRIBUTION AHEAD OF A NOTCH.

Under monotonic conditions, there is usually a notch or crack tip plastic field or zone. Because of the influence of the notch there occurs a stress distribution which effectively polarizes the bulk of material ahead of a notch into two different property regions namely, the plastic and elastic

notch fields which coincide with regions very close to and remote from the said tip respectively. The types of region and the stress distribution in them are shown schematically below:

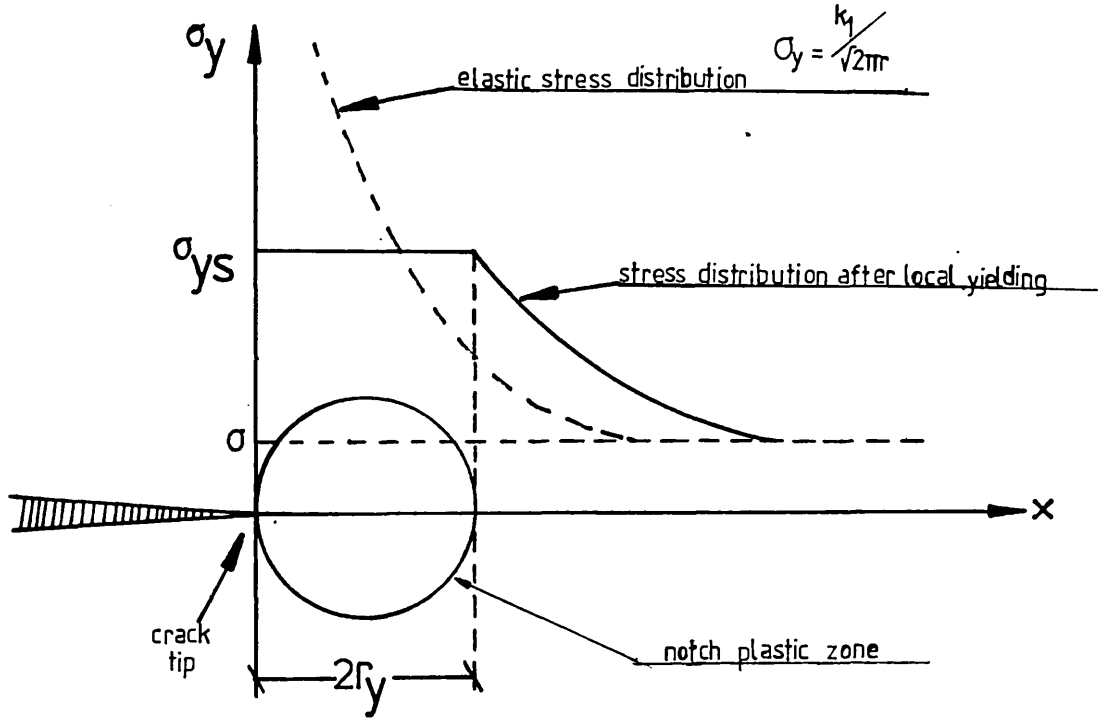


Fig 4.2: Crack tip plastic zone and stress distribution (58)

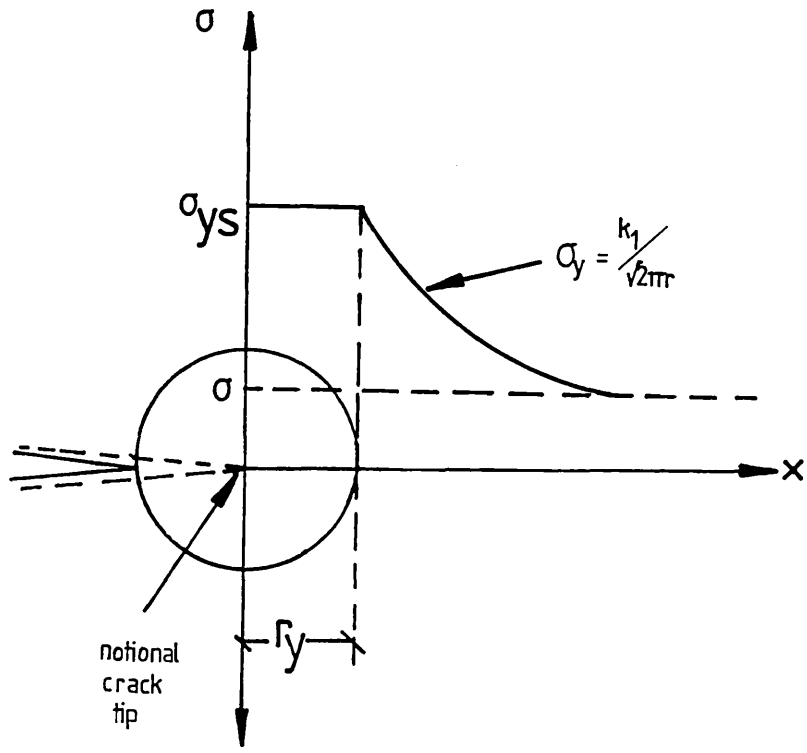


Fig 4.3: Crack tip plastic zone and the effect of Irwin's correction (58)

K can be used in the form expressed in equation (4.2) for a perfectly elastic situation and it may also be modified to include the plastic zone size so that an effective crack size can then be defined in cases of contained yield. In this form:

$$K_1 = \sigma\sqrt{\pi\,(a + r_p)} \qquad (4.5)$$

where,

$a + r_p = a_{eff}$ = effective crack length.

For plane stress,

$$r_p = 1/2\pi\,(K_1/\sigma_0)^2 \qquad (4.6)$$

for plane strain,

$$r_p = 1/2\pi\,(K_1/c\,\sigma_0)^2 \qquad (4.7)$$

where c = 1.7, σ_0 is the uniaxial yield stress under monotonic loading.

Even though this modification works effectively in elastic and strictly contained yield situations, it does not satisfy data correlation requirements for the elastic-plastic and extensive plasticity cases.

4.7 K,ΔK AND FATIGUE ANALYSIS.

Owing to the presence of a notch, crack growth often begins under conditions of local plasticity. At this incipient stage, the crack can be accurately considered a short one. In circumstances of fatigue loading this local region is dominated by fatigue induced plasticity and it is expected that the dominant stress parameter will be the cyclic stress range. Because of this situation, all parameters be they elastic or elastic-plastic in nature should

be calculated using the value of the settled cyclic stress range which is obtainable from a cyclic stress-strain curve.

After initiation, the crack then grows through the plastic region, past the notch elastic field and finally into the bulk stress-strain field where behaviour is unquestionably of the LEFM type and data can be correlated by K or ΔK.

Wherever there is intense local plasticity, as is the case in fatigue circumstances, ΔK or K becomes inadequate for correlation of data especially as the growth rates at this region is either higher (or lower in some metals (62) than those predicted by K and ΔK. The pattern is not dissimilar in the notch elastic field, however, corrected values of ΔK would better satisfy condition in this region. A major reason advanced for the disparity in growth forms between short and long cracks even in the region of notch elastic field is that growth behaviour is affected by the difference in the residual plastic deformation in the wakes of cracks (59). Newman (44), has also argued that the smaller amount of residual deformation (in comparison to that of large cracks) for a short crack results in less crack closure and higher effective K (ΔK_{eff}) and hence a higher crack growth rate.

In a situation where ΔK_{eff} fails to produce reasonable answers, elastic-plastic solutions are opted for. Solutions are often approximate under elastic-plastic assumptions since the concepts are still undergoing

development. Nevertheless, there is no doubt that a lot of investigators favour this approach.

Elastic and elastic-plastic concepts for crack growth correlation in fatigue cases will now be reviewed in order to be able to choose which parameter(s) should be used for the purpose of fatigue data correlation.

El Haddad et al (69)

These workers corrected for the length of the physical crack and suggested an effective crack length a_{eff}:
where,

$$a_{eff} = a + l_o \qquad (4.8)$$

l_o is a material constant.

For a crack growing in the notch elastic field, this modification leads to a formulation,

$$K = K' \ \Delta\sigma\sqrt{\pi(a + l_o)} \qquad (4.9)$$

where K' is the elastic stress concentration factor accounting for increase in crack tip stress owing to the notch.

Evaluation of lo.

l_o is evaluated from the limiting condition where the physical crack size approaches zero. Under this situation,

$$l_o >> a ; \quad K^1 \Delta\sigma \rightarrow \Delta\sigma_e ; \quad \Delta K \longrightarrow \Delta K_{th}$$

and equation (4.9) can then be written as:

$$\Delta K_{th} = \Delta\sigma_e \sqrt{\pi l_o}$$

or

$$l_o = 1/\pi \, [\Delta K_{th} / \Delta\sigma_e]^2 \qquad (4.10)$$

where $\Delta\sigma_e$ is the fatigue limit of the material and ΔK_{th} is the threshold value of the stress intensity factor.

In classical terms, the threshold stress intensity factor is defined as the value of the stress intensity factor below which a long crack cannot grow when under fatigue loading.

Smith and Miller (70).

This is another length correction exercise. If K_T is the theoretical elastic stress concentration factor and K_F is the experimentally

determined fatigue strength reduction factor of a notched specimen, then these authors assumed the following as a basis of analysis:

1 $K_F < K_T$ with the true difference increasing as K_T increases.

2 A size effect occurs for geometrically similar specimens of the same K_T value, ie K_F increases as the size of specimen increases.

3 Non-propagating cracks can occur but only at very sharp notches.

4 The higher K_T values of sharp notches have little or no effect on the stress level separating the propagating and non-propagating crack situations.

These authors argued that the stress value of interest is that which causes crack initiation and its magnitude is expressed as:

$$\Delta\sigma_i = \sigma/K_T \qquad (4.11)$$

where $\Delta\sigma_i$ is the stress that causes crack initiation

σ is the plain specimen fatigue limit.

Based on these assumptions, they suggested that,

for $a < 0.13\sqrt{D\rho}$,

$$\Delta K = \Delta\sigma\sqrt{\pi a\,(1 + 7.69\sqrt{D/\rho})}^{1/2} \qquad (4.12)$$

and

$$\text{for } a > 0.13\sqrt{D\rho},$$

$$\Delta K = \Delta\sigma\sqrt{\pi\ (a + D)} \qquad (4.13)$$

where,

ρ is the actual notch root radius, and

D is the depth of an elliptical notch with the same root radius.

These authors drew some interesting conclusions as regards fatigue crack behaviour. These are summarised as follows:

a All experimental observations of fatigue at notches can be explained by considering the extension of the fatigue crack as being controlled by two plasticity mechanisms namely:

   i) Notch generated plasticity in the early stages of growth being superseded by crack tip plasticity as the crack grows longer.

b That initiation and early growth is a result of the plastic zone generated by the notch.

c Because of applied bulk stress, a crack once initiated will continue to grow to failure in a blunt notch situation.

d Crack growth in regions away from the notch area is as a result of crack tip plasticity.

e The extent of crack tip plasticity must exceed that corresponding to the threshold stress intensity factor ΔK_{th} before an "LEFM"

contribution to crack growth can occur.

f In relatively sharp notches, the stress level required to initiate a crack is low, consequently the notch plasticity is small. Under this condition, it is possible for a crack to arrest after initiation since crack tip plasticity is insufficient to cause continued growth. It was suggested that under this condition,

$$\Delta K > 2\,\Delta\sigma_o\sqrt{D/\Delta K_{TH}} \qquad (4.14)$$

where D is the notch depth.

They argued further that expressions 4.12 and 4.13 can be used to predict if a structure containing a crack will be safe, will initiate non-propagating cracks or fail in service.

4.8 CRACKS WITHIN NOTCH PLASTIC FIELD.

4.8.1 Effective stress intensity factor, K_{eff}.

Elber (71) and Tanaka et al (65) argued separately that the plastically stretched material behind a fatigue crack tip causes the crack to open or close at load levels higher than that inferred from the remote applied loads. This in effect reduces the applied stress intensity factor range to:

$$\Delta K_{eff} = K_{max} - K_{opening} \qquad (4.15)$$

This approach takes into consideration the effect of mean stress on crack

propagation by monitoring crack closure. The authors claim that this modification to the stress intensity factor range will correlate the early stage of notch fatigue crack growth with the long crack growth despite the controversial observations and questioning by some investigators on its capacity to rationalize overloads and environmental effects.

4.9 STRAIN INTENSITY FACTOR.

Having found out that the stress intensity factor, even in most of its modified forms falls short of accurate data correlation below threshold stress (or stress intensity factor).
El Haddad et al (72) argued that a more realistic parameter will be that based on the relatively high strains that develop in the notch plastic region. Consequently, a strain-based intensity factor ΔK_ε was suggested and defined as,

$$\Delta K_\varepsilon = E\ \Delta\varepsilon\sqrt{\pi\,(a + l_o)} \qquad (4.16)$$

where

$\Delta\varepsilon$ is the local plastic strain. It must be noted that $\Delta\varepsilon$ values are not easy to evaluate and usually an elastic-plastic computer program has to be employed in order to be able to obtain these values.

So far, only the models that are fairly representative across board in the vast number of fatigue crack models have been discussed. For full information on fatigue crack growth models, readers should refer to the comprehensive listing by Yokobori (73) and el Haddad et al (74). These papers have not been reviewed here for the sake of briefness.

4.10 THE NEUBER'S RULE.

So far, mention has been of the stress and strain-based intensity factors. The basis of the arguments and assumptions stems up from Neuber's analysis (75) of the local stress-strain field surrounding the notch tip. The conclusion is now known as the Neuber rule.

It states that the elastic stress concentration factor, K_t is equivalent to the geometric mean of the stress and strain concentration characterizing a local stress-strain field, ie,

$$K_t^2 = K_\sigma K_\varepsilon \qquad (4.17)$$

In engineering analysis, the expression

$$K_\sigma K_\varepsilon / K_t^2 = 1 \qquad (4.18)$$

is called the Neuber factor.

Equation (4.17) can be re-written as

$$(\sigma\varepsilon)_{notch} = K_t^2 \ \sigma_o^2/E \qquad (4.19)$$

where,

σ_o is the uniaxial yield stress and E is the Young's modulus. In this form a Neuber hyperbola was defined. Since the right hand side of equation 4.19 is constant for a particular notch configuration, then

$$\sigma\varepsilon = \text{Const.} \qquad (4.20)$$

Equation 4.20 can be represented schematically as follows:

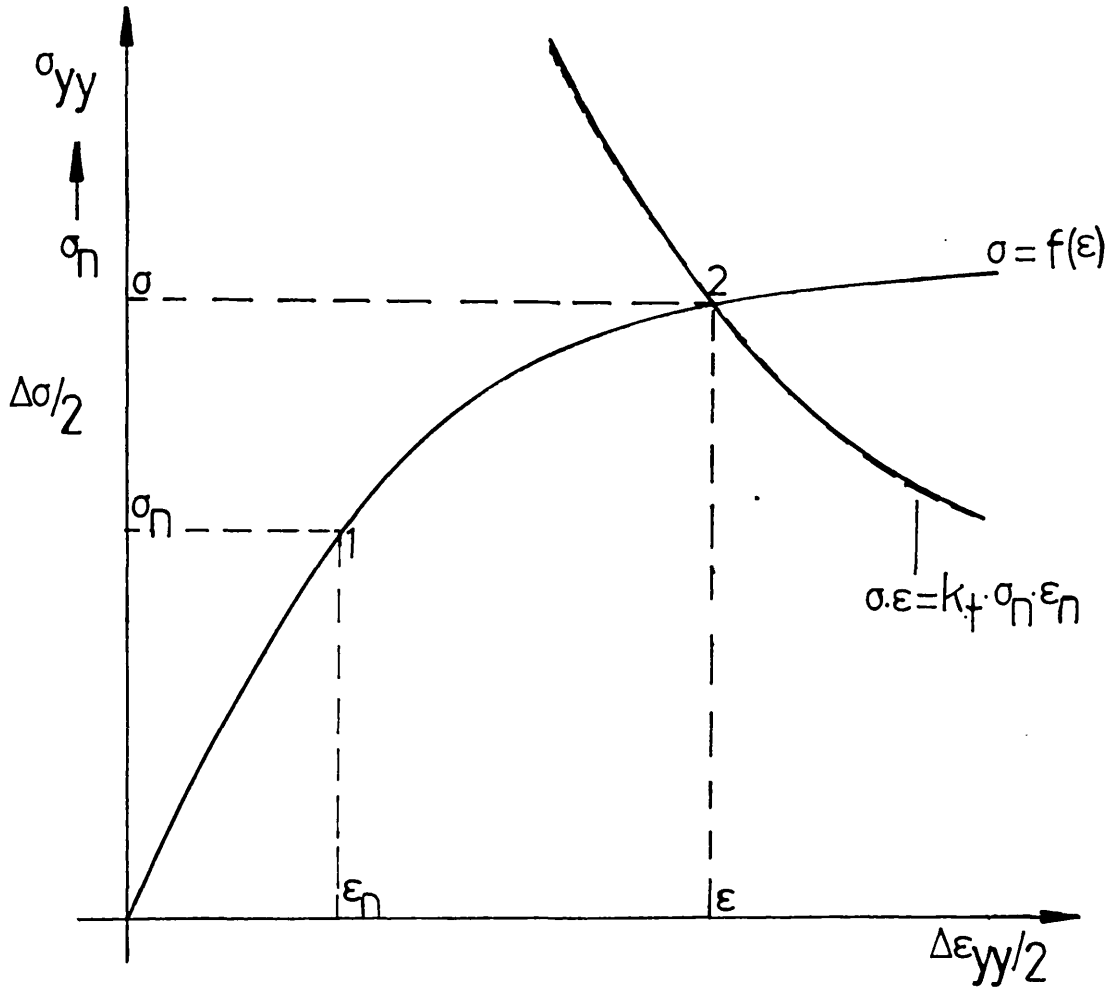


Fig 4.4: Graphical representation of Neuber's rule

For a given notch geometry and a given applied stress, the term $K_t^2\sigma_0\varepsilon_0$ is a constant. The LEFM values are marked by point 1 on the stress-strain curve shown above. The values at the notch root are given by the intersection of the Neuber's hyperbola $(\sigma\varepsilon)_n$ = const,

with the cyclic stress-strain curve $\sigma = f(\varepsilon)$ represented by point 2 on the same figure.

This analysis by Neuber divides the measurable intensity factor at the notch root in two namely K_ε and K_σ as mentioned above. Under LEFM, the constant that is used is the stress intensity factor based on the stress concentration factor K_σ. When contained yield or extensive elastic-plastic situation arises, the value that is referred to is the strain concentration factor K_ε. El Haddad et al as mentioned above adopted this argument in the formulation of the correlation parameter for the two different conditions suggesting specifically that the strain–based intensity factor and stress-based intensity factor correlate the near tip and bulk stress portion of fatigue crack growth respectively. The stress and strain concentration factors are obtainable from an analysis as presented in Figure 4.4.

4.11 TOTAL SHEAR DEFORMATION, ϕ TOTAL.

Hammouda et al (76) suggested that crack growth correlation in fatiguecould be carried out through the consideration of total shear deformation in a material. They suggested that this parameter can be split into two parts namely, ϕ_{LEFM}, which correlates crack tip singularity and a plastic part ϕ_p, which is due to notch plasticity. It is argued that fatigue crack growth rate is proportional to the

quantity ϕ_{total} which is expressed as:

$$\phi_{total} = \phi_{LEFM} + \phi_{Plastic} \qquad (4.21)$$

where ϕ_{LEFM} relates again to the stress intensity factor range as follows:

$$\phi_{LEFM} = \Delta K^2 / \sqrt{2E^2 \Delta\sigma_y^2} \qquad (4.22)$$

and

ϕ_p is calculated from an integral of the shear strain function given as;

$$\phi_p = \int_{l}^{R_p} \gamma \, dx \qquad (4.23)$$

The various parameters used are defined as follows:

$\Delta\sigma_y$ = Cyclic yield stress,

ΔK = Stress intensity factor range,

E = Young's modulus;

ϕ_{LEFM} = Linear elastic fracture mechanics contribution to ϕ total;

ϕ_p = Notch tip plastic field's contribution to ϕ total;

γ = Shear strain ahead of crack tip;

ϕ_{total} = Shear strain ahead of crack tip.

The use of the cyclic stress range is particularly important in this analysis while also the consideration of shear deformation makes it more plausible to represent plasticity effect, and probably in a more accurate way since the analysis of displacement is usually best suited to plastic deformation assessment - a very important aspect of numerical analysis on the computer.

4.12 J BASED CORRELATION OF FATIGUE CRACK GROWTH RATE DATA.

As highlighted above, the stress intensity factor range in its various forms can be used to correlate fatigue crack growth rate data. However, despite the numerous modification, this approach still works best for the notch elastic-field, which neglects short crack growth. Because of the inadequacy of this parameter, several investigations have resorted to the use of some elastic-plastic correlation parameter such as the J-integral and the crack opening displacement (COD). The J-based methods are reviewed here.

Rice's J-Integral

For a homogeneous body of linear or non-linear elastic material free of body forces and subject to a two-dimensional deformation field (plane strain, generalised plane stress, anti-plane strain), in which all stress σ_{ij} depend only on two cartesian coordinates $x_1 (= x)$ and $x_2 (= y)$.

If this body contains a U-notch with rounded tip denoted by the arc as shown in fig 4.5 . In this wise, a straight or sharp crack will be the limiting case.

For this type of notched body, Rice (77), suggested that a path independent integral can be used for analysis around this crack tip.

This integral is defined as follows:

$$J = \int_{\Gamma} (W dy - T.\partial u / \partial x . ds) \qquad (4.24)$$

Here Γ is a curve surrounding the notch tip, this integral being evaluated in a contra clockwise sense starting from the lower flat notch surface and continuing along the path Γ to the upper flat surface.

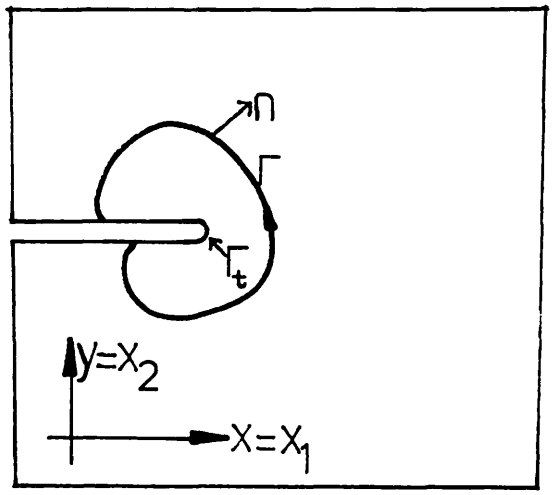


Fig 4.5: Flat surfaced U-notch in a two-dimensional deformation field.
(Γ is any curve surrounding the notch tip; Γ_t denotes the curved notch tip).

T is the traction vector defined according to the outward normal along Γ,
e.g $T_i = \sigma_{ij} n_j$.

u is the displacement vector;

W is strain energy density = $\int_0^{\varepsilon} \sigma_{ij} d\varepsilon_{ij}$;

ds is an element of arc length along Γ.

J is normally regarded as the potential energy available for crack extension. For non-linear elastic materials, it can be estimated as given below.

Experiments are performed at two different crack lengths a and a+da to obtain Fig 4.6.

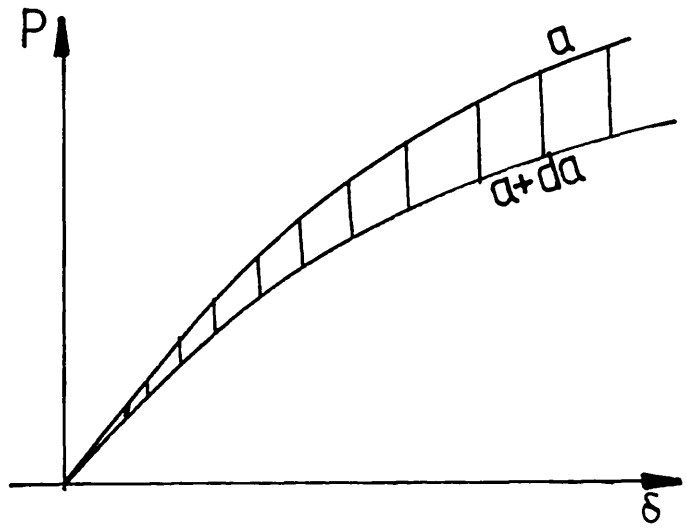


Fig 4.6 Non-linear elasticity - potential energy difference analysis for J.

From this figure,

$$J = -(1/B)(du/da) \qquad (4.25)$$

where,

du = incremental potential energy;

da = incremental crack length; and

b = thickness.

J can be approximated to G, the strain energy release rate under strict and appproximate LEFM conditions.

For plane stress,

$$J_{elastic} = G = K^2/E \qquad (4.25a)$$

where,

K is stress intensity factor;

E is Young's modulus.

4.13 APPLICATION OF THE J-INTEGRAL.

Dowling (78) , assumed a Ramberg-Osgood type of model and used the analysis shown graphically in Figs 4.7a and 4.7b to compute, ΔJ, for half-circular crack surface geometry. This value of ΔJ is given in an approximate form as:

$$\Delta J \cong 3.2 \Delta We_a + 5.0 \Delta W_p \, a \qquad (4.26)$$

where,

ΔWe is the elastic strain energy density;

ΔW_p is the plastic strain energy density;

a, is crack length estimated by taking half the measured surface length in a specimen along the crack line when the specimen is broken open.

It was suggested that ΔJ should be computed by using the compressive part of the cyclic hysteresis loop as against the crack opening or tension part because of problems arising from the inability to observe well -defined opening of cracks.

Using J in this form, the author was able to correlate fatigue crack growth data as presented in Figs 4.8a and 4.8b. Figure 4.9 shows that the scatter band for correlation in which ΔJ was used for small cracks is about the same for long crack scatter. The boundaries of this scatterband were found to be separated by a factor of three in growth rate. This type

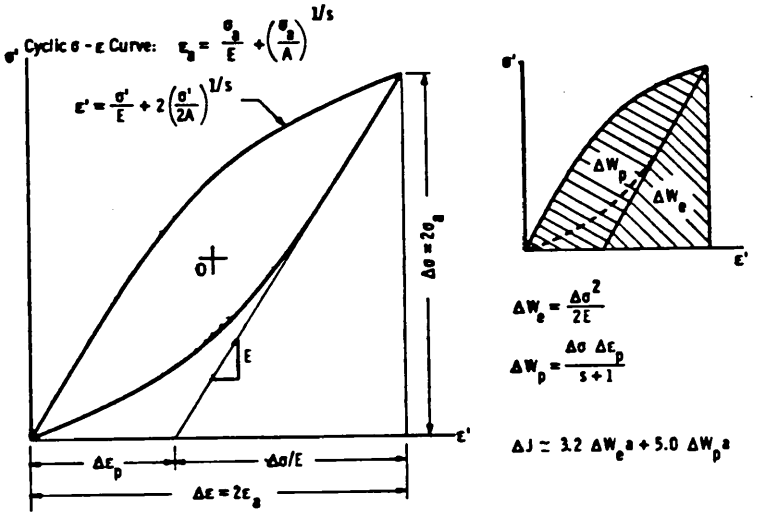


Fig 4. 7a *Estimation of small crack ΔJ from stress-strain hysteresis loops.* (78)

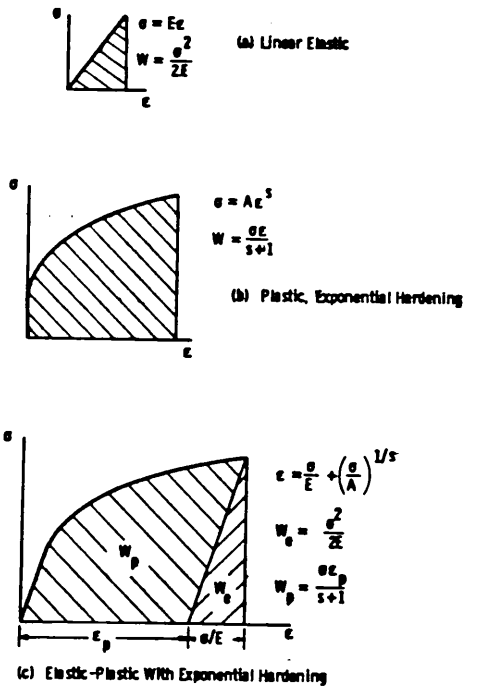


Fig 4. 7b *Three types of idealized stress-strain behavior.* (78)

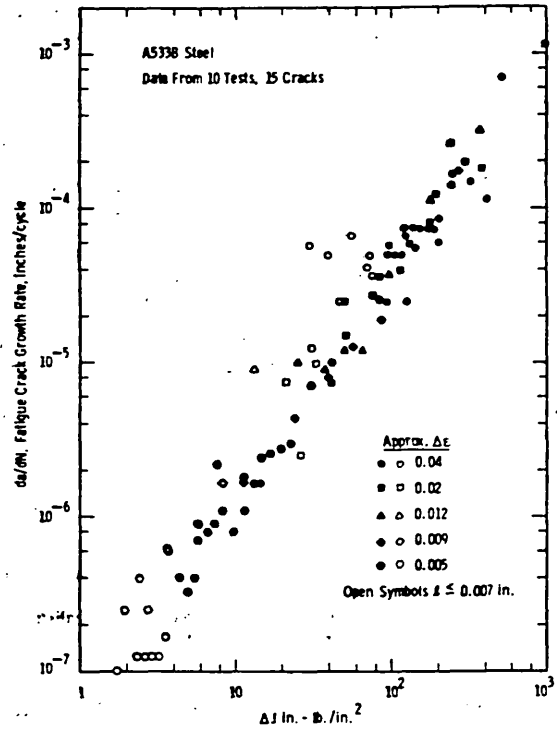


Fig 4. 8a *Fatigue crack growth rate versus Δ J for small cracks under plastic deformation.* (78)

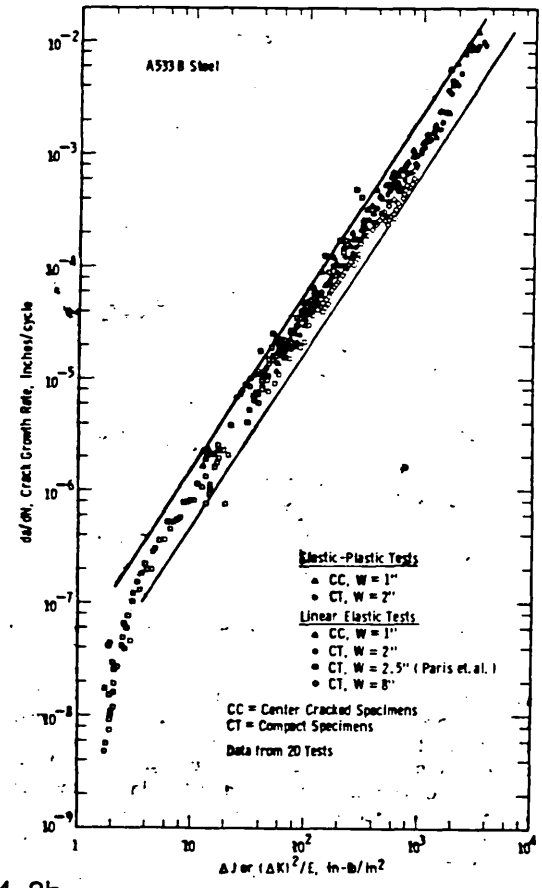


Fig 4. 8b—*Fatigue crack growth rate versus Δ J for various geometries.* (78)

of viability was confirmed as typical for ordinary linear elastic fatigue crack growth rate testing (79).

This treatment was found to offer adequate way of correlating crack growth data except for cracks smaller than 0.007in. At this type of size, the crack is unquestionably well embedded in the notch plastic field and may probably be treatable if something is done to the values of ΔJ or J that are evaluated. This thesis attempts to look at this problem by way of investigating the J-integral further.

El Haddad et al

El Haddad et al (80) also suggested the use of ΔJ for fatigue crack growth correlation when local plastic yielding is involved. Following a type of LEFM modified assumption, they developed the following equations:

$$J_{elastic} = 2\pi F^2 W_e (l + l_o) \qquad (4.27)$$

where

We is the elastic strain energy density, $\Delta S^2/2E$, and

ΔS is the nominal stress range

and

$$\Delta J_p = 2\pi F^2 f(n) W_p (\rho + l_o) \qquad (4.28)$$

where

f(n) is a function of the strain-hardening exponent, n, which is defined in the stress-strain relationship:

$$\Delta S = \alpha (\Delta \varepsilon_p)^n \qquad (4.29)$$

α is the Ramberg-Osgood constant.

$Fe \equiv F_p$ = Geometry correction factor.

W_p is the plastic work, which may be expressed as in Dowling (77) in terms of n, S and plastic strain range

i.e

$$W_p = \sigma \varepsilon_p / (S + 1) \qquad (4.30)$$

in cyclic cases,

$$\Delta W_p = \Delta\sigma \Delta\varepsilon_p / (S + 1) \qquad (4.31)$$

and in general,

$$\Delta J_p = 2\pi F^2 f(n) (\Delta S \Delta \varepsilon_p / (n + 1) (1 + l_o)) \qquad (4.32)$$

since,

$\Delta\varepsilon_p = \Delta\varepsilon - \Delta\varepsilon_e$, the J-integral estimate for a cracked smooth specimen then becomes,

$$\Delta J = 2\pi F^2 (1 + l_o) [(f(n)/n + 1) \{\Delta S \Delta \varepsilon E/E\} - \{(2f(n)/n + 1) - 1\} \Delta S^2/2E] \quad 4.33$$

$\Delta\varepsilon$ is the total strain.

These authors argued that at stress levels causing local notch plasticity but not general yielding, a yield zone develops at the notch

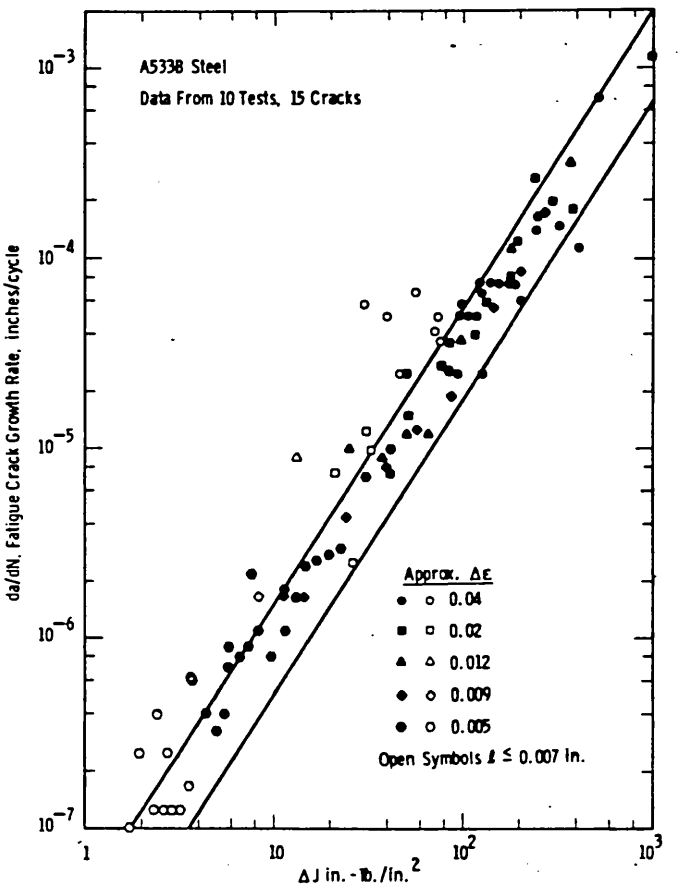


Fig 4. 9—*Comparison of small crack data with scatterband from test results for ordinary and large-size specimens.* (80)

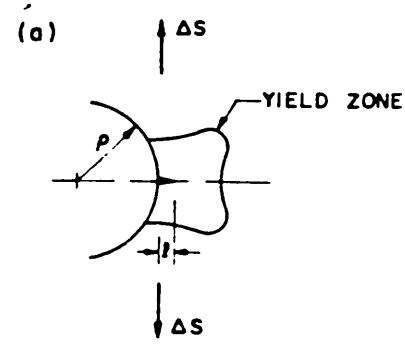


Fig 4.10a Illustration of Yield Zone Around Notch Root for a Short Crack (80)

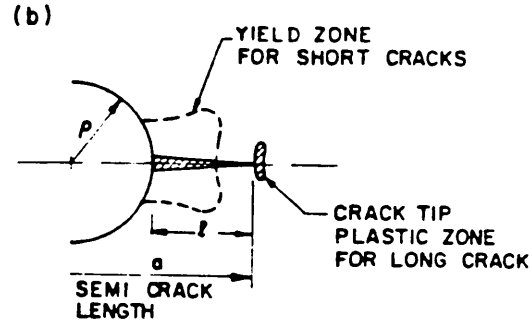


Fig 4.10b Illustration of Yield Zone Around Notch Root for a Long Crack (80)

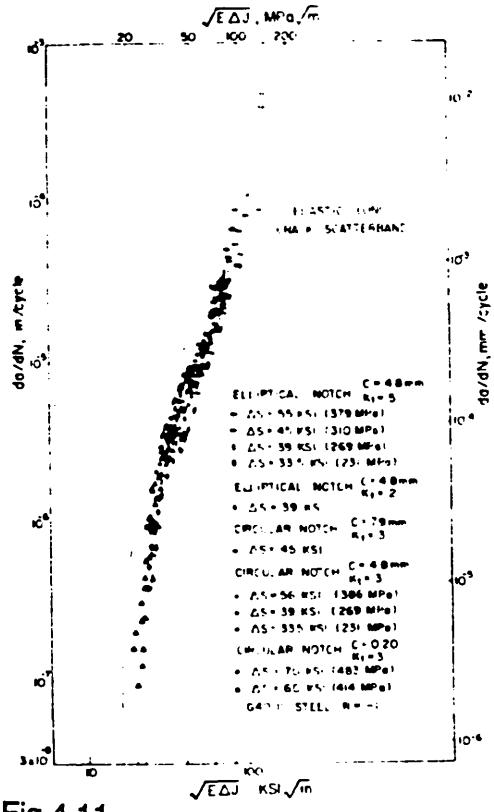


Fig 4.11 Fatigue crack growth rates as a function of ΔJ for G40.11 steel. (80)

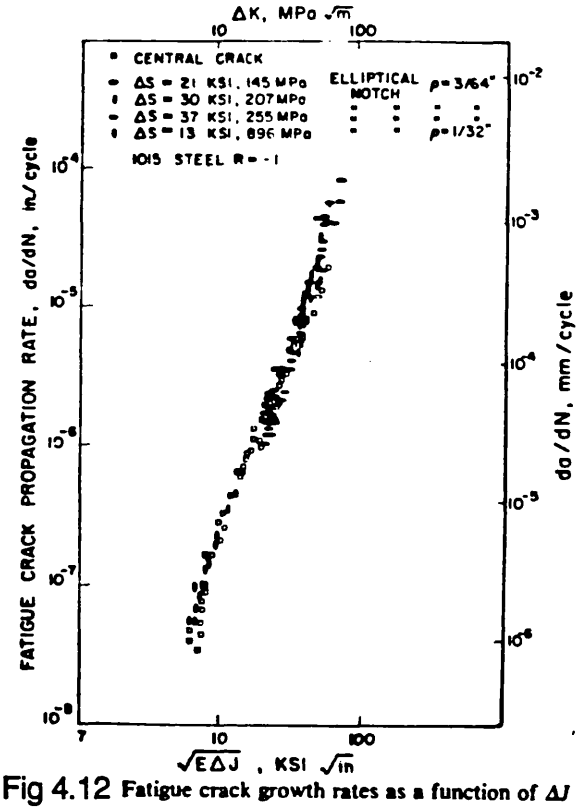


Fig 4.12 Fatigue crack growth rates as a function of ΔJ for 1015 steel. (80)

root as shown in Fig 4.10a. Small cracks may be imbedded in such a yield zone, invalidating linear elastic fracture mechanics and requiring an elastic-plastic solution. Conversely, as shown in Figure 4.10b, long cracks are unaffected by the local notch plasticity and linear elastic fracture mechanics may be applied.

In order to account for these two regions, it is suggested that the stress and strain ranges measurable in the near tip vicinity be used in estimating ΔJ which may then be used for data correlation. Under this condition,

$$\Delta J = 2\pi F^2(l + l_o)\,[(f(n)/n + 1)\,\{\,\Delta\sigma\Delta\varepsilon\,E/E\} - \{(2f(n)/n + 1) - 1\}\,\Delta\sigma^2/2E] \qquad (4.34)$$

l_o is still the characteristic crack length defined in relation to the fatigue limit and the threshold stress intensity factor, written as

$$l_o = 1/\pi\,(\Delta K_{th}/\Delta\sigma_e)^2 \qquad (4.35)$$

where

$\Delta\sigma_e$ is the plain fatigue limit. Here, l_o is assumed independent of the applied strain.

The authors have reasonably correlated fatigue crack growth data by using equation (4.34). Their results are summarized as shown in Figures 4.11 and4.12.

Sehitoglu (81) obtained notch strains using the Neuber's rule and cyclic stress-strain curve of A-36 steel to correlate fatigue crack growth in this material. They found out that the data obtained from slot notched plates at R = -1, using linear regression analysis, could be represented by:

$$da/dN = 1.97 \times 10^{-5} (\Delta J)^{1.78} \qquad (4.36)$$

He argued that plasticity effects must be considered during both the crack-initiation and the crack propagation phases of fatigue life.

The J-integral was found to be able to correlate small crack growth in the vicinity of notches as well as the influence of geometry, material and applied stress level on the crack initiation length and also crack propagation out of the local notch strain field at all stress levels.

A notable conclusion in this work was the emphatic appraisal of the elastic-plastic solution i.e J-integral, in the study of crack growth from the incipient stages of growth to the behavioural pattern in the bulk stress or remote elastic field. A typical result of the proposed method is shown below in Figure 4.13.

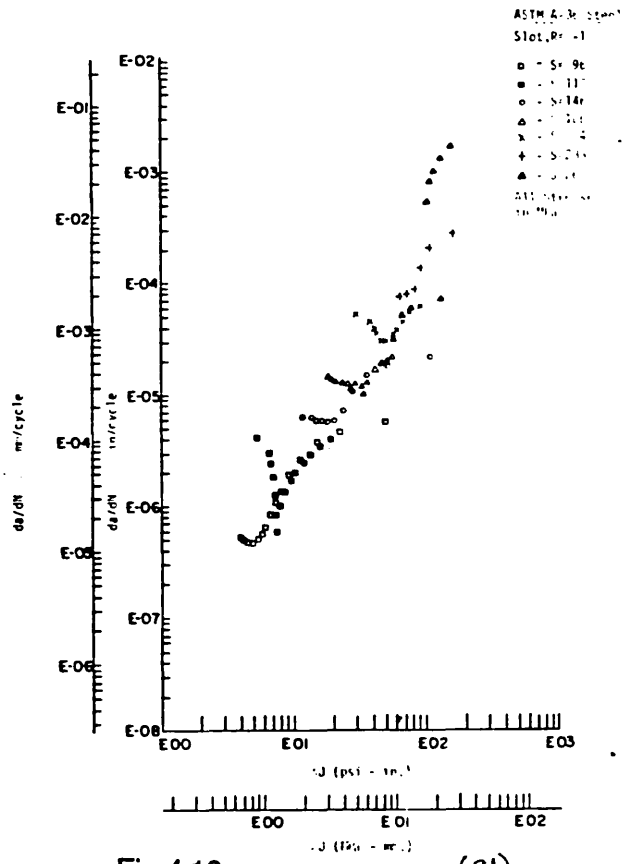


Fig 4.13 (81)

4.14 THE K_R-CURVE CONCEPT TO FATIGUE CRACK GROWTH.

Wilhem and Ratwani (82) investigated the idea of using the crack growth resistance curve to correlate data for both fatigue and fracture (Fig 4.14, Figs 4.15 and 4.16) show fatigue crack growth resistance curves.

They concluded that on a wide range crack growth resistance curve, the lower crack extension range developed from fatigue crack growth data as shown in the Figures, can be considered to be an extension of the statically developed (increasing load) resistance curve.

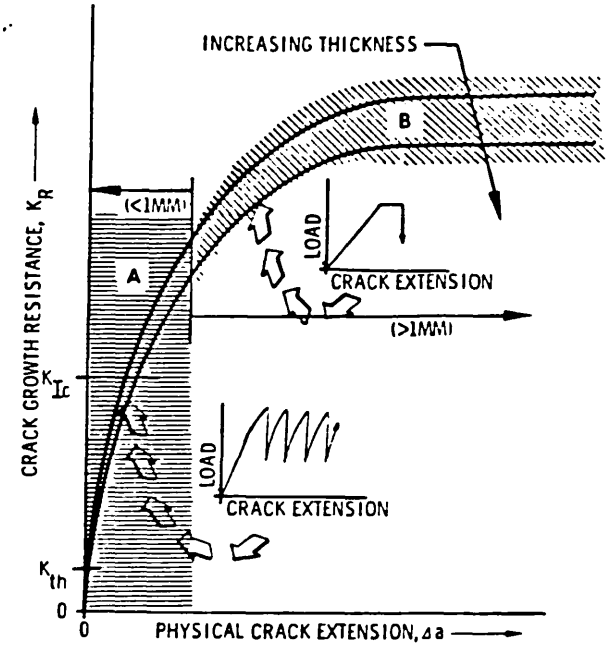


Fig 4.14 **Representation of wide range crack growth resistance** (82)

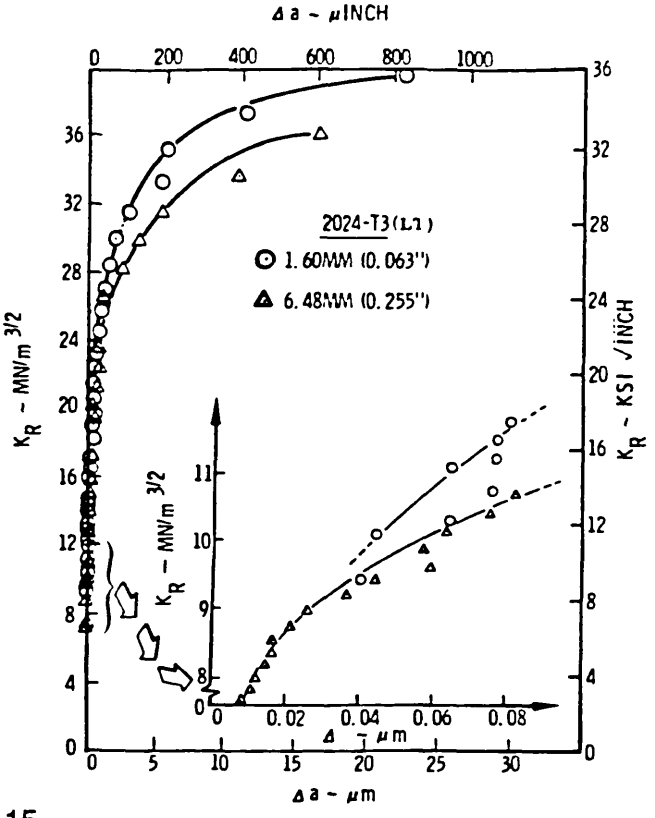


Fig 4.15 **Fatigue crack growth resistance for two thicknesses of 2024-T3 aluminum** (82)

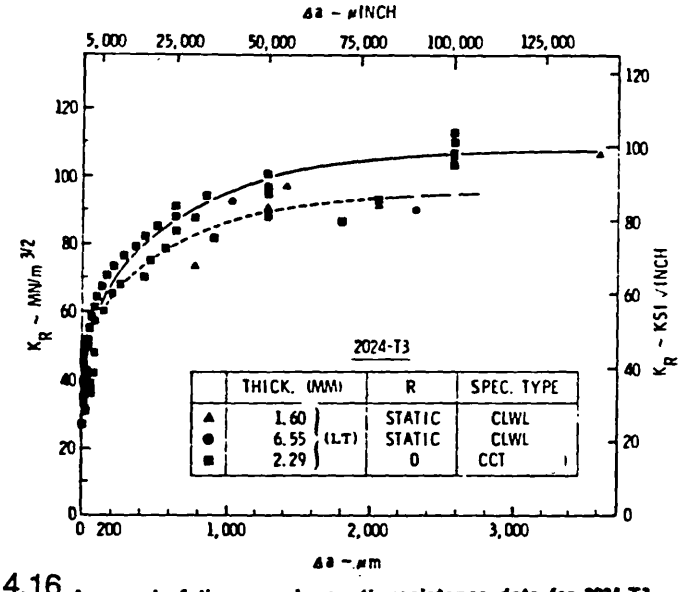


Fig 4.16 **Low cycle fatigue crack growth resistance data for 2024-T3 aluminum** (82)

Furthermore, they showed that cyclic stress ratio influences the production of K_R-curves for fatigue crack growth purposes. Fig 4.16 summarizes this study. However, fatigue crack growth studies via R-curves are still limited and confined to elastic growth only.

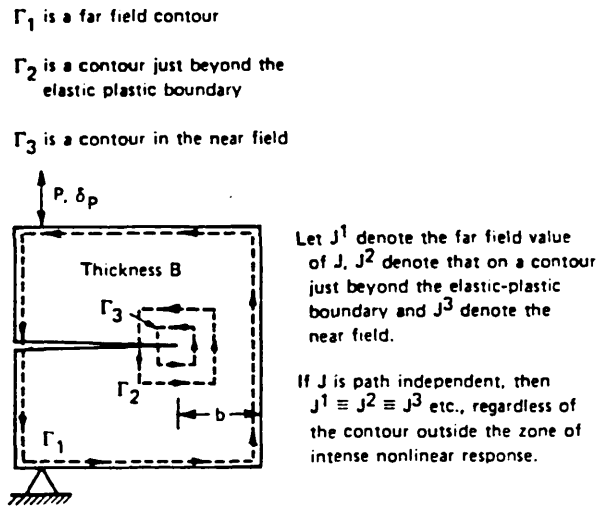


Fig 4.17 Concept of Near Field J in Applications to Variable Amplitude Cyclic Histories (85)

Shih and Smith (83) have done extensive investigation on most of the suggested macroparameters and they found out that ΔK, ΔK_{eff}, ΔK_ε and ϕ_{total} are not able to correlate fully all the notch fatigue crack growth

data in the near notch field, with the corresponding long crack data away from the notch.

They argued that ΔJ is the most reliable candidate for data correlation in fatigue studies. Further studies will be carried out on near and far field J-integral values later in this thesis.

4.15 UNIQUENESS PROBLEM OF THE J-INTEGRAL.

Parks (84), worked with the deformation theory and elastic-plastic finite element method and concluded that J is path dependent within the crack tip element or in the HRR field despite the use of non-linear constitutive law of material behaviour to characterize the region.

Leis and Zahoor (85) on cyclic inelastic deformation used the finite element method and found out that because of crack closure and bifurcation of the specimen, the J-integral ceased to be globally path independent. Furthermore, it was observed that the computation of the J-integral on a contour very close to the crack tip does not follow from simple rules such as the Neuber's rule. Because of these difficulties, they divided J into two, namely the near field J (or J_{NF}) and the far field J (or J_{FF}) for the purpose of analysis. These two parameters were different when computed and thus confirmed J as path dependent. These authors argued that unless concepts such as J_{NF} is valid, it is unlikely that a single parameter measure of the near field will provide general utility in fatigue crack growth analysis. Because of the attendant residual

stresses at stationary crack tips, bifurcation and near tip closure, material transient response in the plastic zone and residual deformations in the wake of the crack, the authors focused on the study of the J_{NF}, (see fig.4.17) They established the existence and uniqueness of J_{NF} and proposed that some simple relationships must exist between J_{NF} and J_{FF}.

McMeeking (86) also using finite elements and the deformation theory under plain strain conditions detected path dependence of J in the crack tip field. Fig 4.18 shows J being path dependent at region very near the notch or crack tip. He argued that a relationship exists between the near field J and the remote J and that for R/b < 0.5, (87).

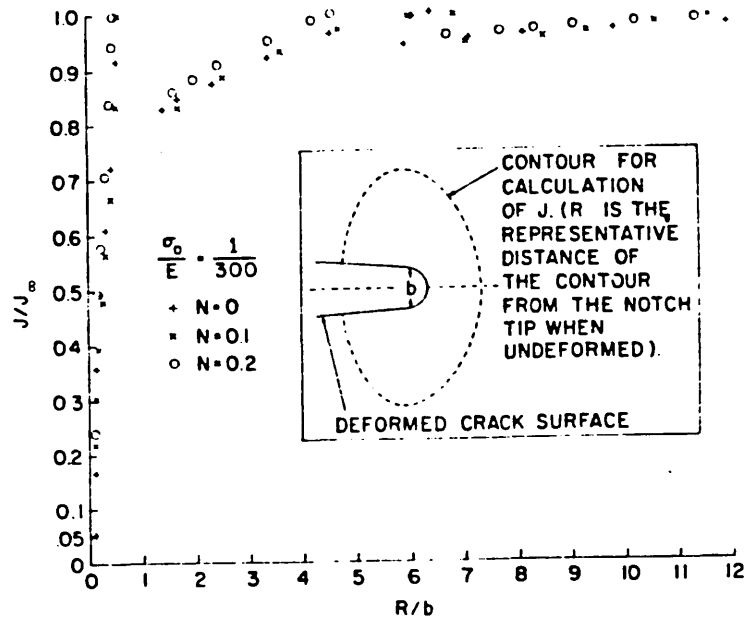


Fig 4.18 J-integral Versus Distance From Notch Tip (Finite Element Analysis) to Show Path Dependence of the J-integral (87)

$$J_{NF}/J_{FF} = \ln (b/b_o) / [(b/b_o - 1) f_o] \qquad (4.37)$$

where,

b is current width of notch tip;

b_o is original width of notch tip (i.e size before deformation starts);

f_o is a non-zero constant chosen to match the gradient of the line for a particular hardening index. Here, $f_o = 1.8$.

In the same paper, it was noted that J is effectively path independent within the region where small strain theory is applicable.

Rice and Tracey (88) and Tracey (89), using singular crack elements and flow theory of plasticity noted that the J-integral is path independent under conditionsof small-scale yielding. Despite the fact that this work fails to throw some light into what might happen to J in the near crack tip element, the authors implied that J might become path dependent inside this near tip field where high residual stresses dominate. When this happens, they suggested that the value of J_{NF} will be a numerical constant times the remote value of J. The result will then be approximate because small-scale yielding assumptions are still valid.

The above studies show that J or ΔJ (for fatigue purposes) is a reliable parameter for correlating crack growth from initiation to bulk field behaviour. When a material is homogeneous, the J-integral is path independent under small scale yielding. In conditions where residual stress etc, cause bifurcation of specimen into regions of different properties, J ceases to be path independent and the reasonable thing to do

is to separate this parameter into the near field and remote field, J_{NF} and J_{FF} respectively. The literature shows that almost all investigators observed that something has to be done in order to unify the characterizing parameter J_{NF} and J_{FF} before J can be used for fatigue crack growth. This special problem is investigated through the use of finite-elements and flow theory of plasticity in the next Chapter.

4.16 THE COD AS A CHARACTERIZING PARAMETER.

The other fracture parameter for correlating crack growth especially in situations of intensive plasticity is the crack opening displacement (COD). First suggested by Wells (90, 91), Ingham et al (92) observed that a cracked loaded specimen tends to rotate about a certain point approximately half way across the remaining ligament as shown in Fig 4.19.

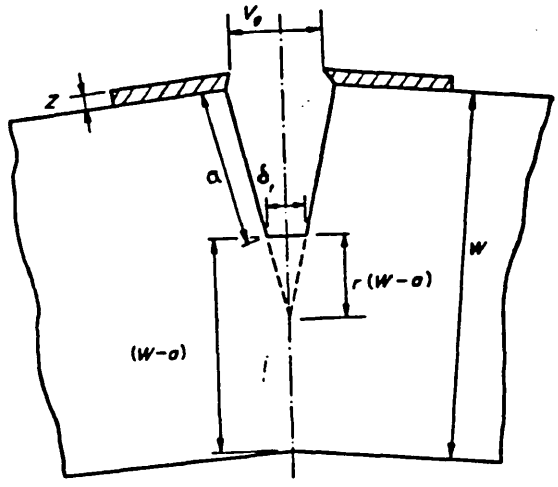


Fig 4.19 Model for the Determination of COD

On this observation, they suggested that the COD can be evaluated from the following expression,

$$Vg/\delta_t = 1 + a + z/\, r(w - a) \qquad (4.38)$$

where V_g is the clip gauge measurement at the edge of the specimen.

δ_t is the crack opening displacement (COD);

w is the total length of ligament;

a is crack length;

r is the rotation factor which has to be determined in order to be able to evaluate δ_t. This factor remains constant over a certain range of values.

z is the height of the clip gauge above the mouth of specimen as shown above.

For the linear elastic (LEFM) situation, generally,

$$\delta = (4\sigma/E)\sqrt{(a + r_p)^2 - x^2} \qquad (4.39)$$

for strict LEFM $r_p = 0$

r_p is plastic zone correction factor;

$a + r_p$ is the effective crack length;

x is distance moved by tip of crack along the horizontal axis;

σ is the remote applied stress.

For the general yielding fracture mechanics, Wells (90) and Burdenkin et al (93) adapted the Dugdale model of strip yielding at the crack tip (94) to express the COD as follows:

$$\delta_t = 8\varepsilon_y a/\pi \log \sec (\pi\sigma/2\sigma_y) \qquad (4.40)$$

On expansion and putting $\varepsilon_y = \sigma_y/E$,

$\delta_t = (8\sigma_y a/\pi E)[1/2\ (\pi\sigma/2\sigma_y)^2 + 1/12\ (\pi\sigma/2\sigma_y)^4 + 1/45(\pi\sigma/2\sigma_y)^6 + ..]$ (4.41)

For small scale yielding ie where σ is close to σ_y, only the first term is significant and the expression reduces to:

$$\delta_t = \pi\sigma^2 a/E\sigma_y \qquad (4.42)$$

In fatigue situation where the stress is reversed every half cycle, the reversed plastic zone must be taken into account. This is about (1/4)x (the monotonic plastic zone size).

Rice (95) suggested the replacement of σ_y by the yield range $2\sigma_y$ experience by a specimen under fatigue loading. Hence in reversed loading situation,

$$\delta_t = \pi\sigma^2 a/E\ 2\sigma_y \qquad (4.43)$$

4.17. APPLICATION OF COD TO FATIGUE CRACK GROWTH.

LEFM Condition.

Donahue et al (96) proposed that the rate of fatigue crack growth in the linear elastic range should be related to the crack tip opening displacement. Following this line of thought a crack growth relationship was suggested as follows:

$$da/dN \times COD = \Delta K^2/\sigma_y E \qquad (4.44)$$

Equation (4.44) was modified for the presence of a threshold for fatigue crack growth and put in the following form;

$$da/dN = A\,(COD - COD_{TH}) = (A/\sigma_y E)(\Delta K^2 - \Delta K_{th}^2) \qquad (4.45)$$

where,

$A \propto \sigma_y/E$ for the linear elastic case.

When A is substituted into (4.45)

$$da/dN = (A'/E^2)(\Delta K^2 - \Delta K_{TH}^2) \qquad (4.46)$$

Some investigator eg Bates and Clark (97), Frost and Dixon (98) and Frost and Pook (99) have noted the dependency of da/dN on $\Delta K^2/E$ away from the threshold region in steel. This observation is encouraging in terms of the use of (4.46) for correcting crack growth under LEFM conditions.

4.18 PLASTICITY CONDITION.

When extensive plastic deformation occurs, the rate of crack growth accelerates compared with the linear elastic behaviour (100)

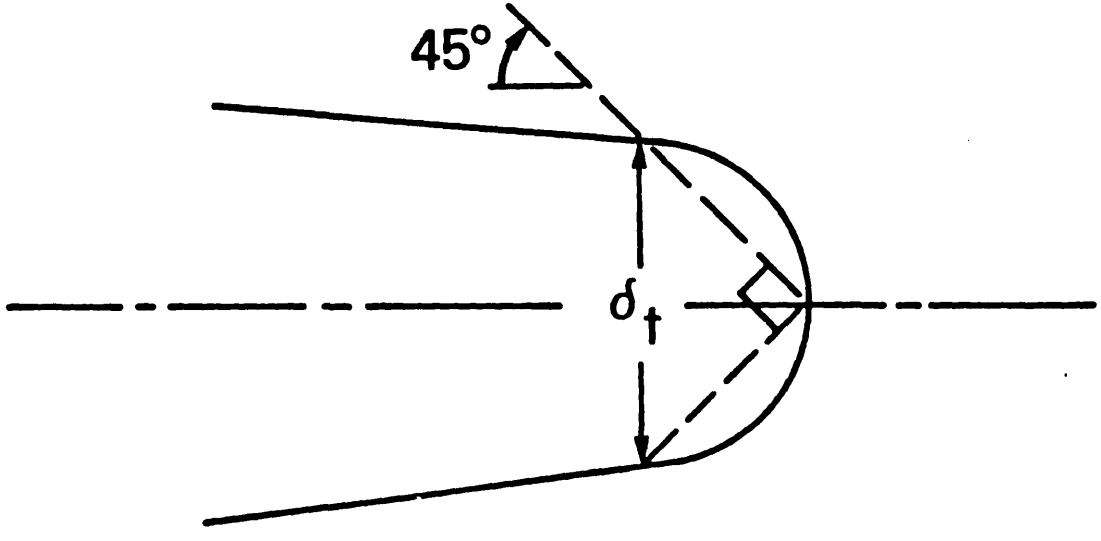


Fig 4.20 Idealization of the Crack Opening Displacement (COD)

and this circumstance is taken care of by means of the ΔJ approach. It is well documented that the use of ΔJ is approximately equivalent to the use of COD concept. For a non-work hardening material of yield strength, σ_o, these two parameters will be related as expressed below:

$$COD = m J/\sigma_o \qquad (4.47)$$

where,

m, is a constant related to the degree of workhardening of a given material.

The magnitude of the COD is reduced by workhardening (101, 102).

Tomkins (103)

This author attempted to correlate crack growth data in the plastic range through the use of the COD. He proposed that crack advance occured by a sliding-off process. The crack tip deformation field is idealized by the introduction of two plastic hinges at ± 45 degress to the crack tip as shown in Fig 4.20, without deformation allowed in the area around and within the hinges. The extent of the hinges, D, was assumed to be proportional to the Dugdale (94) plastic zone size for:

$$D = \sqrt{2}\left\{(\pi^2\sigma^2/4\sigma_c^2)\, a\right\} \qquad (4.48)$$

where σ_c was taken to be the cyclic tensile strength, which is not the

yield strength.

The cyclic stress and strain were presumed related by:

$$\sigma_c = \Delta\sigma = K\Delta\varepsilon_p^{\,n} \qquad (4.49)$$

Substituting 4.49 into 4.48 yields,

$$D = \sqrt{2}\left\{(\pi^2 L^2/4 \;.\; \varepsilon_p^{\,2n}/\; \sigma^2)\right\} \qquad (4.50)$$

where $L^2 = K^2\sqrt{a}$

In this study, Tomkins assumed that incremental sliding-off, $d\delta$, is represented as,

$$d\delta \cong D d\varepsilon_p \qquad (4.50)$$

This allowed a simple estimate of the crack opening to be made and this opening was related to the increment of growth per cycle. This choice ensured that the rate of advance per cycle will be a small fraction of the plastic zone size which accords well with previous experimental observation.

In this wise,

$$da/dN = \delta/\sqrt{2} = (\pi^2/8\,(\Delta\sigma/2\Delta\sigma)^2\;(\Delta\varepsilon_p/(2n+1)))a \qquad (4.51)$$

McEvily (104)

McEvily suggested that the rate of crack advance can be considered as simply proportional to the crack opening displacement and wrote that:

$$da/dN = c_2\delta = C_2\ 16/.\pi\ T_{1a}/E.\ \ln \sec \pi/2\ \sigma/\ T_1 \qquad (4.52)$$

In the fully plastic range, T_1 is taken to be the true cyclic tensile stress at necking instability given by:

$$T_1 = K'\ (M)^{n'} \qquad (4.53)$$

where M is the true tensile strain value measurable at the neck of a smooth specimen, and E is the secant modulus measured from the zero stress point on the compression side of the cyclic stress-strain loop to the peak tensile stress, neglecting the elastic strain. With,

$$\sigma = K'\ (\Delta\varepsilon_p/2\ )^{n'} \qquad (4.54)$$

Combining 4.52, 4.53, 4.54,

$$\Delta a/\Delta N = c_2\delta = C_2\ 16/\pi\ (M)^{n'}\ (\Delta\varepsilon_p/2)^{1\ -\ n'}\ x\ a\ \ln \sec [\pi/2\ (\Delta\varepsilon_p/2M)^{n'}]\ 4.55$$

It was suggested that $C_2 = 0.5$.

Following this stated line of thought, the crack growth behaviour was separated into its plastic and elastic components as follows:

$$\Delta a/\Delta N = [(\Delta a/\Delta N)_e + (\Delta a/\Delta N)p \qquad (4.56)$$

and

$$(\Delta a/\Delta N)_e = A/E^2(\Delta K - \Delta K_{TH})^2 (1 - (\Delta K/Kcc - Kmax)) \qquad (4.57)$$

$$(\Delta a/\Delta N)_p = 8/\pi (M)^{n'} (\Delta\varepsilon_p/2)^{1-n'} \ln \sec [\pi/2 (\Delta\varepsilon_p/2M)^{n'}] f (Jcc) \qquad (4.58)$$

n' is the strain hardening exponent;
A is a constant ; and

J_{cc} is the initial value of the J-integral.

Dover(105)

Stress cycling tests were carried out on the Amsler under axial tension compression cycling on sheet specimens and three point bending tension test on bend specimens. Crack lengths were measured by a travelling microscope.

Fig.(4.21) summarizes the results of COD cycling on 1/2in thick specimens, constituted as described earlier. The parameters used are the total COD δ_t, range δ_{tR}, and the loop width δ_{tL} which are illustrated in the hysteresis loops in Fig 4.22.

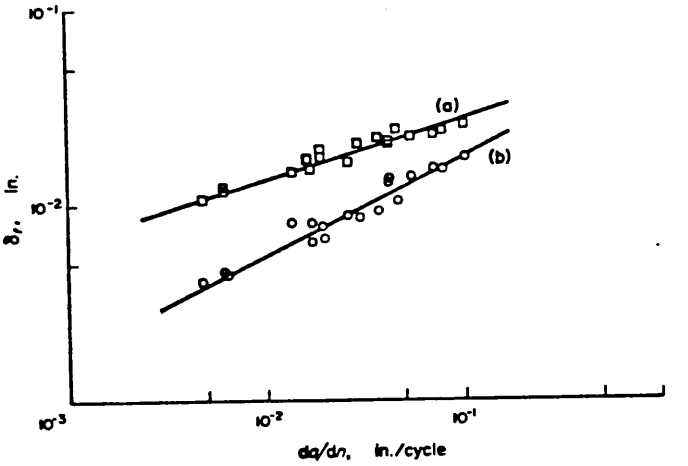


Fig 4.21 Results of COD Cycling Results for 1/2 in Thick Mild Steel (105)

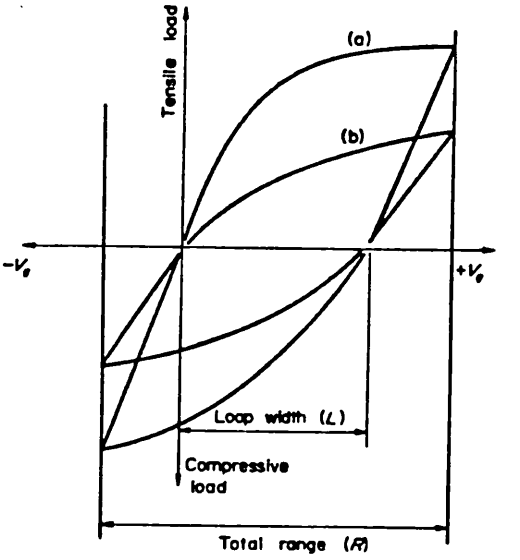


Fig 4.22 Hysteresis Loops: a - Initial Loop; b - Loop After Several Cycles Causing Crack Extension (105)

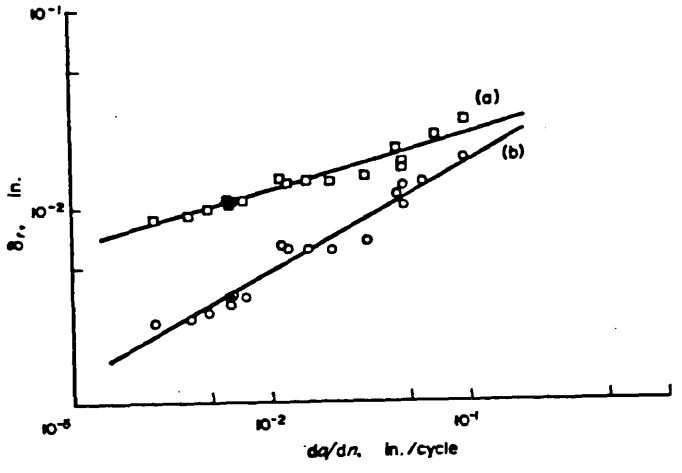


Fig 4.23a Results of COD Cycling Results of 1/4 in Thick Mild Steel (105)

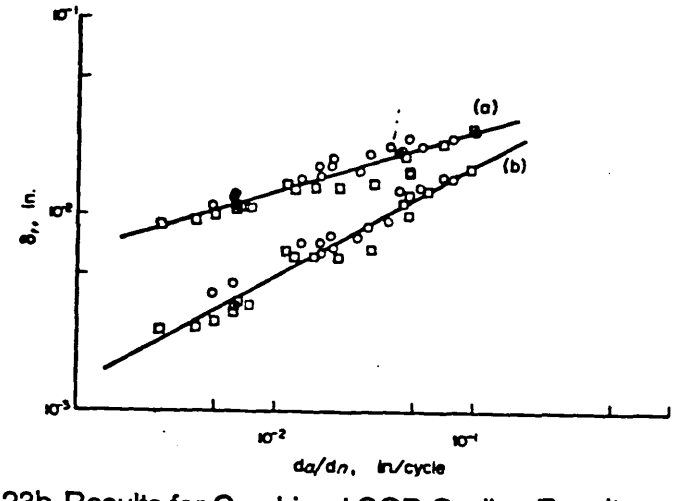


Fig 4.23b Results for Combined COD Cycling Results for 1/4 and 1/2 in Mild Steel (105)

Notches can either be sharp or blunt in configuration. It must be noted that when mention is made of the sharpness or bluntness of a notch, reference is being made to the shape of its root. The root of a notch is therefore very important in studies related to notched members because, as willbe explained in the following Sections, its bluntness or sharpness determines the engineering processes that contribute to crack formation and its subsequent behaviour when still within the region of influence of the notch.

4.20 BLUNT AND SHARP NOTCH BEHAVIOUR.

The definition of blunt and sharp notches can only be done in relative terms. If an arbitrary critical radius, r, is considered as a datum for comparative classification, then arguing according to the work of Topper and El Haddad (106), differentiation can be made between these two groups.

4.21 BLUNT NOTCHES.

A blunt notch will be defined under (106)'s proposition as that which radius is larger than the datum value, r. With this type of notch, the threshold stress continuously decreases with length and its influence will allow a crack to propagate to failure at a value of stress equal to the initiation stress. The implication is that the

maximum threshold stress occurs at initiation. In these notches, the initial condition for propagation of a crack to failure at a constant stress level is that the notch root stress should equal the endurance limit stress and it occurs at the notch root surface rather than at a finite length.

4.22 SHARP NOTCHES.

These notches will be classified as those which radii are smaller than the arbitrary chosen radius r. They occur as short or long cracks in structures. It has been observed that those notches will initiate cracks at stress level equal to the ratio of the endurance limit stress at the theoretical stress concentration factor, K_t. If then the stress at initiation is $\Delta\sigma_i$, $\Delta\sigma_e$, is the endurance limit stress and K_e is the stress concentration factor, then,

$$\Delta\sigma_i = \Delta\sigma_e/K_t \qquad (4.61)$$

It is known that under continuous loading situations, "geometric readjustments" go on at the notch tip as a consequence of the localized high stresses and strains. Because of this process, the value of K_t changes and this causes a change in the value of $\Delta\sigma_i$. For continued propagation to fracture, $\Delta\sigma_i$ must be increased with increasing crack length until it reaches a maximum given by,

$$\Delta\sigma_p = F\,\Delta\sigma_e/(1+\sqrt{c/l_o}) \qquad (4.62)$$

where

$\Delta\sigma_p$ is the stress for stable propagation to failure;

$\Delta\sigma_e$ is the endurance limit stress;

F is a geometry correction factor;

l_o is a notch dependent correction factor and a material constant;

c is the major depth of the notch.

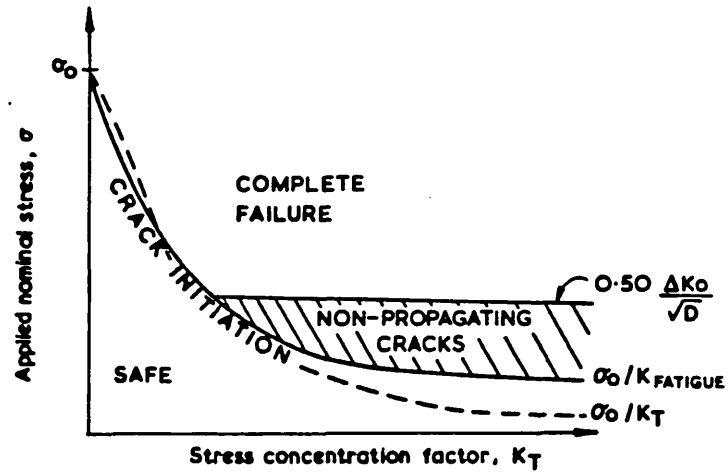


Fig 4.24 Summary of Crack Behaviour Under Completely Reversed Tension - Compression Loading

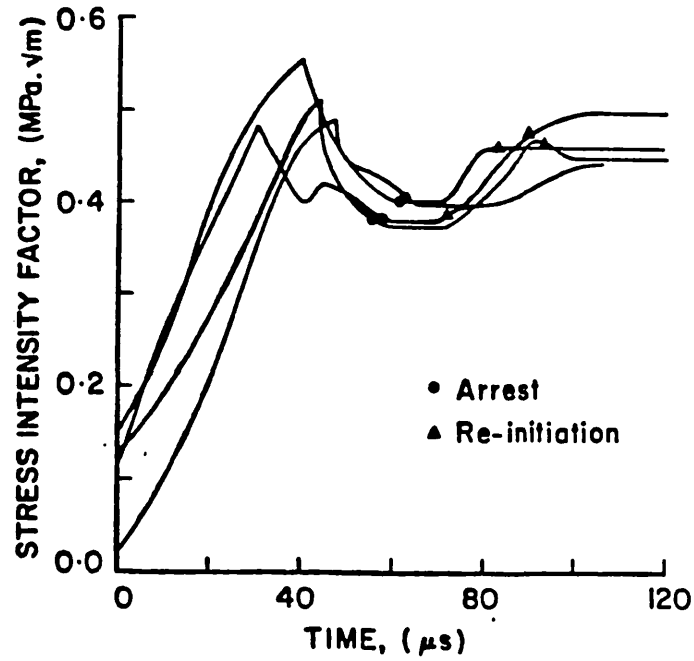


Fig 4.25 Stress Intensity Factor Histories for Crack Arrest Experiments (107)

4.23 CRACK ARREST.

Fenner et al (107) first noted that cracks can initiate at notches, grow for some distance and eventually become non-propagating. Later, Frost separately and with other workers (108 - 112), confirmed that this observation was correct since their metallographic examination of aluminium alloys and mild steel revealed that an initiated crack would grow for sometime and then remain non-propogating for innumerable cycles.

Conditions of notch geometry, nominal stress range and mean stress corresponding to no crack initiation, non-propagating cracks and complete failure were defined in the cited references and summarized in Fig 4.24. The key points illustrated by these data are summarized as follows:

a) That a level of alternating stress, $\Delta\sigma_{th}$, threshold cyclic stress range, exists which is independent of notch configuration, hence K_t. Long cracks do not grow below this stress level.

b) That a critical value of the stress intensity factor exists above which non-propagating cracks can occur.

c) That the alternating stress required to predict the initiation of cracking in a notched member is given by $\Delta\sigma_e/K_t$.

The results of the experiments by Ravi-Chandar and Knauss (113) aimed at investigating crack arrest are compounded in Figs 4.25 and 4.26.

From Fig 4.25, it is clear that when the stress intensity factor reaches

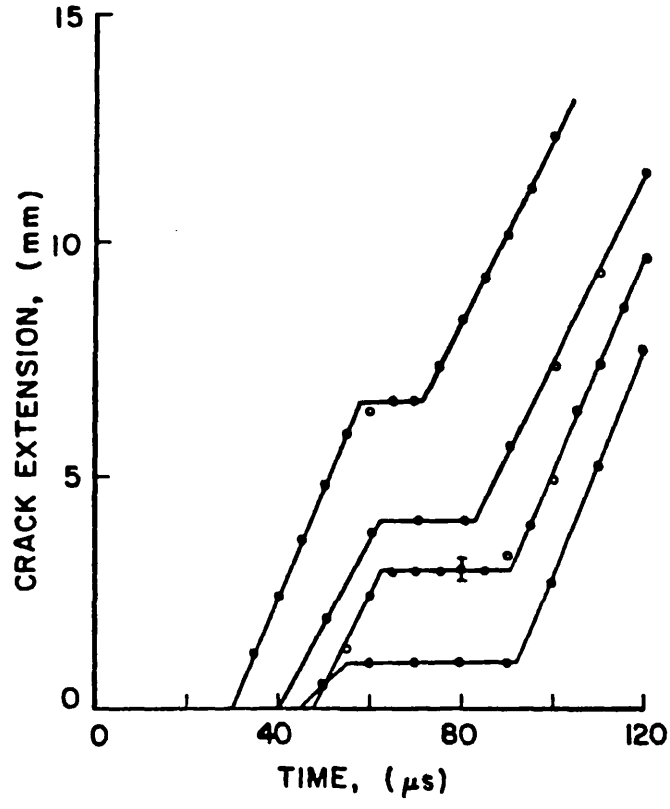


Fig 4.26 Crack Extension Histories for Crack Arrest (113)

the critical value, the crack starts to propagate at a (constant) velocity as shown in the crack extension histories of Fig 4.26. It was argued that as the crack begins to propagate, the accompanying unloading causes the stress intensity factor to decrease. When the stress intensity factor decreases to a level such that the energy release rate is no longer sufficient to maintain stable crack propagation, the crack arrests.

It is worth noting that there was no crack deceleration phase prior to arrest, also they observed that the instantaneous stress intensity factor at crack arrest appears to have a fixed value for the materials investigated. Bradley and Kobayashi (114) and Kalthoff et al (115) came to the same conclusion whilst working with high speed camera to monitor the stress intensity factor history.

In the light of the paper reviewed and the supporting experimental evidence presented earlier, the authors concluded that there exists an "arrest stress intensity factor" which is a material property.

SUMMARY ON NOTCH FATIGUE ANALYSES.

1 Notches in cyclically loaded structural components cause stress intensification in the vicinity of the notch tip. The material element at the tip of the notch is subjected to the maximum stress amplitude $\Delta\sigma_{max}$ which is often more than the yield stress σ_y even if the applied stress is

less than σ_y. Consequently, the localized material element in the tip of a notch is plastically deformed and crack initiation needs to be studied by an elastic-plastic analysis. This observation was closely emphasised in the work by Saanouni and Bathias (116).

2 Notch tip plasticity occurs and dominates the early stages of crack growth. The Neuber's rule can be employed for estimating the local plastic notch field strains and stresses and these can be used to work out approximate values of the J-integral which will in turn be used in establishing ΔJs.

3 The growth rate kinetics for cracks near the notch or small cracks are faster than those for large cracks when analysed according to LEFM assumptions and this growth has been found to be dependent on notch tip geometry. The reason for this was put down to the breakdown of underlying continuum mechanics assumptions (117,118).

4 Small cracks can grow at stress levels which are below the threshold value of the stress intensity factor range ΔK_{TH}. When this happens data are best correlated by the ΔJ concept.

5 In order to be able to correlate fatigue data in a realistic way, the J-integral, hence ΔJ, should be separated into some near field, J_{NF} and far field J_{FF} values. There is the likelihood of a relationship between J_{NF} and J_{FF}.

6 The crack opening displacement (COD) can be adapted for fatigue data correlation especially in the notch plasticity dominated region.

CHAPTER FIVE

THE INFLUENCE OF CYCLIC PLASTICITY ON THE PARAMETERS J-INTEGRAL AND THE CRACK OPENING DISPLACEMENT (COD).

5.1 INTRODUCTION.

It was established in Chapter Four that the J-integral and crack opening displacement, COD, are the most promising parameters available for correlating elastic-plastic, hence, fatigue crack growth rate data. Because fatigue is an essentially plastic phenomenon, these parameters are employed and studied extensively in this Chapter. As noted then, high residual stresses and intensive plastic deformation characterize the region of the crack or notch tip in a given notched structure. Because of this occurence, bifurcation of a test piece occurs and this causes path dependence of the J-integral especially.

The concept of ramifying J into J_{NF} and J_{FF} ie near field and far field values respectively is necessary. The earlier studies cited suggest that the near field parameter, J_{NF} and the far field or uniform material J_{FF} values must be related in some rationalized way. The aim, therefore, in the present study is to establish this relationship and hopefully come out with a unique parameter which is rationally based on the far field J-integral value.

In the following study, the "experimental" test piece used on the computer was constituted in such a way as to monitor real state bifurcation

caused by the interaction of the notch with cyclic plasticity. A plastic/cyclic stress range region of a particular magnitude and size (in area) was introduced each time and its effect on the value of J or COD was noted. The data generated were plotted on the accompanying figures shown. Afterwards, a non-dimensional analysis of the plastic components of J_{NF} and J (uniform material) was attempted. The same type of rationalization, by way of non-dimensional analysis was also carried out for the crack opening displacement, COD, data.

5.2 THE RESIDUAL STRESS FIELD AND CYCLIC PLASTICITY.

A notch of any kind and size is known to produce a residual stress or notch plasticity field. On loading, this field becomes one of material instability. Various micro processes interact to cause crack initiation under loading of various kinds, hence its name the FRACTURE PROCESS ZONE.

As a consequence, of reversed plasticity or cyclic loading, this region is subjected to further instability. After several cycles and at steady state, the residual stresses in the notch tip region assume a steady value, normally referred to as a saturated stress range. The magnitude of this stress is arguably a multiple of the monotonic yield stress ie,

$$\sigma_{notch} = C\,\sigma_o \qquad (5.1)$$

where,

C is a numerical constant and material dependent,

σ_{notch} is the settled cyclic residual stress at the notch plastic field,

σ_o is the uniaxial yield stress.

For a typical hardening material, e.g many of the aluminium alloys, the constant C may have its lower limit as 2. This is substantiated by the study carried out in reference (93). Under these circumstances, a relationship can then be written for this lower limit steady state cyclic stress range as:

$$\Delta\sigma = 2\sigma_o \qquad (5.2)$$

However, on the evidence of the cyclic stress-strain curve for Titanium-6211 presented in Chapter 3 (Appendix F), it is not all materials that settle down to this type of condition, hence equation (5.2) with C = 2 may not be universally representative of minimum stress range in work-hardening materials. Because of this reason, it was argued that some steady-state residual stress field may settle at $\Delta\sigma < 2\sigma_o$. This type of field was therefore investigated.

5.3 THE FINITE-ELEMENT "EXPERIMENTAL" SPECIMEN (MESH).

Fig (5.1) shows the finite-element mesh employed for analysis. It is a 100mm x 200mm plate which contains a very small crack for which a/W = 0.05. Where,

a is crack length, and

W is the total length of ligament along the x-axis.

Fig (5.2) exhibits a typical bifurcated configuration of the same size of mesh. The shaded portion is the notch residual plastic stress and strain field. It is characterized by a stress of a magnitude equal to the settled cyclic stress range.

The mesh in Figs (5.1) and (5.2) contains 99 elements and 346 nodes.

5.4 THE COMPUTER PROGRAM.

The program used is an elastic-plastic one. It has its origin in the work of Owen and Hinton (44). It is used in the form compiled for the section by Bleackley (43). It can monitor up to two materials at a time. This program is displacement controlled and is capable of calculating the elastic -plastic values of most of the fracture mechanics parameters used in analysis such as the J-integral, stresses and strains, plastic and elastic components of work and the crack opening displacement (COD). It can analyse two materials in a run and is able to monitor either plane strain or plane stress condition.

5.5 PATH INDEPENDENCE OF THE J-INTEGRAL FOR HOMOGENEOUS SPECIMENS.

The first set of J-integral values was obtained for a homogeneous mesh. The input data for running the program were set out as suggested in the user

manual prepared by the author of the program (48). This exercise was necessary in order to be able to establish the validity of the said program to the desired purpose. In simple fracture mechanics term and as suggested by Rice (77),J should be path independent for a homogeneous material as long as its values are not measured too close to the notch or crack tip singularity. The data are summarized and compared in Fig (5.3).

In order to plot these curves, the J-integral was evaluated for four contours, one of which was defined very close to the notch singularity, the next two inside elements of approximately equal size and further away from the region of effective notch influence and the third cutting across different element sizes. The graphical presentation shows relative path independence for J in a homogeneous material under different path characteristics.

5.6 THE BIFURCATED SPECIMEN.

5.6.1 Effect of Bifurcation on the J-Integral.

In carrying out these experiments, it was assumed that the region immediately ahead of a very short crack as shown in the meshes presented in Figs (5.1) and (5.2) is characterized by an amount of residual stress as a result of an imposed settled cyclic stress range at the notch plasticity region.

The first set of data was collected by prescribing a settled cyclic plastic

stress range equivalent to $\Delta\sigma = 1.5\sigma_0$ (where σ_0 is the monotonic yield stress of the tested material). The data obtained are presented in graphical form in Fig (5.4). The second category of data, presented in Fig (5.5) was obtained by imposing on the near field a different settled cyclic stress range of $\Delta\sigma = 2\sigma_0$, where σ_0 is as defined before.

Size effects were measured by changing the number of elements that make up the field - with prescribed cyclic stress range - immediately ahead of the notch. The chosen sizes were constituted as 16, 30, 40 and 75 elements in a mesh that was originally made up of 99 homogeneous elements.

The distinctive revelations in Figs (5.4) and (5.5) show that the J-integral decreases with increasing size of the notch cyclic plasticity area. The results here also reveal that the J-integral calculated in the homogeneous specimen is not representative of the practical situation for crack growth especially at the onset of growth or at the short crack growth stage.

5.6.2 Test for Uniqueness.

In an attempt to elucidate the disparity between the values of the J-integral calculated in the plasticity dominated near field and the LEFM far field domain, two paths were chosen in either field and the computed data were plotted in Figs (5.6a and b). The meshes used contained notch plastic areas sized by 30 and 40 elements respectively. It is evident from

these plots that there is no unique value of J across fields in a bifurcated specimen. Also path independence of J was found in paths calculated inside each field within limits of numerical accuracy.

5.6.3 Effect of the Magnitude of Cyclic Stress Range on the J-Integral.

Two data studies were carried out here. They are reported below. The size of the near field cyclic plasticity region is 40 elements.

Data for three different cyclic plastic stress ranges were extracted for this mesh configuration. The values plotted in Fig (5.7) are those of the J-integral computed for paths lying outside the border of the notch plasticity region (J_{FF}). It will be noted from this figure that even for the same size of plastic zone, the values of J are different for different stress ranges. This goes to substantiate that the J-integral may not be path independent when it is calculated from paths drawn to run inside regions of different characteristic strengths.

Fig (5.8) compares data for the same type of mesh configuration at different stress levels for the J-integral calculated inside the notch plasticity zone (J_{NF}). It can be concluded from this plot that the values of J_{NF} are also state dependent. This serves again as a basis for questioning the path independence of the J-integral in real notched specimen behaviour under fatigue loading.

Fig (5.9) is another manifestation of the effect of notch region residual

cyclic stress level on the J-integral for a configuration characterized by a 30 element notch plasticity region. This study also shows that different values of the J-integral result for the three stress ranges of $1.2\sigma_0$, $1.5\sigma_0$, and $2\sigma_0$. Again the non-uniqueness of J with varying path condition is reflected.

The "experimental" evidence above has shown that when a notched specimen ceases to be homogeneous (as assumed in the initial theory of the J-integral), the J-integral becomes path dependent with its values determined by the properties of the region in which a given path is defined. Because of this behavioural pattern of the correlating parameter J, problems like those associated with short crack growth occur.

It is now obvious that the difference in data correlation in the near field fatigue/plasticity dominated region and the LEFM far field when using the J-integral is due to the fact that J is affected by the consequence of the interaction between a notch and cyclic plasticity.

Attempts will now be made to find an adoptable hybrid of the J-integral which can correlate data more accurately from the fatigued or cyclic plasticity region to the LEFM regions of a specimen.

5.7 THE PLASTIC J-INTEGRAL.

The plastic component of the J-integral is of relevance in the following analysis. Fig (5.17) compares the values of contained yield values of the J-integral in the near and far fields. This plot shows that most of the effects so far discussed as regards the disparity in the values of J_{NF} and J_{FF} are absent in the purely elastic situations, hence the emphasis on the plastic component. Having established the uniqueness of the J-integral in the elastic region, we can now proceed.

In order to obtain the plastic parts of the integral, the elastic component had to be deducted from the total value of the parameter. Data were then extracted for those load increments at which there was not more than 10 yielded elements in the mesh. In this wise, the data plotted in Figs (5.11) to (5.17) represent elastic/contained yield ones for the homogeneous and different notch plastic zone size and settled cyclic stress ranges. The common point of deviation is taken as the maximum elastic value of the J-integral in each case. These elastic values were noted for each configuration and then subtracted from the total J of the same configuration to give the plastic values plotted in Figs (5.18) to (5.21).

Having obtained the plastic components, the next objective then is to rationalize the J data by attempting a form of non-dimensional analysis on these plastic values.

5.8 RATIONALIZED NON-DIMENSIONAL ANALYSIS FOR THE J-INTEGRAL.

For the non-dimensional analysis carried out, the plastic component of the J-integral for the homogeneous mesh and those in the plastic region of the bifurcated meshes were used. For example, plastic data were extracted for a path prescribed inside a notch fatigue/plasticity dominated region of say a size of 40 elements.

The other parameters needed are the Young's modulus, and the flow stress of the cyclic and LEFM regions. A numerical constant was also used for complete rationalization.

The rationalized non-dimensional form of J employed is written as:

$$J_{cgc} = J_{pl}\, E/C\sigma^2_{fl}a \qquad (5.3)$$

where J_{cgc} is rationalized non-dimensional J;

J_{pl} is the plastic component of J.

For the homogeneous specimen,

$\sigma_{fl} = \sigma_{LEFM} = \sigma_o$,

C is a numerical constant for a given specimen constitution. It will be explained later in the text.

For the bifurcated specimen,

$\sigma_{fl} = \Delta\sigma$ (the settled cyclic stress range)

and C = 1.

E/a is a constant for all cases.,

E is the Young's modulus.

a is the size of notch or crack.

σ_o is the monotonic yield stress.

5.9 PROCEDURE FOR DETERMINING J_{cgc}.

STEP 1: Take the plastic component of the J-integral calculated for the path inside the notch plasticity zone and divide it by the square of the characteristic notch plastic cyclic stress range. It is not very necessary to multiply with the ratio E/a since this is a constant for a chosen notch configuration and material.

STEP 2: Divide the plastic component of J for the uniform or homogeneous material by the square of the LEFM stress which is assumed to be equivalent to the characteristic monotonic yield stress of the chosen material. Again, it is not necessary to multiply by the ratio E/a for the same reason as that given above.

STEP 3: This part of the analysis deals with the rationalizing constant, C. It is found that there is a large disparity between the non-dimensional values obtained in the two steps explained above. C is then the constant factor that relates one non-dimensional value to the other. Various values of C are chosen and used to divide the non-dimensional value obtained in Step 2 until they were near enough to those calculated in Step 1. The final outcome offers a relationship between the non-dimensional near and far field magnitudes of J-integral.

The data obtained were plotted on Figs (5.18) to (5.21) for reasons of comparison with the initial plastic J data. A good agreement was found between the rationalized non-dimensional values.

5.10 THE CRACK OPENING DISPLACEMENT.

The numerical experiments carried out here are similar to those of the J-integral. These consist of choosing different sizes of notch plastic region and settled cyclic stress ranges in order to compute related values of the crack opening displacement.

5.10.1 EFFECT OF NOTCH PLASTICITY REGION ON THE COD.

Figs (5.22) to (5.24) exhibit the effect of the size of the notch plasticity zone on the crack opening displacement at different values of the notch

zone settled cyclic stress range. The chosen cyclic stress ranges are $1.2\sigma_0$, $1.5\sigma_0$ and $2\sigma_0$.

5.10.2 Effect of Different Notch Zone Settled Cyclic Stress Ranges on The Value of The Cod.

The mesh bifurcated by a plasticity zone of 30 elements in size was used for carrying out these "experiments". Curves were plotted for different stress ranges of $1.2\sigma_0$, $1.5\sigma_0$ and $2\sigma_0$. Fig (5.25) presents these curves. It is explicit that the variation in the settled plasticity/cyclic stress range caused variations in the computed values of the COD for the fixed size of notch plastic zone.

5.11 DETERMINATION OF δ_{cgc}.

In order to carry out this analysis, the elastic parts of the COD were extracted and plotted in Figs (5.26) and (5.27). As done earlier, the common point of deviation for the homogeneous case and the bifurcated mesh cases is noted and used in subsequent analysis which deals with obtaining the plastic component of the crack opening displacement.

These plastic components were computed by subtracting the elastic components from the total COD. In attempting to non-dimensionalize and rationalize the plastic CODs, the following type of analysis was carried out:

If δ_{NDIM} is the non-dimensional plastic component of COD, then

$$\delta_{cgc} = \delta_{pl} \; E/C_1 \, \sigma_{fl} \, a \qquad (5.4)$$

δ_{pl} = plastic component of COD

For the homogeneous or uniform case,

$\sigma_{fl} = \sigma_{LEFM} = \sigma_o$

Once again, C_1 is an emperically determined constant which reconciles the disparity between the non-dimensional values of COD for the uniform and bifurcated meshes,

and E/a is a constant for a chosen notch size and material;

a is the notch or crack size;

E is the Young's modulus of elasticity.

For the bifurcated specimen,

σ_{fl} is the characteristic notch plastic/cyclic stress range, e.g $1.5\sigma_o$.

and $C_1 = 1$.

The three steps highlighted above for J_{cgc} were adopted again but this time the magnitude of σ_{fl} and not its square was used.

These data, were again plotted on the same axis with the plastic components of COD for comparison . Good agreement was found between the rationalized non-dimensional data.

We have now been able to establish unique hybrids of the J-integral and COD by way of rationalizing their plastic non-dimensionalized values. Equations 5.3 and 5.4 will now be applied in the next Chapter in order to establish a way of correlating adequately crack growth from the fatigue affected notch tip region called the near field to the far LEFM dominated field The behaviour of these parameters will be studied in detail and attempts will be made to explain crack arrest and crack propagation to failure once a crack initiates. Also, the adaptability of these new parameters to regions that engulf a small crack, hence, the behaviour a small crack itself is investigated in chapter six.

5.12 THE ORIGIN OF CONSTANT C or C_1.

In the preceeding section, the constants C and C1 were used to rationalize the non-dimensional values of plastic J-integral and crack opening displacement.On a J-displacement curve for the near field and far field regions (Fig. 5.6), it was revealed that the disparity between the two quantities measured i.e, J_{NF} and J_{FF} would be eliminated by using a factor of two and not factors as high as were encountered in our analysis. This observation has then led to ask the following questions,

a). Where does C come from?

b). What is its significance?

The EnJ (119) design method has been adopted for answering these questions. This method allows for studying the response of the J-integral under varying degrees of sectional yielding. In the present situation, the extent of yielding is different in the separate fields of a bifurcated specimen under the same loading condition. When this exists, the two equations employed for producing a relevant design curve are as follows:

for $\sigma/\sigma_y = \varepsilon/\varepsilon_y < 1.2$,

$$J/G_y = (\sigma/\sigma_y)(1 + 0.5(\sigma_f/\sigma_y)^2) \qquad (5.5)$$

for $\varepsilon/\varepsilon y > 1.2$,

$$J/G_y = 2.5(\varepsilon/\varepsilon_f - 0.2) \qquad (5.6)$$

where,

J is the J-integral,

σ_f is applied plastic stress,

ε_f is the applied plastic strain,

σ_y and ε_y are yield stress and strain respectively.

$G_y = \gamma^2 \sigma_1^2 a / E$

The data obtained by using equations 5.5 and 5.6 are plotted on fig. 5.33.

It can be seen from the curves that the magnitude of J increased rapidly immediately after contained yield for the homogeneous specimen. The values of J calculated for the two different sizes of the notch plastic zones

chosen were much lower than those computed for the homogeneous case. When the homogeneous and bifurcated specimens are loaded in tension, for example up to,

$$\sigma_f/\sigma_y = 2,$$

$$J(\text{homogeneous}) \cong 313.25$$
$$J_{NF}(40 \text{ elements}) \cong 6.6$$
$$J_{NF}(75 \text{ elements}) \cong 1.5$$

These data reveal that,

$$J(\text{homogeneous}) \cong 48 \times (J_{NF}\ (40 \text{ elements}))$$
$$J(\text{homogeneous}) \cong 210 \times (J_{NF}\ (75 \text{ elements}))$$

These relationships show clearly the origin of the factor C or C_1 which came up in the empirical determination of the hybrids for different specimen configurations.

5.13 OBSERVATIONS.

5.13.1 THE HOMOGENEOUS SPECIMEN.

Considerable agreement was found between the data collected for different J-paths in the homogeneous material (Fig 5.3).
The agreement between the paths going through different size

configuration and areas of notch effect showed that whatever the attendant condition in a homogeneous specimen, the computed J-integral is path-independent within limits of numerical accuracy. In the investigation carried out, the disparity between data for different paths is about +/- 5%.

5.13.2 INFLUENCE OF THE NOTCH (PLASTIC/CYCLIC STRESS RANGE) FIELD.

Figs (5.4) and (5.5), showed undoubtedly that the introduction of bifurcation through the imposition of a region of cyclic plasticity around the notch tip affected the J data calculated in the region lying outside the notch field region and characterized by the monotonic yield stress.

The pattern of variation is similar for specimens containing notch field cyclic stress ranges of $1.5\sigma_0$ and $2\sigma_0$ (where σ_0 is the uniaxial monotonic yield stress) in that the J-curve decreased with increasing values of the area of notch influence (which is measured in "number of elements").

The curve plotted for data in the far field region when the residual cyclic notch plasticity zone was characterized by 16 elements was found to vary the least from the homogeneous curve. The overall pattern is such that an envelope was defined with the top-most curve corresponding to that of the homogeneous specimen and the lower boundary was defined by the specimen that was assumed to have gone extensively plastic through the imposition of a cyclic stress range on most of the elements of the

representative finite-element mesh. In this case the large cyclic plastic region was sized by 75 elements.

In Fig (5.6) it could be seen that the values of J in either field are unique characteristic of each field.

The values of J calculated in the near field region are higher than those of J evaluated in the far field region. This revelation solved one uniqueness problem only to create another one in that there was agreement between different paths in the same field and none between J_{NF} and J_{FF}.

However, the layout of the curves show that one set of data differed from the other by some factor. This factor is possibly due to the difference in the magnitudes of the characteristic stress in the different fields.

Another interesting point from these figures is that the J calculated in the homogeneous part of the specimen i.e in the far field region is higher than that calculated in the cyclic plasticity notch field.

The magnitude of J in either the homogeneous or plastic near field region was found to vary with the magnitude of the settled cyclic stress range imposed on the near field region for a constant size of the notch plastic zone. Figs (5.7) to (5.9) show these curves.

J was found to decrease with increasing values of the cyclic stress range in the near field.

The contained yield data for J (Figs 5.10 - 5.17) revealed that all the curves coincided until they reached a point where they began to deviate into their respective plastic components. Since this limit point was unique in all cases it was assumed to be of significance. This point was used to establish the magnitude of the maximum elastic value of the J-integral or G, the elastic crack driving energy.

A noteworthy aspect of the study compounded in the Figures mentioned is that the elastic part of the J data for near field and far field agreed reasonably with each other. This observation lends credence to the argument for the universal uniqueness of the elastic limit point for J. Fig (5.10) is especially explicit on this.

5.13.3 PLASTIC AND HYBRID J GRAPHS.

The plastic curves show considerable disparity between data for the homogeneous J and those calculated in the notch cyclic plastic region. On the other hand, the rationalized non-dimensional curves showed considerable agreement within limits of numerical accuracy.

The agreement between these curves show that unique values of J can be established for the different cases studied by way of rationalizing the non-dimensional values in the plastic regime.

These unique values would be tested for fatigue crack growth data correlation in the near and far field regions of a notched specimen.

5.14 THE CRACK OPENING DISPLACEMENT CURVES.

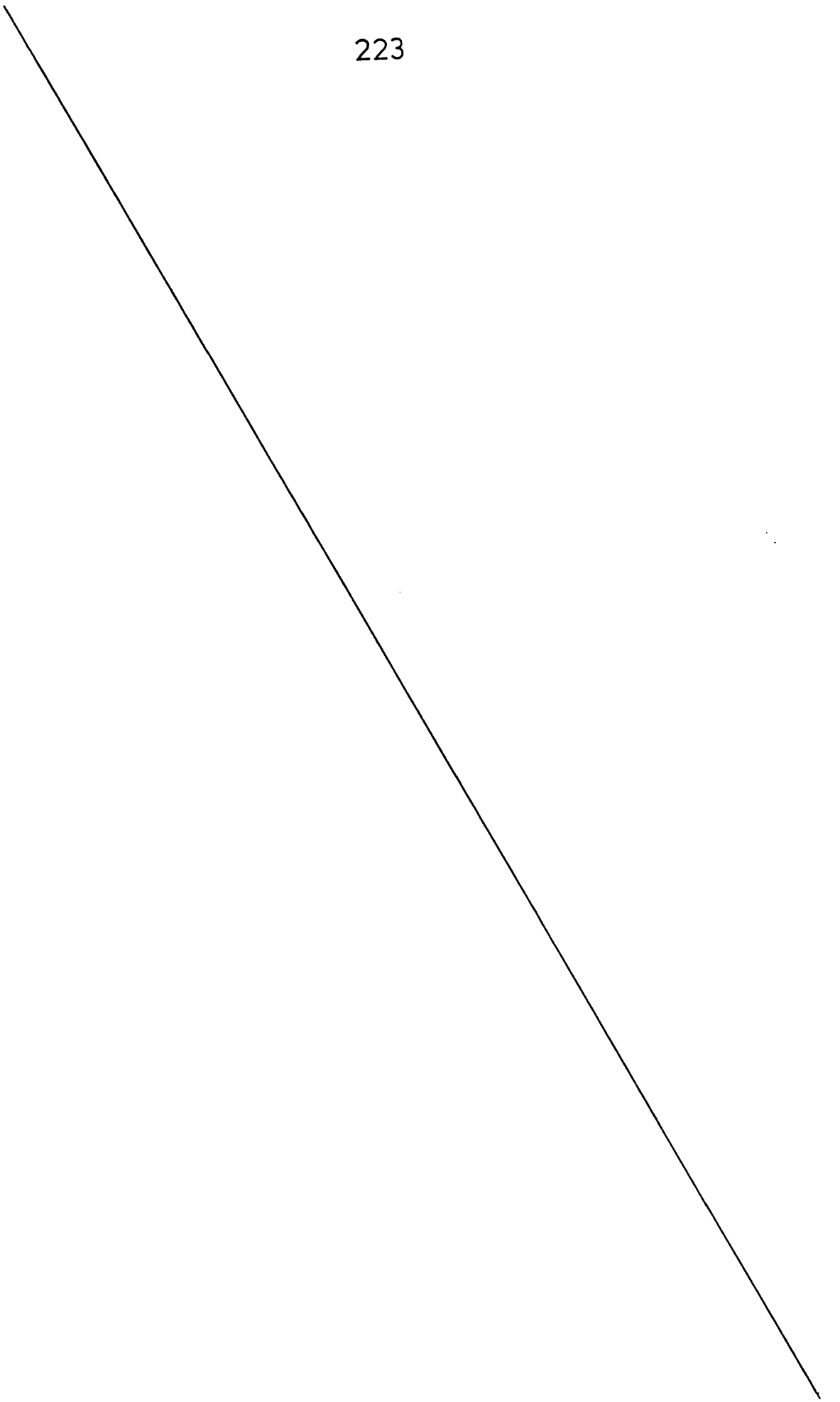
The crack opening displacement (COD) curves presented in Figures (5.22) to (5.24) showed that the data were affected by the size of the notch cyclic plastic field. The variations were similar to those observed for the J-integral with the data decreasing as the size of the notch cyclic plastic field increased.

Similar envelopes were formed for the three stress cases studied. The homogeneous curve and the curve corresponding to the largest size of notch effect region formed the upper and lower boundaries respectively.

The pattern of variation with cyclic stress range magnitude for a chosen size of notch plasticity field was found to be the same as in the J curves. The COD data decreased as the cyclic stress range in the notch plastic stress field was increased for the 30 element case presented. The top-most curve corresponded to a stress range of $1.2\sigma_o$ while the lowest was for a range of $2\sigma_o$.

5.14.1 THE CONTAINED YIELD CASES.

These curves were plotted in order to be able to extract elastic data which was in turn subtracted from the total COD to obtain the plastic component of the COD.



Figs (5.26) and (5.27) revealed that the contained yield curves coincided until about a displacement of 0.3mm before they started to separate into their plastic values. On these figures, the homogeneous curve did not show good agreement with the rest of the curves in the elastic regime. However, the first point of inflexion on the homogeneous curve also laid at about the 0.3mm displacement mark.

In this wise, the elastic components of the COD were taken at the 0.3 mm mark for the homogeneous and bifurcated specimens. The average values of the data were then taken to represent the elastic COD for a chosen configuration.

5.14.2 PLASTIC COD.

Having obtained the elastic magnitudes of the COD, they were subtracted from the respective total COD to obtain the plastic components. These plastic CODs were plotted on Figs 5.28 to 5.32 for different notch constitutions and configurations. The plastic curves plotted were those for the homogeneous specimen and the ones obtained inside defined areas of notch plasticity and settled cyclic stress range. There was no agreement between these data.

Plotted on the same axes were the rationalized non-dimensional values of the plastic COD curves. These hybrids (δ_{cgc}) were found to exhibit encouraging agreement with each other.

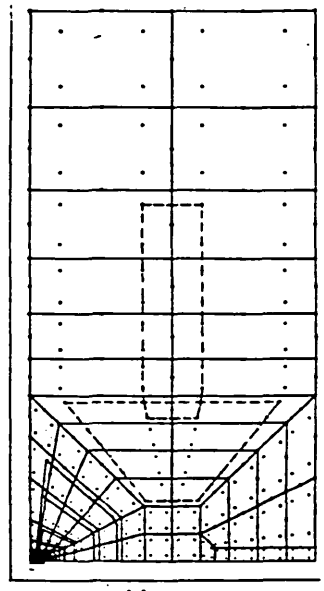


Fig 5. 1 Homogeneous Finite-element Mesh

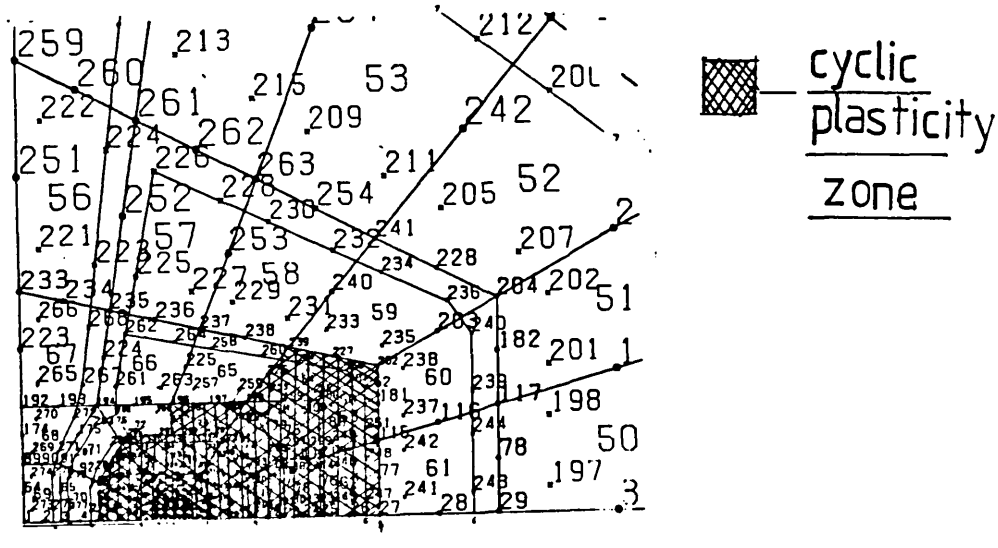


Fig 5. 2 Bifurcated Finite-element Mesh

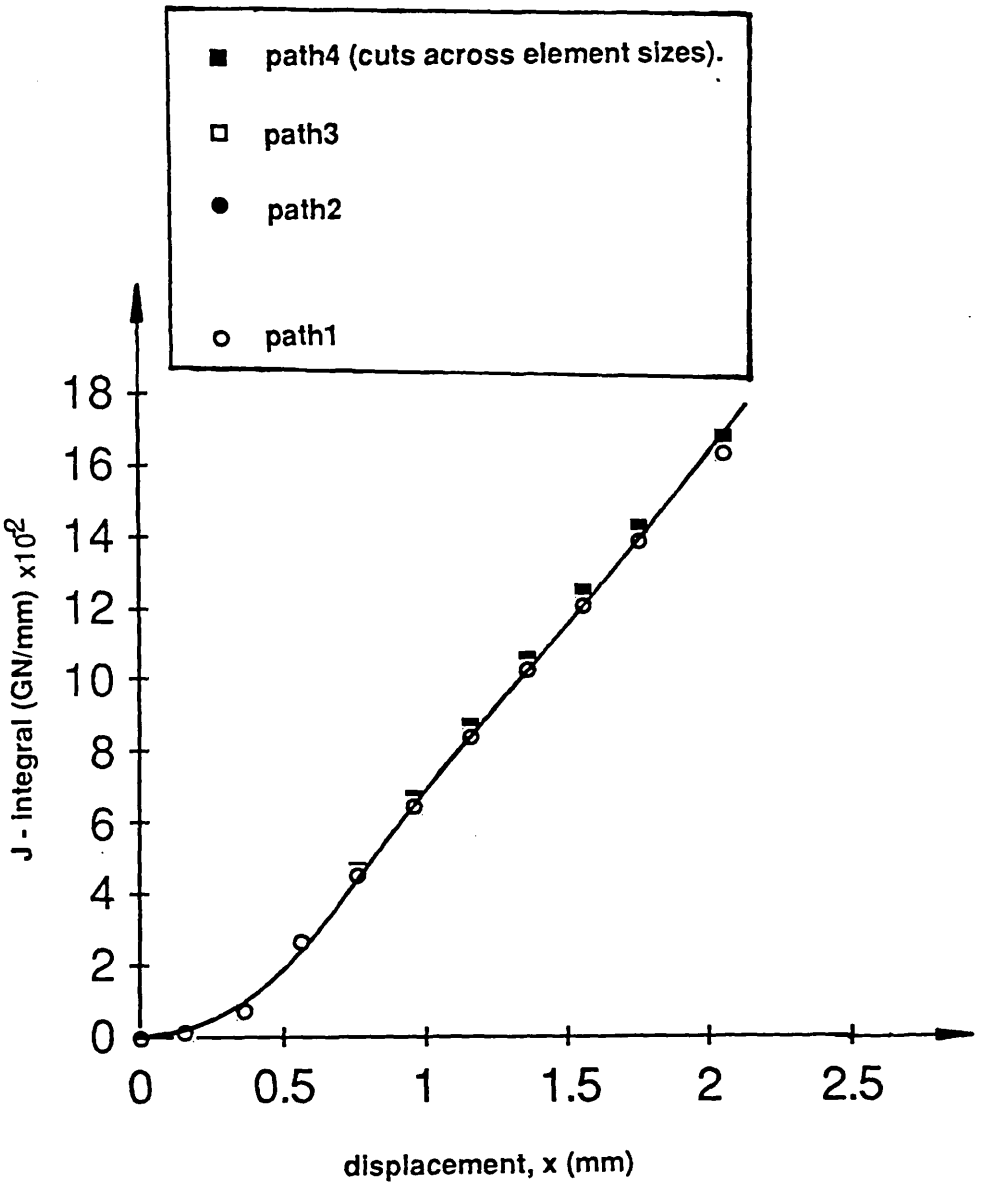


Fig.(5.3) J - Integral for different paths in a homogeneous specimen.

sNPF = Size of Notch Plasticity field.

NFCS = Notch field cyclic yield stress.

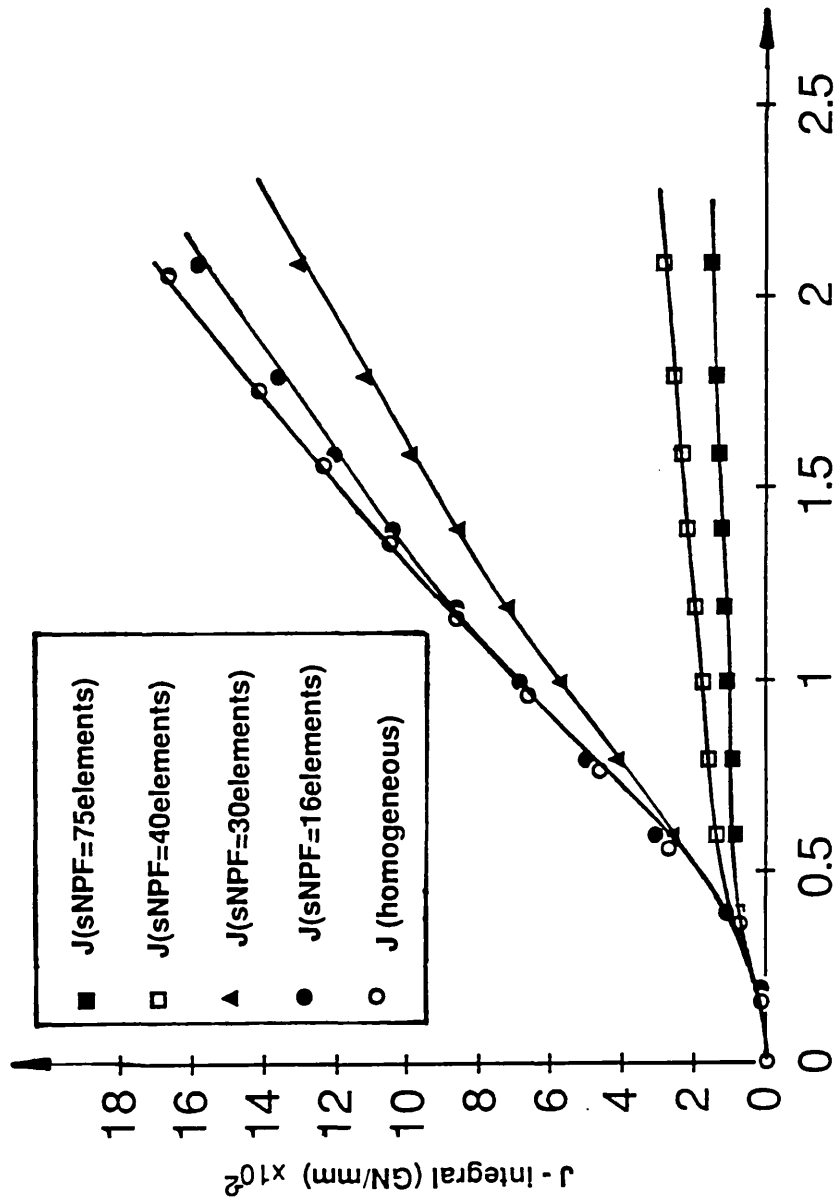


Fig.(5.4) Influence of size of notch plastic field on J_{FF} (NFCS = $1.5\sigma_0$).

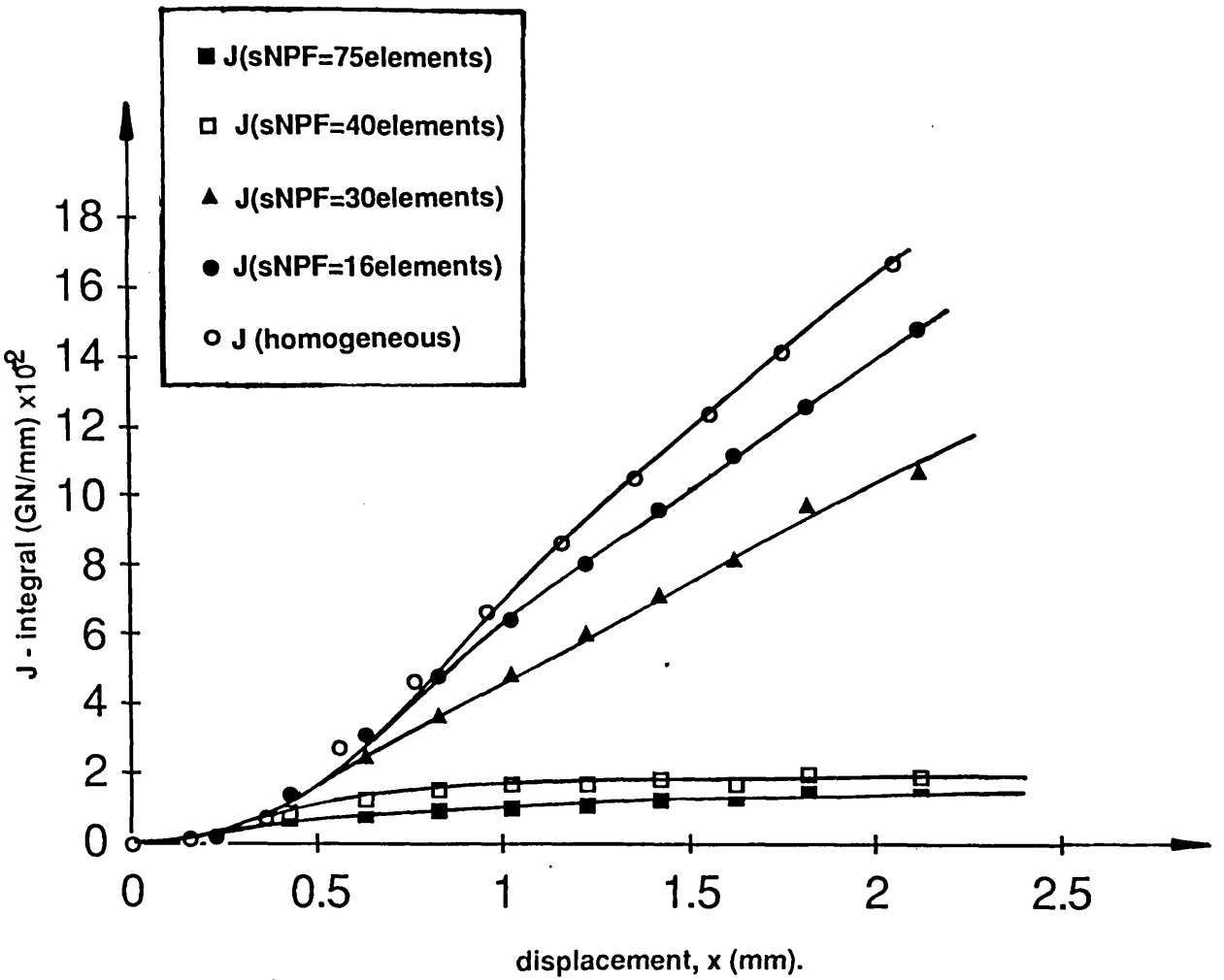


Fig.(5.5) Influence of size of notch plastic field on J_{FF} (NFCS = $2\sigma_0$).

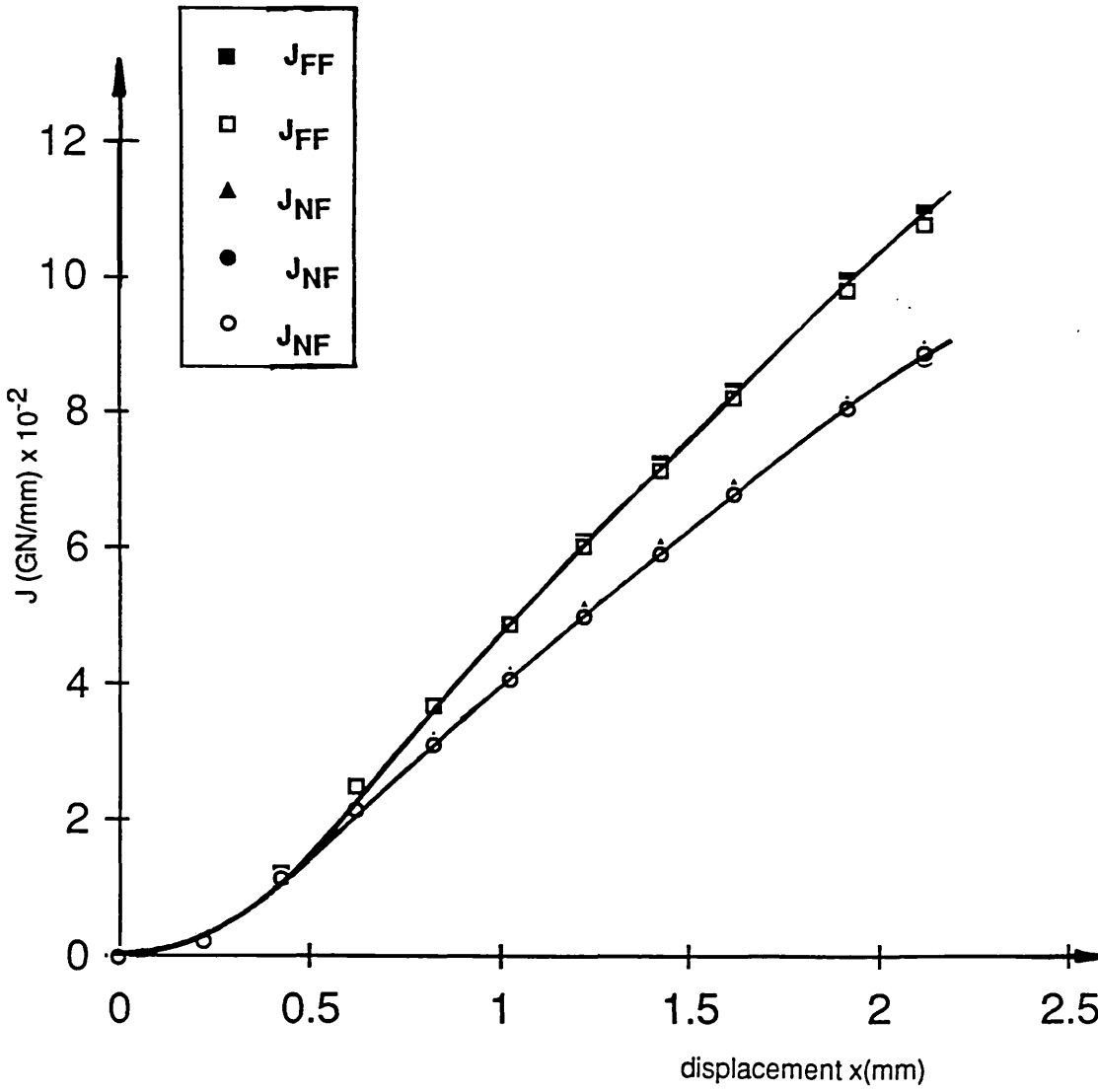


Fig. 5.6a Comparison of J_{NF} and J_{FF} for (sNPF=30elements) and (NFCS=$2\sigma_o$)

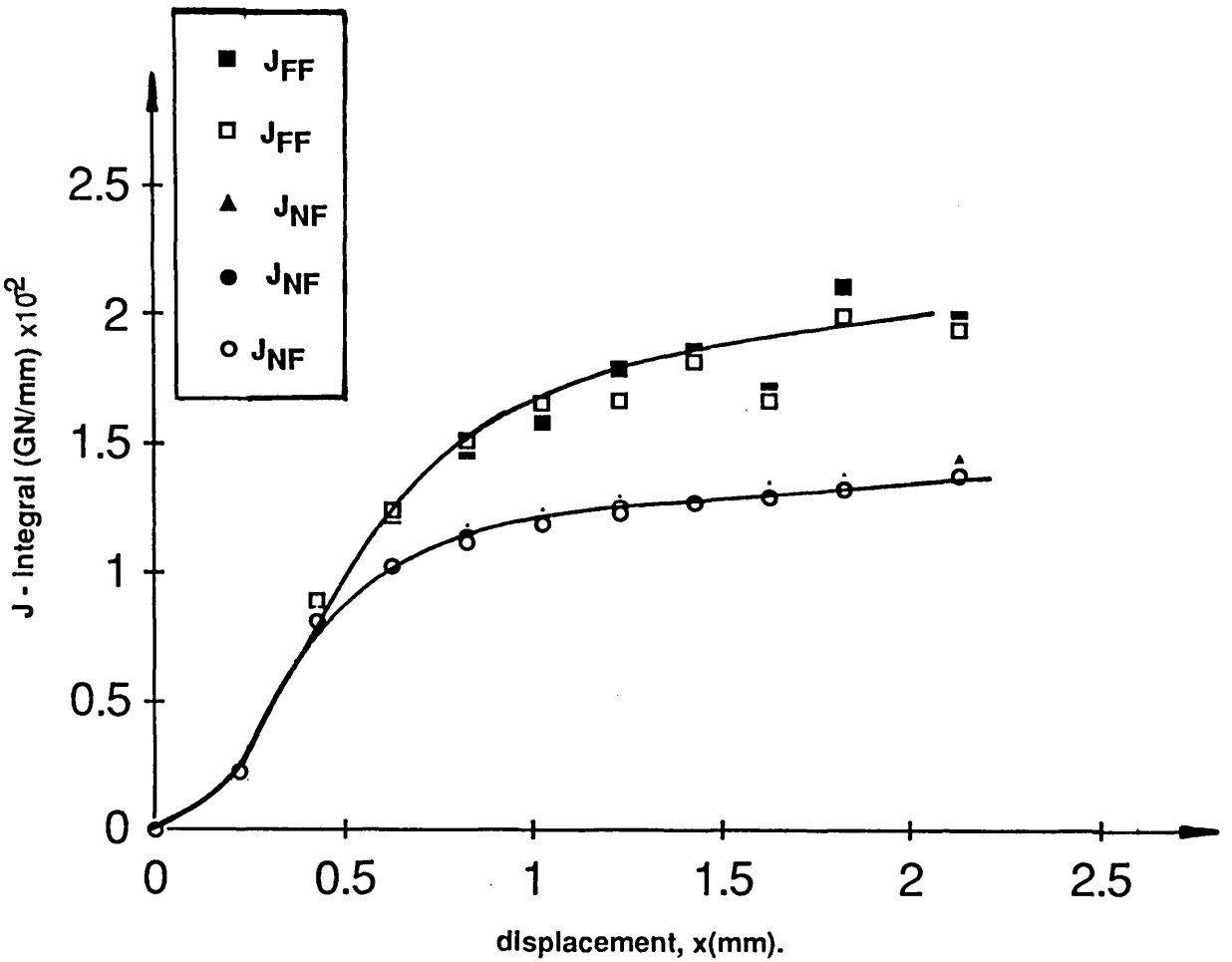


Fig.(5.6b) Comparison of J_{NF} and J_{FF} (sNPF = 40 elements).

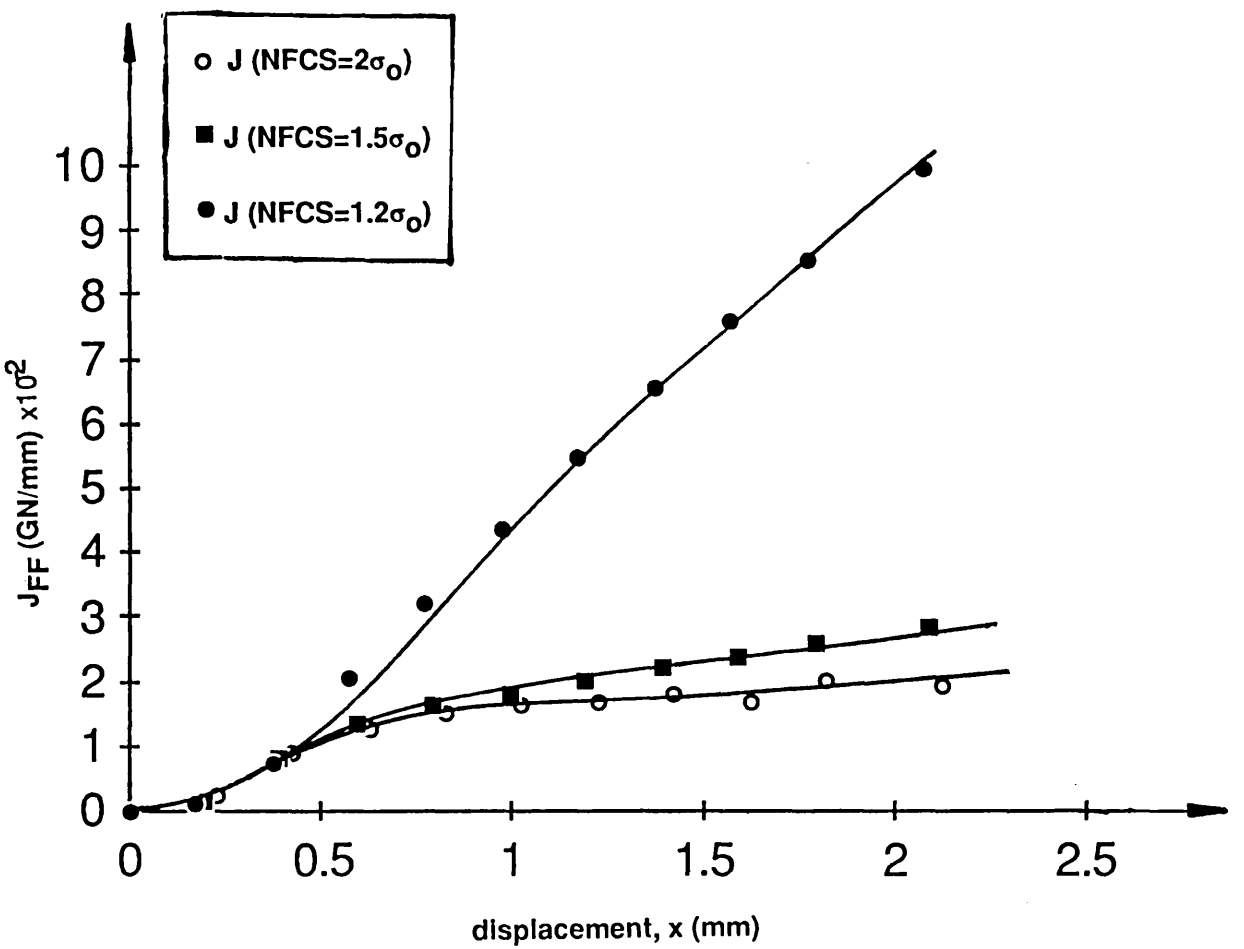


Fig.(5.7) Comparison of J_{FF} for different NFCS values. (sNPF = 40 elements).

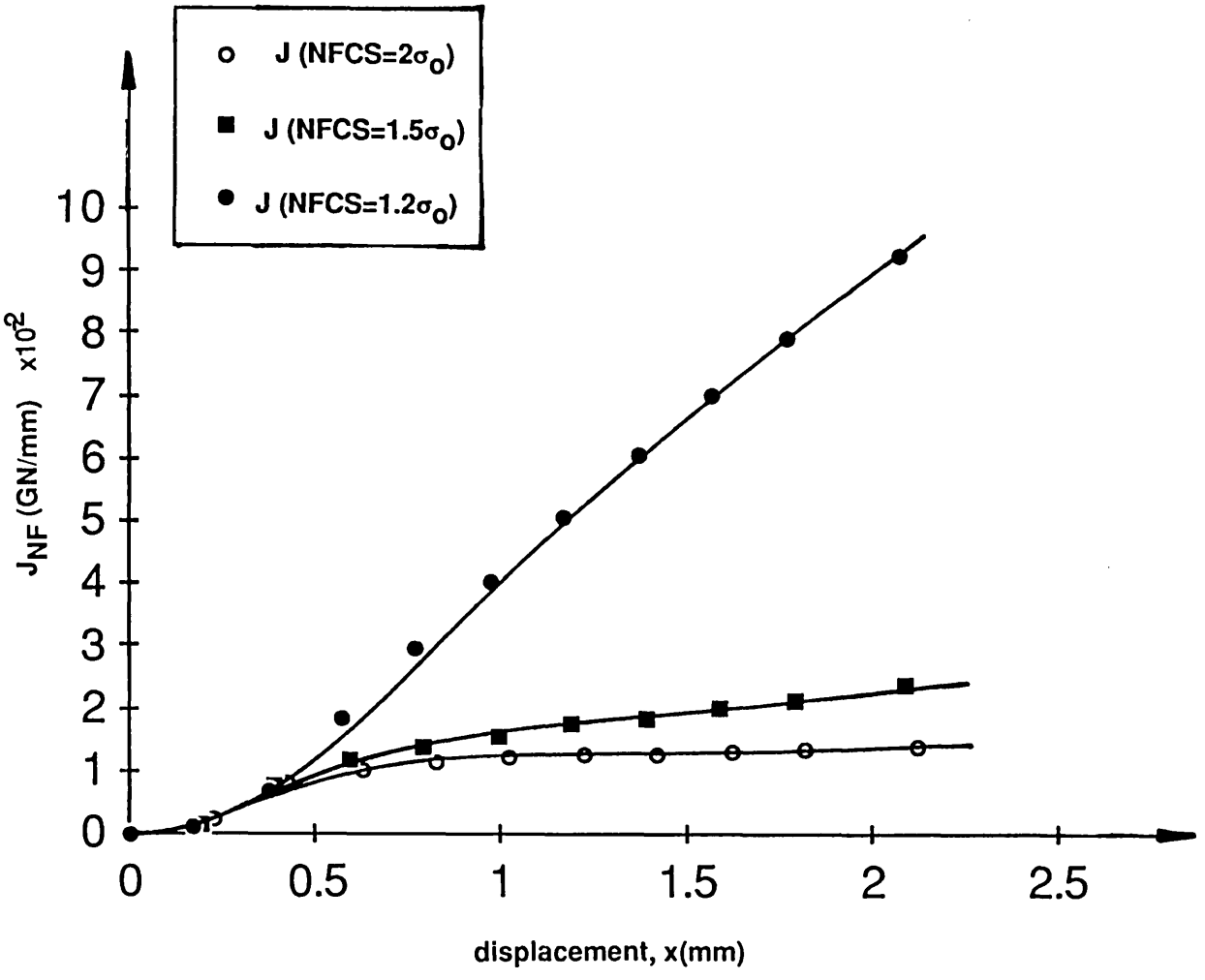


Fig.(5.8) Comparison of J_{NF} for different NFCS values. (sNPF = 40 elements).

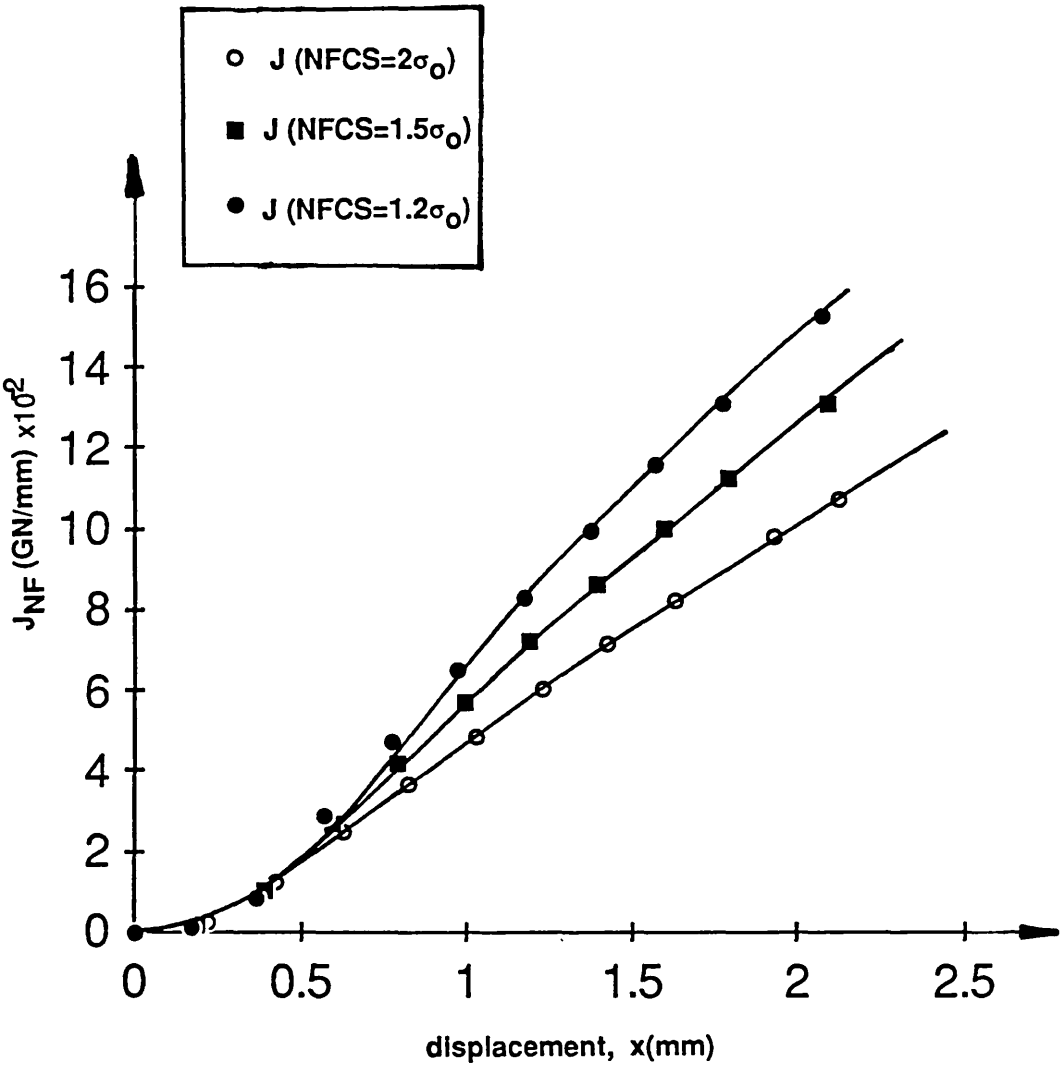


Fig.(5.9) Comparison of J_{NF} for different NFCS values. (sNPF = 30 elements).

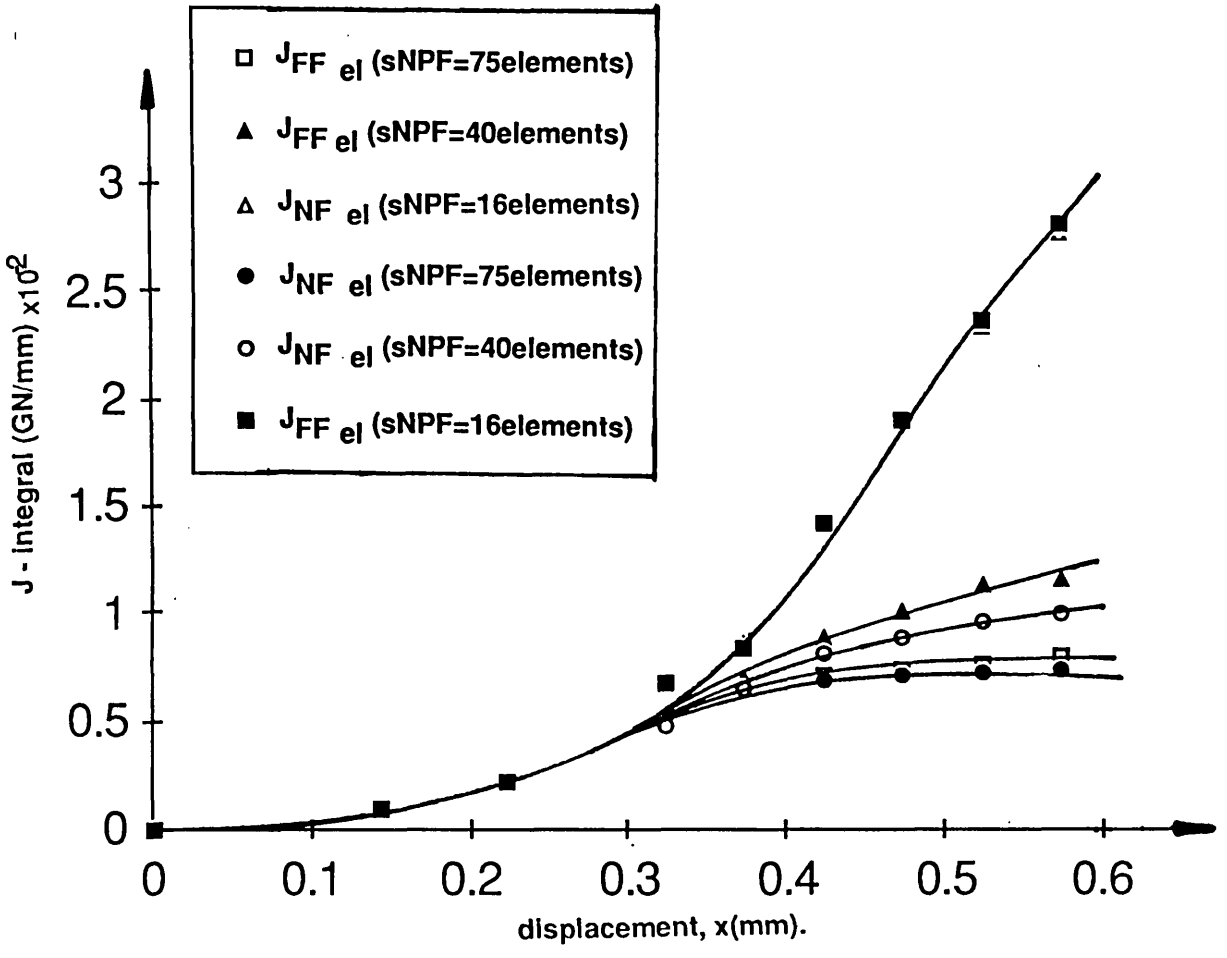


Fig.(5.10) Elastic curves for J_{NF} and J_{FF} for different sNPF (NFCS = $2\sigma_0$).

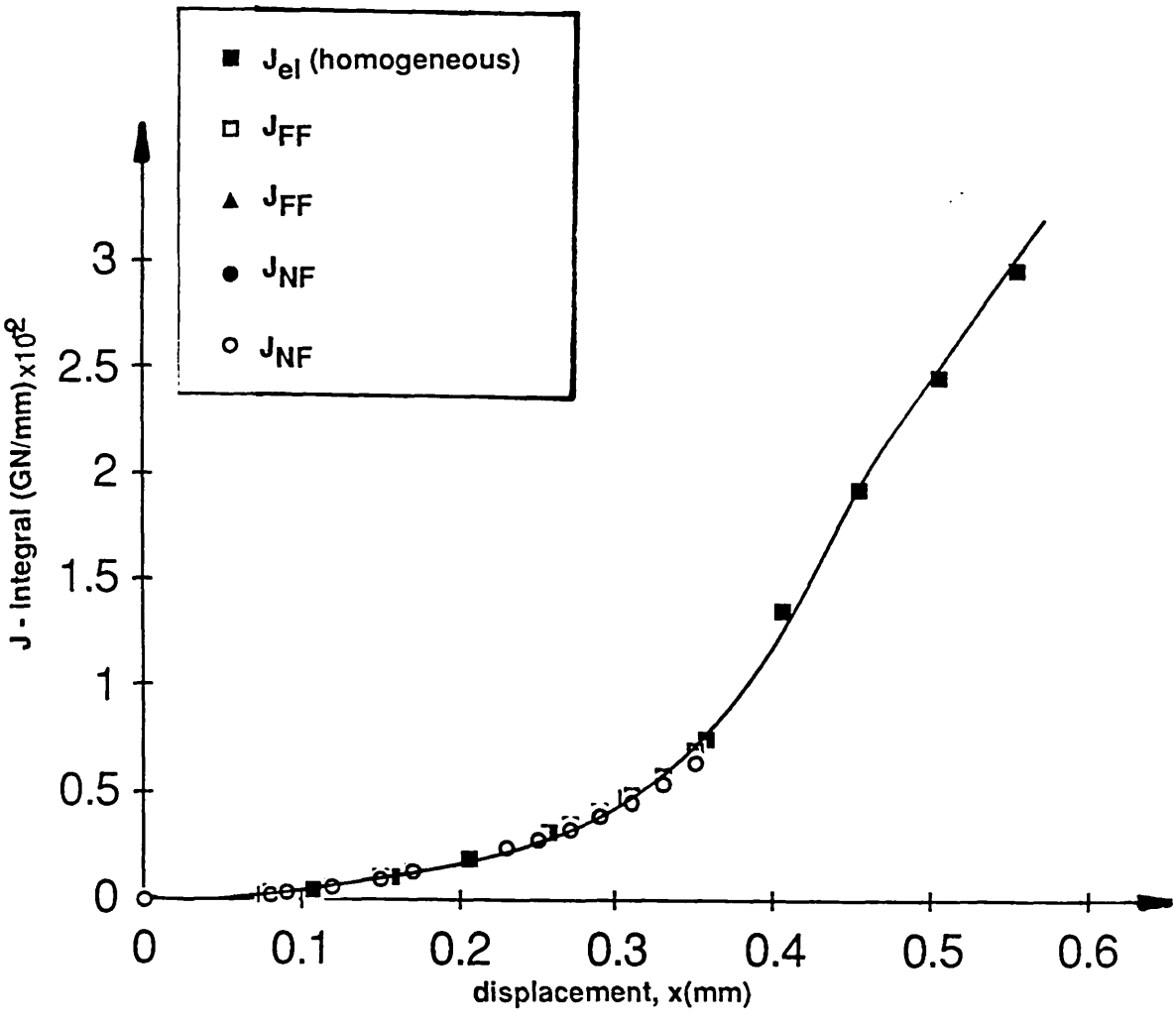


Fig.(5.11) Contained yield values for J_{NF} and J_{FF}. (sNPF = 16elements), (NFCS = $1.2\sigma_0$).

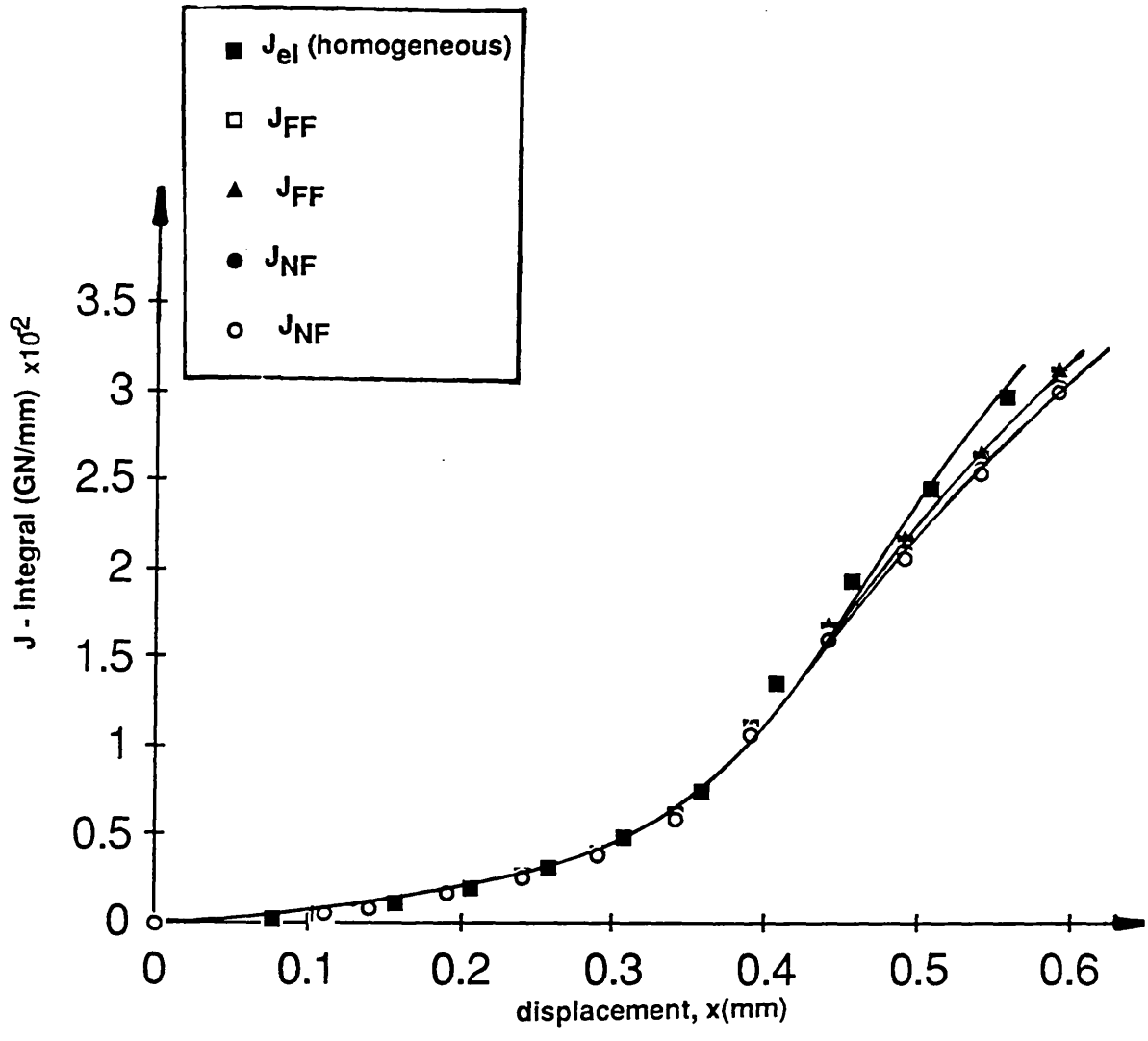


Fig.(5.12) Contained yield values for J_{NF} and J_{FF}. (sNPF = 16elements), (NFCS = $1.5\sigma_0$).

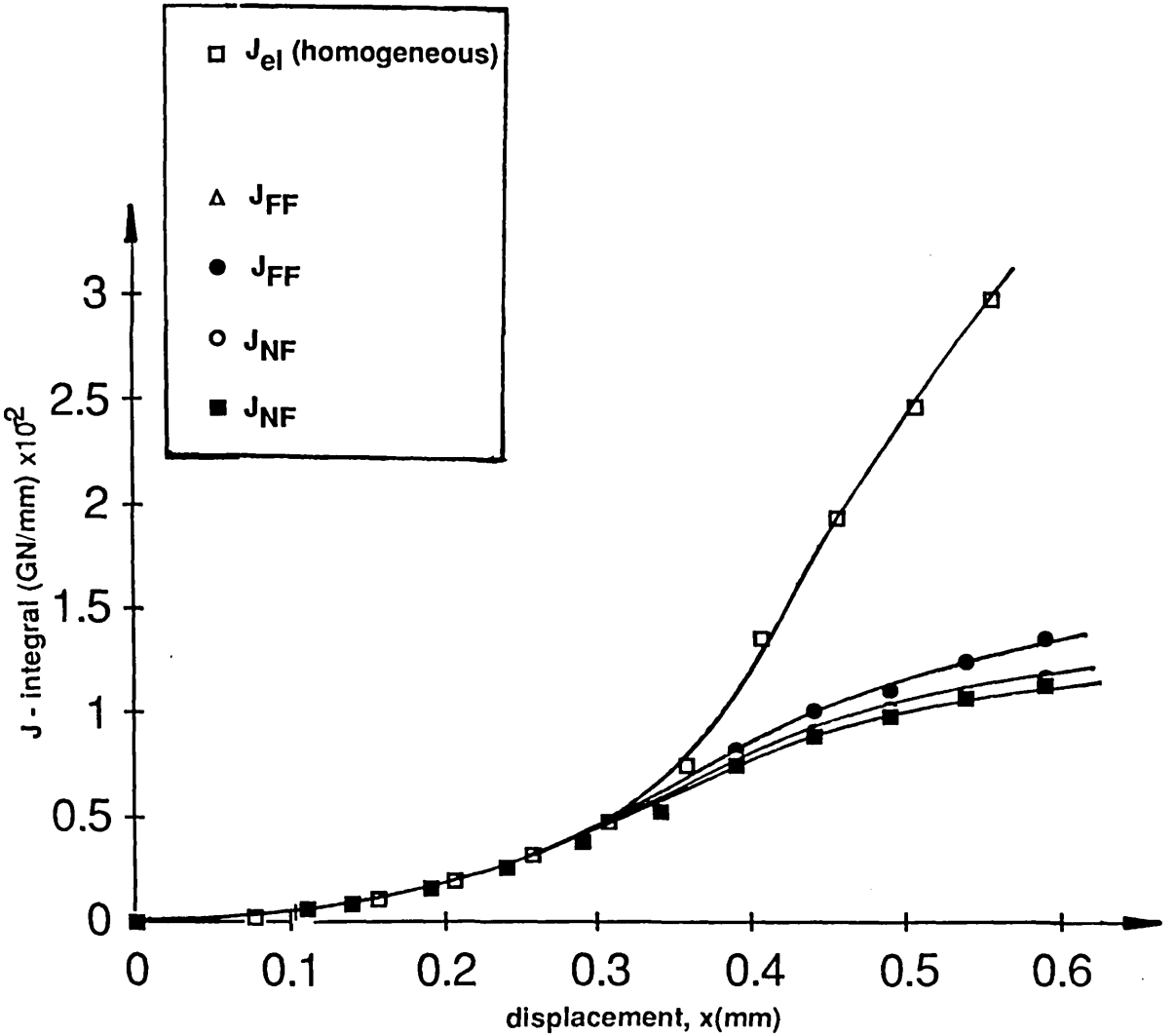


Fig.(5.13) Contained yield values for J_{NF} and J_{FF}. (sNPF = 40elements), (NFCS = $1.5\sigma_0$)

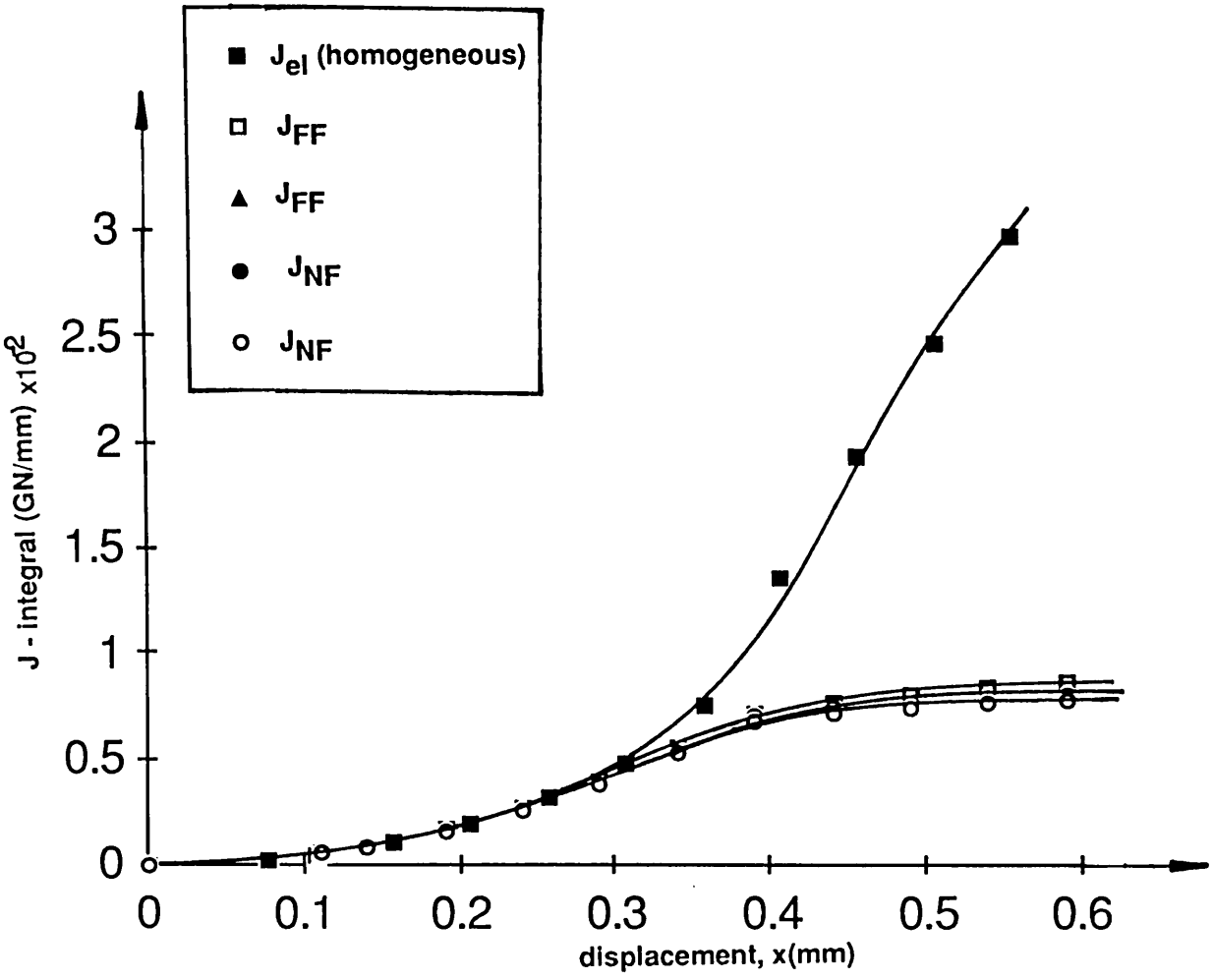


Fig.(5.14) Contained yield values for J_{NF} and J_{FF}. (sNPF = 75elements), (NFCS = $1.5\sigma_0$)

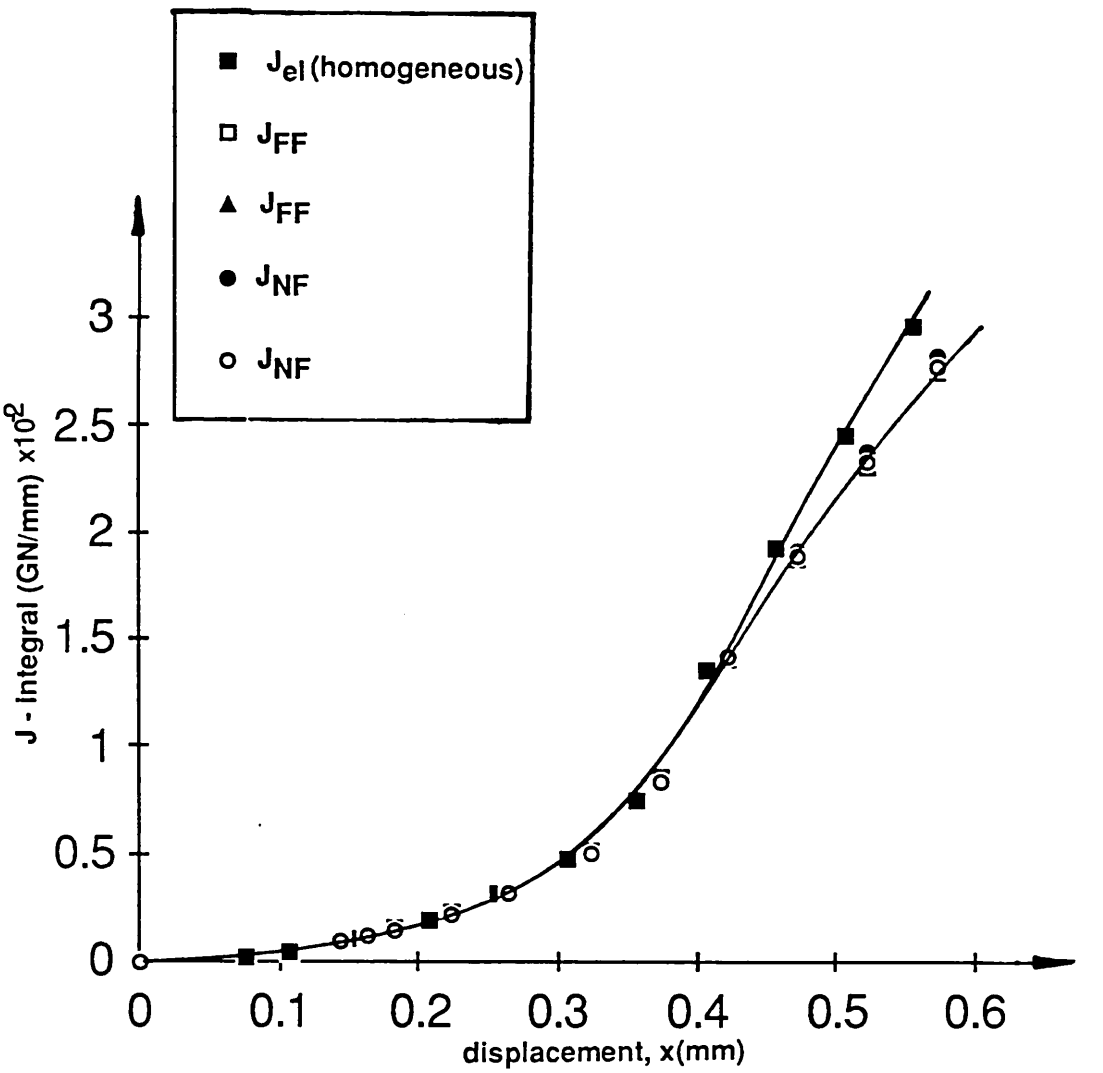


Fig.(5.15) Contained yield values for J_{NF} and J_{FF}. (sNPF = 16elements), (NFCS = $2\sigma_0$).

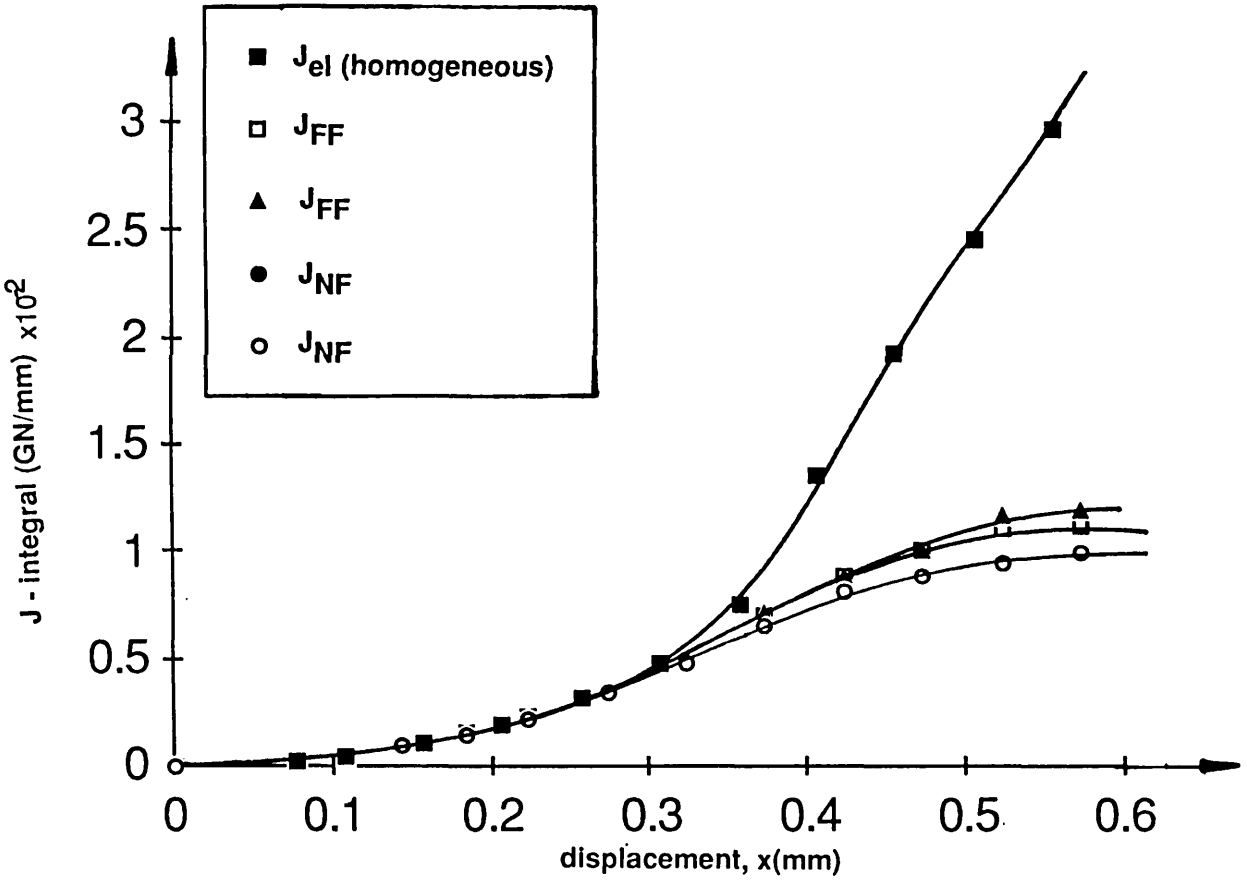


Fig.(5.16) Contained yield values for J_{NF} and J_{FF}. (sNPF = 40elements), (NFCS = $2\sigma_0$)

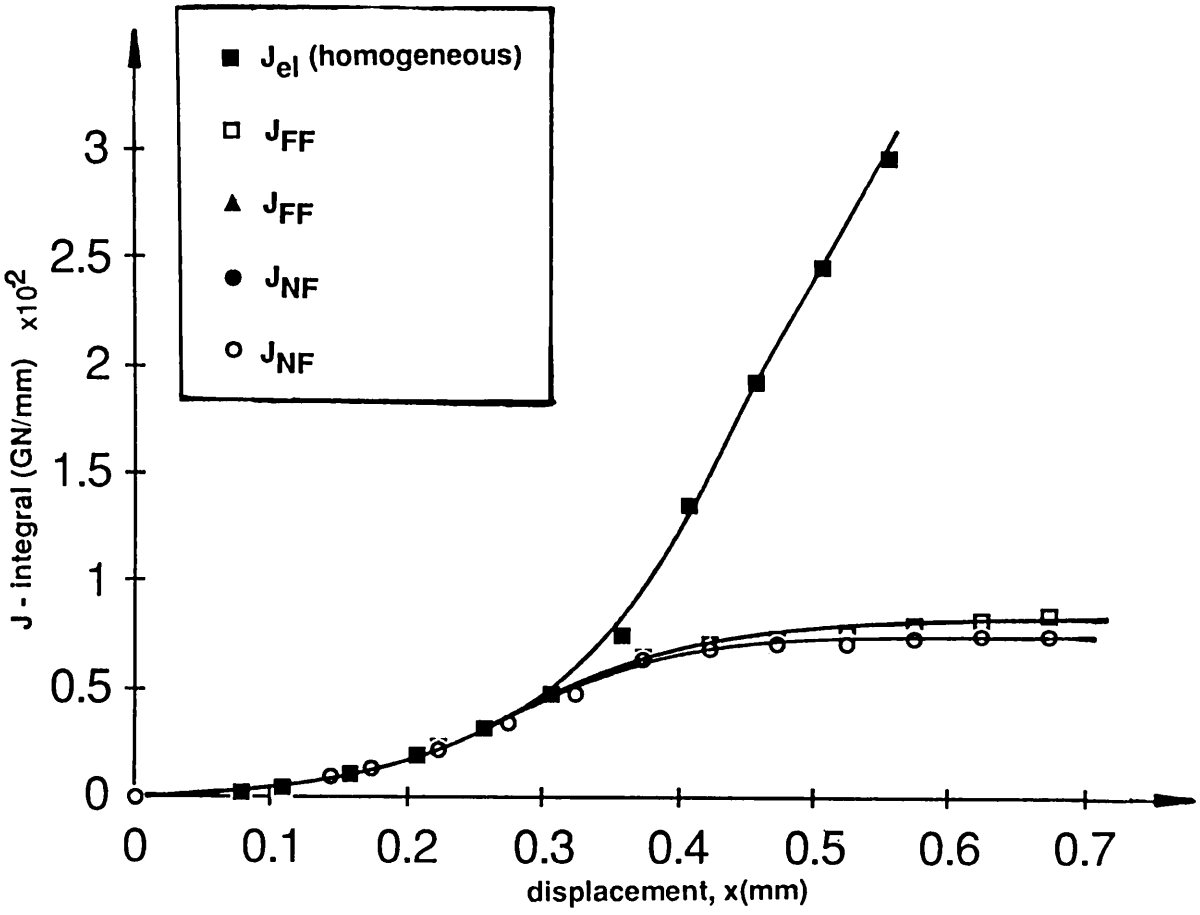


Fig.(5.17) Contained yield values for J_{NF} and J_{FF}. (sNPF = 75elements), (NFCS = $2\sigma_0$).

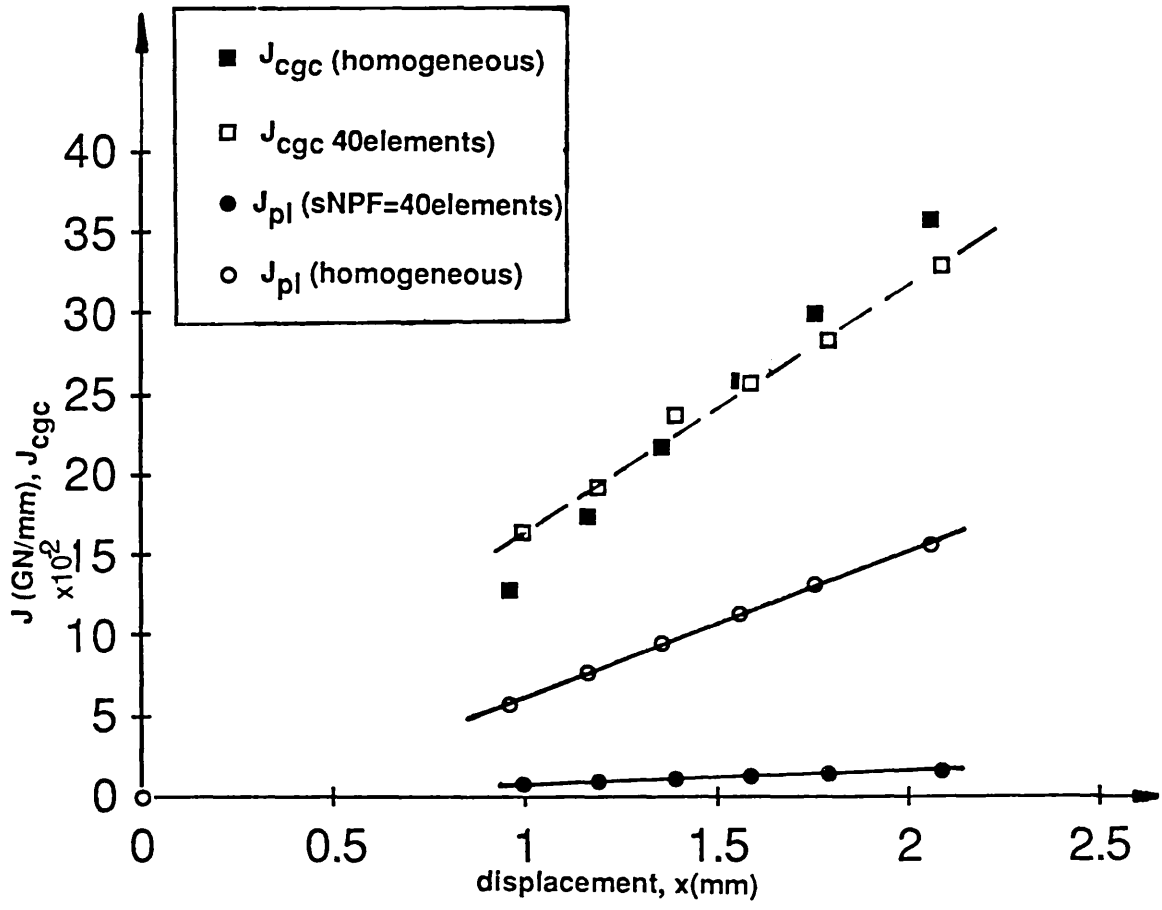


Fig.(5.18) Plastic and rationalized non-dimensional values of J_{NF} and J_{FF}. (sNPF = 40elements, NFCS = $1.5\sigma_0$).

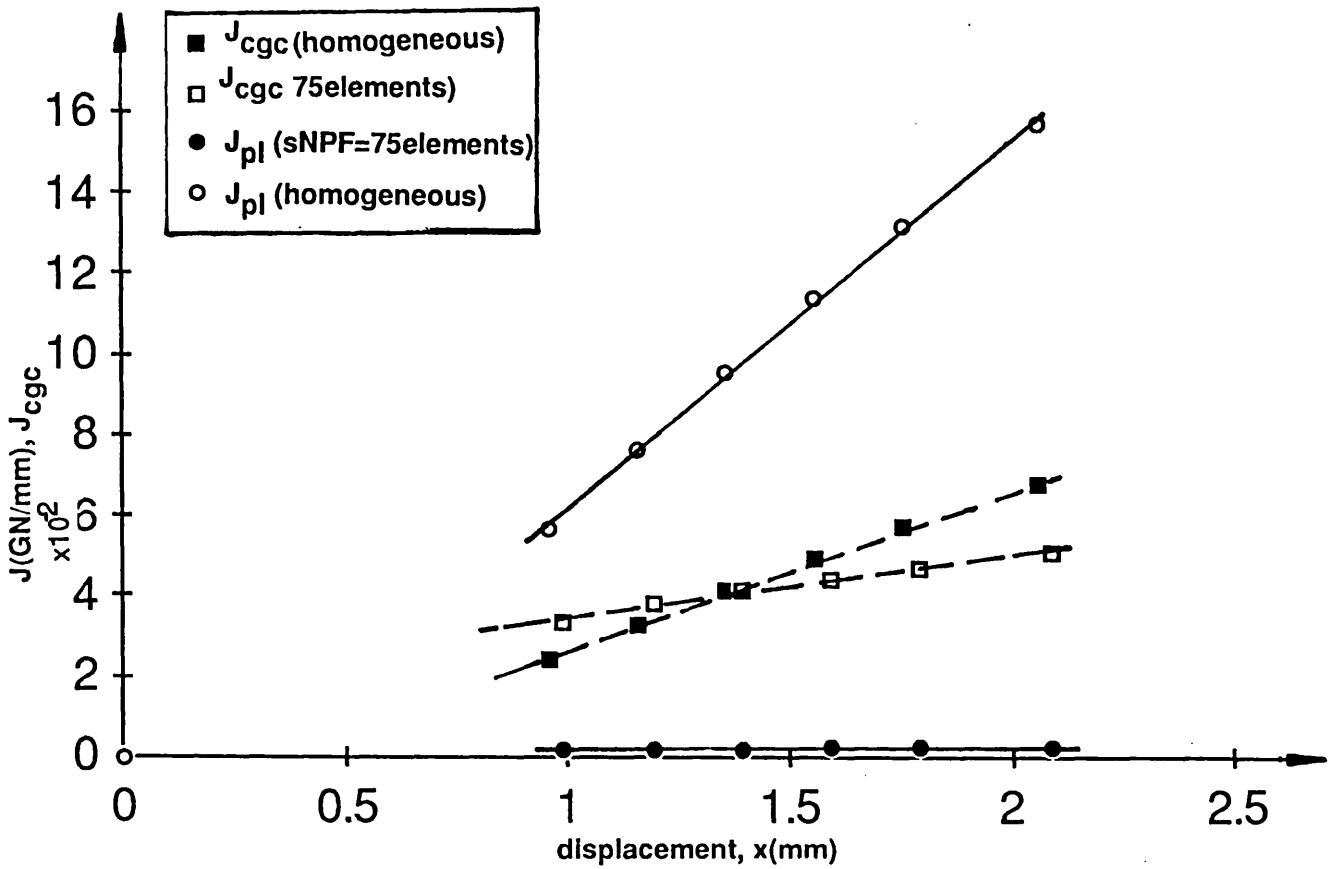


Fig.(5.19) Plastic and rationalized non-dimensional values of J_{NF} and J_{FF}.
(sNPF = 75elements, NFCS = $1.5\sigma_0$).

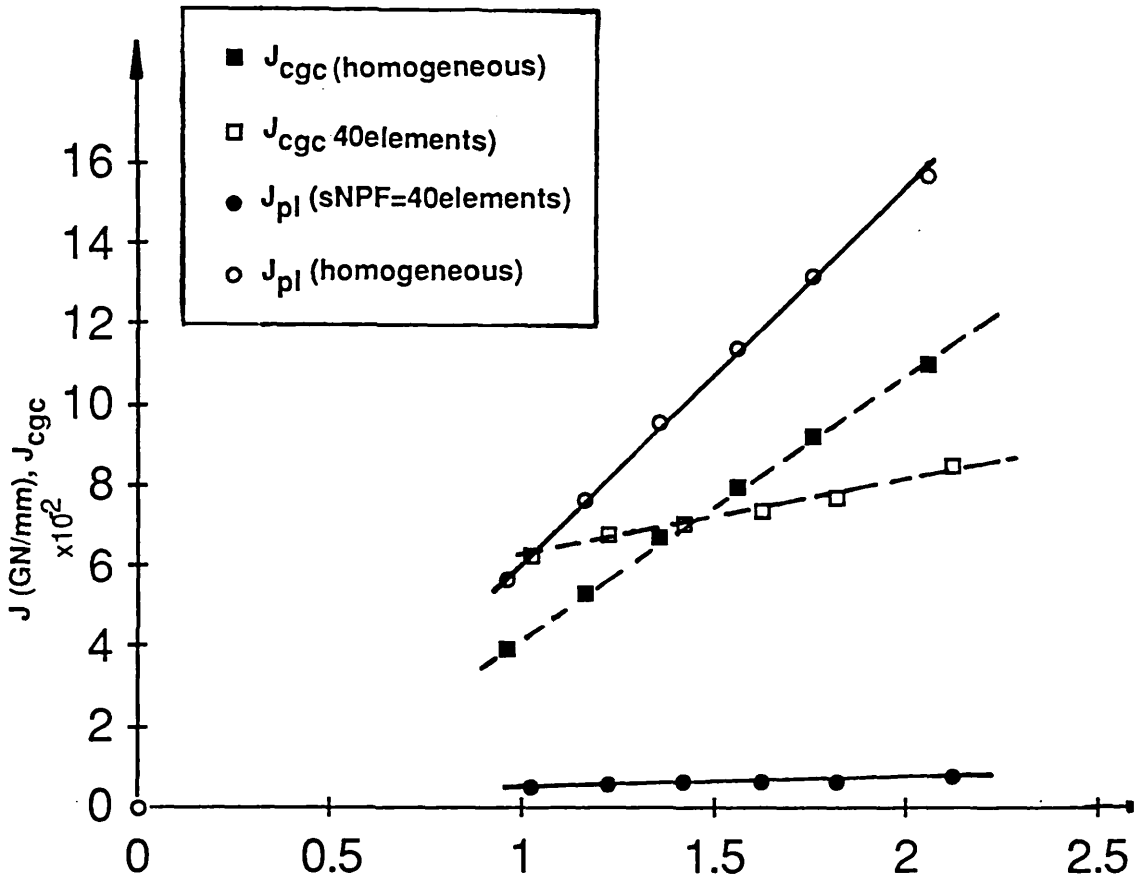


Fig.(5.20) Plastic and rationalized non-dimensional values of J_{NF} and J_{FF}. (sNPF = 40elements, NFCS = $2\sigma_0$).

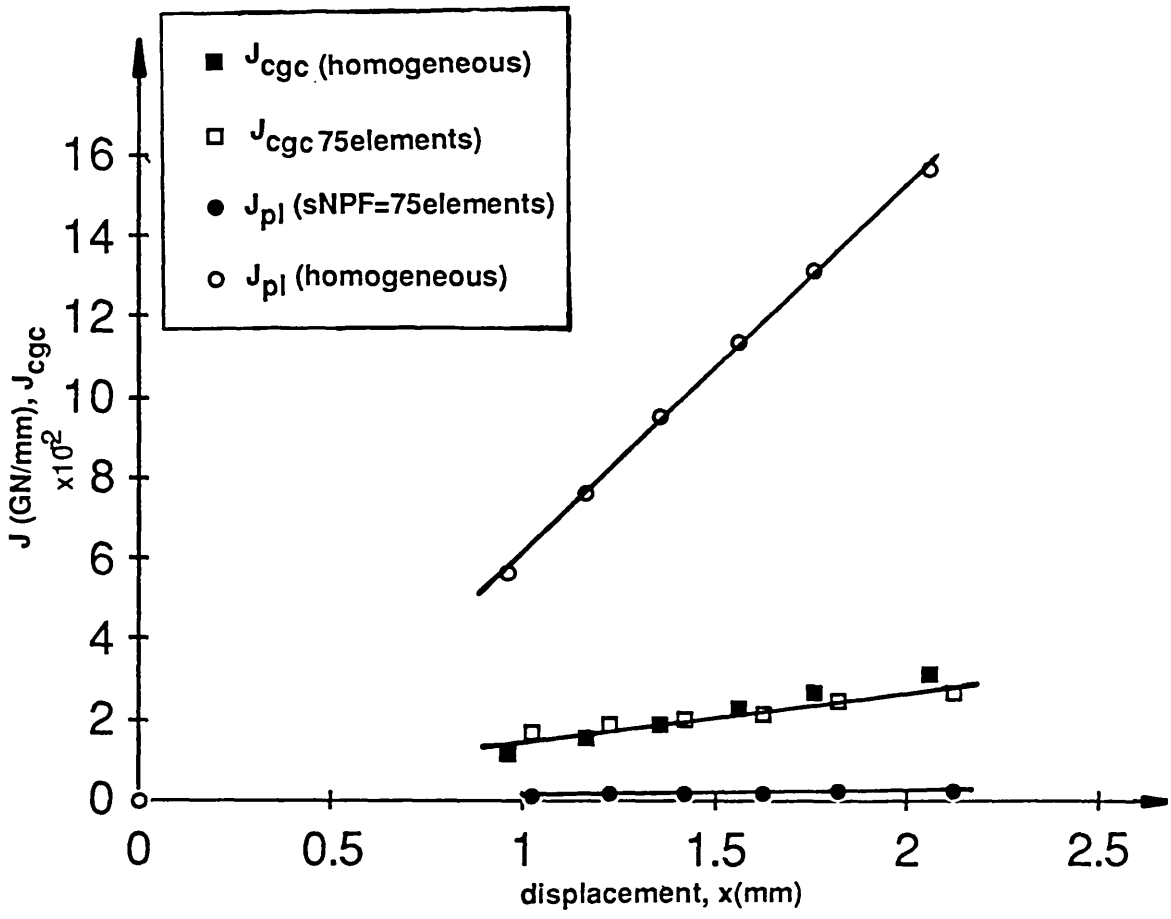


Fig.(5.21) Plastic and rationalized non-dimensional values of J_{NF} and J_{FF}. (sNPF = 75elements, NFCS = $2\sigma_0$).

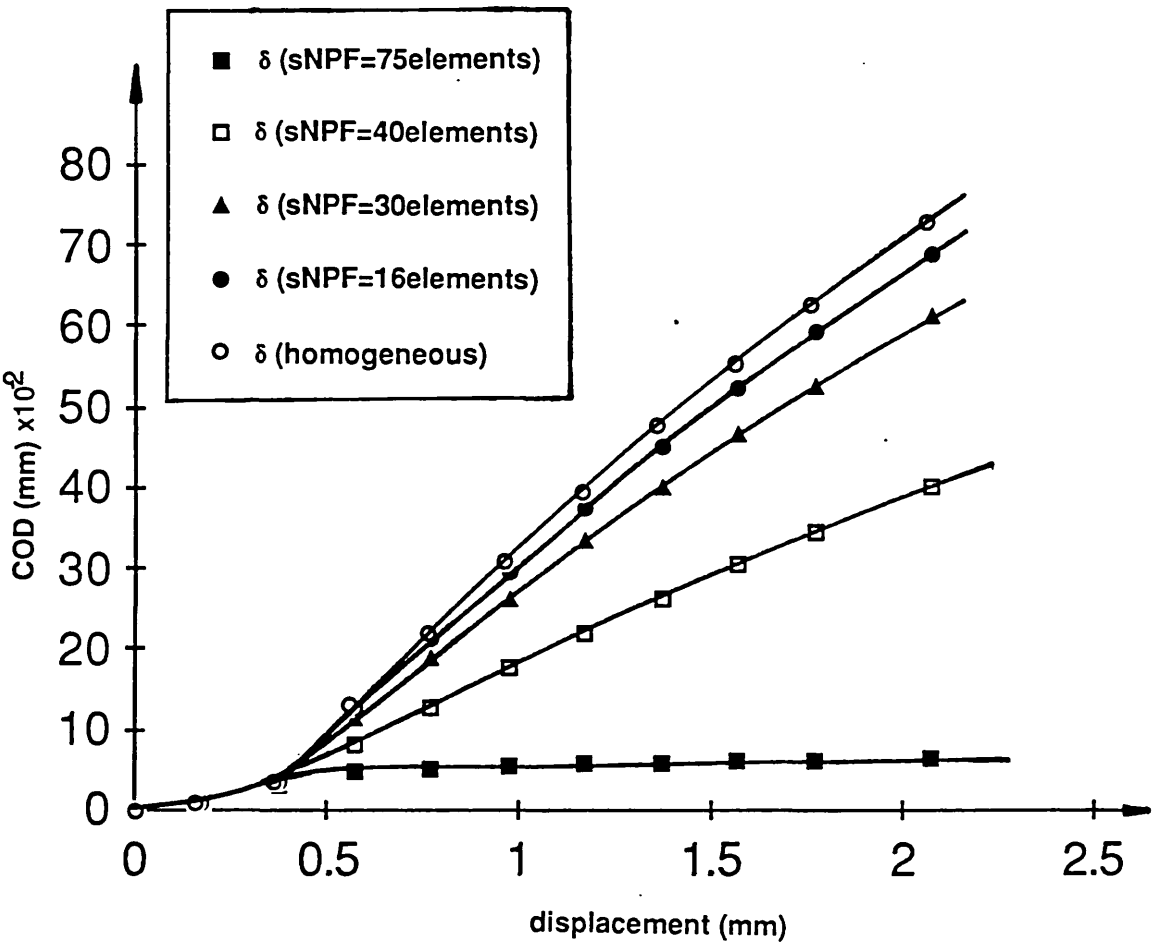


Fig.(5.22) Influence of sNPF on the COD. (NFCS = $1.2\sigma_0$)

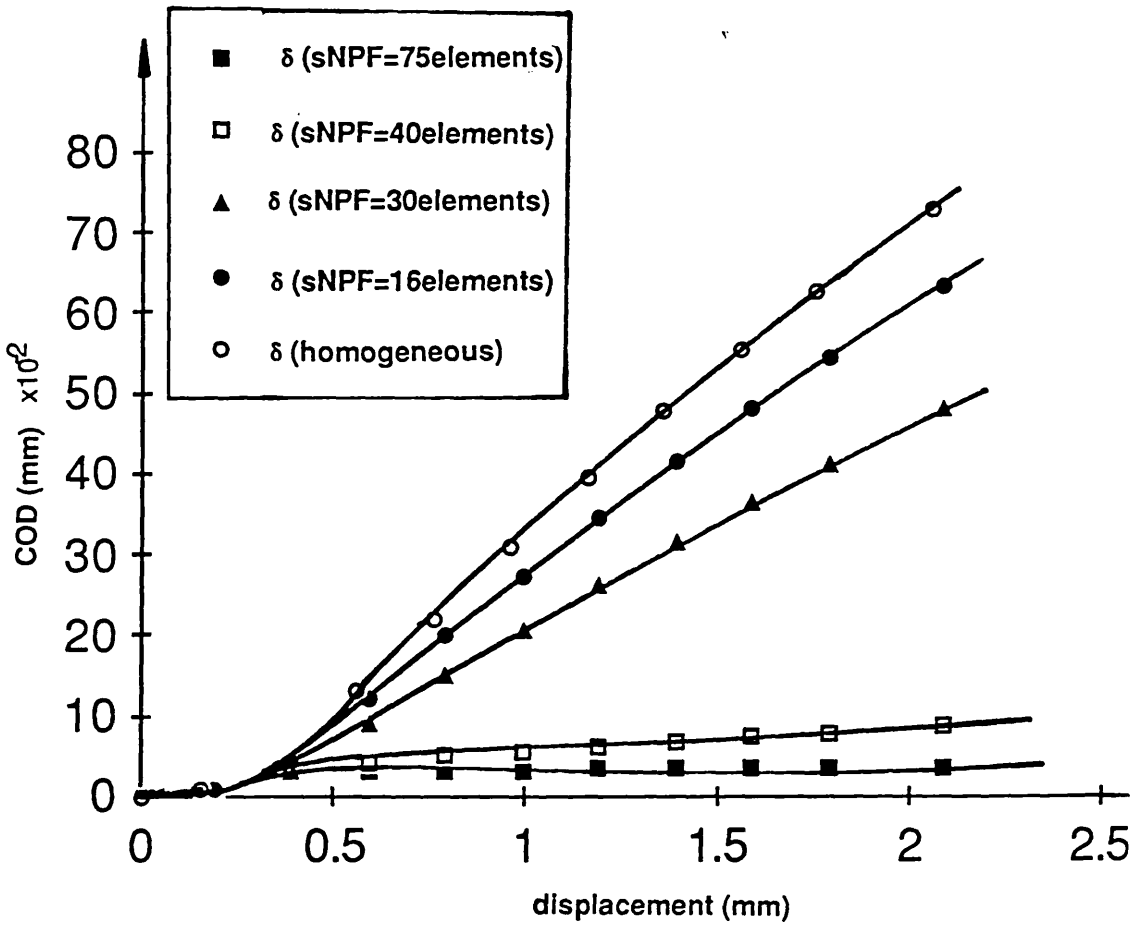


Fig.(5.23) Influence of sNPF on the COD. (NFCS = $1.5\sigma_0$).

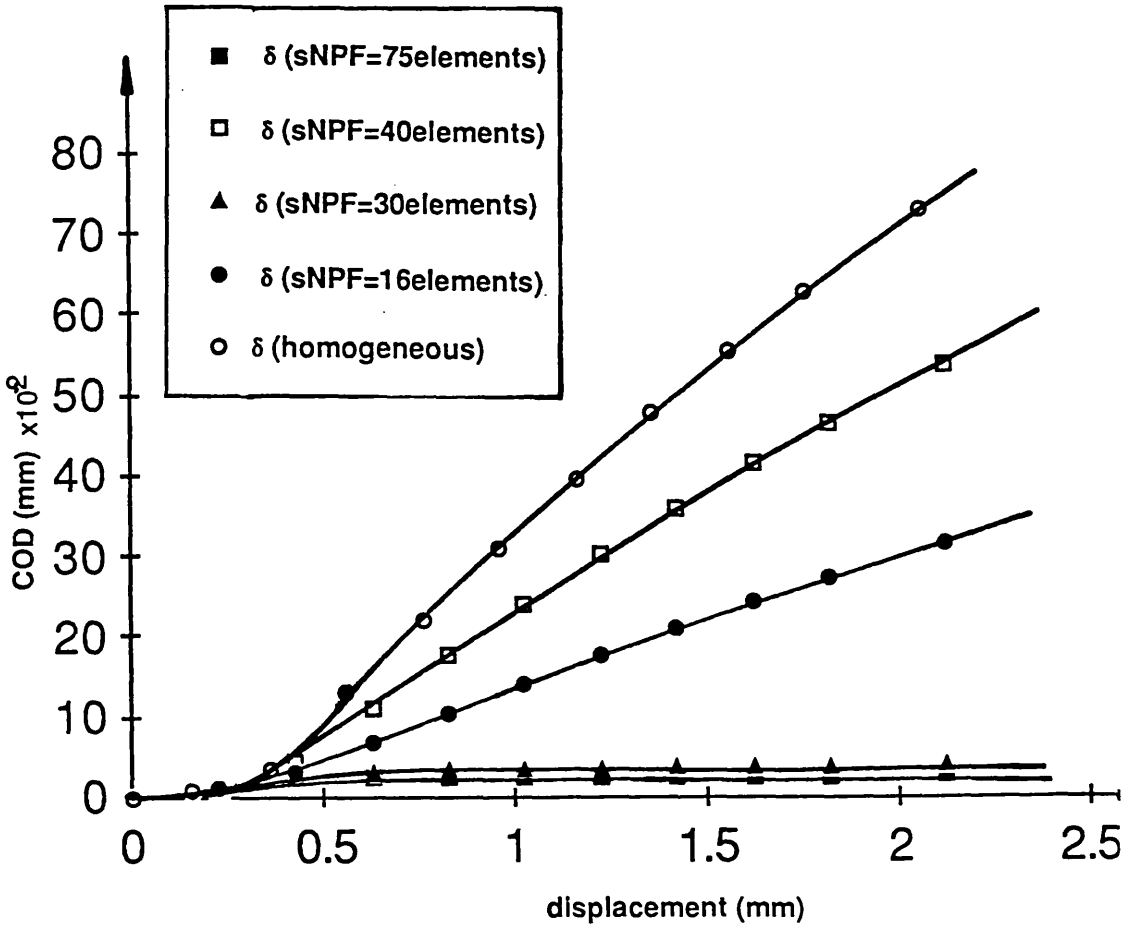


Fig.(5.24) Influence of sNPF on the COD. (NFCS = $2\sigma_0$).

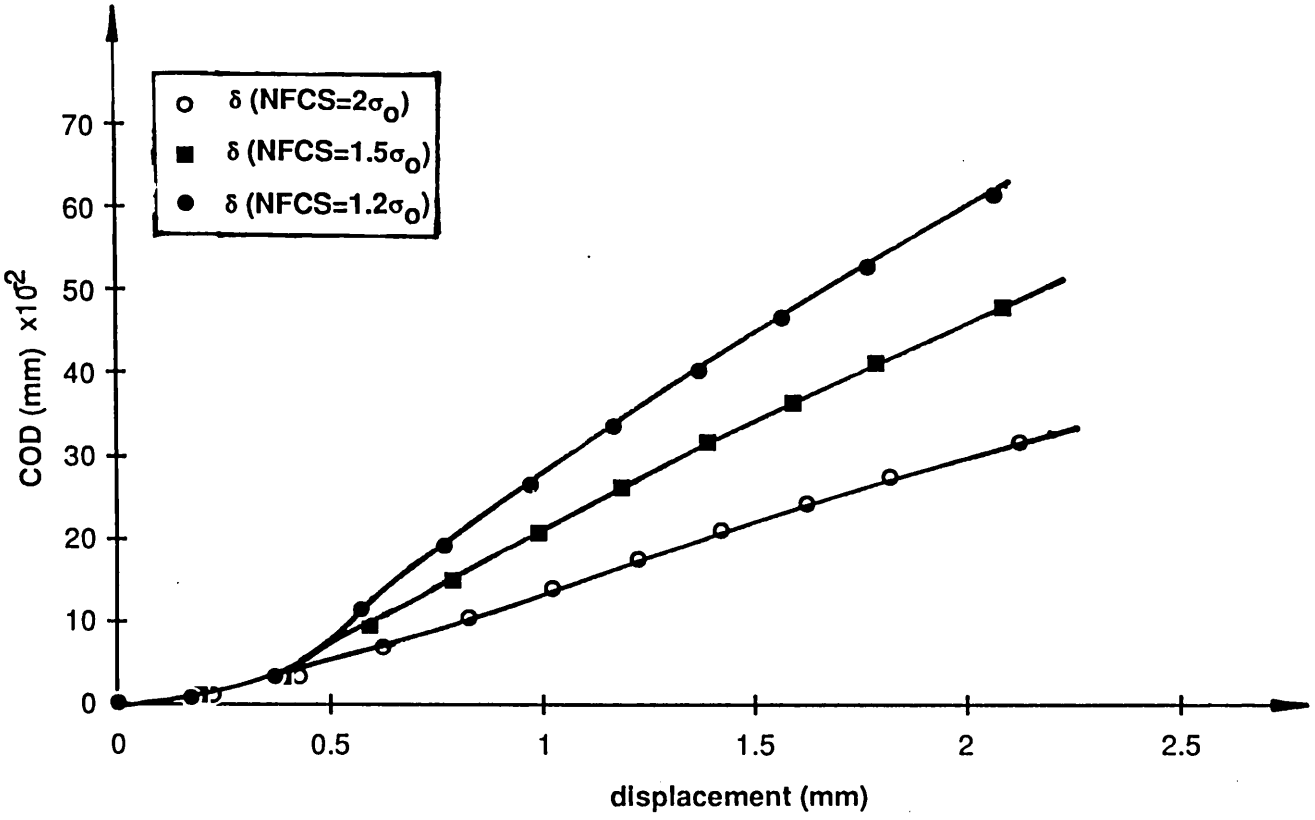


Fig.(5.25) Comparison of the effect different NFCS on COD.
(sNPF = 30elements)

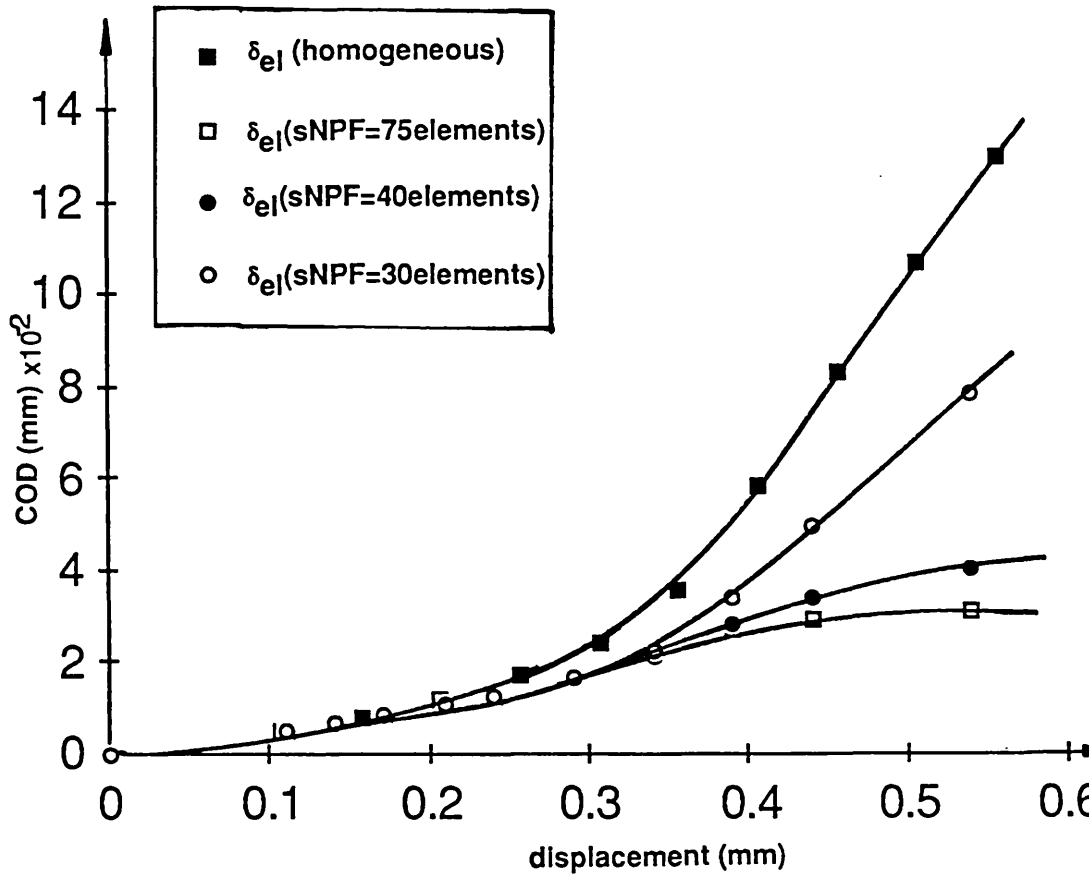


Fig.(5.26) Contained yield values of COD. (NFCS = $1.5\sigma_0$).

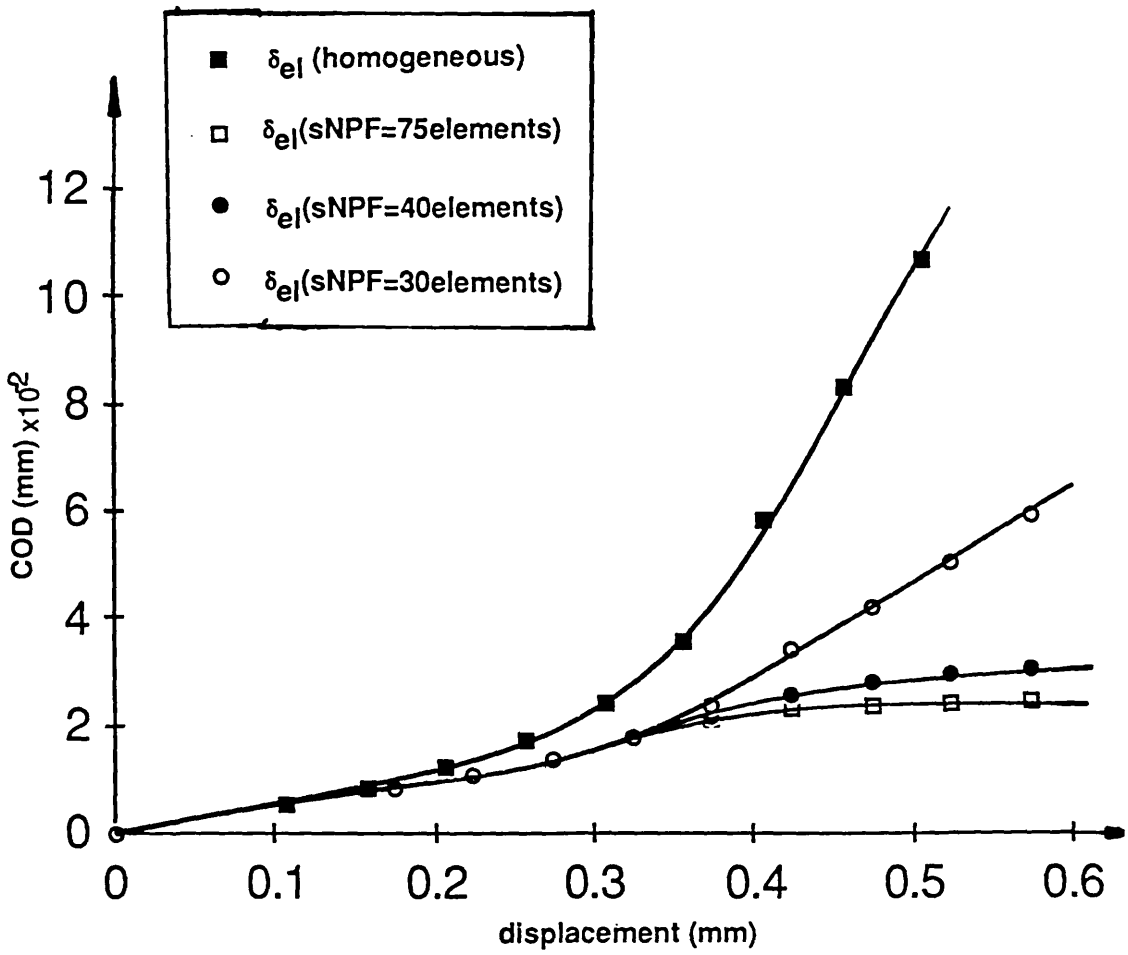


Fig.(5.27) Contained yield values of COD. (NFCS = $2\sigma_0$).

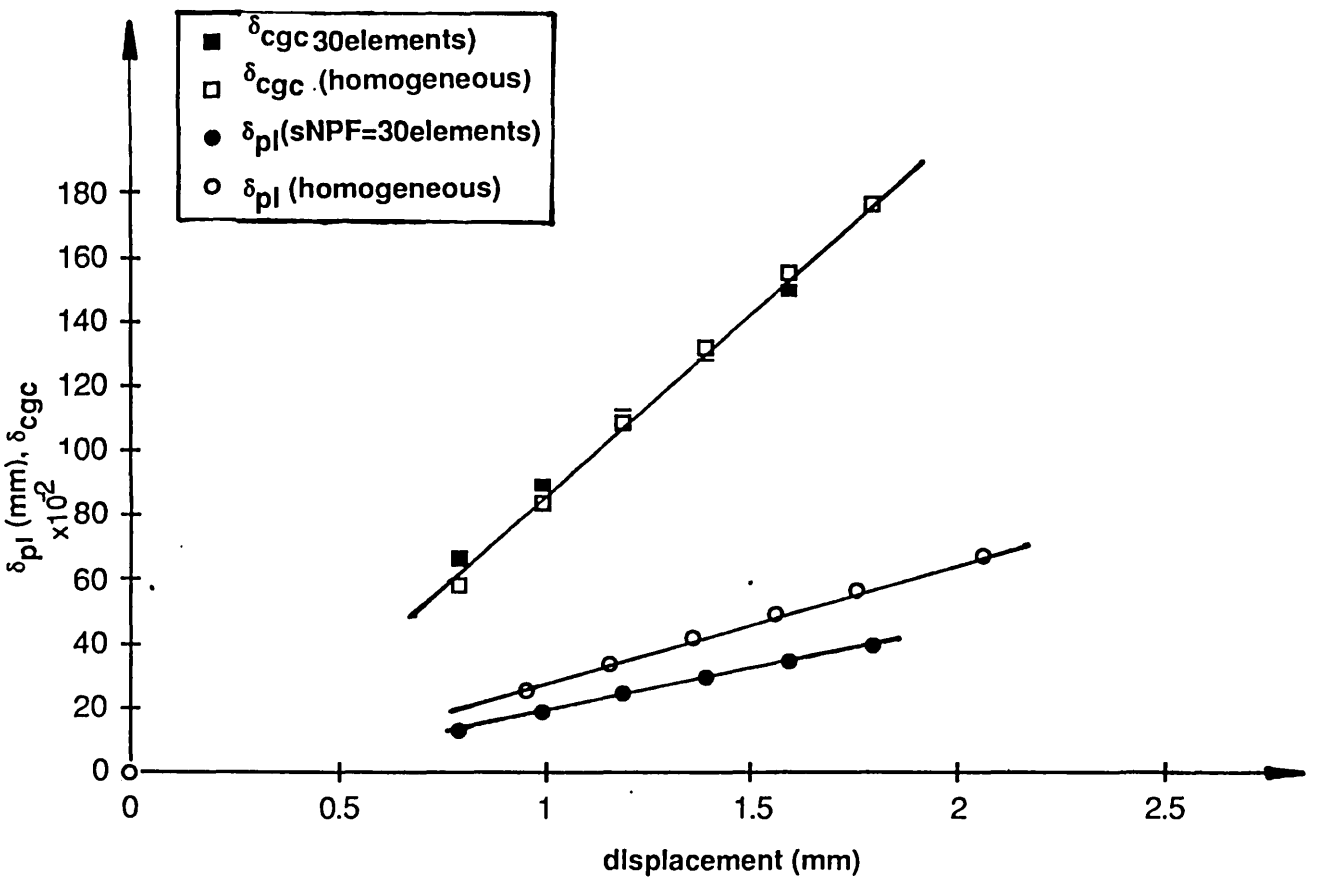


Fig.(5.28) Plastic and rationalized non-dimensional values of COD. (NFCS = $1.5\sigma_0$), sNPF = 30elements).

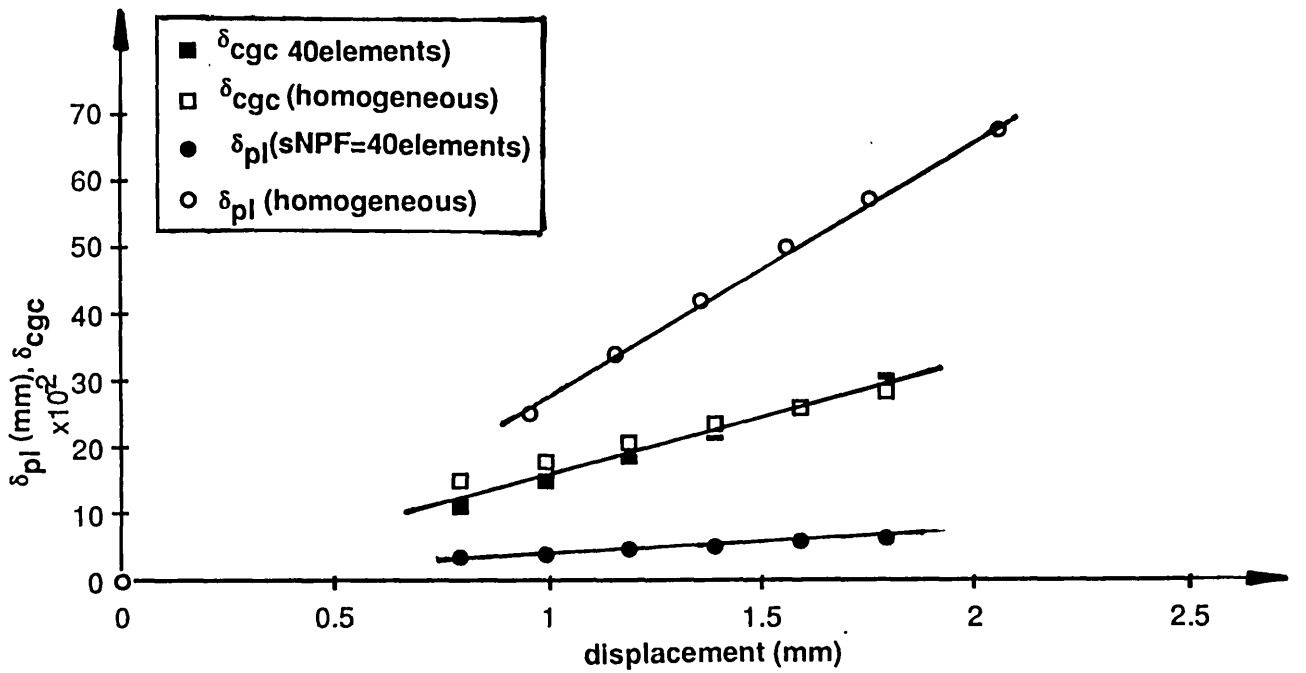


Fig.(5.29) Plastic and rationalized non-dimensional values of COD.
(NFCS = $1.5\sigma_0$, sNPF = 40elements).

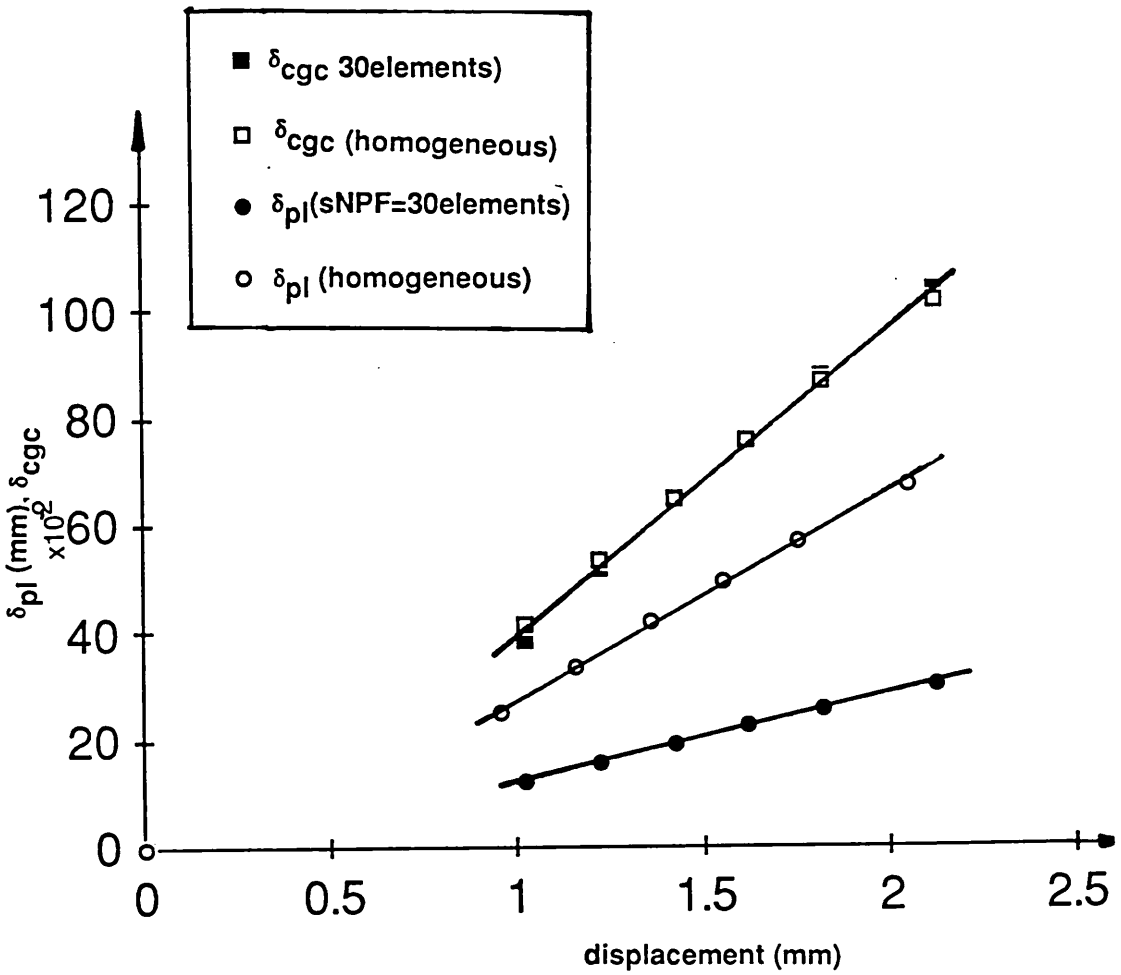


Fig.(5.30) Plastic and rationalized non-dimensional values COD.
(NFCS = $2\sigma_0$, sNPF = 30elements).

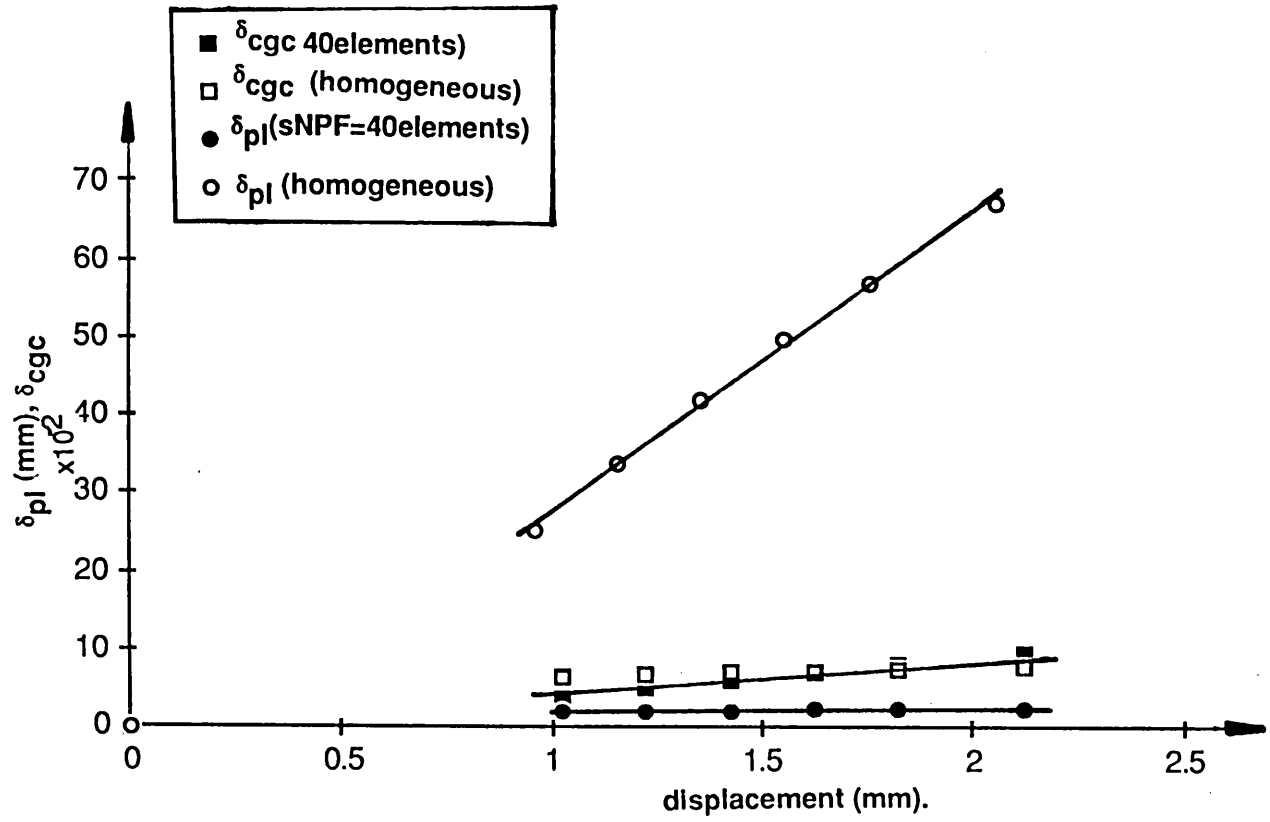


Fig.(5.31) Plastic and rationalized non-dimensional values of COD.
(NFCS = $2\sigma_0$), sNPF = 40elements).

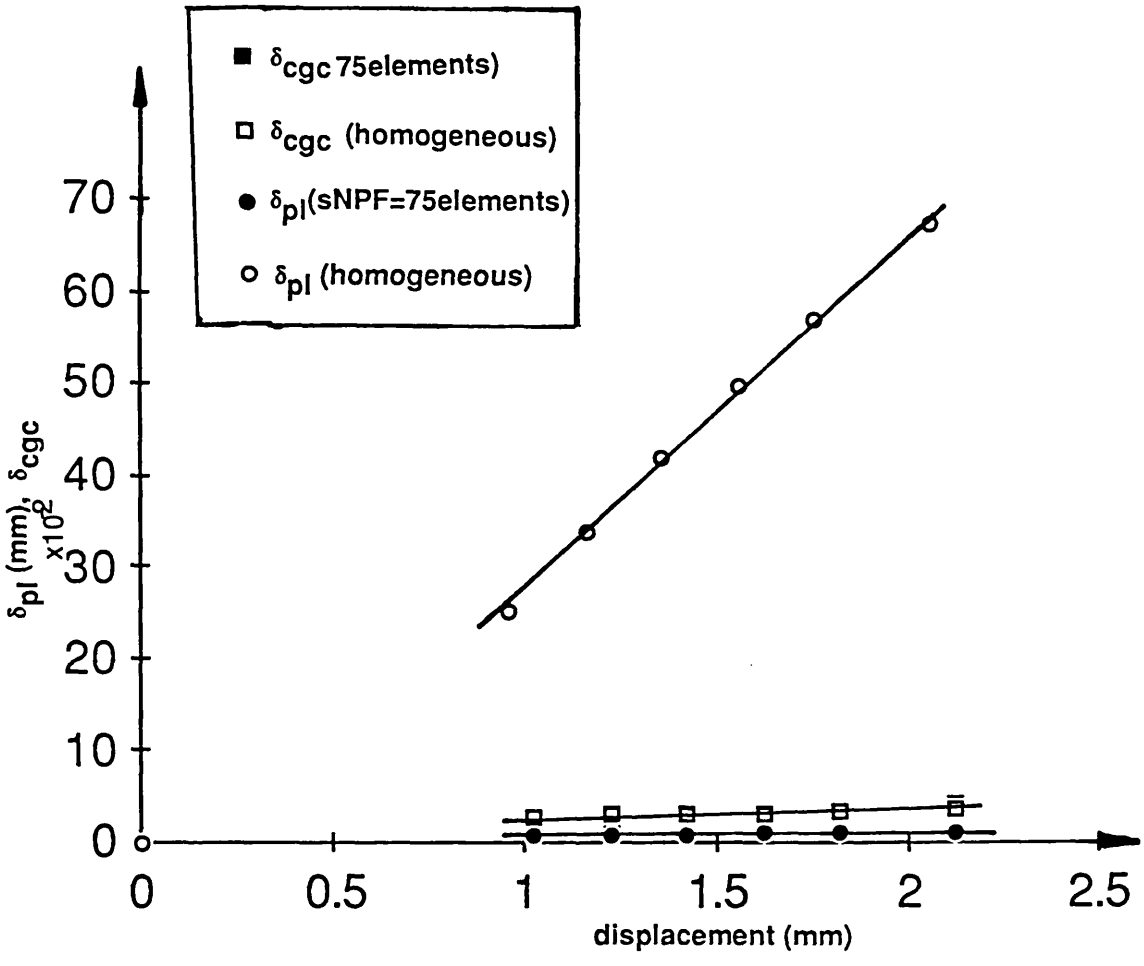


Fig.(5.32) Plastic and rationalized non-dimensional values of COD. (NFCS = 2σ0, sNPF = 75elements).

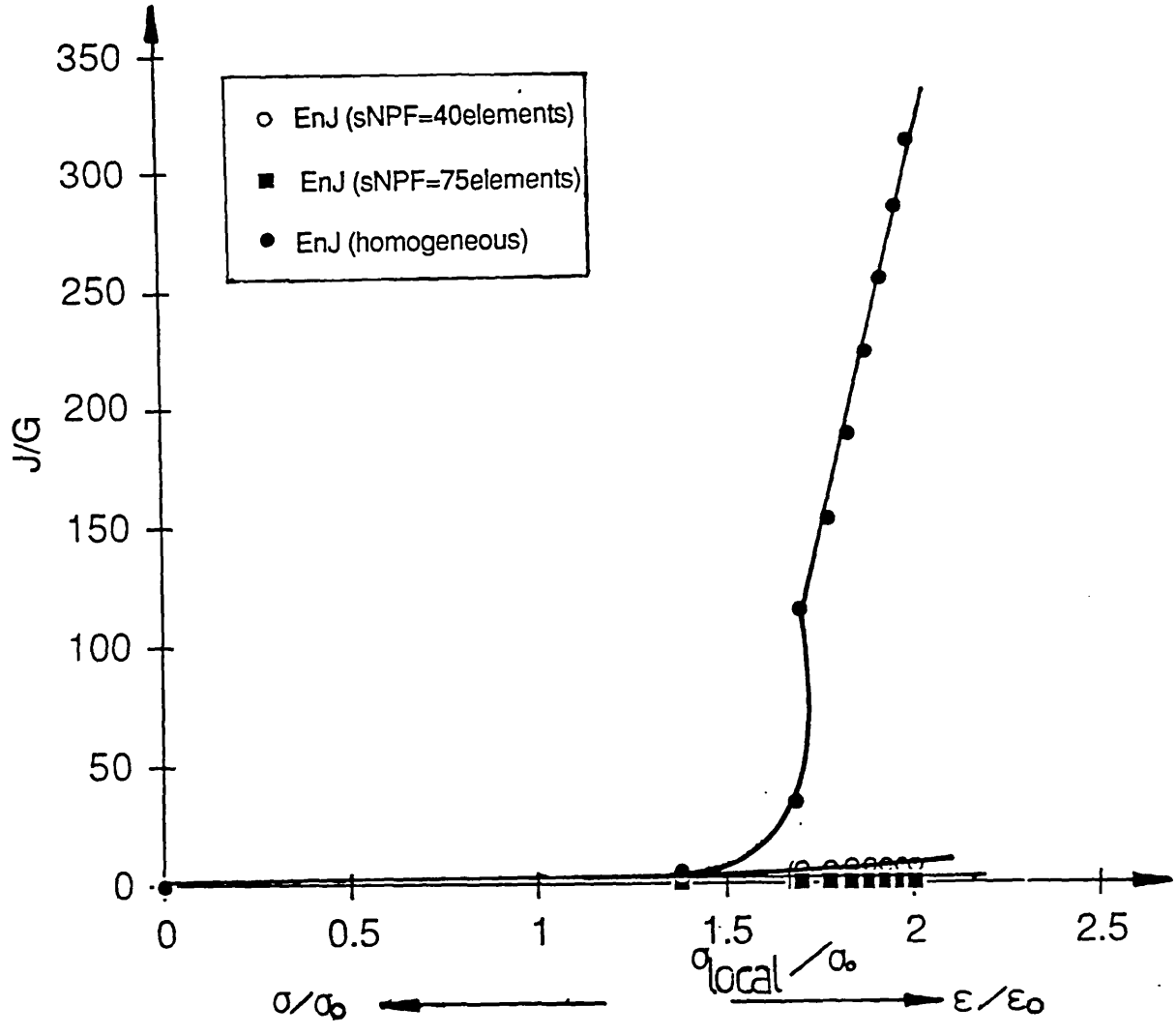


Fig 5.33 The EnJ design curve (based on local yielding).

CHAPTER SIX

CORRELATION OF FATIGUE CRACK GROWTH DATA

6.1 INTRODUCTION

The Paris law, $da/dN = C\Delta K^m$ cited earlier in Chapter Four is known to be able to correlate fatigue crack growth data for secondary or long crack growth stages. It is also known to be inadequate for correlating data at the incipient stages of crack growth when the crack is small and is growing inside the notch plasticity region. In this circumstance, its growth rate is higher than those predicted by a Paris type law. The phenomenon and the efforts that had been made by investigators to describe it has been presented in Chapter Four.

One of the reasons for the failure of the Paris law in the vicinity of the notch tip is because it is essentially based on the stress component, K_σ, of the overall stress concentration factor, K_t, expressed by the Neuber's rule and is then unable to correlate data in the notch plasticity region where events are influenced by the strain component, $K\varepsilon$, of the SCF.

The other factor may be due to the effect of the residual stress - be it monotonically or cyclically imposed - field through which a newly initiated and small crack has to travel before acquiring a size big enough tc make it behave like a long crack. In this notch plasticity field, stresses and strains are higher than what would normally be the case in the LEFM situations, hence the necessity for large crack driving parameters to pull

the crack through this field.

The J-integral is an example of such a driving parameter and it is now known that its values in a region of high strains and stresses vary significantly from those calculated in the adjacent LEFM or far field region.

It was possible in the previous Chapter to unify the J-integral and COD by rationalizing their non-dimensional values. The aims in this chapter are to:

a) Introduce the use of a combination of monotonic and cyclic data in the form of monotonic strains ahead of the notch and the cyclic stress-strain curve for fatigue crack growth data correlation. This idea though approximate, would help in overcoming the problems associated with experiment for measuring stresses and strains in the fracture process zone. It also offers a way of reflecting the effects of K_{ε} and K_{σ}, hence the effect of bifurcation in notched specimens.

b) To correlate fatigue crack growth from short crack to the long crack growth stage. The consequential aspect of this study will be the modification of the Paris law.

c) To look at the behavioural pattern of a correlation parameter with crack length and use the opportunity to predict crack arrest or crack propagation to failure.

d) To apply the newly derived unique expression for the J-integral (J_{cgc}) and the crack opening displacement (δ_{cgc}).

6.2 THEORETICAL BASIS FOR CRACK GROWTH CORRELATION PARAMETER.

The unique expression derived earlier for crack growth correlation are:

1) $JE/C\sigma_{fl}^2a$ or J_{cgc}

2) $\delta E/C_1\sigma_{fl}a$ or δ_{cgc}

The method of analysis so far is computational and empirical, hence there is need to look for a theoretical basis for the established relationships. Consequently, linear elastic fracture mechanics assumptions were adapted and modified for contained yield condition as presented below.

6.2.1 EXPRESSIONS FOR CRACK GROWTH CORRELATION FOR CONTAINED YIELD SITUATION.

6.2.1.1 The J-Integral Analogy.

In simple LEFM terms:

$$K = \sigma\sqrt{\pi a} = Y\sigma\sqrt{a} \qquad (6.1)$$

where

K is the stress intensity factor,

Y is the geometry correction factor,

a is crack length.

$$K^2 = Y^2 \sigma^2 a \qquad (6.2)$$

also,

$$K^2 = EG \qquad (6.3)$$

where

G is the elastic crack driving energy.

E is the Young's modulus.

For contained yield,

$$K^2 \cong EJ \qquad (6.4)$$

Substituting (6.4) into (6.2), we get:

$$EJ = Y^2 \sigma^2 a \qquad (6.5)$$

Divide (5) through by σ_Y^2, then

$$JE/\sigma_Y^2 = Y^2 (\sigma/\sigma_y)^2 a \qquad (6.6)$$

σ/σ_y = non-dimensional notch stress distribution and it is constant for a given notch configuration.

Therefore, $\sigma/\sigma_y = K_n$; hence,

$$JE/\sigma_y^2 = Y^2 K_n^2 a$$

or

$$JE/\sigma_y^2 a = Const = C_o \qquad (6.7)$$

Since, the produce $Y^2 K_n^2$ is constant for a chosen crack length and notch configuration.

6.2.2 The COD Analogy.

Recalling the relationship,

$$J = m \sigma_y \delta \qquad (6.8)$$

Substituting for J

$$C_o (\sigma_y)^2 a/E = m \sigma_y \delta$$

to get

$$\delta E/(\sigma_y)a = C_o/m = C_1 \qquad (6.9)$$

Equations (6.7) and (6.9) are of the same form as the two hybrid parameters obtained in Chapter Five.

Having been able to establish a theoretical basis for the suggested parameters, we shall proceed to apply them to crack growth under monotonic and cyclic loading conditions.

In the above expressions, σ_y, is not a constant yield stress but a flow stress that varies according to the type of analysis to be carried out.

In the LEFM case,

σ_y assumes the magnitude of the monotonic uniaxial tensile yield stress.

For the cyclic plasticity case,

$$\sigma_y = \Delta\sigma \qquad (6.10)$$

$\Delta\sigma$ is the cyclic stress range which can be obtained from a cyclic stress-strain curve. (This curve was obtained in Chapter Three.) A stress range is twice the magnitude of a measured stress amplitude,(σ_a).

$$\text{i.e} \qquad \Delta\sigma = 2\sigma_a = 2\sigma_{fl} \qquad (6.11)$$

σ_{fl} is a more general way of representing stress measured along the plastic part of the cyclic stress-strain curve.

6.3 CORRELATION OF CRACK GROWTH DATA.

In correlating crack growth data from the cyclic plastic dominated near field region to the LEFM dominated region, the applicable parameters will be put in the forms shown below:

From $JE/\sigma_y^2 a = C_o$

$J \propto J_{cgc} = CY^2 \sigma_{fl}^2 a$

where,

$C = K_n^2/E$ = constant for a given notch configuration, either for the monotonic or cyclic case.

In this light, an approximation is made, and

$$J \propto J_{cgc} = (Y^2 \sigma_{fl}^2 a)/E \quad (6.12)$$

also

$$\delta \propto \delta_{cgc} = (Y^2 \sigma_{fl} a)/E \quad (6.13)$$

Using the appropriate σ_{fl} or σ_y the values of J_{cgc} and δ_{cgc} were determined for increments of crack length or distance along the uncracked ligament. These incremental crack lengths are fictitious in that the crack is not physically growing, However, the values are near enough approximation of

what probably happens along the uncracked ligament.

After calculating J_{cgc} and δ_{cgc} they were plotted against the increments of crack length as shown in Figs (6.7) to (6.14). The curves that result were used to predict crack behaviour.

6.4 DETERMINATION OF STRENGTH PARAMETERS FOR ANALYSIS.

6.4.1 Monotonic.

The monotonic data are presented in Figs (6.2) to (6.6) i.e strain distribution ahead of notch tips. The most important part of these data is the region of high strains. The "tails" of the curves were assumed to be characterized by LEFM strength distribution i.e σ_y (monotonic or uniaxial yield stress).

In applying these data, the striation model by Laird (120,121) was assumed. Under this model a striation was assumed to be created per fatigue cycle and each striation was considered a crack length increment. The assumption here, is that on the macroscopic scale, an increment of length measured ahead of a notch along the crack growth direction is made up of several striations culminating in a macroscopic increment of crack length.

For every incremental length, a corresponding strain was obtained from

the strain distribution curve and these strains were used to extract data from the settled cyclic stress-strain curve by measuring the stress amplitudes at these values of strain.

6.4.2 Cyclic Data.

These are taken from the cyclic stress-strain curve. The cyclic stress amplitudes were multiplied by 2 to get the stress range . The cyclic stress range was used in the calculation of the cyclic component of the hybrids. Recall that they replace σ_{fl} in analysis.
It was not feasible to construct cyclic stress-strain curve for high strain amplitudes from experiments. Consequently, one of the cyclic stress-strain curves (for aluminium) obtained in chapter 3 was used to formulate an empirical formula as given below:

$$\sigma_a/\sigma_o = 1.25 \left(\varepsilon_a/\varepsilon_o \right)^{0.15} \qquad (6.14)$$

Using equation (6.14), it was possible to find $\Delta\sigma$ for the very high magnitudes of strain measured immediately ahead of the notch.

6.5 THE GEOMETRY CORRECTION FACTOR, Y.

This factor was used because analyses were done on finite plates. For compact tension case, it is calculated from the formula,

$$Y = (w/a)^{1/2} \cdot f(a/w) \qquad (6.15)$$

where

$$f(a/w) = (2 + a/w)\,(0.886 + 4.64\,a/w - 13.32\,(a/w)^2 + 14.72\,(a/w)^3 - 5.6\,(a/w)^4\} \qquad (6.16)$$

a is the crack length, and
w is the total size of ligament (or the total width of plate inclusive of the crack).

6.6 OBSERVATIONS.

6.6.1 STRAIN DISTRIBUTION CURVES.

With reference to the strain distribution curves, it is noticeable that the length of region of high strain values lying ahead of a notch varied with type of notch. In exact terms, the size of the region of influence of notch (region of high strain values) decreased as the notch tended to a sharp crack.

The cyclic and monotonic strain distribution curves for SCF = 5 were plotted on Fig (6.5). The cyclic curve which was obtained after ten cycles was found to settle down at a maximum strain value of about a quarter of the highest strain measured for the monotonic loading situation. It is however noteworthy that the cyclic and monotonic curves

came close to each other at a distance of length approximately equal to 1/2 x (notch depth). It is therefore arguable that the data came to good agreement at a distance away from the notch tip where realistic strains were measured.

In this wise, the possibility of a cyclically induced region of residual stress range becomes plausible. Also, the strains computed in the monotonic case could be used for analysis as against taking the trouble to cycle meshes on the computer for definite cyclic strain distribution.

Finally, the ellipsoidal strain distribution curves started the formation of "tails" from a distance equivalent to approximately a notch depth. The regions of interest on these curves are the small areas of high plastic strains. The "tail" region is assumed to be LEFM dominated.

6.6.2 J_{cgc} CURVES.

The J_{cgc} versus x/h curve for the various notches studied showed that the hybrid parameter J_{cgc} was able to correlate fatigue crack growth, in that it predicted curves that conform with LEFM types for the monotonic cases and the high small crack growth curves for the fatigue or cyclic situation.

x/h = Length along ligament / notch depth.

6.6.3 SCF = 2.

In case of the stress concentration factor of 2 Fig (6.7), the driving parameter, J_{cgc}, for the cyclic case grew to about 35 times more than the monotonic curve at a distance of about one notch depth on the ligament and then to slowed down. The point of inflexion is possibly the magnitude of this parameter at crack initiation. After this point, the crack driving force slowed down until about a length of 3 notch depths after when it rose again. It continued to rise without meeting the monotonic curve for up to a ligament length of about 5 notch depths. The pattern of this cyclic curve suggests that it might meet the monotonic curve eventually.

The slope of the cyclic curve for the J_{cgc} measured on the tangent from zero is $400\ N/m^{-1}$ and that of the monotonic one is $37.2\ m^{-1}$. Consequently, the slope of the cyclic curve is about 11 times that of the monotonic curve.

Using the δ_{cgc} for the same notch configuration Fig (6.11), it was observed that the point of inflexion on the cyclic curve lies just beyond one notch depth from the notch tip. There was a slowing down between 1.5 and 3 notch depths after which this curve began to rise steeply away from the monotonic curve.

The slope of the cyclic curve measured on the tangent from zero is about $40\ N/m^{-1}$ and that of the monotonic curve is $9.09\ N/m^{-1}$. Consequently, cyclic slope = 4 x (monotonic slope).

6.6.4 SCF = 3.

Data correlation for the case of a circular hole in a plate (SCF = 3) using the two hybrids J_{cgc} and δ_{cgc} revealed the same pattern of the cyclic curve being higher than the monotonic one in the vicinity of the crack tip. There was hardly a unique maximum value on this cyclic curve. There is a lower and upper point of inflexion at about 0.5 notch depth and 2 notch depths respectively. After the second point of inflexion, the curve rose very rapidly showing a pattern as if it would eventually meet the monotonic curve at a distance much beyond the 3.5 notch depths shown.

The slope on the tangent at zero for the cyclic case is about 300, whilst that of the monotonic curve is about 20.3. Therefore, the cyclic slope is approximately 15 times the monotonic one.

Fig (6.12) gives the monotonic and cyclic curves when the δ_{cgc} is used. The pattern of the curve was similar to that of the SCF = 2 case. Two points of inflexion were barely visible at about 0.5 and 1 notch depth away. The cyclic curve rose steeply afterwards running almost parallel to the monotonic one.

The slopes from zero are as follows:

cyclic = 506.33 m^{-1}

monotonic = 141.18 m^{-1}

so that

cyclic slope = 3.586 x monotonic slope.

6.6.5 SCF = 5.

In the case of the ellipsoidal notch of stress concentration factor of 5, the J_{cgc} curve rose to an initiation point at about 0.5 notch depths away from the notch tip. The point of inflexion and commencement of decline of this cyclic curve laid just beyond the point of initiation. The decline measured about 102 units before joining the monotonic curve at about 1.5 notch depths away from the notch tip.

The slope of the tangent drawn from zero on the cyclic curve is approximately 442.86. The monotonic slope is 25. Consequently, the cyclic slope is about 17.71 x (monotonic slope).

Using the δ_{cgc} parameter, we arrive at the graph presented as Fig (6.13). The cyclic curve rose gradually until it reaches a maximum at about 0.6 notch depth away from the notch tip. The curve began to drop just after this point and it eventually met the parabolic monotonic curve at about 1.5 notch depths away from the notch tip.

The slope of the cyclic curve is 483.325 whilst that of the monotonic curve is 125. Hence, the cyclic slope is equal to 3.8666 x (monotonic slope)

6.6.6 SHARP NOTCH (THE SMALL CRACK CASE).

For the sharp notch studied, the initiation point occured at about 0 .25 (notch depth) away from the notch tip. After inflexion, the curve declined curvilinearly for about 77 units before finally linking up with the

monotonic curve at about 0 .625 notch depth away.
The slope of the cyclic curve measured on the tangent from zero is about $342.86\Delta^{m-1}$.The monotonic slope is $11.88\Delta^{m-1}$so that:

cyclic slope = 28.86 x (monotonic slope).

The COD curve had a gradual ascent until it reaches a point of inflexion at about 1 notch depth away from the notch tip. The decline measured about 147 units. The link up with the monotonic curve occured at about 1 notch depth away from the notch tip.

The cyclic slope is approximately $222\Delta^{m-1}$.The monotonic slope is $66.67\Delta^{m-1}$.In this wise,

The cyclic slope = 3.33 x (monotonic slope).

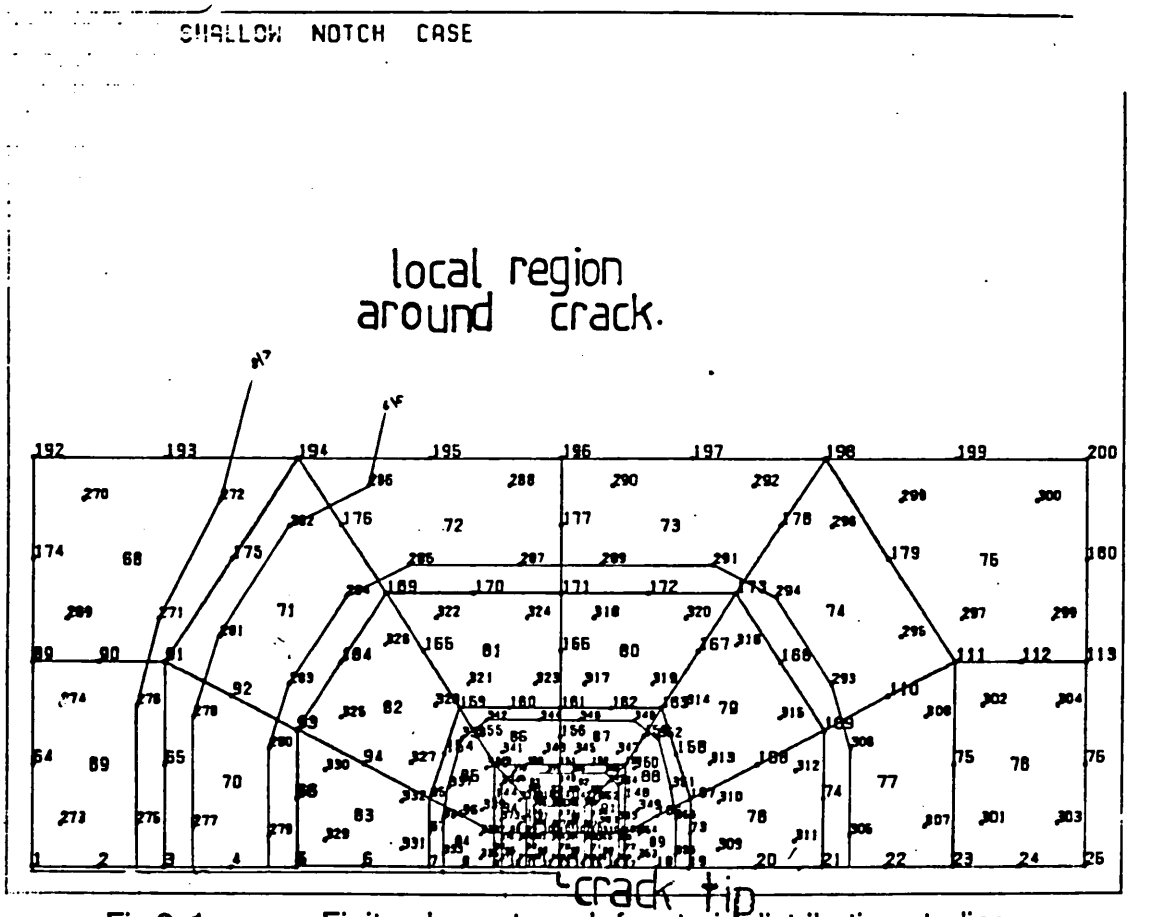


Fig 6. 1 Finite-element mesh for strain distribution studies.

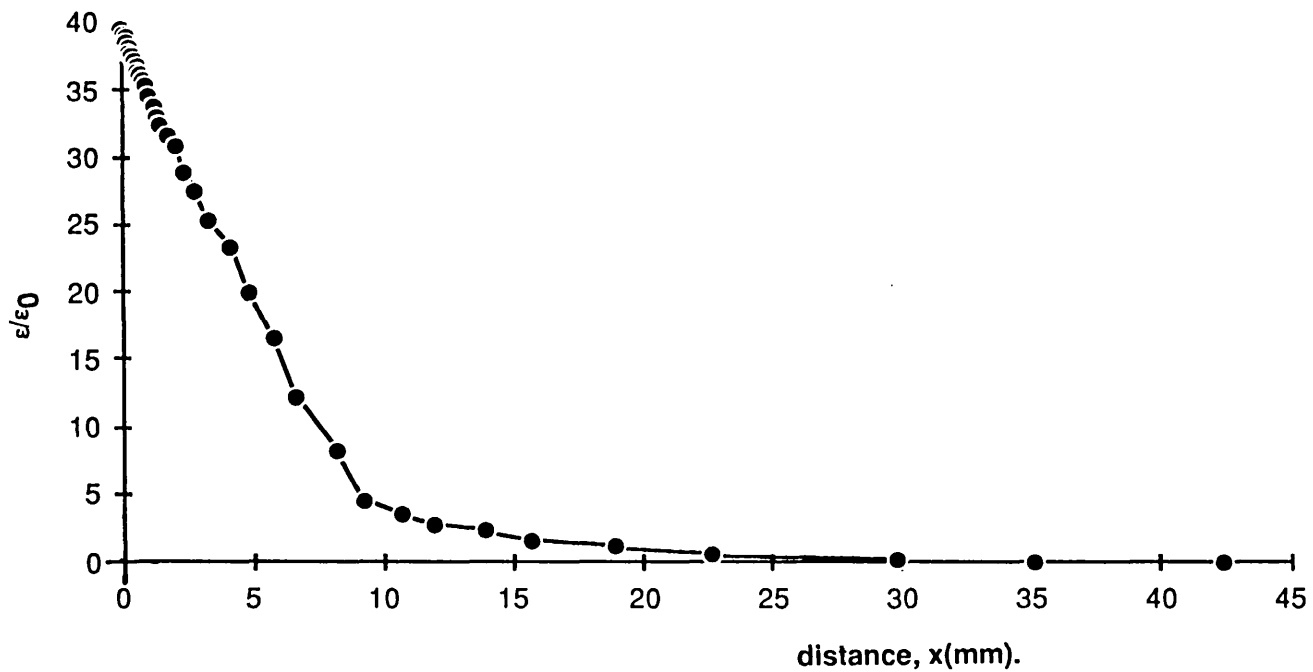


Fig.(6.2). Strain distribution ahead of a notch. (SCF=2).

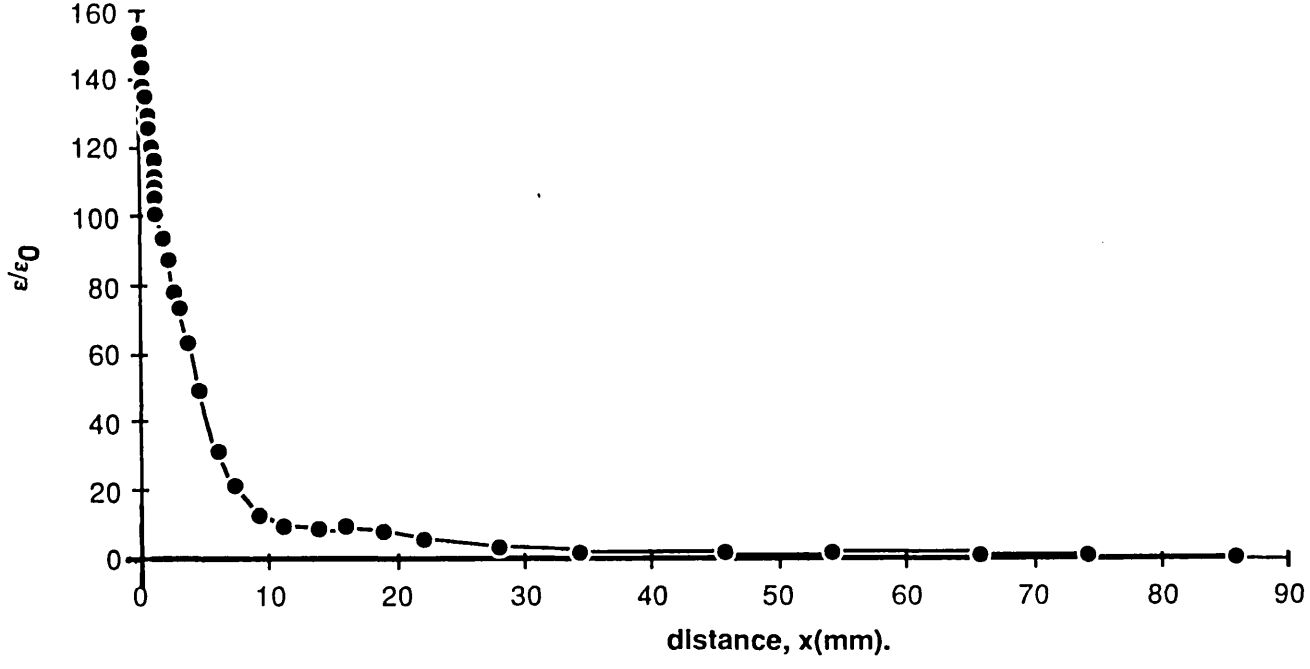


Fig.(6.3). Strain distribution ahead of a notch. (SCF=3).

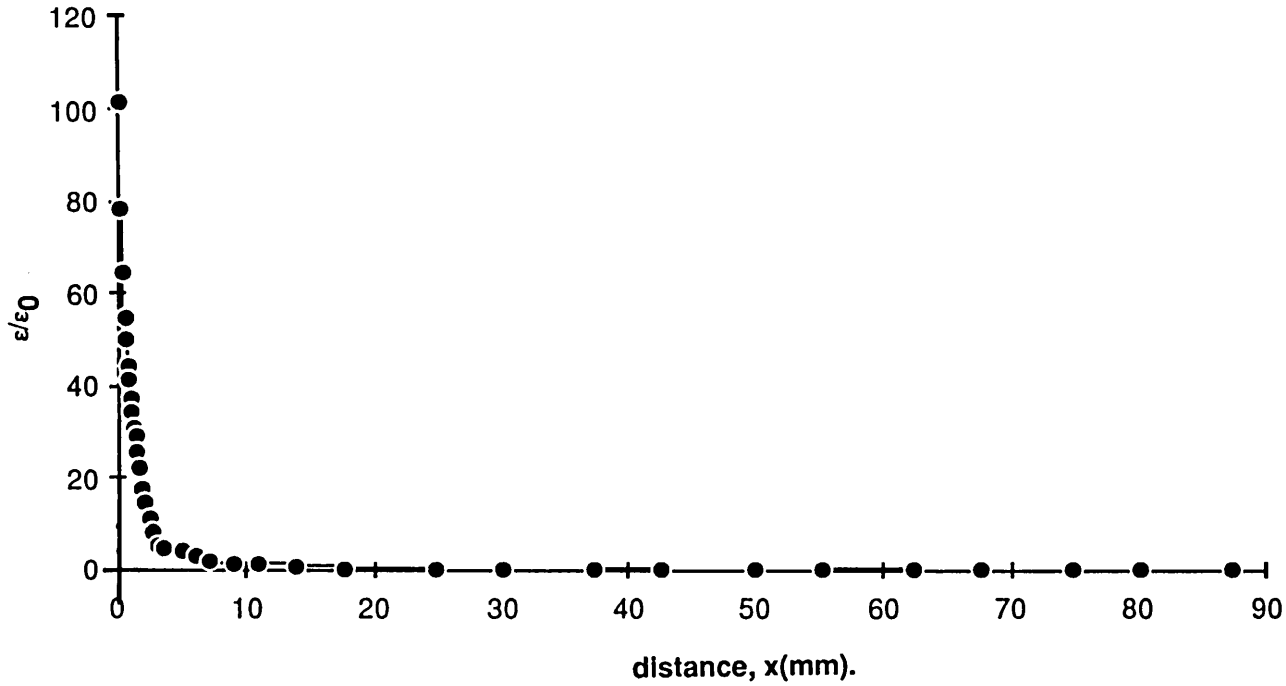


Fig.(6.4). Strain distribution ahead of a notch. (SCF=5).

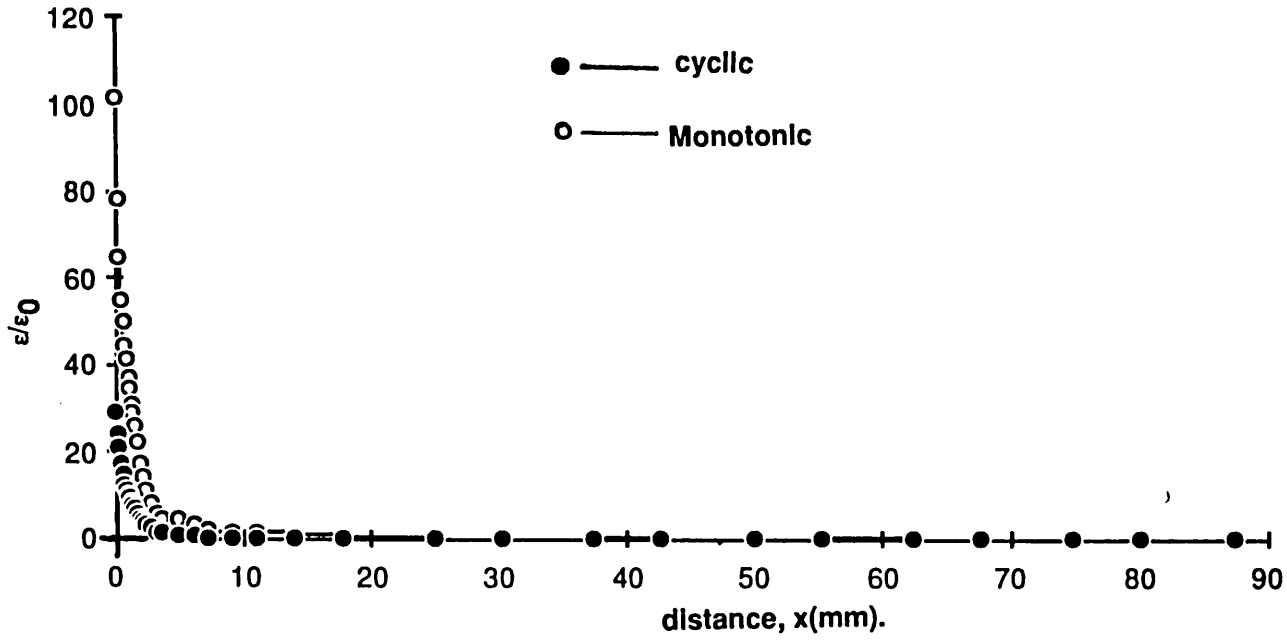


Fig.(6.5). Comparison of strain distribution ahead of a notch for monotonic and cyclic loading. (SCF=5).

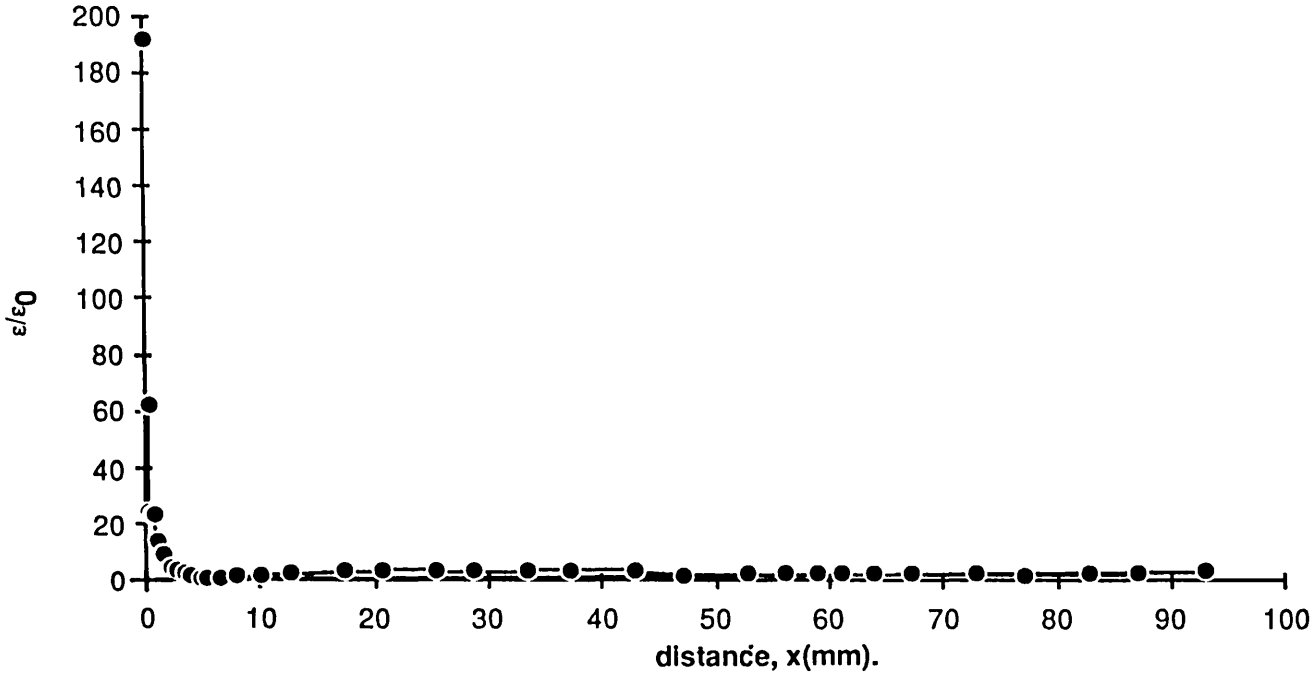


Fig.(6.6). Strain distribution ahead of a sharp crack. (a/w = 0.05).

SCF=2, h=5.0mm σ_o=0.165 GN/mm^2.

x/h	Y^2	$\Delta\sigma^2$	J_{cgc}	ΔJ_{cgc}	δ_{cgc}	$\Delta\delta_{cgc}$
.0052	88.897	.9332	.0629	2.157	.3814	2.2327
.0302	88.477	.9262	.3634	12.37	2.204	12.858
.0552	88.060	.9193	.661	22.343	4.010	23.300
.0802	87.723	.9128	.9568	32.109	5.804	33.608
.1052	87.401	.9193	1.250	42.263	7.586	44.079
.1302	87.081	.9155	1.542	51.899	9.354	54.241
.1606	86.751	.9067	1.895	63.162	11.494	66.331
.2106	86.258	.8765	2.471	79.612	14.987	85.035
.2632	85.910	.8616	3.075	97.410	18.655	104.94
.3416	88.733	.8435	4.122	127.84	25.007	139.19
.4816	88.619	.8050	5.804	171.78	35.210	191.46
.6634	88.263	.7555	7.963	221.19	48.307	254.47
.9690	91.062	.6587	12.00	290.62	72.797	358.07
1.336	103.77	.4987	18.85	345.63	114.36	489.44
1.850	102.54	.3519	25.80	333.82	156.52	562.73
2.776	124.71	.2177	47.09	376.894	285.66	807.80
4.528	238.28	.0880	146.75	474.770	890.19	1601.3

Table 1 Values of Jcgc, ΔJcgc, δcgc and $\Delta\delta$cgc for SCF=2

SCF=3, h=10.0mm σ_0=0.165 GN/mm^2.

x/h	Y^2	$\Delta\sigma^2$	J_{cgc}	ΔJ_{cgc}	δ_{cgc}	$\Delta\delta_{cgc}$
.0303	91.188	.3961	.7567	10.937	4.556	17.51
.0553	90.855	.3806	1.366	19.115	8.287	30.98
.0803	90.480	.3699	1.976	26.869	11.99	44.18
.1105	90.165	.3590	2.711	35.778	16.45	35.78
.1197	87.199	.3527	2.840	36.819	17.23	61.99
.1130	90.127	.3494	2.771	35.594	16.81	60.22
.1145	90.123	.3449	2.806	35.581	17.02	60.59
.1161	90.120	.3392	2.845	36.075	17.26	60.92
.1894	86.470	.3290	4.455	53.890	27.02	93.96
.2159	89.263	.3202	5.241	61.694	31.79	109.0
.2592	89.048	.3063	6.277	70.684	38.08	127.7
.3014	88.91	.2982	7.289	79.915	44.22	146.4
.3736	88.64	.2818	9.007	93.316	54.64	175.8
.4528	88.60	.2554	10.92	102.47	66.20	202.8
.5972	88.86	.2134	14.43	113.24	87.56	245.2
.7240	89.39	.1811	17.60	117.20	106.78	275.4
.9260	90.72	.1491	22.85	125.26	138.62	324.4
1.106	92.30	.1329	27.76	135.63	168.39	372.1
1.894	103.3	.1254	53.23	245.44	322.94	693.1
3.422	150.5	.0668	140.1	344.11	849.97	1332

Table 2 Values of Jcgc, ΔJcgc, δcgc and $\Delta\delta$cgc for SCF=3

SCF=5, h=10mm σ_0=0.165 GN/mm^2.

x/h	Y^2	$\Delta\sigma^2$	J_{cgc}	ΔJ_{cgc}	δ_{cgc}	$\Delta\delta_{cgc}$
.0197	88.648	1.2264	.4750	21.428	2.8830	19.3490
.0447	88.262	1.0566	1.074	41.705	6.5130	40.576
.0697	87.853	.9765	1.666	59.812	10.106	60.528
.0947	87.536	.9036	2.255	74.92	13.681	78.82
.1197	87.199	.8448	2.840	88.193	17.225	95.949
.1447	86.918	.7861	3.421	98.868	20.752	111.51
.1894	86.470	.6561	4.455	107.47	27.027	132.68
.2394	86.059	.5625	5.605	115.90	33.998	154.54
.4243	85.197	.3770	9.833	136.28	59.656	221.96
.6077	85.114	.2715	14.069	140.43	85.344	269.48
.7187	89.360	.1989	17.469	127.74	105.97	286.44
.9063	86.172	.0272	21.243	21.243	128.86	128.86
1.389	89.820	.0272	33.937	33.937	205.87	205.87
3.014	119.69	.0272	98.131	98.131	595.28	595.28
4.986	260.11	.0272	352.75	352.75	2139.8	2139.8

Table 3 Values of Jcgc, ΔJcgc, δcgc and $\Delta\delta$cgc for SCF=5

Sharp crack a/w=0.05, σ_0=0.165 GN/mm^2.

x/h	Y^2	$\Delta\sigma^2$	J_{cgc}	ΔJ_{cgc}	δ_{cgc}	$\Delta\delta_{cgc}$
.0132	114.96	1.755	.2064	13.32	1.252	10.05
.0493	113.12	1.119	.7585	31.21	4.601	29.50
.1118	110.03	.7611	1.673	46.81	10.15	53.66
.2236	105.89	.6195	3.220	73.33	19.53	93.17
.3028	105.67	.5219	4.352	83.51	26.40	115.59
.4472	99.615	.3919	6.058	87.28	36.75	139.42
.5528	97.434	.3286	7.326	88.50	44.44	154.38
.8028	93.654	.2876	10.23	108.1	62.03	201.62
1.085	91.017	.2131	13.43	105.2	81.44	227.88
1.569	88.906	.0272	18.97	18.97	115.1	115.10
4.138	97.989	.0272	55.15	55.15	334.5	334.5
7.423	140.80	.0272	142.1	142.1	862.2	862.2
10.58	274.16	.0272	394.4	394.4	2392	2392

Table 4 Values of Jcgc, ΔJcgc, δcgc and $\Delta\delta$cgc for a small sharp crack, a/w 0.05.

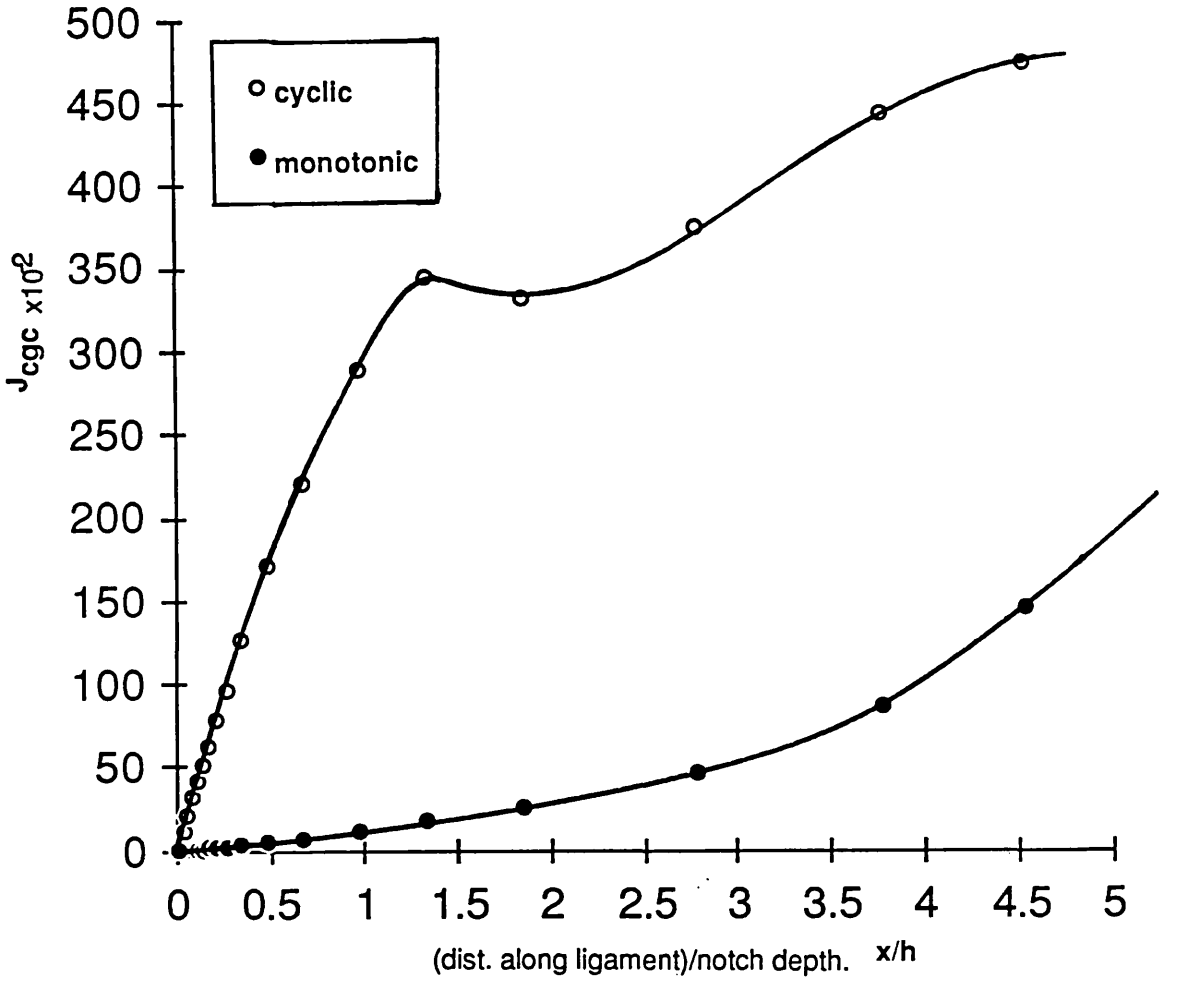


Fig.(6.7). Monotonic and fatigue crack growth correlation using J_{cgc}, SCF=2.

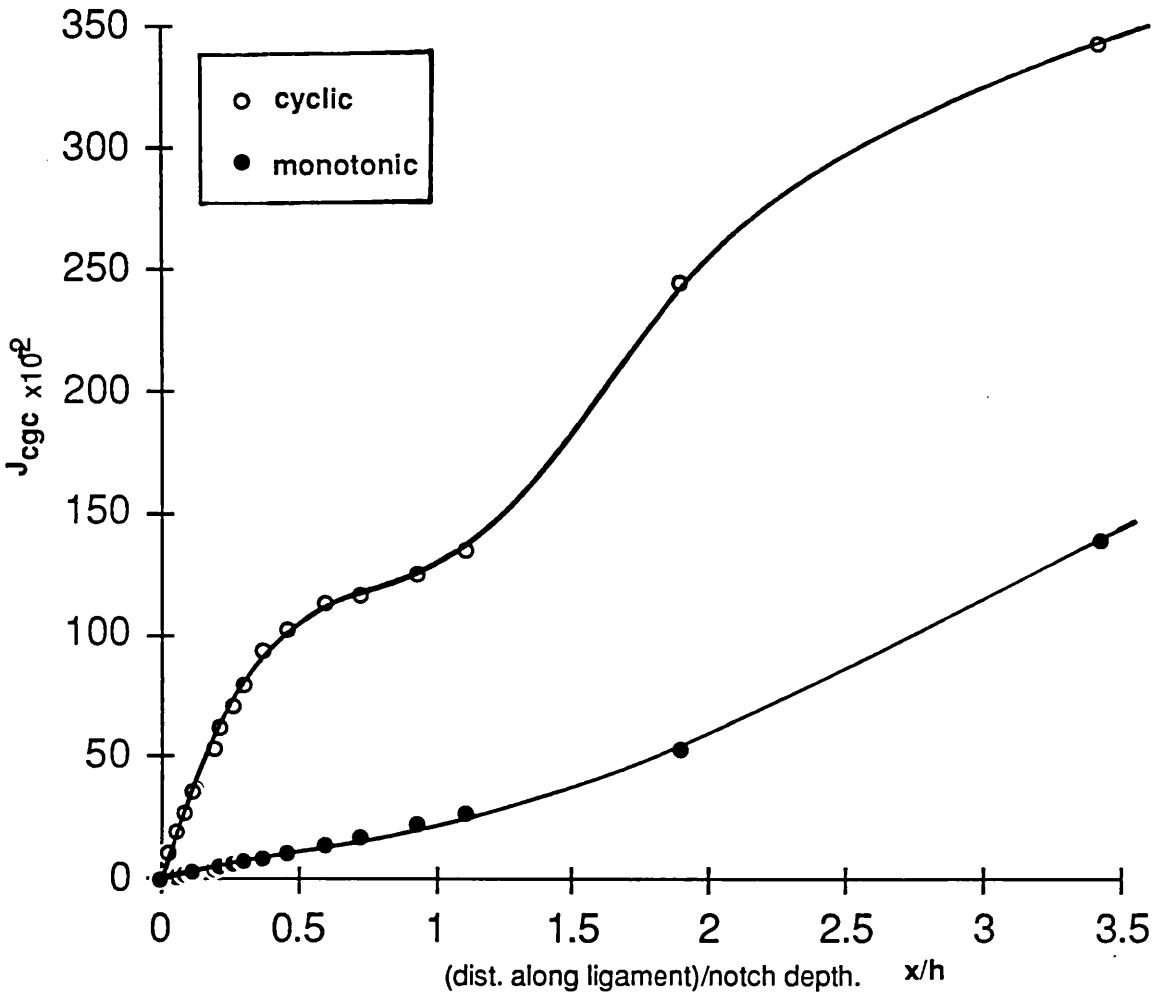


Fig.(6.8). Monotonic and fatigue crack growth correlation using Jcgc, SCF=3.

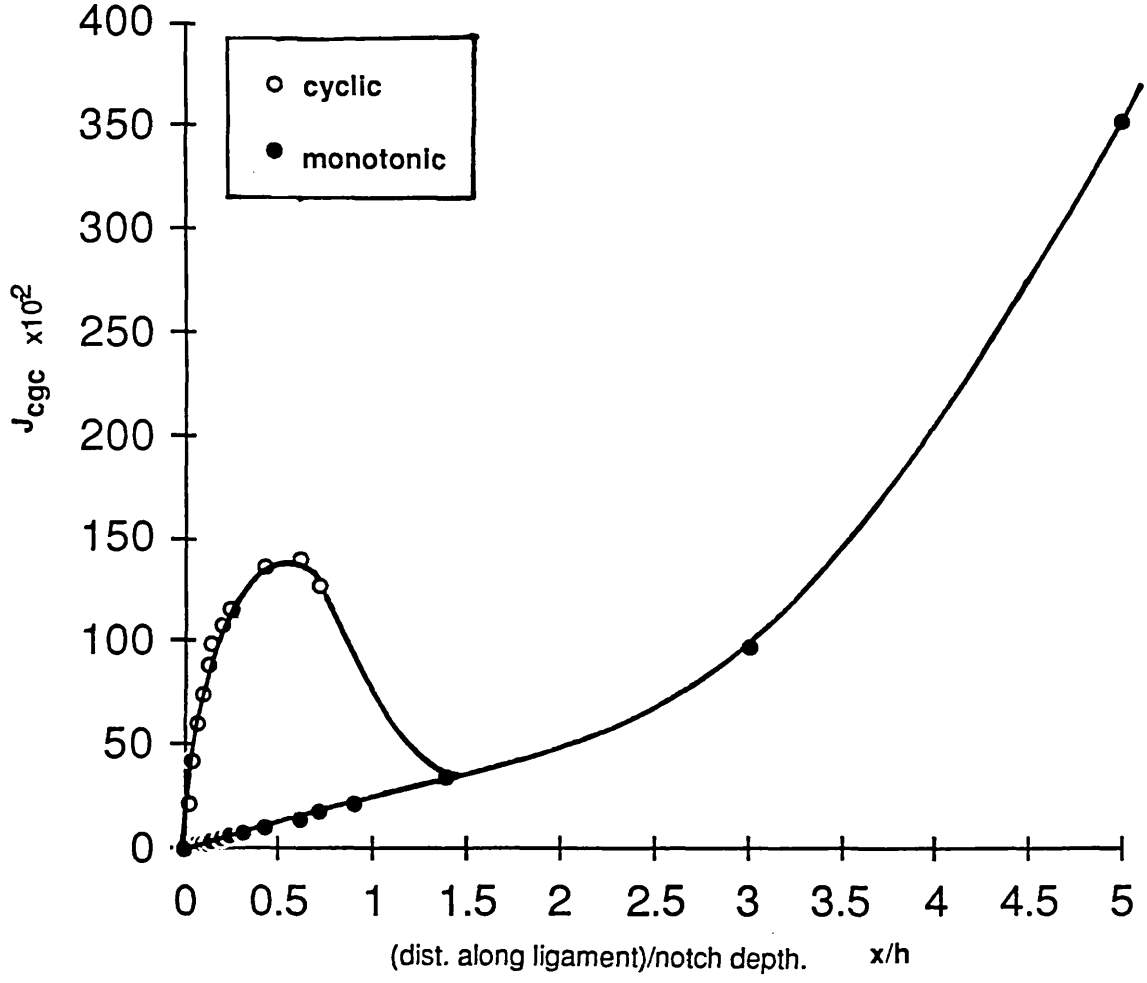


Fig.(6.9). Monotonic and fatigue crack growth correlation using Jcgc, SCF=5.

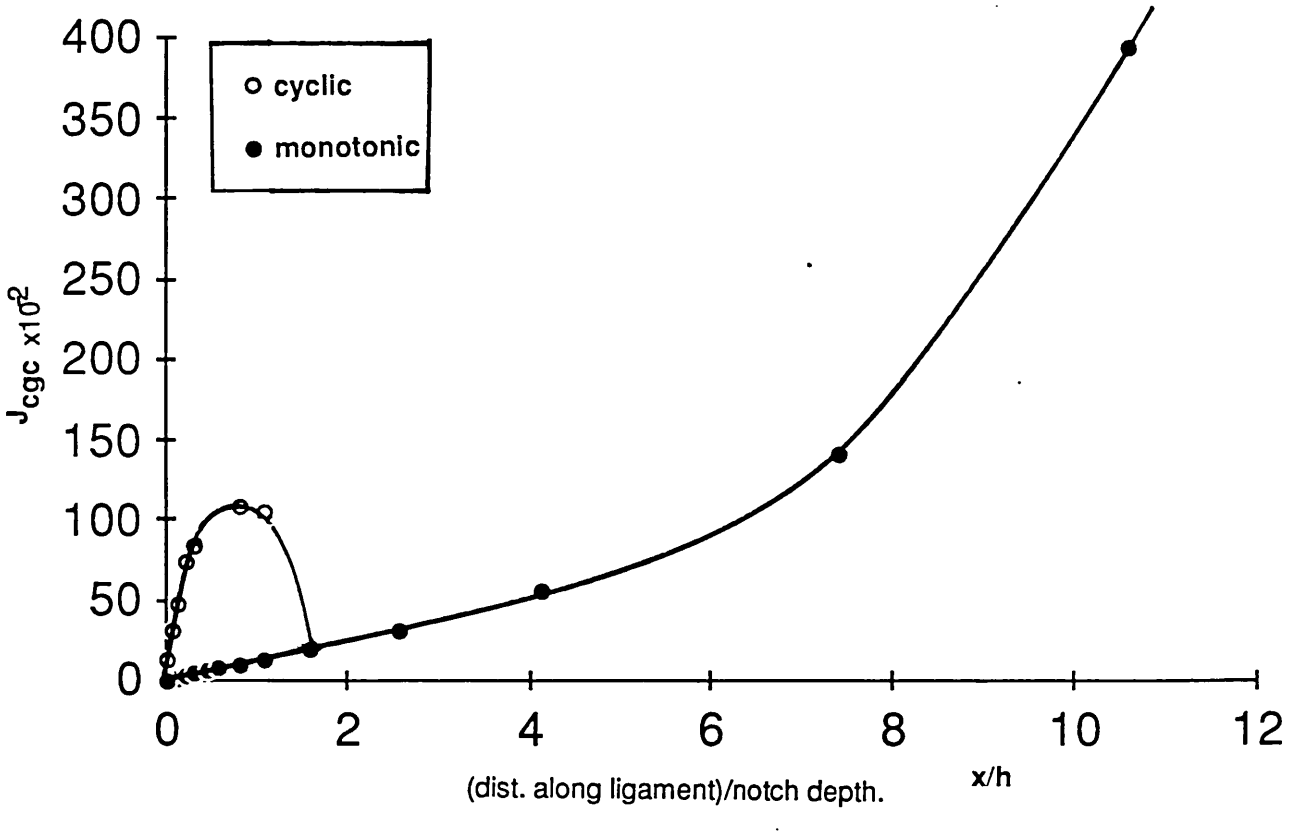


Fig.(6.10). Monotonic and fatigue crack growth correlation using Jcgc, sharp crack a/w=0.05.

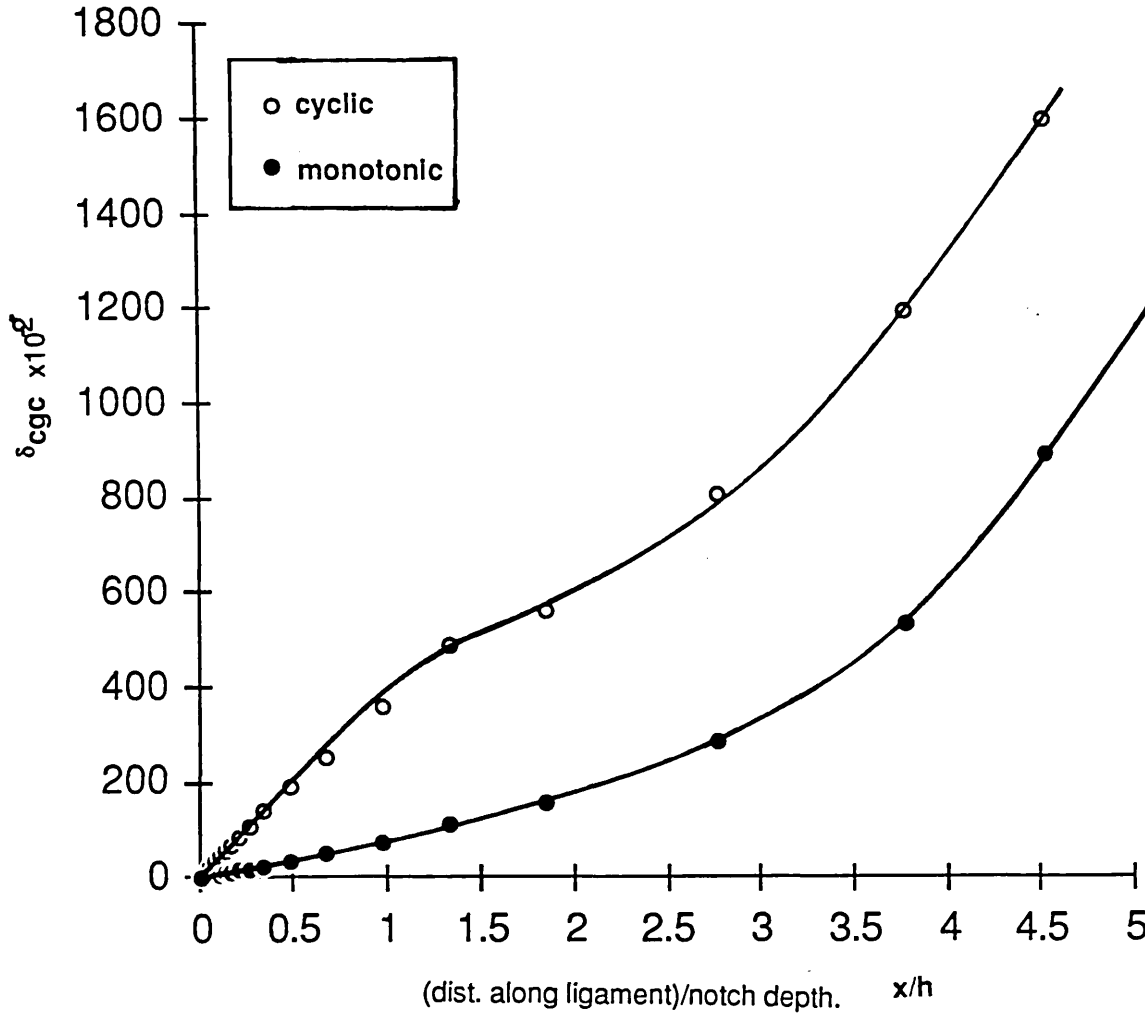


Fig.(6.11). Monotonic and fatigue crack growth correlation using δcgc, SCF=2.

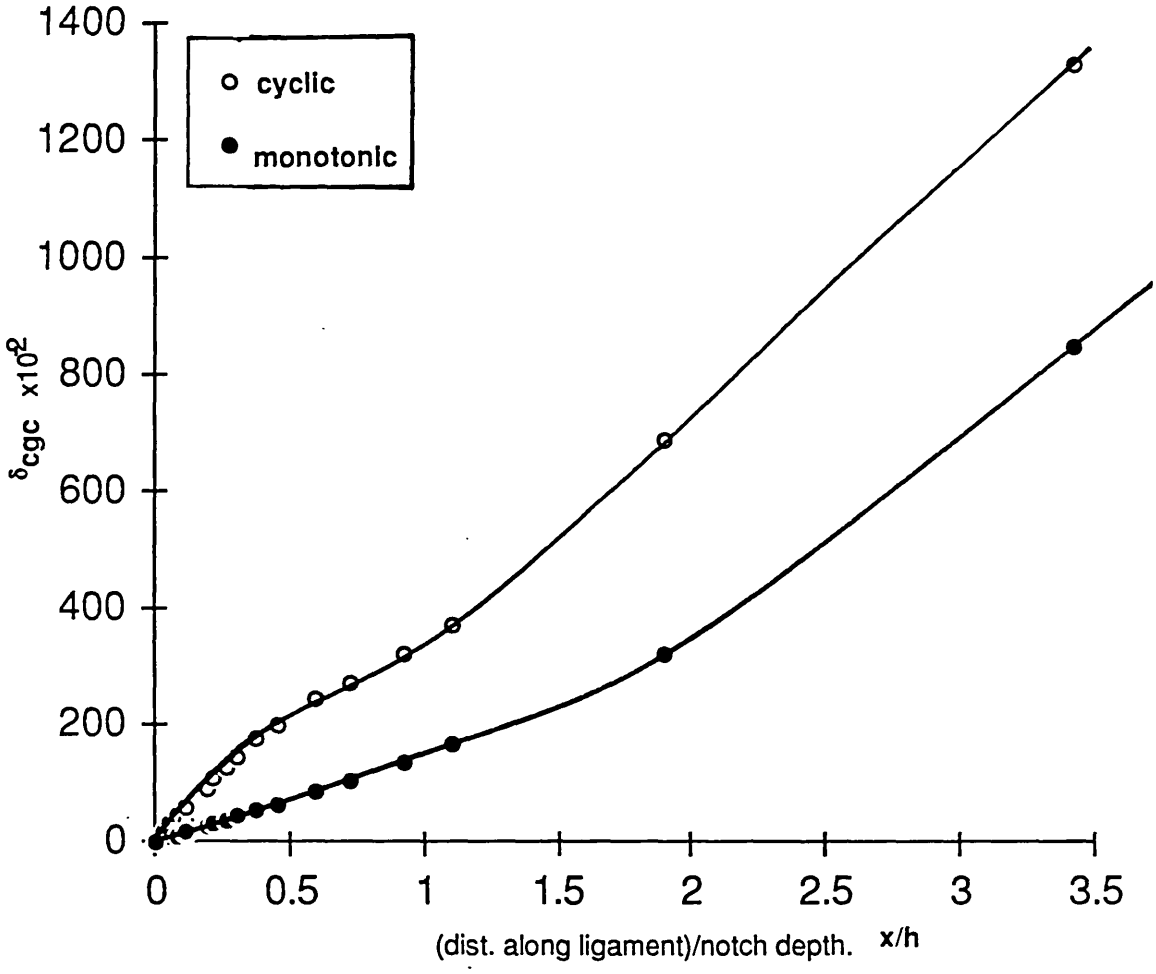


Fig.(6.12). Monotonic and fatigue crack growth correlation using δcgc, SCF=3.

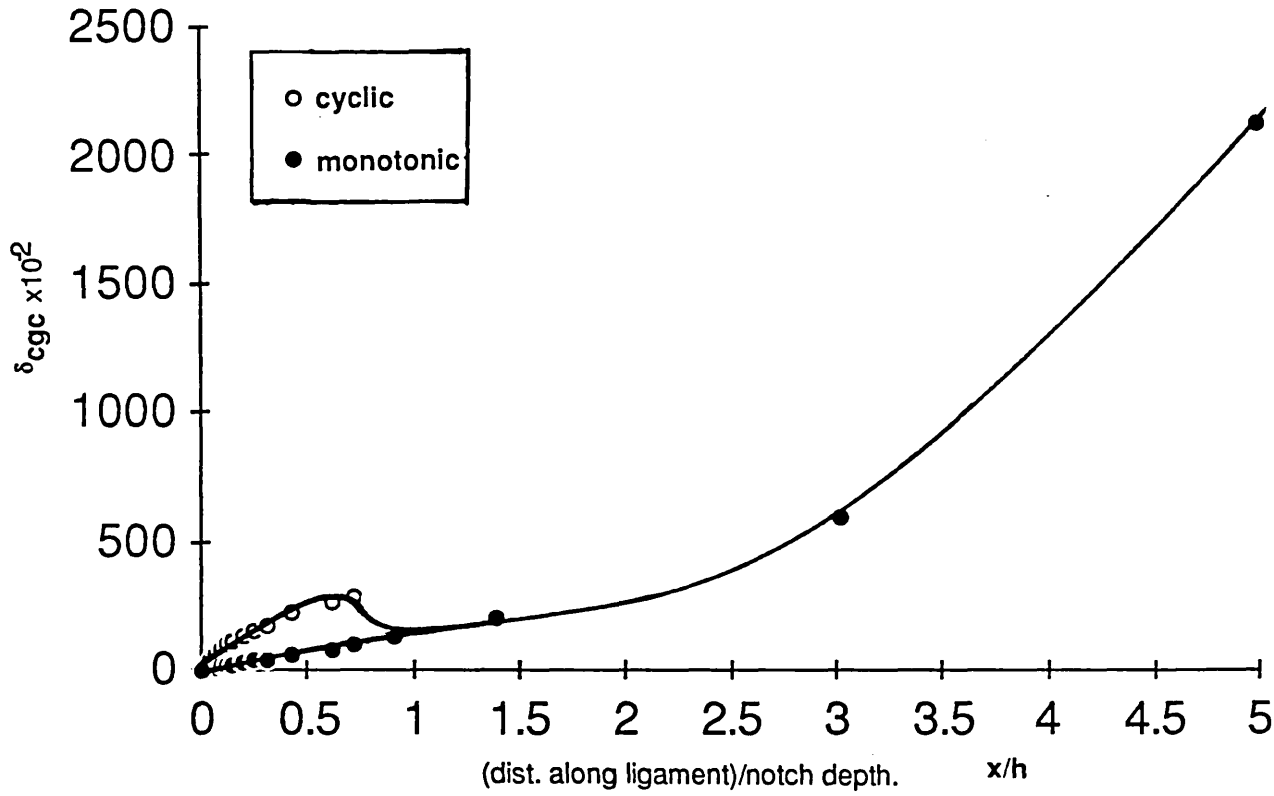


Fig.(6.13). Monotonic and fatigue crack growth correlation using δcgc, SCF=5.

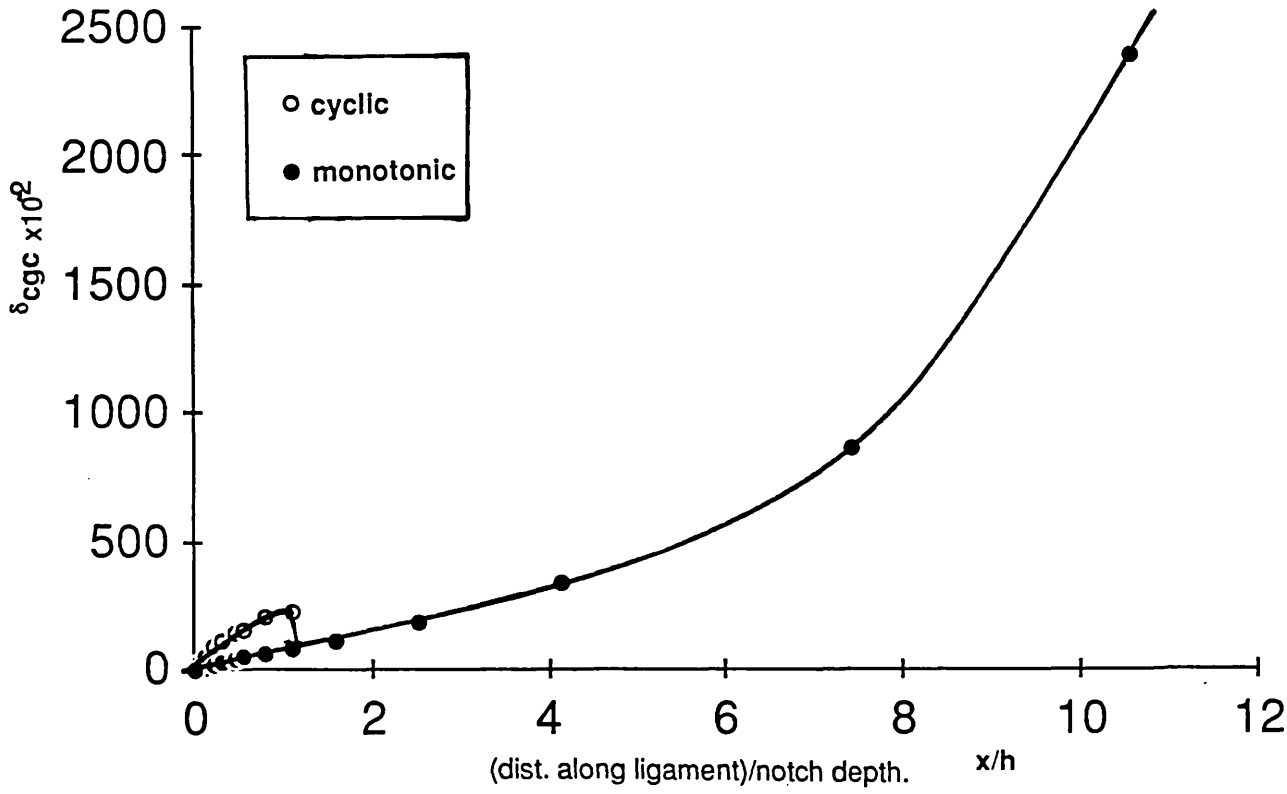


Fig.(6.14). Monotonic and fatigue crack growth correlation using δcgc, sharp crack, a/w=0.05

CHAPTER SEVEN

DISCUSSION AND CONCLUSION.

Studies on experimental investigations of fatigue processes reported in Chapter Two led to the conclusion that the response of an engineering material to cyclic loading is essentially plastic. Also, it was noted that the von-Mises yield criterion and hence yield surface, is suited to the investigation of initial and subsequent yielding of a material. Under plastic loading, the ellipsiodal von-Mises yield surface expands and translates rigidly in a chosen stress space.

Theoretical elastic-plastic analyses were employed for describing the observable behavioural patterns. Various elastic-plastic models exist in the form of isotropic-hardening, kinematic-hardening and combined-hardening models. The isotropic hardening models suggests that during plastic loading the von-Mises yield surface expands concentrically about a fixed origin (ie centre of the initial yield surface). The kinematic-hardening model expresses a situation of hardening in which the Bauschinger effect, exhibited by materials when unloaded from a plastic loading state to beyond reversed yield, is considered. Under this model, the yield surface retains its shape and size and is allowed to translate rigidly along a vectorial path. Experiments show that this vectorial or loading path coincides with the direction of the pre-strain or pre-stress vector and it is perpendicular to the tangent drawn through the loading point on the yield surface.

Traditionally, the combined-hardening theory unifies the two theories already defined. For most materials it accords with experimentally observable behavioural pattern since it allows for expansion and translation of yield surface at the same time. The route through combined hardening theory was particularly attractive and was exploited throughout the cyclic study carried out in this thesis.

The combined -hardening theory developed offers an improvement on established ones in that it offers a tripartite combination of hardening rules instead of the usual dual ones (ie the isotropic - and kinematic-hardening rules). The proposed model is a union of the isotropic-hardening, kinematic-hardening and the anisotropic-hardening models.

Usually, it is wrongly assumed that the kinematic-hardening model is also the anisotropic-hardening model. It is argued in this thesis that the kinematic-hardening model refers to the aspect of anisotropic-yielding behaviour in which the yield stress value in tension is different from that measured in the reverse direction due to the Bauschinger effect. Anisotropic-hardening however, seeks to recognise the situation in which the hardening rate is different in forward and reversed loading directions. On a plastic loading and unloading curve of a material, the slopes of the plastic parts of the stress-strain curves are often found to be different and this has to be accounted for in any attempt to describe material behaviour fully.

The isotropic-hardening and kinematic-hardening models were used in their conventional forms. Prager's model for kinematic-hardening was opted for because of its simplicity and Drucker's flow theory of plasticity was used to establish the relationship between the plastic strain and the translation of the yield surface in a stress sub-space. In the original Prager's model, the relationship $d\alpha_{ij} = cd\varepsilon^{p}_{ij}$ was used to establish the flow process, where, $d\alpha_{ij}$ is the infinitesimal translation of a yield surface to a subsequent position and $d\varepsilon^{p}_{ij}$ is the incremental plastic strain. In earlier works, the constant of proportionality, c, was taken as the tangent or plastic modulus of rigidity. The present work redefines the constant c as a Bauschinger effect related parameter obtainable from analysing a single cycle load-unloading curve. The consideration of anisotropic-hardening negates the appropriateness of the use of the tangent modulus as a constant of proportionality in yield surface translation characteristics . Under anisotropic-hardening assumptions, there will be no unique value of the tangent modulus, hence it cannot be accurate as a characterizing constant. On the other hand the Bauschinger effect parameter is such that it is calculated from a phenomenon characteristic of a material at a given state of loading. Its value is unique for a given loading condition and it does not vary with direction. In this wise, the flow relationship was rewritten as $d\alpha_{ij} = \beta d\varepsilon^{p}_{ij}$ and β is called the kinematic translation parameter.

The kinematic translation parameter was measured from a single cycle stress-strain curve using the stress criterion mentioned in the main text. This stress-strain loop was used to pre-strain/pre-stress (as applicable),

a specimen before cycling it between specified strain amplitudes. The sufficiency of this method of analysis for various types of cyclic loading (following either a tensile or torsional pre-strain) is borne out of the experimental observation that after a pre-strain, the translation characteristic of subsequent yield surfaces is such that they orientate themselves and translate in the direction of the initial pre-strain vector. For example, when a material is initially prestrained in tension and then cycled under any combination of loading the subsequent yield surfaces will translate along an axis coincident with the tensile axis. In the present study the yield surface should translate along the tensile axis under any type of cyclic loading because all prestraining works were done in tension before cycling was carried out. Experimental evidence shows that this parameter varies with strain and prestrain and that it is material dependent.

For the materials studied, the value of $\beta = 0$ corresponded to an isotropic situation under which the monotonic stress-strain curve was calculated. When $\beta = 1.0$, kinematic-hardening resulted. Combined-hardening was observed for values of $0 < \beta < 1$. The situation at magnitudes of β close to 1.0 e.g 0.9 - 1.0 was found to be susceptible to numerical errors which resulted in curves that almost coincided with the kinematic-hardening curve for $\beta = 1.0$.

In conflict with previous arguments e.g those of Newman, it was noticed that $\beta > 1.0$ is a meaningful case. Combined-softening was noted for cases in which $\beta > 1.0$. A good manifestation of this was found in the computer derivation of the cyclic

stress-strain curve for Titanium, Ti6211. This alloy was found experimentally to soften at low plastic strain amplitudes and harden at high plastic strain amplitudes. Softening and hardening being defined as situations in which the cyclic curve is lower or higher than the monotonic stress-strain curve respectively. On the computer, the use of values of β extracted from the β vs ε_p curve successfully produced a cyclic stress-strain curve that softened at low plastic strain values when $\beta > 1.0$ and hardened at high plastic strain values when the values of β laid between 0 and 1.

The process of computing cyclic stress-strain curves consisted of using the values of β and plastic strain read off a βvs ε_p curve. ε_p was then used as the cyclic strain amplitude. After several cycles of loading a settled stress-strain hysteresis loop results. The cyclic stress-strain curve was constructed by using either the multistep approach or the Morrow method. For the multistep approach, several steady hysteresis loops were produced under different combination of β and ε_p. The tips of these loops were then joined together to form the cyclic stress-strain curve. In the case of the Morrow analysis, a large steady hysteresis loop was produced by cycling at a large value of plastic strain amplitude and its corresponding β. The cyclic stress-strain curve was derived by analysing the single hysteresis loop as previously highlighted in the text.The Morrow method or single cycle hysteresis loop was particularly favoured by the author because of its economic value as regards computing time and cost. Steady-state for cyclic processes was achieved within the first 10 cycles and this was established by the constancy of the values of the amount of

plastic work done over a few cycles (note that the area of a hysteresis loop is a measure of plastic work done in a material).

At this juncture, the reader may ask questions about the pertinence of the theory of plasticity, Bauschinger effect and behaviour of the yield surface (re isotropic-hardening, kinematic-hardening or combined-hardening) to the cyclic behaviour of materials, since these assumptions formed the basis of the computational work offered in this thesis for the derivation of cyclic stress-strain curve. A hysteresis loop will be adopted for explaining the relationships.

During cycling microscopic changes occur very quickly. The manifestation of these on a macroscopic scale is the production of hysteresis loops which eventually settle down into a steady-state. A stable or steady-state cyclic hysteresis loop, provides data for constructing the cyclic stress-strain curve.

The area of the cyclic hysteresis loop is a measure of the plastic work done on a specimen whilst the distance measured across its width is the plastic strain amplitude. Because all measurements related to the cyclic hysteresis loop are plastic, plasticity theories are necessary for establishing relationships in cyclic analysis.

As said earlier, when a specimen is loaded in tension to a magnitude of plastic strain and then unloaded, the yield stress in tension is usually different from that of the reversed yield stress in compression. This phenomenon is known as the Bauschinger effect and was demonstrated in

the laboratory by taking an hour-glass specimen through one cycle of loading. On a physical perspective, this happens during every cycle of loading until steady-state is reached. During fixed strain amplitude cycling, the characteristic of the intermediate hysteresis loops change according to the relationship between the Bauschinger effect and the plastic strain. Each hysteresis loop corresponds to a yield surface whose centre has moved an amount $d\alpha_{ij}$ (which is equal to the product $\beta d\varepsilon^{p}_{ij}$). Each of these intermediate hysteresis loops has an associated value of β. For a given test, the limit of these instantaneous values of β is the input value of β which was experimentally determined. Also, at instances during strain cycling, the stress amplitudes change even though the strain amplitude was kept constant. This lends credence to the use of the stress criterion for calculating the kinematic translation parameter.

As regards the relevance of the behaviour of yield surface, consider a cyclically hardening material for which the stress in tension increases, causing a corresponding decrease in the re-yield stress. The measurement of the forward and reversed yield stresses from corresponding hysteresis loops give points on a von-Mises type yield surface, along the axial direction. The movement of the hysteresis loop along this tensile axis as hardening progresses corresponds to an amount of translation of the centre of the yield surface. Conceptually then, a stable hysteresis loop corresponds to the final state and position of a von-Mises yield surface whose centre has translated progressively from the initial position to the final or steady-state in a stress subspace.

Following the conceptual approach described above, an elastic-plastic combined-hardening model was developed as presented in Appendix A. This model was implemented in a finite-element computer program called "OYIN".The program is displacement controlled. An unloading routine was inter-woven into the program such that loading and unloading sequences could be carried out for the production of cyclic hysteresis loops. Unloading was approached as a perfectly elastic phenomenon. This program is batch-run and a typical data file is presented in Appendix C. The program requires a value of β and other material properties such as the Young's modulus, uniaxial yield stress, poisson's ratio, material density, thickness, yield strain, hardening index and the Ramberg-Osgood constant to run it. These parameters are obtainable from a monotonic stress- strain curve. The translation of the centre of the yield surface was calculated by the plasticity subroutine using the input value of β and the values of plastic strain calculated from the prescribed displacements. The translation of the yield surface causes changes in the cyclic stress calculated and this in turn causes changes in the hysteresis loop area. A settled cyclic state is assumed when the plastic work measured over a number of cycles remains appreciably constant.

Since the program is elastic-plastic and displacement controlled meaningful simulation were carried out through careful management of the displacement factors input under sub-routine RELOAD and the prescribed displacements input at the section of the program that deals with boundary constraints. Displacement control was done in two stages. The first part followed Hooke's law and assumes proportional loading from zero to yield point. In this wise, only two points

were necessary to construct the elastic line namely (0,0) and the (1,1) or yield point (stress) in exact dimensions. To describe the yield point, a displacement corresponding to the yield strain was input as a constraint boundary condition. Once this was done, the first displacement factor input in the displacement loading section of RELOAD was set to 1.00. This displacement factor was the datum and all incremental factors were made as increments on this initial data. For good numerical accuracy, the loading increments were done in small steps. Compressive loading was achieved by inputting negative displacement factors as shown on the sample data file in Appendix C. These displacements were converted to incremental plastic strains which are then used in Function HHH of the program to calculate the corresponding hardening indices. Once the incremental plastic strains, H' or A_X (values returned from FUNCTION HHH) and the β are known, the incremental displacement of the centre of the yield surface are calculated and the incremental plastic stresses are corrected accordingly. This exercise continues until steady-state is reached. These incremental plastic stresses were then used to update the elastic stresses into their elastic-plastic values. The data obtained were then used to construct whole hysteresis loops from which settled cyclic stress-strain curves were calculated. It should be noted that the Function HHH has its origin in assumptions related to anisotropic hardening (explained earlier) and is derived in the present work from the Ramberg Osgood stress-strain relationship.

Following the processes described above and especially using the various combinations of A_X, β and ε_p, it was possible to fit the

monotonic and predict cyclic stress-strain curves on the computer. The curves obtained compared favourably with experimental data.

The later part of the thesis dealt with the application of cyclic plasticity to the prediction of the behaviour of loaded notched specimens. In particular the possibility of combining monotonic and cyclic data to predict the behaviour of macro engineering parameters such as the J-integral (J) and the crack opening displacement (COD) in regions close to the notch tip where events are poorly defined and dominated by cyclic plasticity and in the relatively steady LEFM dominated stress region. The J and COD parameters were favoured by earlier investigators as suitable parameters for correlating crack growth data under fatigue in contained plasticity conditions.

A notch will cause a local region of high stresses and strains. The local region is called the notch influence zone. Customarily, this region is divided into two namely the notch plastic and notch elastic regions. Data correlation in the notch plastic region is usually approximate. Several scholars have attempted data correlation in this region and have used parameters like the J-integral and COD. Their results showed that these plastic or non-linear elastic parameters could account for crack behaviour under the characteristics of the notch plasticity region, otherwise known as the fracture process zone.

In the present study, it was assumed that after plastic straining a notch

imposes a region of high plastic residual stresses around its own tip. Because fatigue crack growth correlation and the behaviour of small cracks were of particular interest to the author, it is argued that when a rectangular plate containing a notch is subjected to cyclic or fatigue loading, the regions of high residual stresses undergo several changes with respect to the number of cycles and then settle down to a steady-state. At steady-state, a cyclic stress range replaces the initial residual stresses originally characterizing the notch region. It is also argued that for a cyclically work-hardening material, the local region surrounding the notch becomes dominated by cyclic plasticity with a stress range equivalent to $C\sigma_0$. σ_0 is the initial yield stress of the material whilst C is a constant depending on the cyclic behaviour of the material. The size of this region is also argued to be material dependent. For work-hardening aluminium, the minimum value of C obtained experimentally and computationally is approximately 2.

Having assumed the occurence of a zone of cyclic plasticity around the notch region early in the fatigue process , it then became mandatory that a small crack emanating from a notch under this circumstances must grow through this field at the incipient stages of growth before it can establish itself as a long crack for which the behaviour is describable under LEFM assumptions. The various processes in this field and their interaction with the crack could culminate in the slowing down of a crack, the arrest of a crack or in the crack becoming a long crack which eventually will propagate under elastic conditions to failure.

A crack grows under the influence of an externally imposed driving

force and also under its own tip plasticity. Two types of crack "driving" parameters or crack growth correlation parameters, namely the J-integral and the crack opening displacement were studied under a bifurcated specimen region. The bifurcation of a specimen was caused by the process described above in which there are both a zone of cyclic plasticity with a characteristic cyclic stress range surrounding the notch and an LEFM region in the remote region.

The first half of the work done under this analysis was to study the effect of the size of cyclic plasticity zone on the J and COD parameters by using a finite element two-dimensional computer program. The magnitude of the area covered by cyclic plasticity was measured in number of elements. Also stress ranges of 1.2 σ_0, 1.5σ_0 and 2.σ_0 were imposed as the cyclic yield stress on these regions. The J values were calculated for J paths lying in the LEFM region of the bifurcated specimen. It was observed that the magnitude of the J-integral and the crack opening displacement decreased relative to the data obtained for the same parameters in a homogeneous specimen. The curve closest to the homogeneous curve corresponded to that of the smallest field sized by 16 elements whilst the curve that showed the largest disparity with the homogeneous curve was that calculated when the cyclic plastic zone was sized by 75 elements. The variation was such that an envelope was formed with the upper boundary being the homogeneous J data and the lower one being the J curve plotted from data calculated for a mesh bifurcated by the introduction of a plastic field of 75 elements. Again J was calculated outside the notch cyclic plasticity zone. Both J and COD were found to decrease with increasing magnitude of the cyclic stress

range. Again J was calculated outside the notch cyclic plasticity zone.

Finite element investigation of the bifurcated specimen revealed that the data calculated inside and outside of the notch plastic zone differ and that J is path dependent in a bifurcated specimen as expected where properties vary. There were unique values of J for each field but the data, when plotted against displacement, differed from each other by a factor of about 2 across fields. Detailed studies were carried out in meshes with cyclic plasticity zone of 30 and 40 elements characterized with a stress range of $2\sigma_o$. Because of the disparity shown, especially in the plastic components of the J integral (and the COD), a rational non-dimensional analysis of these parameters was carried out so as to derive unique parameters for the two fields defined. Consequently, the hybrid parameters J_{cgc} and δ_{cgc} were derived in chapter five. These parameters were unique for all paths across the specimen regions, hence were able to correlate data from one field to the other. In doing the non-dimensional analysis a factor called C in the body of the text (see Chapter Five) came up as a rationalizing parameter to reconcile the large disparity between the non-dimensional plastic data for the homogeneous specimen and those obtained inside the cyclic plasticity region. This factor varied significantly from one case to the other and from one parameter to the other. For the J-integral, it was about 60 for the 40 element sized cyclic plasticity field whilst being about 200 for some case of notch field of 75 elements. The values obtained for the J cases were between 4 and 6 times their magnitudes for COD data using the same type of mesh condition.

An analysis based on the EnJ design curve revealed that the occurence of the factor C or rationalizing factor was justifiable and that the curves of J against displacement that showed a difference by a factor of about 2 were only suitable e.g. for studying the uniqueness/non-uniqueness of the J-integral and did not give the full picture about J in terms of the yielding characteristic of the two separate regions in which it was calculated. In the bifurcated specimen studied, there were two regions one very close to the notch characterized by a plastic stress greater than the original yield stress of the material used caused by cyclic plasticity whilst the other region was characterized by the monotonic yield stress or original yield stress of material.

When this specimen was subjected to uniform loading or displacement in tension, the outer zone (or homogeneous LEFM zone) yielded before the inner zone, since the inner zone was already work-hardened. Because of this different yielding characteristics in the two regions, the J-integrals measured in these fields differ and C is a reflection of this difference. The EnJ method was found to be suitable because it considers the variation of the non-dimensional parameter J/G_y, with net section yielding.

In the present work, a slight variation of the EnJ equations was adopted so that G was substituted for G_y. G was calculated using local stresses (per load increment) instead of using a constant yield stress as suggested in the determination of G_y (119). Also, it was observed that the kink at the point of meeting of the stress based (curve) and strain based (straight line) parts of the curves was more pronounced than in the original EnJ curves. A possible explanation for this difference could be due to the

error incurred when switching from local parameters to LEFM parameters. Note that the original separation of the stress based and strain based analyses were done on homogeneous meshes. It is possible that the equations of the EnJ analysis would have been slightly different if the original analysis was based on the study of bifurcated specimens, thereby producing distinct kinks of discontinuity as revealed by the authors analysis. However, the approximate curves obtained were good enough for establishing the origin of the rationalizing parameter C. For example, the difference between the values of J/G read for the 75 element bifurcation and homogeneous cases was found to be reconcilable by a factor of 210. This value is very close to the empirical value of C of 225 obtained in chapter five. Errors of 6 - 10% between the empirically determined C and the EnJ curves C were incurred in all the cases studied. This error is acceptable within limits of numerical accuracy and the original formulation of EnJ.

The parameters J_{cgc} and δ_{cgc} have a distinct feature of being related to the characteristic stress in the region in which they are being calculated. Because of this, they offer a way of combining cyclic and monotonic data for the correlation of fatigue crack growth data.

The plastic data of J and COD calculated in any region was non-dimensionalized by using the value of the yield stress or stress range characterizing that region. For the cyclic case, J_{cgc} is calculated by using the square of the characteristic yield stress.

J_{cgc} and δ_{cgc} were calculated for different notched configurations using monotonic strain distribution ahead of notches of SCF = 2, 3, 5 and a sharp "small" crack, the monotonic yield stress, and the cyclic stress-strain curve.

For the monotonic values of these parameters, the flow stress used was the uniaxial yield stress and it was assumed constant for calculating the monotonic data. The monotonic values of the hybrid parameters were seen to follow LEFM assumptions. The cyclic values of these parameters were calculated by substituting the cyclic stress range for the flow stress introduced in Chapters 5 and 6. Also, the underlying assumption follows the argument that the local region in which a crack is nucleated and grows as a small crack is dominated by cyclic plasticity with a characteristic cyclic stress range and very high plastic strains.

It should be recalled that experiments cited in chapter four have shown that small cracks (but still larger than the grain size) grow faster than long cracks in the below threshold regime. Even though this observation has been registered by many investigators, there has not been co-ordinated effort to explain this phenomenon in macroscopic or engineering terms. The object therefore was to find an explanation for the phenomenon of small crack growth in the fatigue process at a notch.

On a cartesian system, the pattern of variation of J_{cgc} and δ_{cgc} with displacement was such that the cyclic curves were higher than the monotonic curves in regions close to the notch tip. This is encouraging because it shows the ability of the hybrid parameters to correlate fatigue

and monotonic data in accordance with experimental observations.

The curves for small stress concentration factors (SCF = 2 and 3), showed such patterns that will possibly explain why crack arrest is a rare occurence in notches of this kind. The cyclic curves grew to a maximum point (interpreted as the value corresponding to initiation), then showed some inflexion which is indicative of a slowing down of the force and then rose again to another point of inflexion after which it shows a possibility of linking up with the monotonic curves at a distance several notch-depths away from the notch tip. On the other hand, the history of behaviour of the cyclic curve for the higher stress concentration factors (SCF = 5, sharp crack) is that of a curve rising to a maximum point (point of initiation) and then making a decline to join the monotonic curve at a length much closer to the notch top and in the vicinity of the notch plasticity zone.

The decline of the cyclic curve for the SCF = 5 case was about 102 (non-dimensional) units whilst that of the small sharp crack was about 70 units. The comparison between these figures points to the fact that under the same loading condition, the driving force for the sharp crack decreases more quickly to low values where it joins the monotonic curve, hence crack arrest is more likely to occur for the sharp crack case.

The relationships between the slopes of the monotonic and cyclic curves for the J_{cgc} cases showed that the ratio of the cyclic to the monotonic slope increased towards the sharp notch case. The cyclic slopes were much higher than their monotonic equivalents. This observation relates

to the difference between the local plastic strain concentration factor ($K\varepsilon$) and elastic stress concentration factor ($K\sigma$) which are the two components of the universal notch stress concentration factor (K_t). The slope of the cyclic curve is germane to the magnitude of the $K\varepsilon$ as it occurs when the notch root undergoes plastic deformation.

The relationship between the cyclic and monotonic slopes for the δ_{cgc} curves revealed an interesting pattern in which the ratios are approximately constant at about 4, This factor of 4 is seemingly indicative of the settled range of imposed residual stress range ($2 \times \{2\sigma_o\}$ in the studied case) around the notch root region rather than the effect of the plastic strain concentration factor, $K\varepsilon$. This can be explained as due to the fact that the COD was measured at a point defined on the crack line bordering the free surface and before the notch root deformation field, so that the data obtained did not reflect the deformation characteristics of the notch tip. Instead, the influence of the surrounding cyclic plasticity field was enhanced. With respect to this COD observation, it can be said that the J_{cgc} data were subject to the dual effect of the characteristic cyclic plasticity field and the deformation of the notch root caused by plastic local yielding.

In the light of the above, it can be said the J_{cgc} and δ_{cgc} behaved in such a way that gave credence to their application for fatigue crack growth correlation. Small crack faster growth data can be correlated by using these parameters once the monotonic strain

distribution and cyclic stress range in the region surrounding the notch root in which it grows are known. Also, crack arrest or possible growth to failure and the deformation characteristics of the notch tip (eg by way of $K\varepsilon$) can be predicted by using the curves produced through this method.

It is the considered opinion of the author that following the above revelation, the missing link in the Paris relationship which bears reference to the growth of cracks at below threshold conditions can be established by using the hybrid parameters J_{cgc} and δ_{cgc}.

CONCLUSION.

A viable tripartite combined-hardening theory which accounted for some of the observable behaviour of materials under plastic loading such as the Bauschinger effect and unequal hardening in different directions of loading was developed.

A Bauschinger effect parameter called the **Kinematic translation parameter, β,** was introduced. This parameter accounted for the flow behaviour of the von-Mises yield surface during plastic loading. It is state and material dependent. It was possible to predict material response to cyclic loading through a numerical value of β. For example, when $0 < \beta < 1$, a material would cyclically harden. $\beta = 0$ and $\beta = 1$ represent isotropic and

kinematic-hardening respectively, whilst, $\beta > 1$ signifies cyclic softening. The theory was successfully incorporated into a two-dimensional elastic-plastic finite-element fortran program from which cyclic stress-strain curves were obtained. The curves obtained showed good agreement with experimental data.

The various processes that characterize fatigue loading at a notch cause bifurcation of an initially homogeneous specimen by imposing a region of cyclic plasticity immediately ahead of a crack or notch contained in the specimen, with a characteristic stress range, and an LEFM dominated region in the remote sections.

The studies carried out showed that the J-integral and crack opening displacement (COD) parameters varied according to the size of the cyclic plastic zone and the magnitude of the cyclic stress range.

These parameters were found to be relatively path and state independent in the linear elastic regime e.g the J-integral which reduces to G in the LEFM case is path independent for various combinations of imposed plasticity conditions. The studied parameters showed large disparity in the plastic regime. The J-integral in particular, was path independent within the same field irrespective of whether the data was plastic or elastic. Also, the J-integral was path independent when measured within a defined field, be it dominated by cyclic plasticity or LEFM condition. However, this parameter showed path dependence when calculated and compared for two different fields.
The disparity in the plastic data of the J and COD curves, hence the

non-uniqueness, across fields were rationalized by way of non-dimensional analysis involving the characteristic strength in any field where the path integral was evaluated. By doing this, it was possible to use cyclic data (i.e cyclic stress-strain curve) in the cyclic plasticity region and monotonic data, namely the uniaxial yield stress, in the LEFM region for the correlation of fatigue crack growth data.

The rational non-dimensional analysis introduced in chapter five and applied in chapter six gave rise to the development of the hybrid parameters J_{cgc} and δ_{cgc}. These parameter were calculated using a combination of monotonic and cyclic data as explained in the text. The behavioural patterns of the correlation parameters $J_{cgc} = J_{pl}E/C\sigma_{fl}^2a$ and $\delta_{cgc} = \delta_{pl}E/C_1\sigma_{fl}a$, where, ($\sigma_{fl}= \Delta\sigma$ in the cyclic plasticity field and $\sigma_{fl}= \sigma_0$ for the LEFM region), suggests the appropriateness of the use of a combination of monotonic and cyclic data for analysing crack growth data as well as showing the capability of the two parameters to correlate fatigue crack growth fully.

The variational patterns show that faster crack growth behaviour normally observed for small cracks growing within the cyclic plasticity region could be due to the high magnitudes of the crack driving parameters ΔJ_{cgc} and $\Delta\delta_{cgc}$ shown on the graphs presented in chapter six.

Also, the behaviour of these parameters with incremental crack length, in comparison to their LEFM counterparts, in which the cyclic curve either grew divergently to well over 5(notch depths) across the unbroken

ligament before an inflexion which was suggestive of an intention to join the LEFM or secondary stage crack growth curve (small SCF cases), or grew to a maximum point and then decline to join the LEFM curve at a relatively closer distance of between 1 and 1.5(notch depths) from the notch tip (sharp crack case), seem to throw some light into why crack arrest is virtually non-existent in cases involving small notch stress concentration factors e.g. a hole in a plate SCF=3 and why cracks can arrest in notches of high stress concentration factors (sharp cracks) (See figures 6.7-6.14).

Finally, the problem of computational derivation of cyclic stress- strain curves was solved. The effect of a cyclic plasticity region embedded in a cracked specimen on the crack correlation parameters J and COD were studied. As a result of this, two hybrid parameters J_{cgc} and δ_{cgc} based on the plastic components of these parameters were introduced for purposes of fatigue crack growth correlation.

These parameters showed the capability of correlating crack growth data in the primary and secondary crack growth stages. The Paris law of fatigue crack growth can now be generalized to cater for the incipient stage of crack growth by using the suggested hybrid parameters.

1 **ZIEGLER, H.**: "A Modification of Prager's Hardening Rule";
Quart Appl Math, (1959), 17, 55 - 65.

2 **DRUCKER, D. C.**: "A More Fundamental Approach to Plastic Stress-strain Relations";
Proc Ist US Natl Congr Appl Mech, Chicago (1957), New York (1952), P 487.

3 **PRAGER, W.**: "A New Method of Analysing Stresses and Strains in Work Hardening Plastic Solids";
J Applied Mech, (1956), 23, 493 - 496.

4 **ISAKSON, G/ARMEN, H. Jnr & PIFKO, A.**: "Discrete Element Methods for the Plastic Analysis of Structures";
NASA CR- 803, (Oct 1967).

5 **BUDIANSKY, B.**: "A Reassessment of Deformation Theories of Plasticity";
J Appl Mech, Vol 26, (June 1959), P 259.

6 **MENDELSON, A.**: "Plasticity: Theory and Application";
Macmillan Publishing Company, New York. (First Published 1968), P 106 - 108.

7 **BESSELING, J. F.**: "Matrix Analysis of Creep and Plasticity Problems";
Proc of Conf on Matrix Methods in Structural Mechanics, Wright-Patterson AFB, Ohio, (26 - 28 October 1965), AFFDL-TR-66-80, P 655.

8 **SHIELD, R. T. & ZIEGLER, H.**: "On Prager's Hardening Rule";
J Appl Math Phys - ZAMP, (1958), 9a, 260 - 271.

9 **REES, D. W. A.**: "Anisotropic Hardening Theory and the Bauschinger Effect";
J of Strain Analysis, Vol 16, No 2, (1981), 85 - 95.

10 **PHILLIPS, A. & KAECHELE, L.**: "Combined Stress Tests in Plasticity";
J Appl Mech, Vol 23, (1956), P 43.

11 **MARIN, J. & HU, L. W.**: "Biaxial Plastic Stress-strain Relations of a Mild Steel for Variable Stress Ratios";
Trans ASME, (April 1956),, P 499.

12 **HU, L. W. & BRATT, J. F.**: "Effect of Tensile Plastic Deformation or the Yield Condition";
J Appl Mech, Vol 25, (Sept 1958), P 111.

13 **MARIN, J. & HU, L. W.**: "On the Validity of Assumptions Made in Theories of Plastic Flow for Metals";
Trans ASME, Vol 75, No 6, (1953), P 1181.

14 **BATDORF, S. B. & BUDIANSKY, B.**: "A Mathematical Theory of Plasticity Based on the Concept of Slip";
NACA TN 1871 (1949).

15 **PETERS, R. W./DOW, N. F. & BATDORF, S. B.**: "Preliminary Experiments for Testing Basic Assumptions of Plasticity Theories";
Proc Soc Exp Stress Analysis, Vol 7, (1950), P 127.

16 **SANDERS, J. L. Jnr.**: "Plastic Stress Strain Relations Based on Linear Loading Functions";
Proc 2nd US Nat Congr Appl Mech (1954), P 455.

17 **HODGE, P. G. Jnr.**: "Piecewise Linear Plasticity";
Proc 9th Intern Congr Appl Mech, (Brussels 1956), Vol C, P 65 (1957).

18 **STRICKLIN, J.A.**: "Large Elastic, Plastic and Creep Deflections of Curved Beams and Axisymmetric Shells";
AIAAA Jour, Vol 2, No 9, (Sept 1964), P 1613.

19 **MROZ, Z.**: "On the Description of Anisotropic Work-Hardening";
Journal of the Mechanics and Physics of Solids, Vol 15, ND 3, (May 1967) P 163 - 176.

20 **MROZ, Z.**: "An Attempt to Describe the Behaviour of Metals Under Cyclic Loads Using a More General Work-hardening Model";
Acta Mechanica, Vol 7, No 2 - 3, (1969), P 199 - 212.

21 **DUWEZ, P.**: "On the Plasticity of Crystal";
Review, Vol 47, No 6, (15 March 1935), P 494 - 501.

22 **WHITE, G. N. Jnr.**: "Application of the Theory of Perfectly Plastic Solids to Stress Analysis of Strain Hardening Solids";
Tech Report 51, Gradual Division of Applied Mathematics, Brown University, (August 1950).

23 **HUNSAKER, B. Jnr/VAUGHAN, D. K. & STRICKLIN, J. A.**: "A Comparison of the Capability of Four Hardening Rules to Predict a Material's Plastic Behaviour";
Journal of Pressure Vessel Technology, ASME, P 66 - 74, (Feb 1976).

24 **LIU, K. C.**: "An Experimental Study of Yield Surfaces in a Combined Axial-Torsional Space for Type 304 Stainless Steel";
Paper presented at the Office of Naval Research Plasticity Workshop (3 - 5 October 1974), Texas A & M University, College Station, Texas.

25 **NAGHDI, P. M./ ESSENBURG, F & KOFF, W.**: "An Experimental Study of Initial and Subsequent Yield Surfaces in Plasticity";
J Appl Mech, Vol 25, (June 1958), P 201.

26 **MORETON, D. N./MOFFAT, D. G. & PARKINSON, D. B.**: "The Yield Surface Behaviour of Pressure Vessel Steels";
Jr Strain Analysis, Vol 16, No 2, (1981).

27 **HOLLOWAY, G. & SHELTON, A.**: "The Plastic Behaviour of Annealed OFHC Copper";
Jr Mech Engrg Sci, Vol 21, No 4, (1979).

28 **SHAHABI, S. N.**: "The Anisotropic Yield, Flow and Creep Behaviour of Pre-strained En 24 Steel";
J Mech Engrg Sci, Vol 17, No 2, (1975).

29 **ROGAN, J. & SHELTON, A**: "Effect of Pre-stress on the Yield and Flow of En 25 Steel";
Journal of Strain Analysis, Vol 4, No 2, (1969).

30 **HILL, R.**: "The Mathematical Theory of Plasticity"
Clarendon Press, Oxford, (1950).

31 **EDELMAN, F. & DRUCKER, D. C.**: "Some Extensions to Elementary Plasticity Theory";
J Franklin Inst, (1951), No 251, P 581.

32 **HOLLOWAY, G. & SHELTON, A.**: "Journal of Mechanical Engineering Science, Vol 21, No 4, (1979).

33 **WILLIAMS, J. F. & SVENSSON, N. L.**: "Journal of Strain Analysis", Vol 5, No 2, (1970).

34 **WILLIAMS, J. F.**: "A Rationally Based Yield Criterion for Work-hardening Materials";
Phd Thesis, University of Melbourne, Australia, (1969).

35 **WILLIAMS, J. F. & SVENSSON, N. L.**: "A Rationally Based Yield Criterion for Work-Hardening Materials";

36 **HANCELL, P. J. & HARVEY, S. J.**: "The Use of Kinematic Hardening Models in Multi-axial Cyclic Plasticity";
Fatigue of Engineering Materials and Structures, Pergamon Press, Great Britain, Vol 1, P 271 - 279, (1979).

37 **ELLYIN, F. & NEALE, K. W.**: "Effect of Cyclic Loading on the Yield Surface";
Journal of Pressure Vessel Technology, Vol 101, P 59 - 63, (1979).

38 **PARKER, J. & BASSET, M. B.**: "Plastic Stress-strain Relationships - Some Experiments to Derive a Subsequent Yield Surface";
J Appl Mech, Vol 31, (Dec 1964), P 676.

39 **BERTSCH, P. K. & FINDLEY, W. N.**: "An Experimental Study of Subsequent Corners, Normality, Bauschinger and Allied Effects";
Proceedings, 4th Us National Congress of Applied Mechanics, (1962), P 893.

40 **YOSHIMURA, Y.**: "Hypothetical Theory of Anisotrophy and the Bauschinger Effect Due to a Plastic Strain History";
Aero Res Inst, Tokyo University, (1959), 349, 224 - 246.

41 **BALTOV, A. & SAWCZUK, A.**: "A Rule of Anisotropic Hardening"
Acta Mechanica, (1965), 1, 81 - 92.

42 **HODGE, P. G. Jnr.**: Discussion of "A New Method of Analyzing Stresses and Strains in Work-hardening Plastic Solids"
Journ of Applied Mechanics, Vol 23, No 4, (Dec 1956), P 493 -496.
Journ of Applied Mechanics, Vol 24, No 3, (Sept 1957), P 482 - 483.

43 **KRIEG, R. D.**: "A Practical Two Surface Plasticity Theory";
Paper Presented at the Office of Naval Research Plasticity Workshop (3 - 5 October 1974), Texas A & M University, College Station, Texas.

44 **NEWMAN, J. C.**: "Finite Element Analysis of Crack Growth Under Monotonic and Cyclic Loading";
Cyclic Stress-strain and Plastic Deformation Aspects of Fatigue Crack Growth, ASTM, STP 637. ASTM, (1977), P 56 - 80.

45 **ZIENKIEWICZ, O. C./VALLIAPPAN, S. & KING, I. P.**:
"International Journal for Numerical Methods in Engineering", Vol 1, (1969), P 75 - 100.

46 **OWEN, D. R. J. & HINTON, E.**: "Finite Elements in Plasticity - Theory and Practice"
Pineridge Press, Swansea, UK (1980).

47 **BRAY, A./CRESTO, P. C./ FERRO-MILONE, A. & GABOLA, G.**: "A Computerized Method for the Evaluation of the Bauschinger Effect - Application to Different Types of Steel";
Material pruf, 22 (1980) Nr 6, Juni, Torino, Italy.

48 **BLEACKLEY, M. H.**: Private Contract - Post Doctoral - Imperial College, Department of Mechanical Engineering.

49 **KLESNIL, M. & LUKAS, P.**: "Fatigue of Metallic Materials";
Elsivier Scientific Publishing Company (1980).

50 **WUNDT, B. M.**: "Effect of Notches on Low Cycle Fatigue" - a Literature Survey.
Metals Property Council, ASTM STP 490 (May 1972).

51 **BAIRSTON, L.**: "The Elastic Limits of Iron and Steel Under Cyclic Variations of Stress";
Philosophical Transactions of the Royal Society of London, Series A, Vol 210, (1910), P 35 - 55.

52 **DUGDALE, D. S.**: "Stress-strain Cycles of Large Amplitudes";
Journal of the Mechanics and Physics of Solids, Vol 7, No 2,, (1959),,
P 135 - 142.

53 **LANDGRAF, R. W./MORROW, JoDEAN & ENDO, T.**: "Determination of Cyclic Stress-strain Curves";
Journal of Materials, JMLSA, Vol 4, No 1, (March 1969), P 176 - 188.

54 **MORROW, JoDEAN.**: "Cyclic Plastic Strain Energy and Fatigue of Metals";
Internal Friction, Damping and Cyclic Plasticity, ASTM STP 378 (1965), P 45 - 87.

55 **MINAS, A.**: "The Behaviour of the Low-alloy steel B543600 - 50D Under Cycles of Plastic Deformation";
MSc Thesis, Imperial College , London (Sept 1983).

56 Laboratory Manual on Maye's Machines - Strength of Materials Section - Mech Engrg Dept, Imperial College, London.

57 **SMITH, R. W./HIRSCHBERG, M. H. & MANSON, S. S.**: "Fatigue Behaviour of Materials Under Strain Cycling in Low and Intermediate Life Range";
NASA Technical Note D-15574, (April 1963), National Aeronautics and Space Administration

58 **EWALDS, H. L. & WANHILL, R. J. H.**: "Fracture Mechanics"
Published by Edward Arnold and Delftse Uitgevers Maatschappij, (1984).

59 **SMITH, R. A.**: "Short Fatigue Cracks";
Fatigue Mechanisms: Advances in Quantitative Measurement of Physical Damage, ASTM STP, 811, (1983), P 264 - 279.

60 **LANKFORD, J./COOK, T. S. & SHELDON, G. P.:** "International Journal of Fracture"
Vol 17, No 2, (1981), P 143 - 155.

61 **MORRIS, W. L.:** "Metallurgical Transactions";
Vol 11A, No 7, (1980), P 1117 - 1123.

62 **SCHIJVE, J.:** " Engineering Fracture Mechanics";
Vol 14, No 3, (1981), P 467 - 475.

63 **TRUYENS, P.:** "Crack Growth Under Variable Loads in Ships";
Doctoral Thesis, University of Ghent, Belgium, (1976).

64 **KITAGAWA, H. & TAKAHASHI, S.**
In Proceedings, Second International Conference on Mechanical Behaviour of Materials, Boston, Mass, (1976), P 627 - 631.

65 **TANAKA, K./NAKAI, Y. & YAMASHITA, M.:** "International Journal of Fracture";
Vol 17, No 5, (1981), P 519 - 533.

66 **ELSENDER, A./HOPKINS, P. & BATTE, A. D.:** "Metals Technology";
Vol 15, (June 1980), P 256 - 258.

67 **MILLER, K. J.:** "Initiation and Growth Rates of Short Fatigue Cracks";
Eshelby Memorial Conference held under the auspices of the International Union of Theoretical and Applied Mech, University of Sheffield, (2 - 5 April 1984).

68 **SNEDDON, I. N.:** "The Distribution of Stress in the Neighbourhood of a Crack in an Elastic Solid";
Proc Royal Society, London A, 187, (1946), P 229 - 60.

69 **EL HADDAD, M. H./SMITH, K. N. & TOPPER, T. H.**: "Fatigue Crack Propagation of Short Cracks"
Journal of Engineering Materials and Technology, ASME, Vol 101, (Jan 1979), P 42 - 46.

70 **SMITH, R. A. & MILLER, K. J.**: "Predict ion of Fatigue Regimes in Notched Components";
Int Journal of Mechanics and Science, Vol 20, P 201 - 206, (1978).

71 **ELBER, W.**: "In Damage Tolerance in Aircraft Structures,"
ASTM, STP 486, American Society of Testing and Materials, (1971), P 230 - 242.

72 **EL HADDAD,/ M. H. SMITH & TOPPER, T. H.**: "A Strain Based Intensity Factor Solution for Short Fatigue Cracks Initiating from Notches";
Fracture Mechanics, ASTM STP 677, American Society for Testing anc Materials, (1979), P 274 - 289.

73 **YOKOBORI, T.**: "In Fatigue Mechanisms";
ASTM STP 675, American Society of Testing and Materials (1979), P 683 - 706.

74 **EL HADDAD, M. H./TOPPER, T. H. & MUKHERJEE, B.**: "Review of New Developments in Crack Propagation Studies";
Journal of Testing and Evaluation, JTEVA, ASTM, Vol 9, No 2, (March 1981), P 65 - 81.

75 **NEUBER, H.**: "Journal of Applied Mechanics"
Vol 28, No 4, (Dec 1961), P 544 - 560.

76 **HAMMOUDA, M. M./SMITH, R. A. & MILLER, K. J.**: "Elastic-plastic Fracture Mechanics for Initiation and Propagation of Notch Fatigue Cracks";
Fatigue of Engineering Materials and Structures, 2, 139 - 154, (1979).

77 **RICE, J. R.**: "Mathematical Analysis in the Mechanics of Fracture";
Treatise on Fracture, Vol 2, Edited by Liebowitx, H., Academic Press.

78 **DOWLING, N. E.**: "Crack Growth During Low-cycle Fatigue of Smooth Axial Speciments";
Cyclic Stress-strain and Plastic Deformation Aspects of Fatigue Crack Growth. ASTM STP 637, American Society for Testing and Materials, (1977), P 97 - 121.

79 **CLARK, W. G. Jnr & HUDAK, S. J. Jnr.**: "Journal of Testing and Evaluation",
American Society for Testing and Materials, Vol 3, No 6, (Nov 1975), P 454 - 476.

80 **EL HADDAD, M. H./DOWLING, N. E. & TOPPER, T. H.**: "J Integral Applications for Short Fatigue Cracks at Notches";
Int Journal of Fracture, Vol 16, (1980), P 15 - 30.

81 **SEHITOGLU, H.**: "Fatigue Life Prediction of Notched Members Based on Local Strain and Elastic-plastic Fracture Mechanics Concepts";
Engineering Fracture Mechanics, Vol 18, No 3, P 609 - 621, (1983).

82 **WILHEM, D. P. & RATWANI, M. M.**: "Application of the R-curve Concept to Fatigue Crack Growth";
Journal of Engineering Materials and Technology, Vol 100, (Oct 1978), P 416 - 420.

83 **SHIH, C. F. & SMITH, R. A.**: "International Journal of Fatigue"; Vol 7, No 2, P 87 - 93, (1985).

84 **PARKS, D. M.**: "Some Problems of Elastic-plastic Finite Element Analysis of Cracks";
Phd Dissertation, Brown University,, Providence, RI, (1975).

85 **LEIS, B. N. & AKRAM ZAHOOR**: "Cyclic Inelastic Deformation Aspects of Fatigue Crack Growth Analysis";
Fracture Mechanics, 12th Conference, ASTM STP 700, American Society for Testing and Materials, P 65 - 96, (1980).

86 **McMEEKING, R. M.**: "Finite Deformation Analysis of Crack Tip Opening in Elastic-plastic Materials and Implication for Fracture Initiation";
Journal of the Mechanics of Plastics and Solids, Vol 25, (1977), P 357 - 381.

87 **McMEEKING, R. M.**: In Flow Growth and Fracture, ASTM STP 631, American Society for Testing and Materials (1977).

88 **RICE, J. R. & TRACEY, D. M.**: "Numerical and Computer Methods in Structural Mechanics"
S J Fenves et al, Eds, Academic Press, New York, (1973), P 585 - 623.

89 **TRACEY, D. M.**: "Transactions, Series H, American Society for Mechanical Engineers, Vol 98, (1976), P 146.

90 **WELLS, A. A.**: "Unstable Crack Propagation in Metals - Cleavage and Fast Fracture";
Proc Crack Propagation Symposium, Cranfield (1961) P 210 - 230.

91 **WELLS,, A. A.**: "Application of Fracture Mechanics at and Beyond General Yielding";
British Welding Research Ass Rep M13, (1963).

92 **INGRAM, T./EGAN, G. R./ELLIOT, D. & HARRISON, T. C.**: "The Effects of Geometry on the Interpretation of COD test data"
Practical Appl of Fracture Mechanics to Pressure Vessel Tech, Inst o Mech Engr, P 200 - 208, (1971).

93 **BURDEKIN, F. M. & STONE, D. E. W.**: "COD Approach to Fracture Mechanism in Yielding Materials";
Journal of Strain Analysis 1, P 145 - 153, (1966).

94 **DUGDALE, D. S.**: "Yielding of Steel Sheets Containing Slits";
J Mech Physics and Solids, No 8, P 100 - 108.

95 **RICE, J. R.**: "Mechanics of Crack Tip Deformation and Extension by Fatigue";
ASTM STP 4115, P 247 - 309, (1968).

96 **DONAHUE, R. J./CLARK, H. M./ATANMO, P. ET AL**:
"International Journal of Fracture Mechanics, Vol 8, P 209, (1972).

97 **BATES, R. C. &CLARK, W. G.**: "Transactions of ASM, Vol 62, (1969), P 380.

98 **FROST, N. E. & DIXON, J. R.**: "International Journal of Fracture Mechanics";
Vol 3, (1967), P 301.

99 **POOK, L. P. & FROST, N. E.**: "International Journal of Fracture";
Vol 9, (1973), P 53.

100 **PARIS, P. C./BUCCI, R. J./WESSEL, E. T./CLARK, W. G. & MAGER, T. R.:** "In Stress Analysis and Growth of Cracks"
ASTM STP 513, American Society for Testing and Materials, (1972), P 141 - 176.

101 **RICE, J. R.:** "In Fracture"
H Liebowitz, Ed, Vol 2, Academic Press, New York, (1968), P 191.

102 **SHIH, C. F./ANDREWS, W. R./de LORENZI, H. G./GERMAN, M. D. VAN STONE, R. H. & MOWBRAY, D. F.:** "Methodology for Plastic Fracture";
EPRI Report NP-1735, (March 1981).

103 **TOMKINS, B.:** "Philosophical Magazine";
Vol 18, (1968), P 1041.

104 **McEVILY, A. J.:** "On the Quantitative Analysis of Fatigue Crack Propagation";
Fatigue Mechanisms: Advances in Quantitative Measurement of Physical Damage, ASTM STP 811, P 283 - 312, (1983).

105 **DOVER, W. D.:** "Fatigue Crack Growth Under COD Cycling";
Symp on Fracture and Fatigue at the School of Engineering and Applied Science, George Washington University, Washington D C, (3 - 5 May 1972).

106 **TOPPER, T. H. & EL HADDAD, M. H.:** "Fatigue Strength Prediction of Notches Based on Fracture Mechanics"

107 **FENNER, A. J./OWEN, N. B. & PHILLIPS, C. E.:** "The Fatigue Crack at a Stress Raiser"
Engineering, Vol 171, (1951), P 637 - 638.

108 **FROST, N. E.**: "Crack Formation and Stress Concentration Effects" Direct Stress Fatigue - No 1. The Engineer, Vol 200, (1955), P 464 - 467, P 501 - 503.

109 **FROST, N. E. & DUGDALE, D. S.**: "Fatigue Tests on Notched Mild Steel Plates with Measurement of Fatigue Cracks";
J Mech and Physics of Solids, Vol 5, P 182 - 192, (1957).

110 **FROST, N. E.**" "A Relation Between the Critical Alternating Propagation Stress and Crack Length for Mild Steels";
Proc Institution of Mech Engrs, Vol 173, No 35, (1959), P 811 - 827.

111 **FROST, N. E.**: "Notch Effects and the Critical Alternating Stress Required to Propagate a Crack in an Aluminium Alloy Subjected to Fatigue Loading";
J of Mech Engineering Science, Vol 2, No 2, (1960), P 109 - 119.

112 **FROST, N. E./MARSH, K. J. & POOK, L. P.**: "Metal Fatigue"
Clarendon Press, Oxford, (1974), P 166 - 173.

113 **RAVI-CHANDAR, K. & KNAUSS, W. G.**: "An Experimental Investigation Into Dynamic Fracture: 1 - Crack Initiation and Arrest";
International Journal of Fracture 25 (1984), P 247 - 262.

114 **BRADLEY, W. B. & KOBAYASHI, A. S.**: "Engineering Fracture Mechanics 3";
(1971), P 317 - 332.

115 **KALTHOFF, J. F.**: "In Fast Fracture and Crack Arrest";
ASTM STP 627 (1977), P 161 - 176, American Society of Testing anc Materials.

116 **SAANOUNI, K. & BATHIAS, C.**: "Study of Fatigue Crack Initiation in the Vicinity of Notches";
Engrg Fracture Mechanics, Vol 16, No 5, P 695 - 706, (1982).

117 **SUMPTER, J. D. G. & TURNER, C. E.**: "Fracture Analysis in Areas of High Norminal Strain";
2nd Inter Conf on Pressure Vessel Tech, San Antanio, Texas, (1 - 4 Oct 1973), ASME, Part II: Materials, Fabrication and Inspection.

118 **HUDAK, S. J. Jnr.**: "Small Crack Behaviour and the Prediction of Fatigue Life";
Journal of Engineering Materials and Technology, Vol 103, (Jan 1981), P 26 - 35.

119 **TURNER, C. E.**: "On Design Methods - Post Yield Fracture Mechanics";
- Latzko, D. G. H., Turner, C. E., Landes, J, D., McCabe, D. E., Hellen, T. K.: 2nd Edition, Elsivier Applied Science Publishers (1984), P 351.

120 **LAIRD, C.**: "In ASTM STP" 415, (1967), P 131.

121 **LAIRD, C. & De La VEAUX, R.**: "Metallurgical Transactions";
8A (1977), P 657.

APPENDIX A

A GENERALISED ELASTO-PLASTICITY MODEL TO ACCOUNT FOR THE BAUSCHINGER EFFECT.

-Tripartite combined-hardening model.

1 ABSTRACT.

An elasto-plastic finite element program that contains certain features relevant to cyclic loading is described. Monotonic hardening can be followed by elastic unloading and re-yielding, according to isotropic, kinematic, anisotropic or combined-hardening rules for the movement of the yield surface. Tentative suggestions are made to represent the parameters required in the computation as constants from the material stress-strain data and a few simple cyclic behaviours are illustrated. More complex behaviour where the computational parameters would be funtions of deformation is outlined briefly.

2 INTRODUCTION

The elastic-plastic finite elements methods (EPFEM) have been accepted by many researchers in stress analysis in recent years. With the great flexibility of the finite element method (FEM) and the advanced computer technology, undoubtedly it will play a more important role in future. Many EPFE programs(46) have been

written to perform elasto-plastic (e-p) stress analyses. Most of them can model a certain type of e-p stress-strain behaviour or experimental data fitted stress-strain curves. However, most of them have adopted the isotropic strain hardening rule which cannot model the Bauschinger effect and anisotropic-hardening behaviour.

The Bauschinger effect, which means that the yield stresses are different in different directions of loading after initial yielding, is observed in most real structural materials. This effect must be taken into account while carrying out cyclic stress analyses, otherwise the isotropic hardening assumptions may give misleading results. It is also important for these analyses where local unloading is involved, such as in crack propagation problems.

An elasto-plastic model suitable for F-E programming is derived in this paper as a generalization of the existing models. The model has been applied to a 2D FE program[3]. It is thought that the steady cyclic stress-strain curve can be derived by the computational numerical 'experiments' based on this model.

2 SUMMARY OF PREVIOUS WORK

Previous work of immediate relevance to this problem has been carried out by Isakson et al who included unloading in their elastic-plastic program. They noted isotropic hardening was inappropriate since it could not model the Bauschinger effect and used the Prager concept of kinematic hardening(3)· Anisotropy,

due to deformation during manufacture, was allowed for, whereby initial yield in compression did not equal initial yield in tension.

The work was applied to low cycle fatigue of uncracked bodies. Some time later Newman(44) developed the method further to include also Hodge's concept of combined hardening(42) with behaviour intermediate between isotropic or kinematic. Newman used an elastic plus linear hardening stress-strain curve to study fatigue crack growth, mainly using a critical strain criterion of separation for fatigue crack growth and discussed the effect of hardening rules on the critical strain and subsequent fatigue crack growth.

3 THEORY

The incremental theory of plasticity, which is better than the deformation theory is used throughout all the arguments.

First, the relationships for the isotropic hardening rule are listed below:

a) The yield surface is

$$F(\sigma_{ij},k) = 0$$

or

$$f(\sigma_{ij}) - Y(k) = 0 \qquad (1)$$

where $f(\sigma_{ij})$ is the yield function,

k is the hardening parameter.

The well-known von Mises yield function is given by

$$\sqrt{3/2\sigma'_{ij}\,\sigma'_{ij}} - \sigma = 0 \qquad (2)$$

where $\sigma'_{ij} = \sigma_{ij} - (1/3\ \delta_{ij}\ \sigma_{ij})$ and is the deviatoric stres component,

while σ is the equivalent stress. Here, Einstein's tensor summation convention is used.

b) The incremental flow law (stress-strain relationship) is

$$d\varepsilon^{p}_{ij} = d\lambda\,\sigma_{ij} \qquad (3)$$

including the elastic components

$$d\varepsilon_{ij} = D^{-1}\,d\sigma_{ij} + d\lambda\,\sigma_{ij} \qquad (4)$$

where D is the elasticity matrix.

Restricting $f(\sigma_{ij})$ to the first degree homogeneous function,

$$d\lambda = \sigma_{ij}\,D\,d\varepsilon_{ij}/A + \sigma_{ij}\,D\,\sigma_{ij} \qquad (5)$$

and $A = H' = d\,\sigma/d\varepsilon_{p}$ which is the slope of the σ~ε_{p} curve and can be derived from a uniaxial stress test.

The kinematic hardening model(3) proposed that the actual yield surface does not change its shape and size but its centre can be moved. It can model the Bauschinger effect in a certain way. Because of the complexity, it can only be used analytically in very simple cases. The anisotropic-hardening model describes a situation in which the hardening rate along the plastic stress-strain curve is not the same in forward and reversed loading directions.

The generalized model is described below.
Letting α_{ij} denote the centre position of the yield surface in the stress space, we define:

a) the yield surface

$$f(X_{ij}) - Y(k) = o \qquad (6)$$

where $f(X_{ij})$ is a first degree homogeneous function of X_{ij}, and $X_{ij} = \sigma_{ij} - \alpha_{ij}$;

b) the flow law

$$d\varepsilon^p_{ij} = d\lambda \; \partial f / \partial X_{ij} = d\lambda \, S_{ij} \qquad (7)$$

Equation (4) now becomes

$$d\varepsilon^{ij} = D^{-1} \, d\sigma_{ij} + d\lambda \, S_{ij} \qquad (8)$$

Note that the actual expressions for yield surface and flow law in terms of stress components now are different from that for the

isotropic hardening model and also that the yield surface can change its shape and size as well as its centre position.

c) The movement of the surface centre is specified by

$$d\alpha_{ij} - \beta\, d\varepsilon^{p}_{ij} \qquad (9)$$

where β is considered as a material constant.

Differentiating (6), we have

$$S_{ij}\, dX_{ij} - A_x d\lambda = 0 \qquad (10)$$

where $A_x = 1/d\lambda\{(dY/d\,k)dk\}$ (11)

Substituting (9) - (11), into (8), some simple algebraic operations produce,

$$d\lambda = S_{ij}\, D\, d\varepsilon_{ij}/(A_x + S_{kl}\, \beta\, S_{kl} + S_{kl}\, D\, S_{kl}) \qquad (12)$$

which is similar to Equation (5).

By rearranging Equation (8), the incremental stress-strain relationship is obtained which is most suitable for the finite element program.

$$d\sigma_{ij} = [D - D\, S_{kl}\, S_{kl}\, D/A_x + S_{mn}\beta\, S_{mn} + S_{mn}\, D\, S_{mn}]\, d\varepsilon_{ij} \qquad (13)$$

3 DETERMINATION OF THE PARAMETERS.

The meaning of the parameters A and β can be demonstrated by examining the sequential yield surface. In Fig3.1, a yield surface in 2-D principal stress space is shown. When the material is stressed by a small strain increment $d\varepsilon^p_{ij}$, from point 1 to 2, which are on the original and sequential yield surfaces respectively, the stress changes are caused by two parts, the change of the characteristic size Y and the movement of the centre $d\alpha_{ij}$.

The parameter A represents the size change with the plastic strain,

ie $A = dY/d\varepsilon_p$

where $d\varepsilon_p$ is the effective strain increment.

The quantity $\beta S_{ij} S_{ij}$ represents the movement $d\alpha_{ij}$ projected in the S_{ij} direction.

The proof is given as follows:

Because $f(X_{ij})$ is a first degreee homogeneous function, we can choose suitable constant factors so that in a uniaxial case $f(X_{ij}) = X_1 = \sigma_X - \alpha_X$.

$$f = \sqrt{X_{ij} X_{ij}} \qquad (14)$$

Now the hardening parameter is defined by,

$$dk = (\sigma_{ij} - \alpha_{ij})\, d\varepsilon^{p}_{ij} \qquad (15)$$

Due to the property of the homogeneous function, (Euler's theorem)

$$dk = X_{ij}\, d\lambda\ \partial f/\partial X_{ij} = d\lambda\, f \qquad (16)$$

In uniaxial tension, $dk = (\sigma_x - \alpha_x)\, d\varepsilon^{p}_{x} = d\varepsilon_p\, f$ (17)

Comparing (16) and (17),

$$d\lambda = d\varepsilon_p$$

Normally, Y(k) can be expressed only in terms of λ. Substituting into (11),

$$A_* = 1/d\lambda\,(dY/d\lambda)d\lambda/dk.dk = dY/d\lambda = dY/d\varepsilon = df/d\varepsilon \qquad (18)$$

With the chosen function f, it is easy to understand that

$$\| S_{ij} \| = \| \partial f/\partial X_{ij} \| = 1 \qquad (19)$$

where $||S_{ij}||$ denotes the modulus of S_{ij}.

Then the projection of $d\alpha_{ij}$ on S_{ij} will be

$$S_{ij}\, d\alpha_{ij}/||S_{ij}|| = S_{ij}\, \beta\, S_{ij}\, d\lambda/1 = \beta\, S_{ij}\ S_{ij}\, d\varepsilon_p \qquad (20)$$

From the above proof, a method to obtain A and β from uniaxial stress test data can also be constructed.

First, load the test piece beyond the tensile yield point, then unload and compress it to reach the reversed yield point as shown in Fig.1.

From Fig.1,

$H_1 = f_1 + \alpha_1$

$H_2 = f_2 - \alpha_2$

At the beginning of the reversed yielding, the yield surface has not changed yet, so that

$f_2 = f_1$, $\alpha_2 = \alpha_1$

Then,

$f_1 = H_1 + H_2/2$

$\alpha_1 = H_1 - H_2/2$ (21)

Substituting into (18) and (20)

$A = f_1 - f_o/\varepsilon_p = \partial f/\partial \varepsilon_p$

$\beta = (\alpha_1 - \alpha_o)/\varepsilon_p$ (22)

where $f_o = H_o$ and $\alpha_o = 0$

In general, to represent the real material best, A and β may be functions of ε_p. By loading the specimens to different strain, ε^t,

the curves $f \sim \varepsilon_p$ and $\alpha \sim \varepsilon_p$ can be constructed as shown in Fig.1 where

$\varepsilon_p = \varepsilon^p{}_x = \varepsilon^t - \sigma_x/E$ (see Fig.1).

Performing the differentiation with respect to ε_p, the following is obtained:

$$A(\varepsilon_p) = df/d\varepsilon_p$$
$$\beta(\varepsilon_p) = d\alpha/d\varepsilon_p$$
$$H' = dH/d\varepsilon_p = A + \beta \qquad (23)$$

The model construction and the parameter determination have now been completed. The model can be used with any general first degree homogeneous yield function. The $A(\varepsilon_p)$, $\beta(\varepsilon_p)$ can be used to give a best fit to most experimental results.

In particular, for non-hardening materials,

$H' = A = \beta = 0$

For isotropic hardening materials,

$H' = A \neq 0, \beta = 0$

For kinematic hardening materials,

$H' = \beta \neq 0, A = 0.$

For combined-hardening,

$H' = A_x \neq \beta \neq 0$

4 SIMPLE EXAMPLES

The model has been applied to a 2-D finite element program "OYIN". Two examples will be given to show the generality of the model.

4.1 The Von Mises-like Yield Surface

$$\sqrt{3/2\,(\sigma'_{ij} - \alpha_{ij})\,(\sigma'_{ij} - \alpha_{ij})} - Y(k) = 0 \qquad (24)$$

This is thought suitable to describe the behaviour of most metallic materials.

EXPERIMENT

A monotonic load-unloading experiment is suggested. Under this programme, Fig (1) will be produced. The parameters β, α_c and n are then calculated.

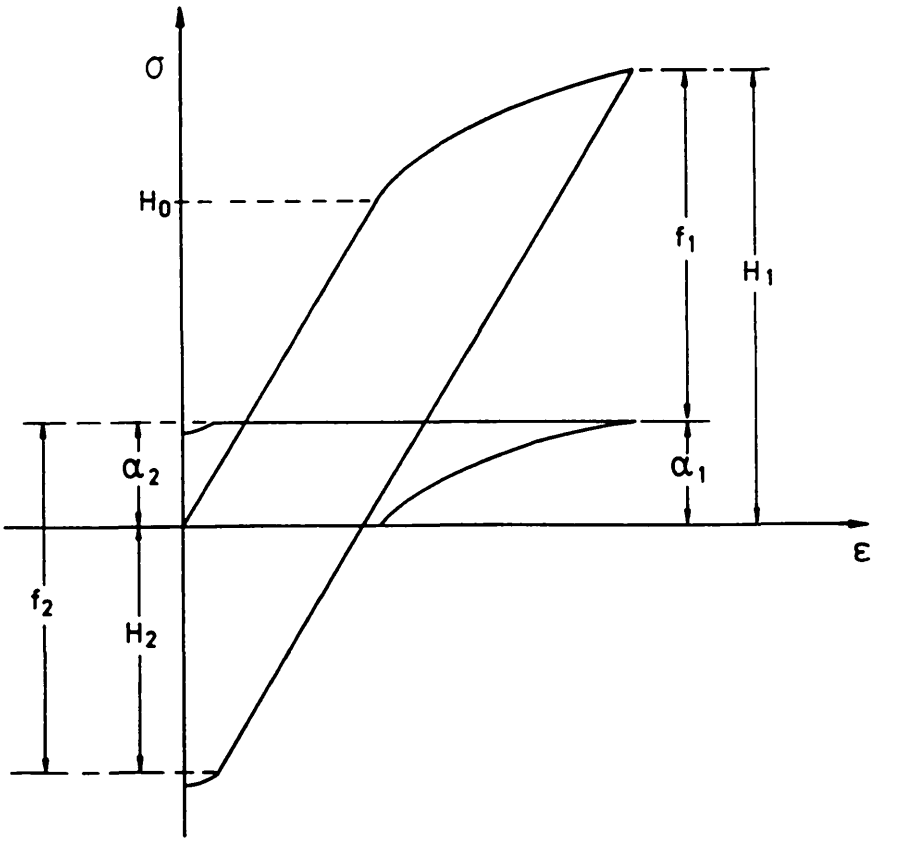


FIG.1: MONOTONIC LOAD-UNLOADING LOOP

All parameters are calculated as described in the thesis

ANISOTROPIC HARDENING.

It is usual to assume a constant hardening index, n, in tension and compression.

The argument here is that this claim is not representative of what happens along the plastic parts of the stress-strain curves in tension and compression. The reality of material behaviour is such that the hardening rate is not always the same for forward and reverse loading sequences. Consequently, material hardening behaviour has been reconstituted as a function which tends to the constant hardening index (n).

For this purpose, the Ramberg-Osgood model for plastic loading is assumed namely,

$$\sigma_p/\sigma_o = \alpha_c (\varepsilon_p/\varepsilon_o)^n$$

and the derived function H^1 is written as:

$$H^1 = E(\varepsilon/\varepsilon_o)^n / (E/\alpha_c [\varepsilon/\sigma_o] - n [\varepsilon/\varepsilon_o]^n)$$

H^1 is implemented in function HHH of program "OYIN" and it replaces A_x as the anisotropic hardening function.

APPENDIX B

USER MANUAL FOR COMPUTER PROGRAM.

The original program is called "IFE" and accesible on UMEMM 26. It can be compiled using FTN 5. The compiled program is called "OYIN".

Two files are needed for running the compiled program. They are 'FILE 1" and "DATAN" when N is any integer.

File 1 contains the geometery data which describe the Finite-element mesh. Also, some computed data are stored on it during program execution. These data will be needed if the main frame is to be used for plotting data on graphs.

LAYOUT OF FILES

Card No	Format	Data
1	2(I5)	Total Number of elements ($\leq$ 127)
1		Total Number of nodes ($\leq$ 439)
Element No (1)		Element Definition
	11(I5)	Element number, followed by 8 nodes arranged anti-clockwisely starting from
Element (N)		a corner, material type and Element type. (Order of arrangement can be random.)

Node (1)	([I5], 2F14.6)	Node number followed by the X- and Y-coordinates. The order can be random but the node with the highest number must be input last. Usually the midside nodes are
Node (N)		not input since the program is capable of interpolating between corner nodes in order to calculate them.

This file is always kept and can be used everytime a run is carried out as long as the same mesh is being used.

LAYOUT OF DATA (N)

Card No	Variables	Format	Description
1	TITLE	(8A10)	It specifies a format to print the title and the words for title.
2	CPLIMT FACT B	(8F10.1)	Specifies the central process time limit and the load scale factor (applied to all loads).
3	ICYCLE, NCYCLE ICODE, ILOAD, IALF	(1615)	ICYCLE - starting cycle NCYCLE - ending cycle ICODE - identification code of previous record (0 for first run) ILOAD - no of load increments

calculated (counted from first cycle; = 0 for first run)

IALF - gauss point no to output movement of centre of yield surface, α_{ij}.

4 IPLANE, ICOND, NPROB(2) 12(A7)

written as:

		STRESS		ELASTICITY
[SPACE]	PLANE [SPACE]	or	[SPACE]	or
		STRAIN		PLASTICITY

5 MAXMAT, MAXITE, NPUT, MAXJI, NCKIN, MTYPE (1615)

MAXMAT - Maximum no of materials.

MAXITE - Maximum iteration time for first load

NPUT - Output control code:

= 0 (energy terms)

1 (displacement for selected points)

2 (stresses for selected points)

3 (restraint forces)

4 (total stresses)

5 (total displacement)

> 8 (accelerator)

The biggest code incorporates the contents of the smaller ones.

MAXJI - No of J paths selected to average

NCKIN - Crack extension indicator
(1 for crack extension, 0 for no crack extension)

MTYPE - No of element types.

6 Material Properties (I3, 9F11.5)

№ of material, followed by E (Young's modulus), υ (poisson ratio) ρ (density), σ_y (yield stress), εpy(yield strain), α_c (Ramberg Osgood plastic constant), n (hardening index), B (thickness), β (kinematic translation parameter).

REPEATED FOR ALL MATERIALS

7 MAXDIS, MAXRCT, MAXPRS, MAXTN (16I5)

MAXDIS - Total no of restrained nodes (includes those which will close during unloading)

MAXRCT - Total no of point loads

MAXPRS - Total no of edges (element) which have distributed loads

MAXTN - Total no of local axes.

8 Restraint condition (215, 2F14.6)

Number of node, condition (x-restraint value, Y-value) condition may be:

00 - No restraint

01 - Y-direction restrained

10 - X-direction restrained

11 - both fixed.

9 Local axes definition. If MAXTN = 0, the set of data will not be necessary.

9a θ Angle (in degree), No of nodes with θ (F14.6,I5).

9b No of nodes with θ (16I5) repeat (9b) if nodes are more than 16. Repeat (9a) and (9b) until MAXTN.

10 Point load data. No, X-load, Y-load (I5,4F14.6). Repeat to MAXRCT (MAXRCT = 0, omit it).

11 Distributed load data:

11a NEPRS, NODPR (16I5)

(Ele No) (Node No anticlockwise).

11b PN(3), PT(3), (6F12.6).

PN = normal stress; towards element as positive;

PT = tangential stress; anticlockwise as positive.

Repeat (11a) and (11b) to MAXPRS.

12 TOLER GRAX GRAY WIRL (6F12.6)

Convergence tolerance, X-gravity, Y-gravity, rotary speed (Rad/sec)

13 MAXDPT, MAXGPT, NCYL, NDTIP (16I5)

MAXDPT - No of selected points to output displacement ($\leqslant$ 30)

MAXGPT - No of selected points to output stresses ($\leqslant$ 32)

NCYL - No of load increment in half cycle

NDTIP - No of crack tip node.

13a MOUTD (1615)) - No of selected displacement nodes, till MACDPT

13b MOUTS (1615) - No of selected stress point.

14 Data block for crack extension if NCKIN = 1:

a) CKIN (A4) identify CKIN block

b) NCRIT, NDTIP, MRELA, NTIME, NCRIT: criterion for crack extension:

1 - ε_p (accumulative plastic strain)

2 - S (strain energy density factor)

3 - δ (COD)

4 - ϕ (Flank angle).

MRELA - max. no of nodes to release (< 2.1)

NTIMES - steps to release the restraint forces (< 6).

c) VCRIT: (value of criterion), ALENG (crack length), FACTD (factor of 8) (6F12.6)

d) FACTR (6F12.6): factor for release of restraints.

e) NRELA: (16I5) - No of nodes to release.

f) NCPTS: (16I5) - No of critical points when NCRIT = 1 or 2 , NCPTs (1, 3, 5 ...) = stress points (2, 4, 6 ...): Nodes vice versa.

15 Data block for J-integral:

a) CJINT (A5)

b) MAXJ, FACTJ (15F14.6) - no of paths factor for J

c) No of points followed by GP No. (16I5). Repeat C to MAXJ.

16 LOAD INCREMENT DATA

a) RELOAD (A7)

b) IE (15) - No of load increments before the cyclic load starts.

Used for $P_{min} = 0$

c) FACT, TOLER, MAXITE, NPUT, NSTOP (2F14.6, 10I5)

FACT - increment factor (to basic load) for first load, it

is better to be 1.0.

TOLER - convergence tolerance

MAXITE - maximum iterations

NPUT - output control code

NSTOP - stop control

= 0 - continue to the next increment

= 1 - restart for the next cycle

= 2 - stop.

VARIABLES IN COMMON.

These information are useful for understanding and modifying the program.

1 Block JACi - constants for quadrate element:

XX(δ), YY(δ) - local co-ordinates (ξ_i, η_i) for nodes;

VECTL (4), WTFUN (4) - local co-ordinates and weight function for all Gaussian points.

2 Block JACZ - the same as JAC1 but for triangular element.

3 Block CYCL - for cyclic loading:

APLWK - accumulative plastic work during half cycle;

NCYL - Number of load increments in half cycle.

4 JAC12 - for Jacobian matrix:

SHP (δ) - shape function N;

DX(δ) - $\alpha N_i/\alpha x$;

DY(δ) - $\alpha N_i/\alpha Y$;

AW(4) - [J];

CW(4) - $[J]^{-1}$;

NELDES(δ) - destination in FRONT of element nodes;

NELDEF (δ) - elemental definition;

X(δ), Y(δ), ψ(δ), V(δ) - co-ordinates and displacements of elemental nodes.

5 TOT1 - control parameters:

NNODδ - maximum nodes for element

8 - for quadrate element

6 - for triangular element;

MAXTNP - maximum number of points restrained in local areas;

MAXSTR - maximum number of stress points;

ICASE - iteration counter;

NLOAD - load counter;

RESMAX - maximum residual nodal force;

FORMAX - maximum external incremental nodal force;

NORMAX - number of the maximum residual nodal force six;

SQLOAD - $|F|^2$;

NACCEL - acceleration and control;

INLOAD - load increment indicator;

NCHEK - convergence indicator;

1 - converged;

2 - converging;

3 - not converged;

EWORK - elastic energy (integrated);

PLASWK - total plastic energy (integrated);

PZEWORK - current (reversed) plastic energy for this load increment;

WORK - external work for P - δ curve;

TPARZA - total plastic zone area;

PAREA - current;

MPLAS - total number of yielded points;

NPLAS - total number of current yielded points.

6 RED

IRED = 1: indicates that the elastic stress at some point deviated from yield;

FACTB - factor to reduce the applied load. It applies to all sequential load.

7 TOT2

DISPL - Displacements : first two for incremental displacement; last two for total displacement;

CORD - nodal co-ordinates;

LDEST - nodal destination vector, ie position in FRONT;

LDEF - definition of elements;

RS - incremental or residual load of elements (RHS of equation);

S - elemental stiffness;

TRS - total applied load;

ERS - equivalent nodal forces of an element;

NPYED - number of current yielded points;

SIG - stress components: σ_x, σ_y, σ_z, τ_{xy}

TEEP - accumulative plastic strain;

SIGB - flow stress.

8 BOUND - for boundary conditions:

KREAS - stiffness reassembly indicator: 1 = reassemble;

IDSP - restraint indicator;

DSP - restrained displacement;

REFOR - restraint forces;

REFIN - incremental restrain forces;

PRERF - previous REFOR.

9 FRBK - for solving equation:

REQ - buffer area for co-efficients;

SKS - assembled RS in FRONT;

SRKP - assembled RS no elimination (for | R |);

TRSKP - assembled total RS (for | F |);

SS - assembled global stiffness.

OUTLINE OF THE OUTPUT.

Firstly almost all input data are printed out for check. Then the coordinate of Gaussian points can be printed out controlled by NPUT(> 4). Some information about front length and the use of the buffer area will print out. The line "RECORD N WRITTEN ON TAPE Z, MZM = NN" will help one arrange the buffer area match with each other.

One line of convergence information will print out each iteration. The results for each load increment after convergence are basically the same controlled by parameter NPUT. They are all self-explanatory. Only the heading for the stress components need a little explanation:

GP - number of Gaussian point;

S1, S2, SZ - three principal stresses;

SX, SY, SXY - σ_x, σ_y, τ_{xy};

DX - X-distance from a reference point (usually crack tip);

EEP - accumulative plastic strain;

WP - plastic strain energy density;

ANGL - angle θ of principal stress with X-axis.

ALUMINIUM - DATA FILE - MONITORING CYCLIC HARDENING

```
FATIGUE CYCLING OF ISO ELECTROPLAL SPECIMEN-
    P00.0          1.00
   1   8   0   0   0
PLANE STRAIN. PLASTICITY
   1   5   2   0   0   2
 1       1.00       0.2000      0.00      0.1650     0.00230      0.620      0.200      1.00    0.25500
  22     0   0   0
    1   01          0.0000          .030
    2   000                         .030
    3   000                         .030
    4   000                         .030
    5   000                         .030
    6   000                         .030
    7   000                         .030
    8   000                         .030
    9   000                         .030
   10   000                         .030
   11   000                         .030
  171   000
  172   000
  173   000
  174   000
  175   001
  176   011
  177   100
  178   000
  179   000
  180   000
  181   05
      0.5000          0.0         0.00          0.0
   11   1   2   3   4   5   6   7   8   9  10  11
    1   1   2   3   4   5   6   7   8   9  10  11
    0
          1.000          5.000          5          0
          0.400          5.000
          0.300          5.000
          0.100          5.000
          0.069          5.000
          1.000          5.000
          0.400          5.000
          0.300          5.000
          0.100          5.000
          0.069          5.000
          1.000          5.000
          0.400          5.000
          0.300          5.000
          0.100          5.000
          0.069          5.000
          1.000          5.000
          0.400          5.000
          0.300          5.000
          0.100          5.000
          0.069          5.000
```

APPENDIX D

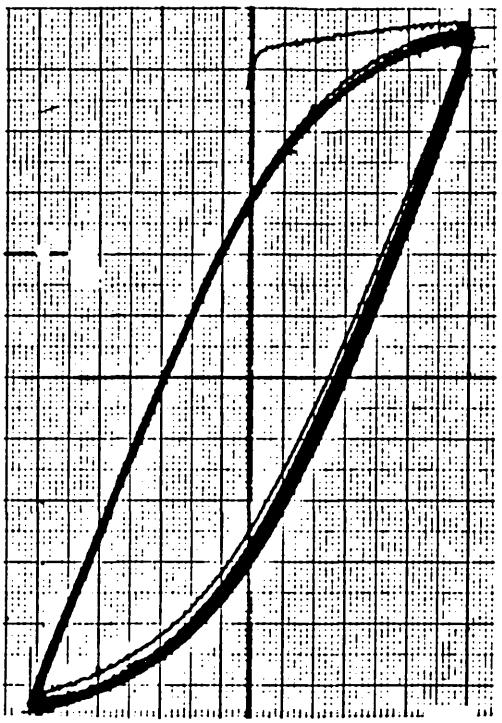


Fig.D.1a Experimental cyclic hysteresis loops for aluminium (Displacement amplitude = 8.8%).

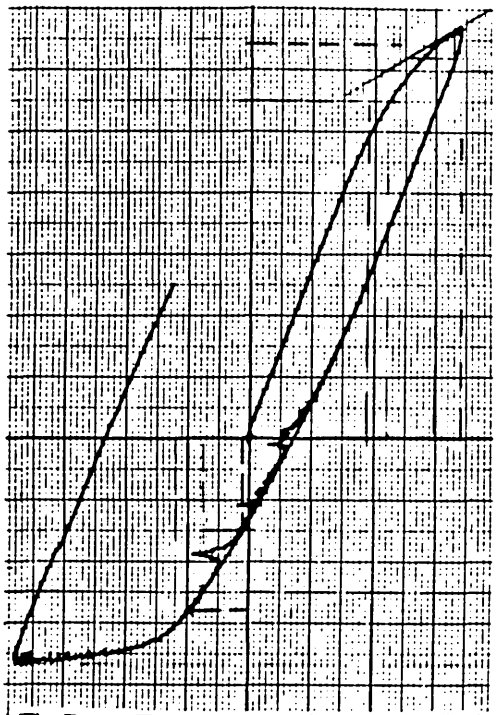


Fig.D.1b Experimental monotonic loop for aluminium (Displacement amplitude = 8.8%).

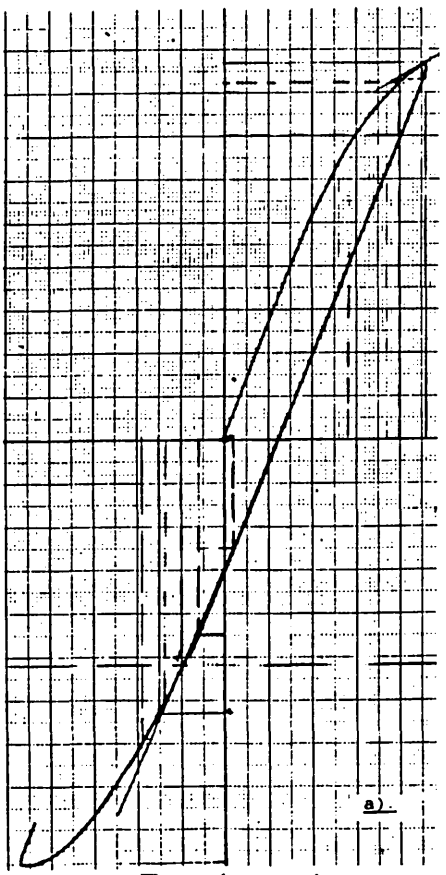


Fig.D.2a Experimental monotonic loop for aluminium (Displacement amplitude = 12%).

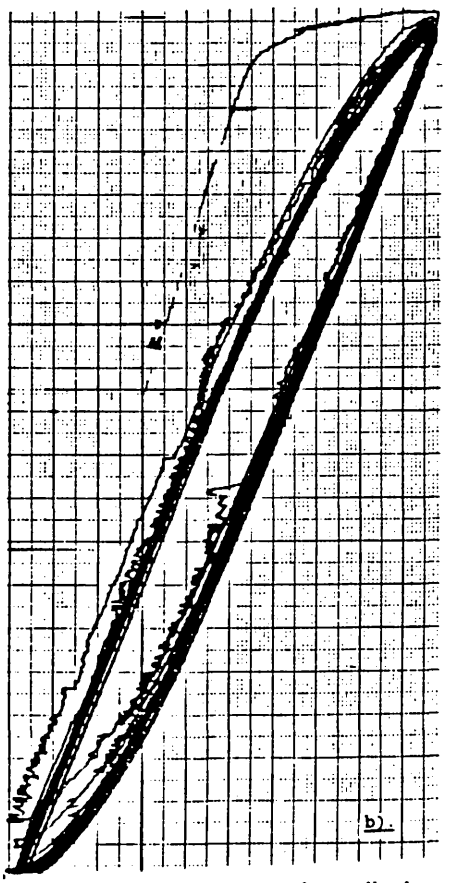


Fig.D.2b Experimental cyclic hysteres loops for aluminium (Displacement amplitude = 12%).

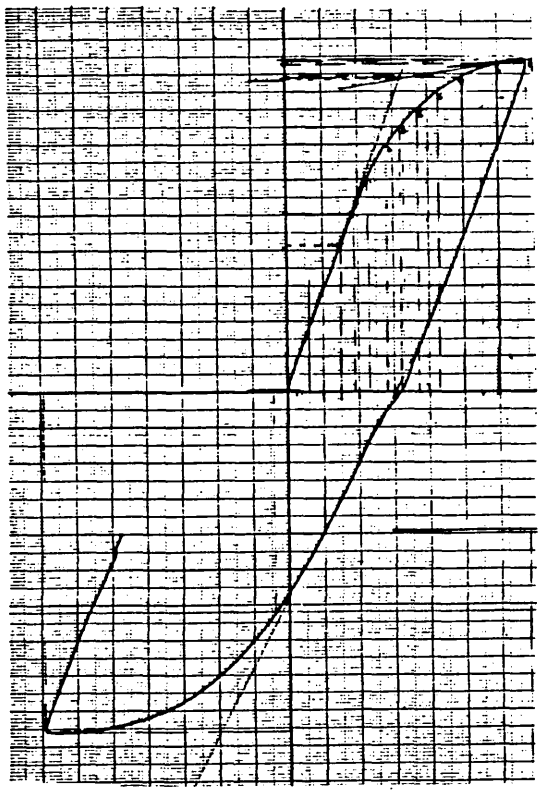


Fig.D.3a Experimental monotonic loop for loops for aluminium (Displacement amplitude = 14.5%).

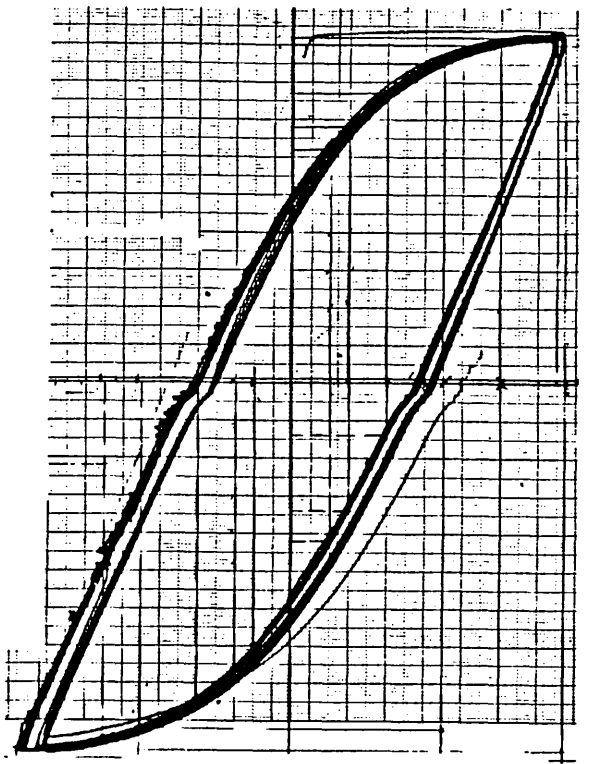


Fig.D.3b Experimental cyclic hysteresis aluminium (Displacement amplitude = 14.5%).

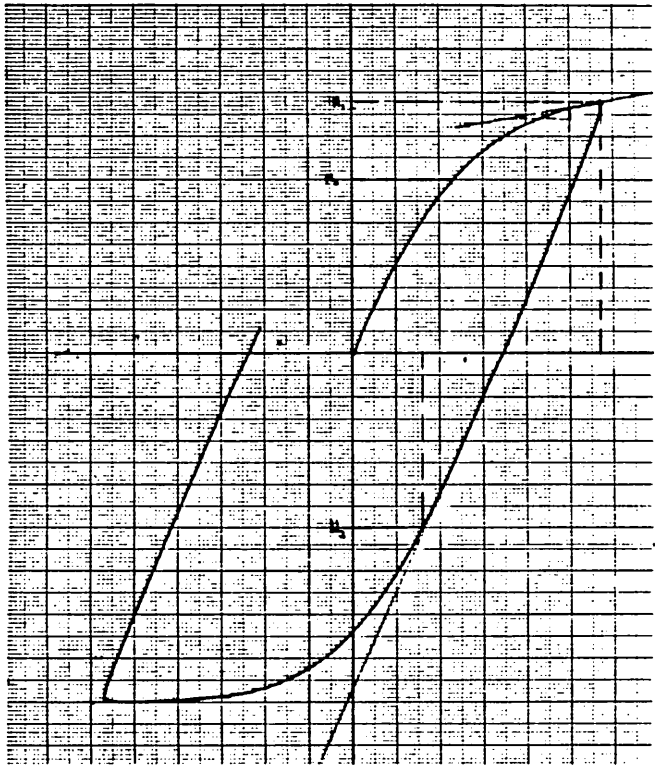


Fig.D.4a Experimental monotonic loop for aluminium

(Displacement amplitude = 16%).

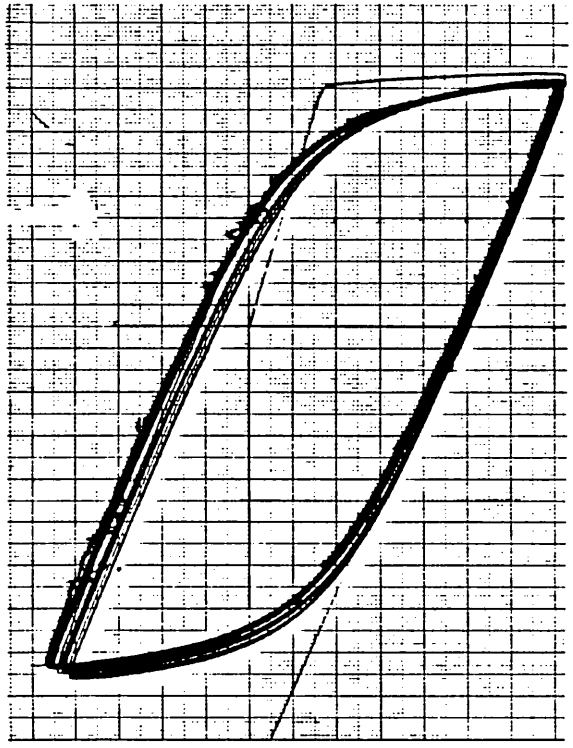


Fig.D.4b Experimental cyclic hysteresis loops for aluminium

(Displacement amplitude = 16%).

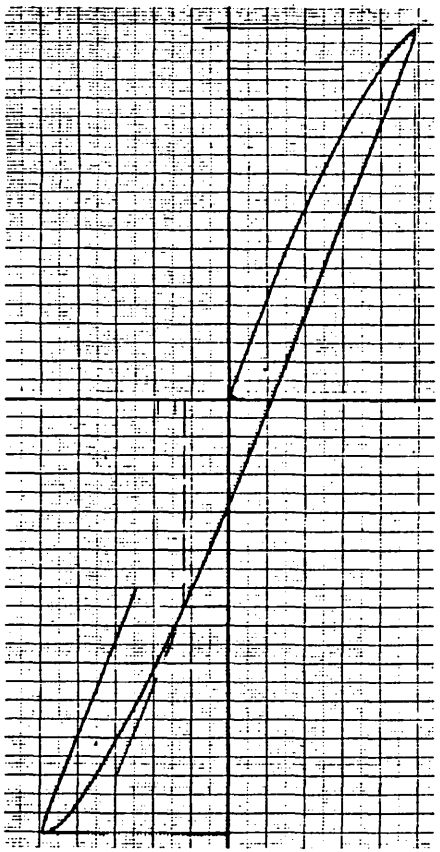


Fig.D.5a Experimental monotonic loop for Titanium

(Displacement amplitude = 13%).

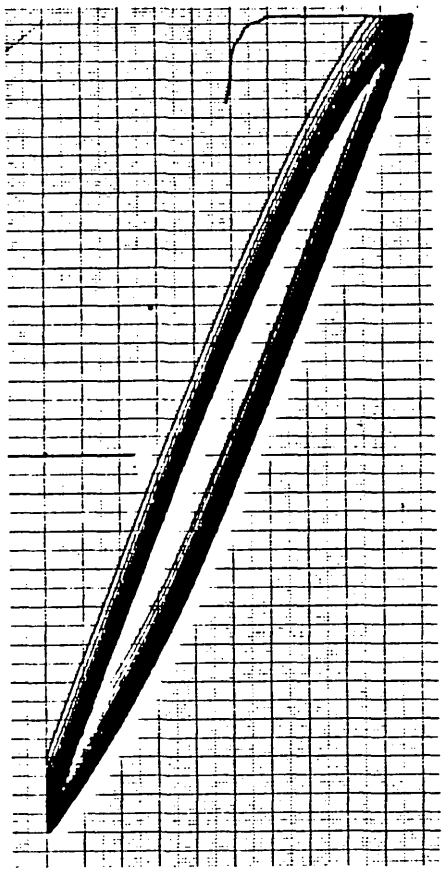


Fig.D.5b Experimental cyclic hysteresis loops for Titanium

(Displacement amplitude = 13%).

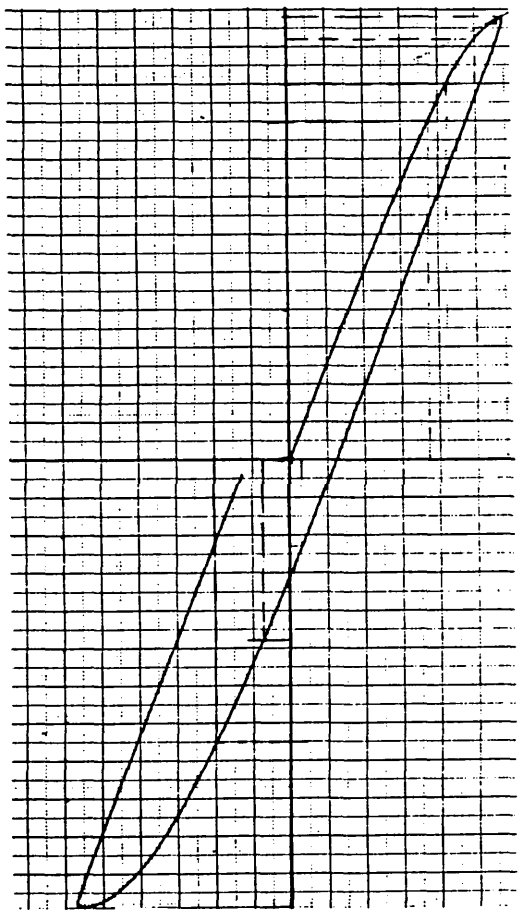


Fig.D.6a Experimental monotonic loop for Titanium

(Displacement amplitude = 16%).

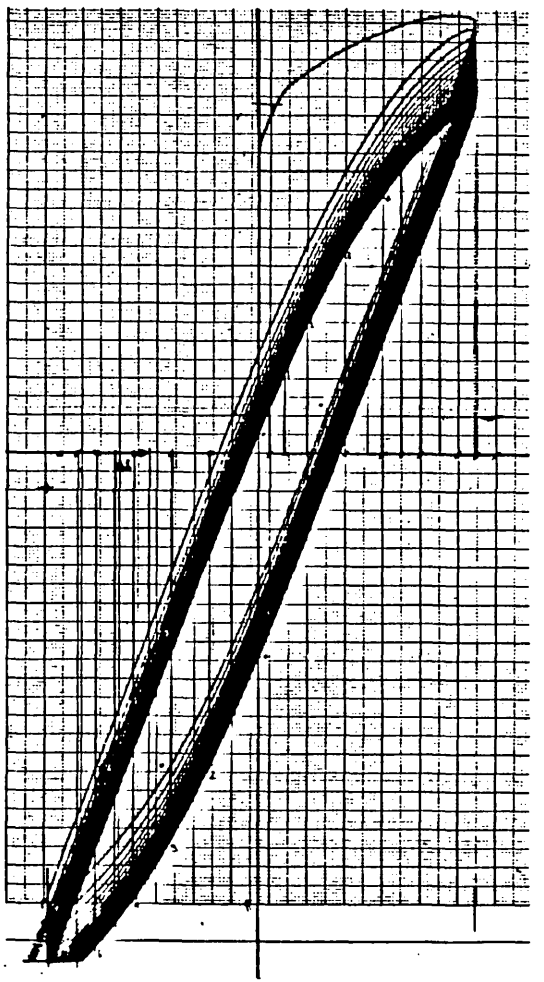


Fig.D.6b Experimental cyclic hysteresis loops for Titanium

(Displacement amplitude = 16%).

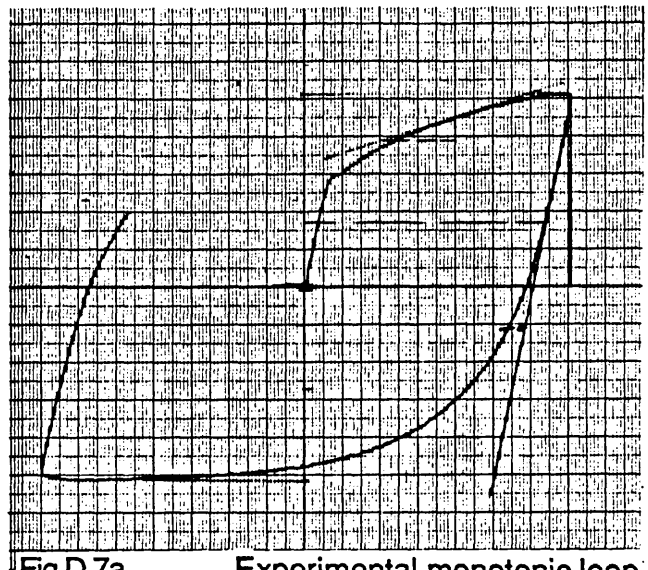


Fig.D.7a Experimental monotonic loop for stainless steel (Displacement amplitude = 15%).

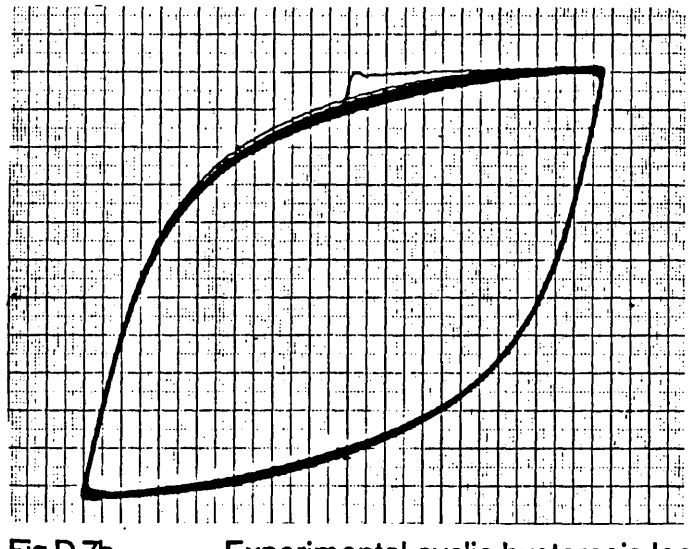


Fig.D.7b Experimental cyclic hysteresis loops for stainless steel (Displacement amplitude = 15%).

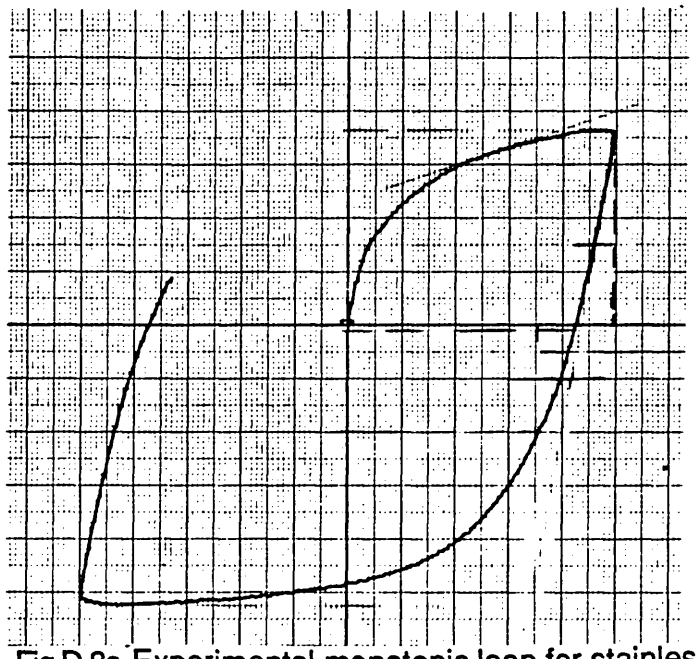


Fig.D.8a Experimental monotonic loop for stainless steel (Displacement amplitude = 18.8%).

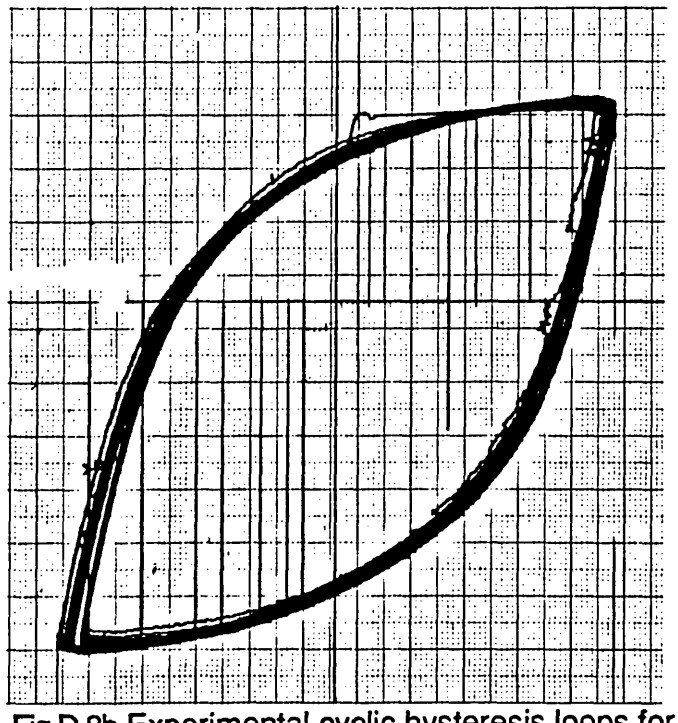


Fig.D.8b Experimental cyclic hysteresis loops for stainless steel (Displacement amplitude = 18.8%).

APPENDIX E

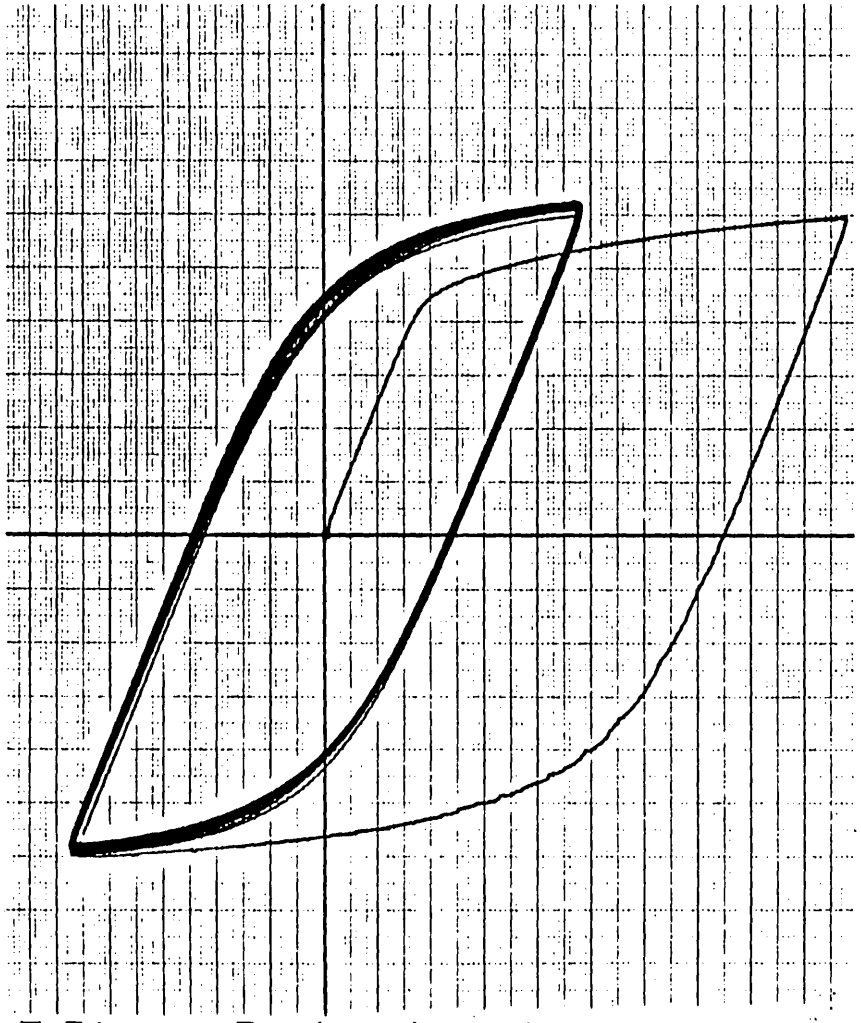


Fig.E.1 Experimental prestrain and cyclic hysteresis loops for aluminium (25.2% prestrain, cyclic ampl.= 10.5%).

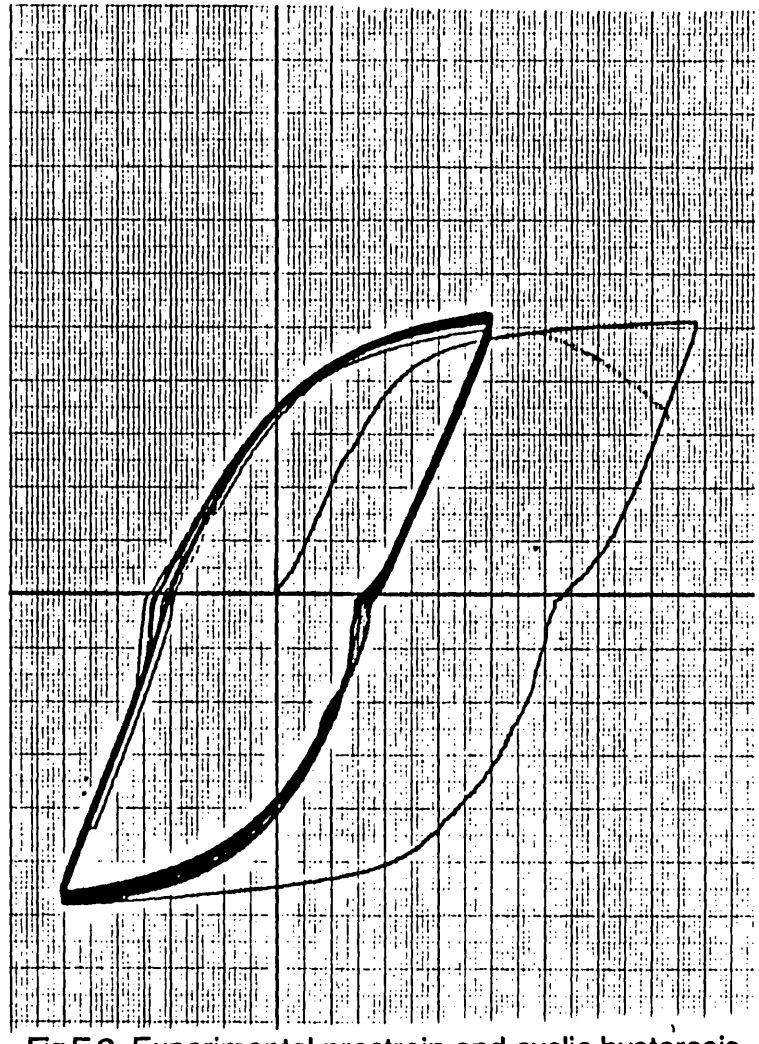


Fig.E.2 Experimental prestrain and cyclic hysteresis loops for aluminium (20% prestrain, cyclic ampl.= 10.5%).

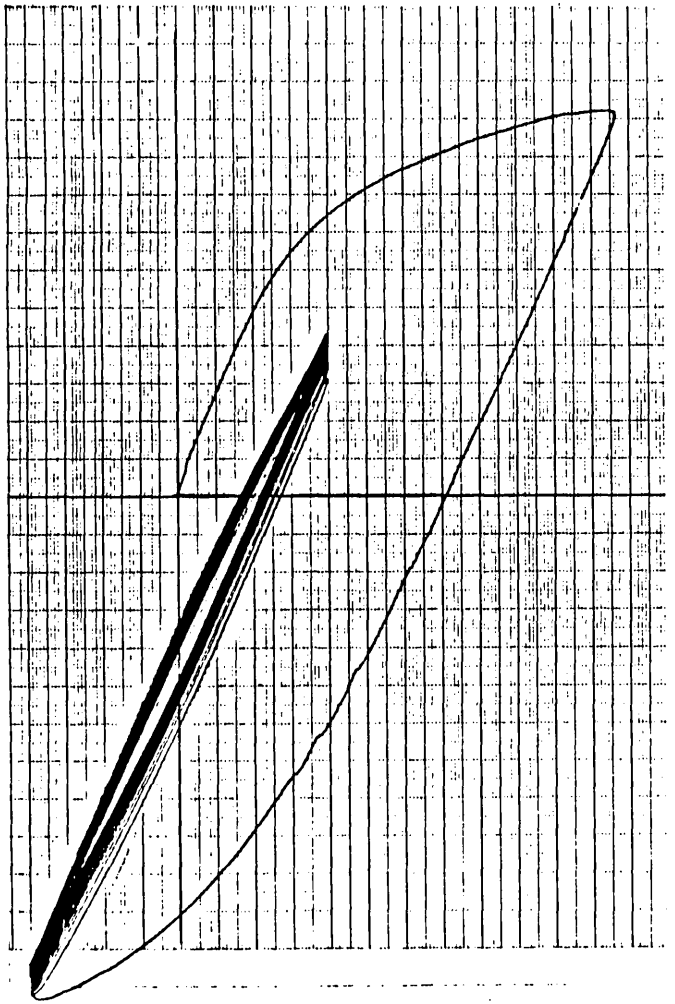


Fig.E.3 Experimental prestrain and cyclic hysteresis loops for Titanium (31.5% prestrain, cyclic ampl.= 10.5%).

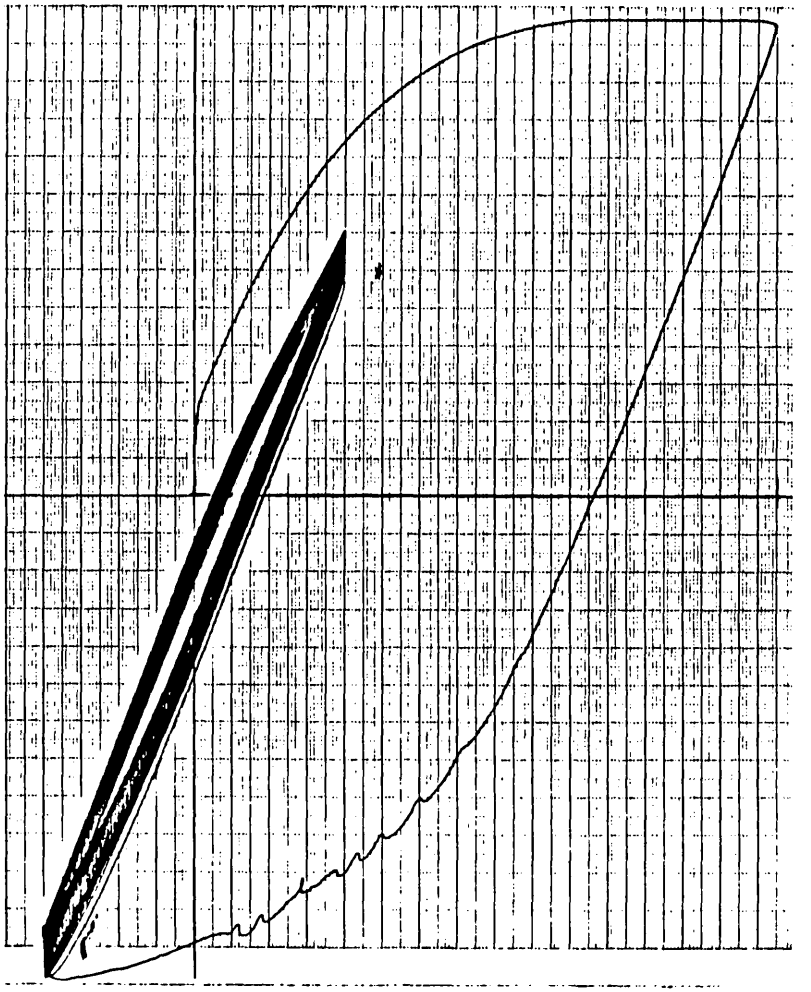


Fig.E.4 Experimental prestrain and cyclic hysteresis loops for Titanium (42% prestrain, cyclic ampl.= 10.5%).

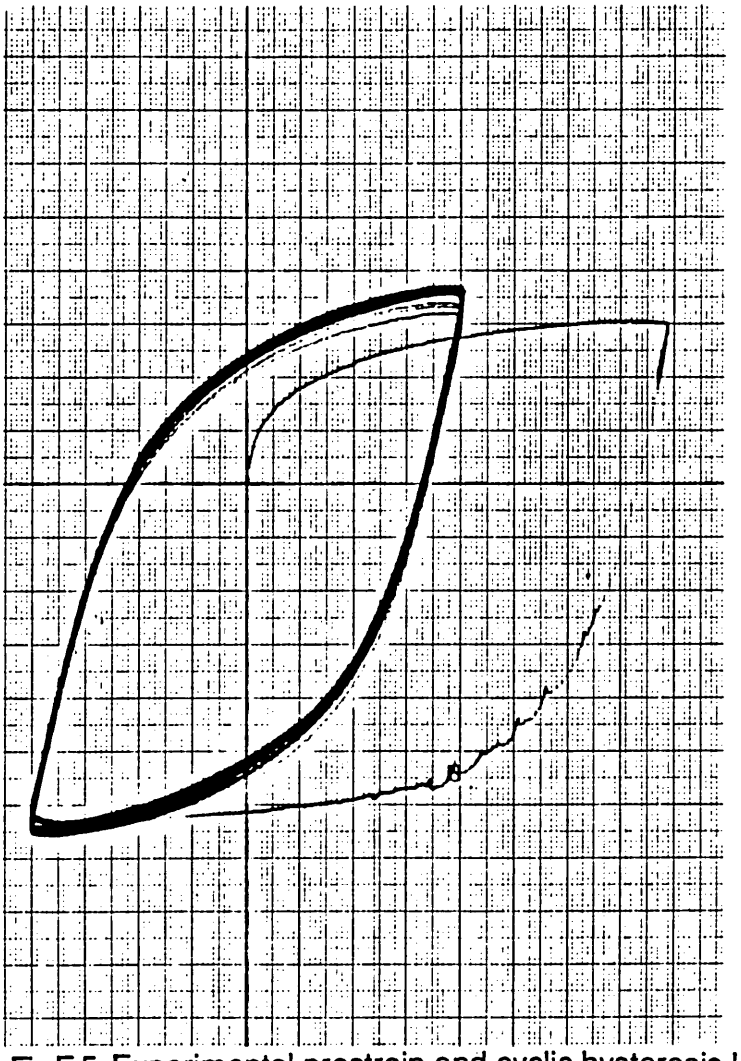


Fig.E.5 Experimental prestrain and cyclic hysteresis loops for stainless steel (20.8% prestrain, cyclic ampl.=10.5%).

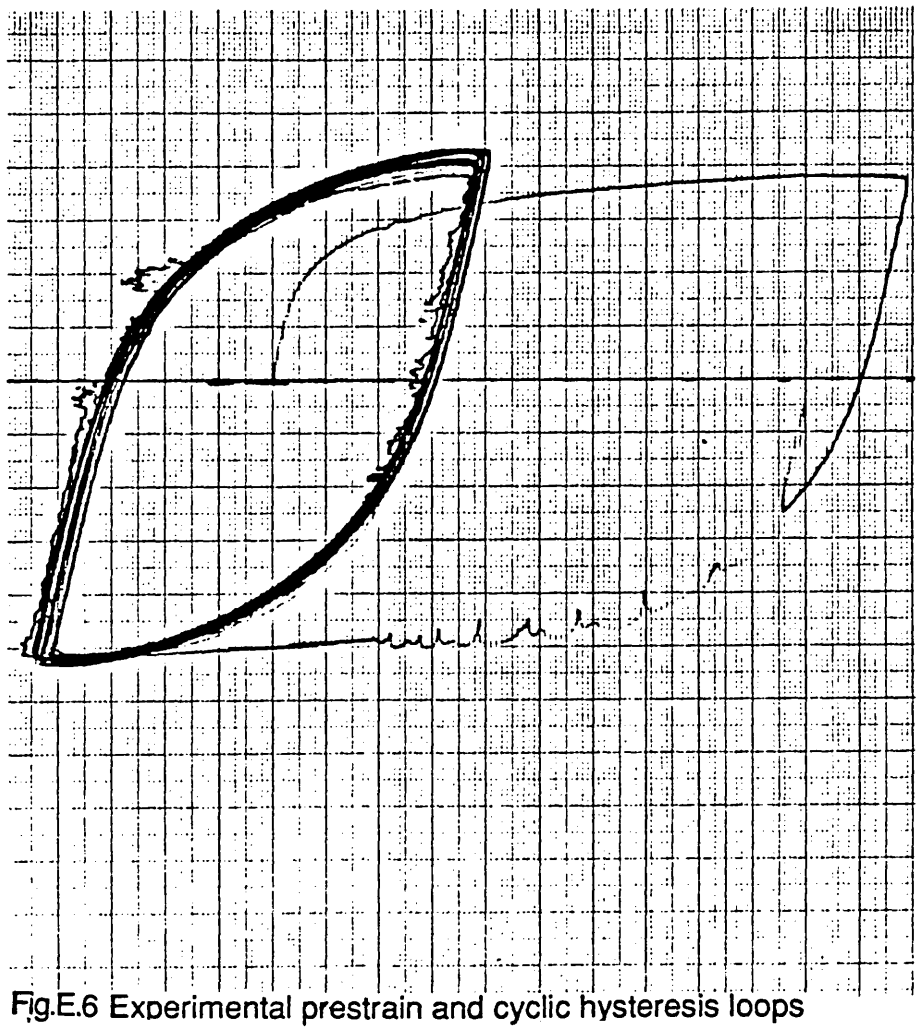


Fig.E.6 Experimental prestrain and cyclic hysteresis loops for stainless steel (31.5% prestrain, cyclic ampl.= 10.5%).

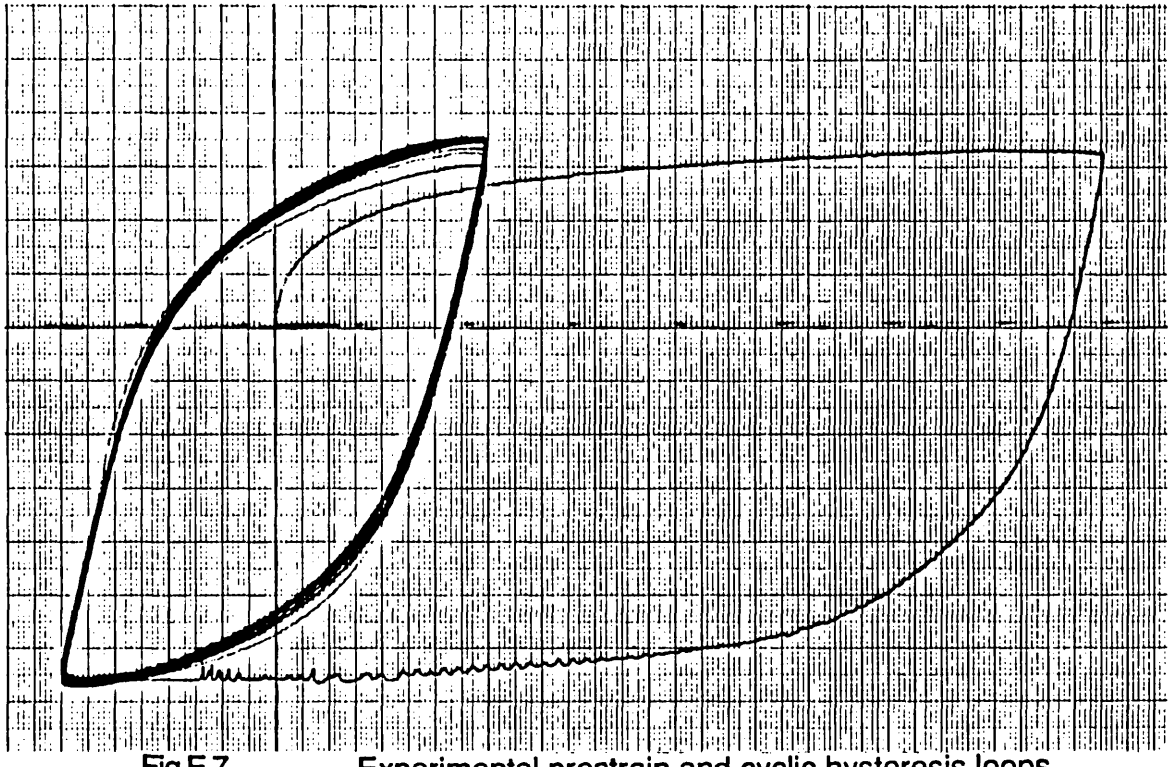


Fig.E.7 Experimental prestrain and cyclic hysteresis loops for stainless steel (42% prestrain, cyclic ampl.= 10.5%).

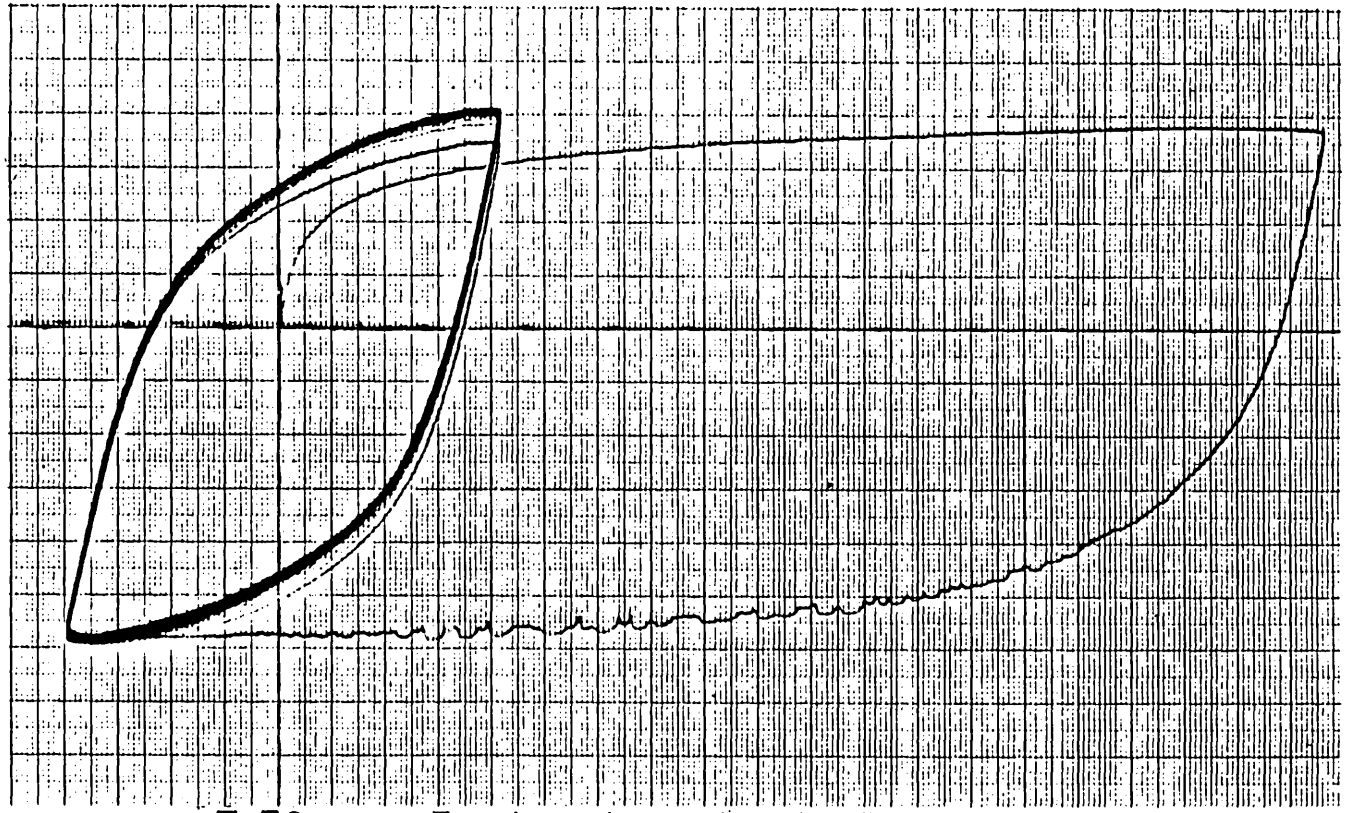


Fig.E.8 Experimental prestrain and cyclic hysteresis loops for stainless steel (52.5% prestrain, cyclic ampl.=10.5%).

APPENDIX F

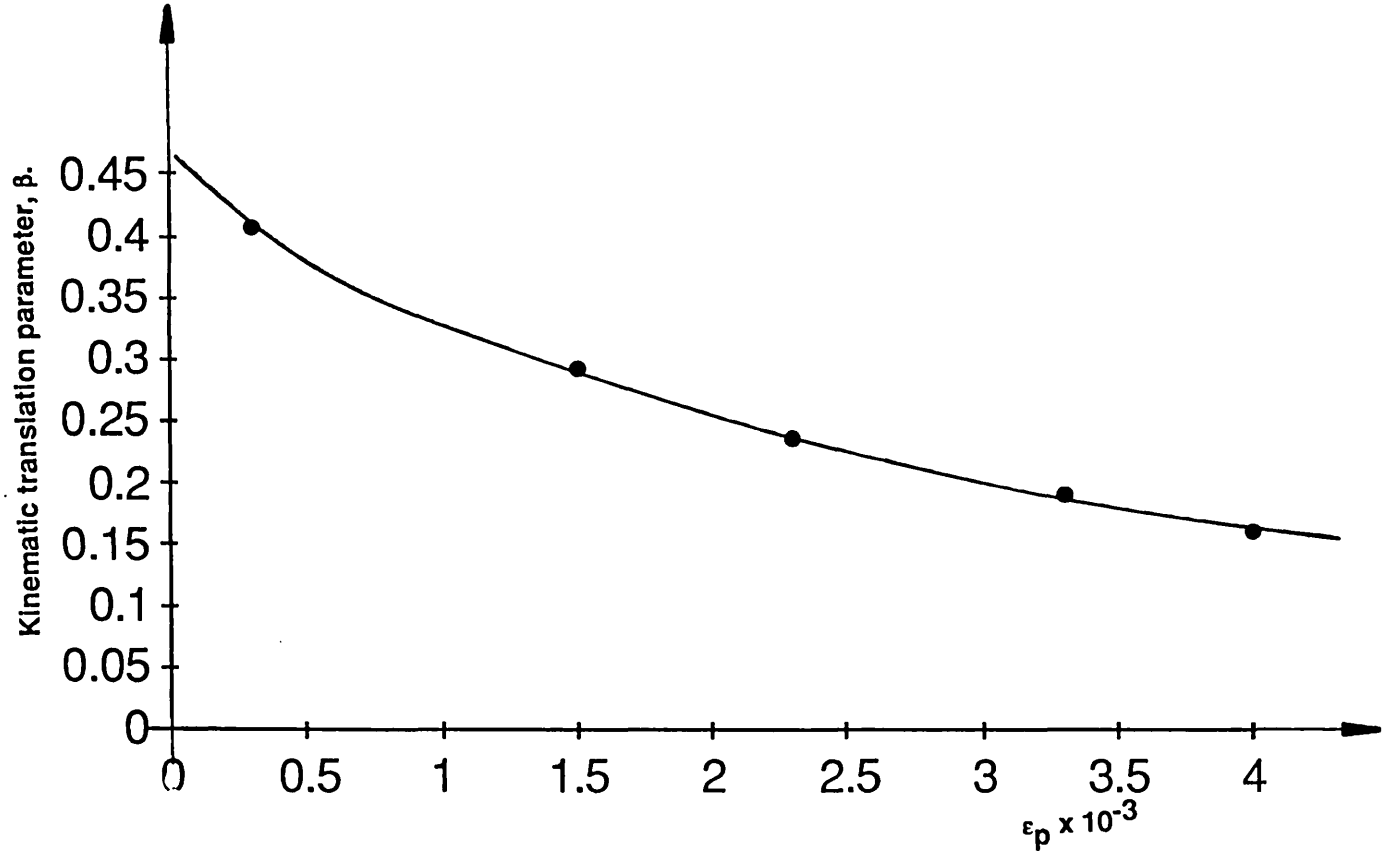


Fig. F.1 Variation of the kinematic translation parameter with initial plastic strain for aluminium H18.

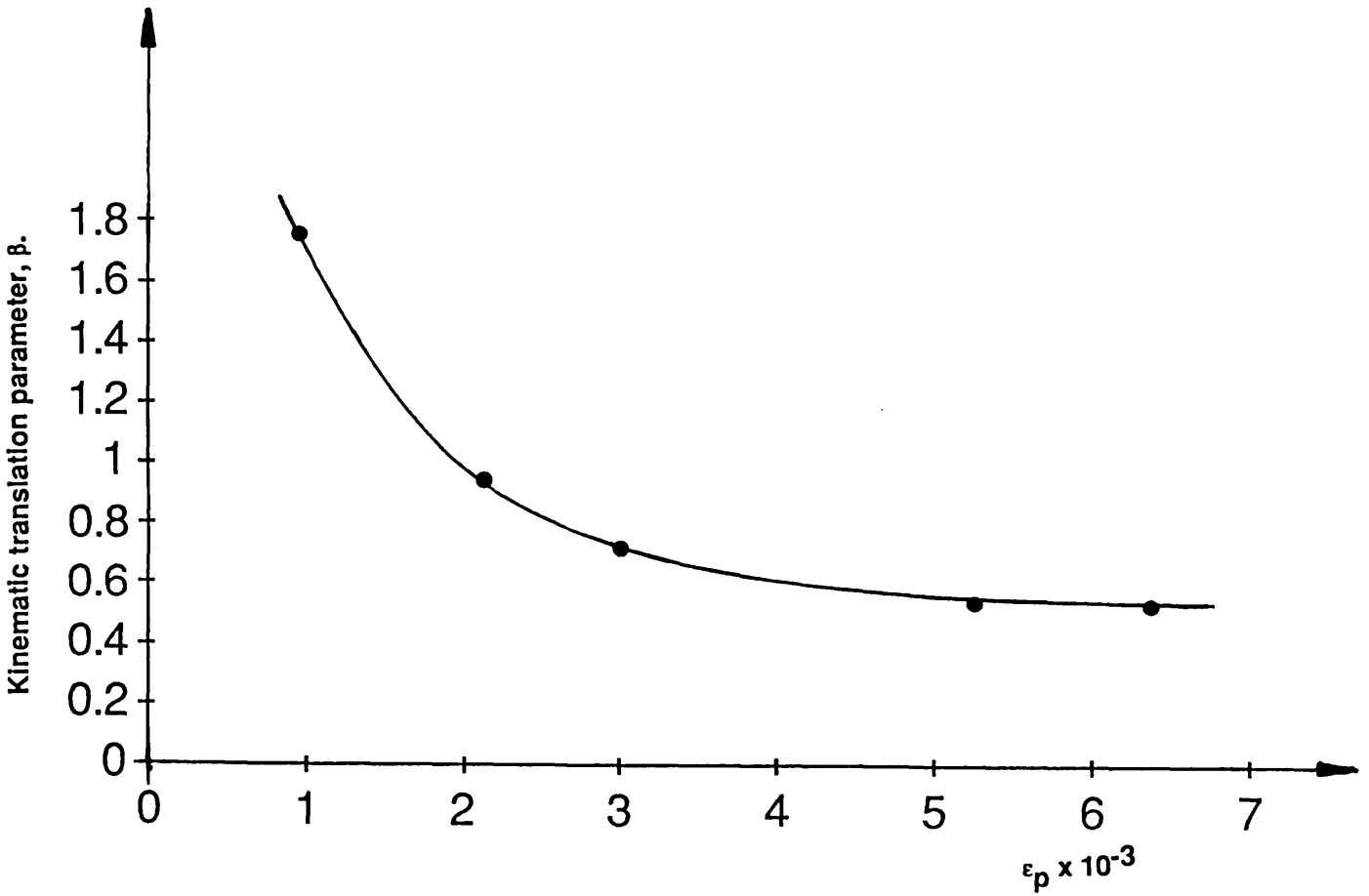


Fig. F.2 Variation of the kinematic translation parameter with initial plastic strain for Titanium (Ti-6211).

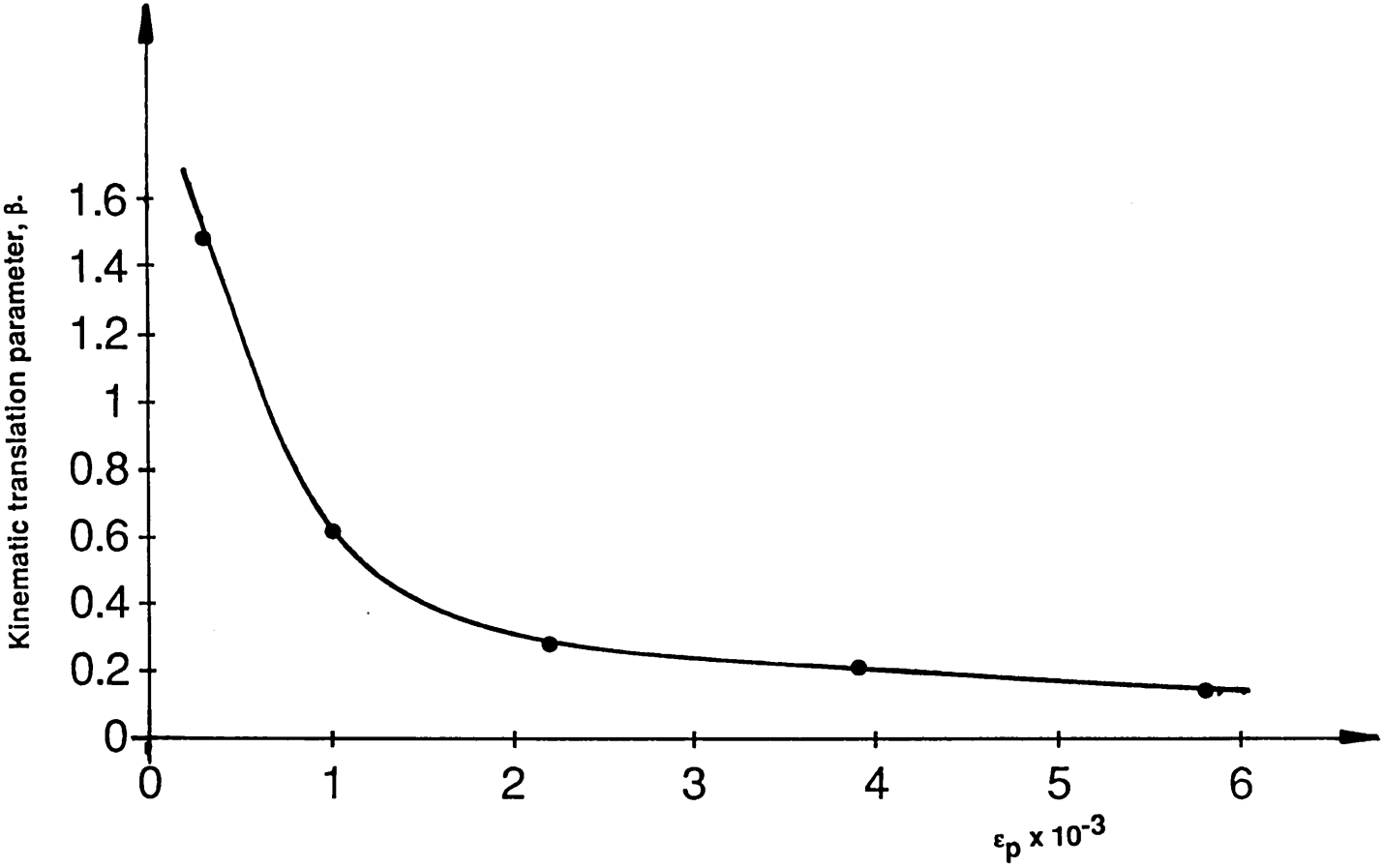


Fig. F.3 Variation of the kinematic translation parameter with initial plastic strain for stainless steel.

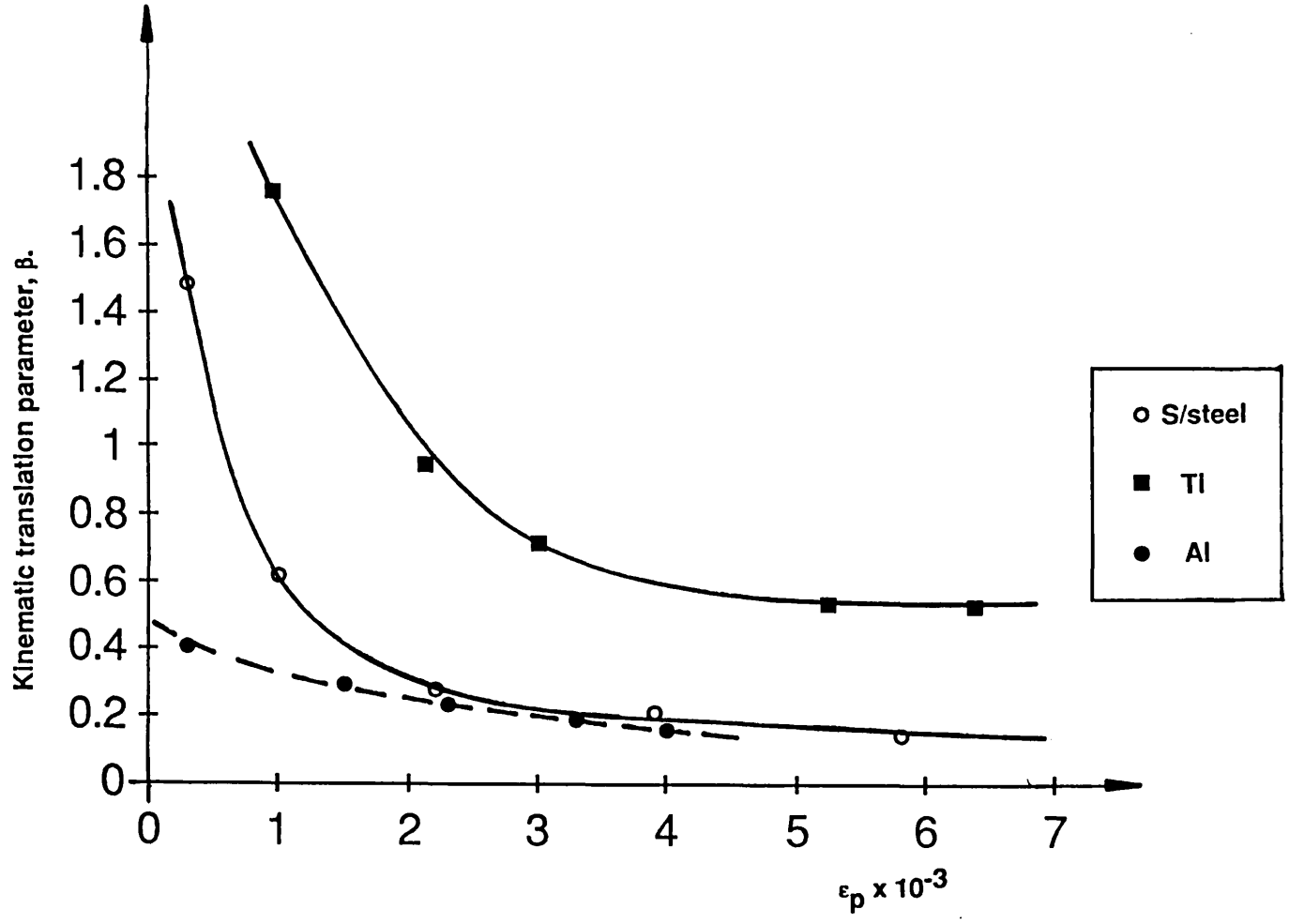


Fig. F.4 Comparison of the variation of β with ε_p to show material dependence of β.

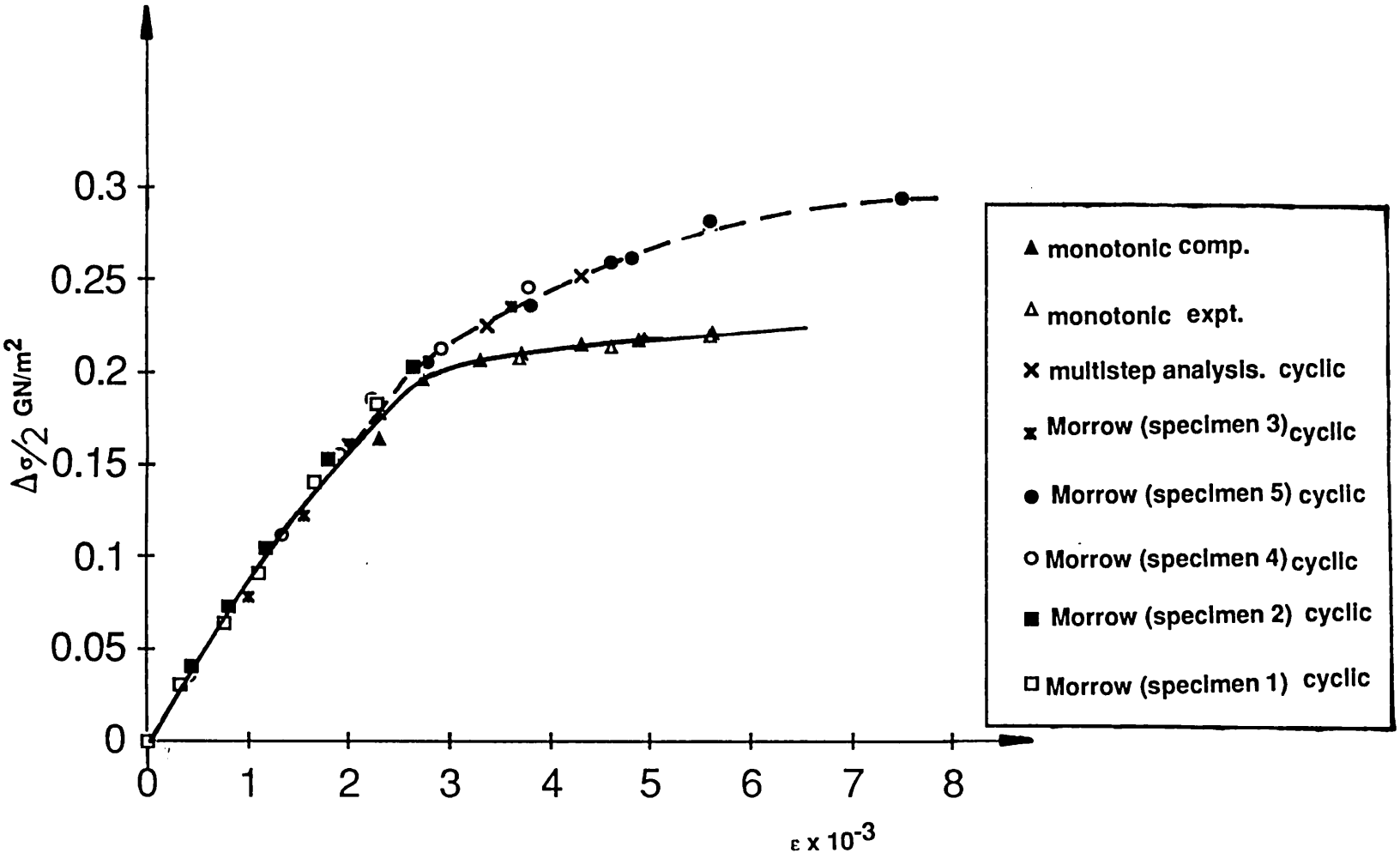


Fig.F.5 Experimental and computed monotonic and cyclic stress-strain curves for aluminium H18.

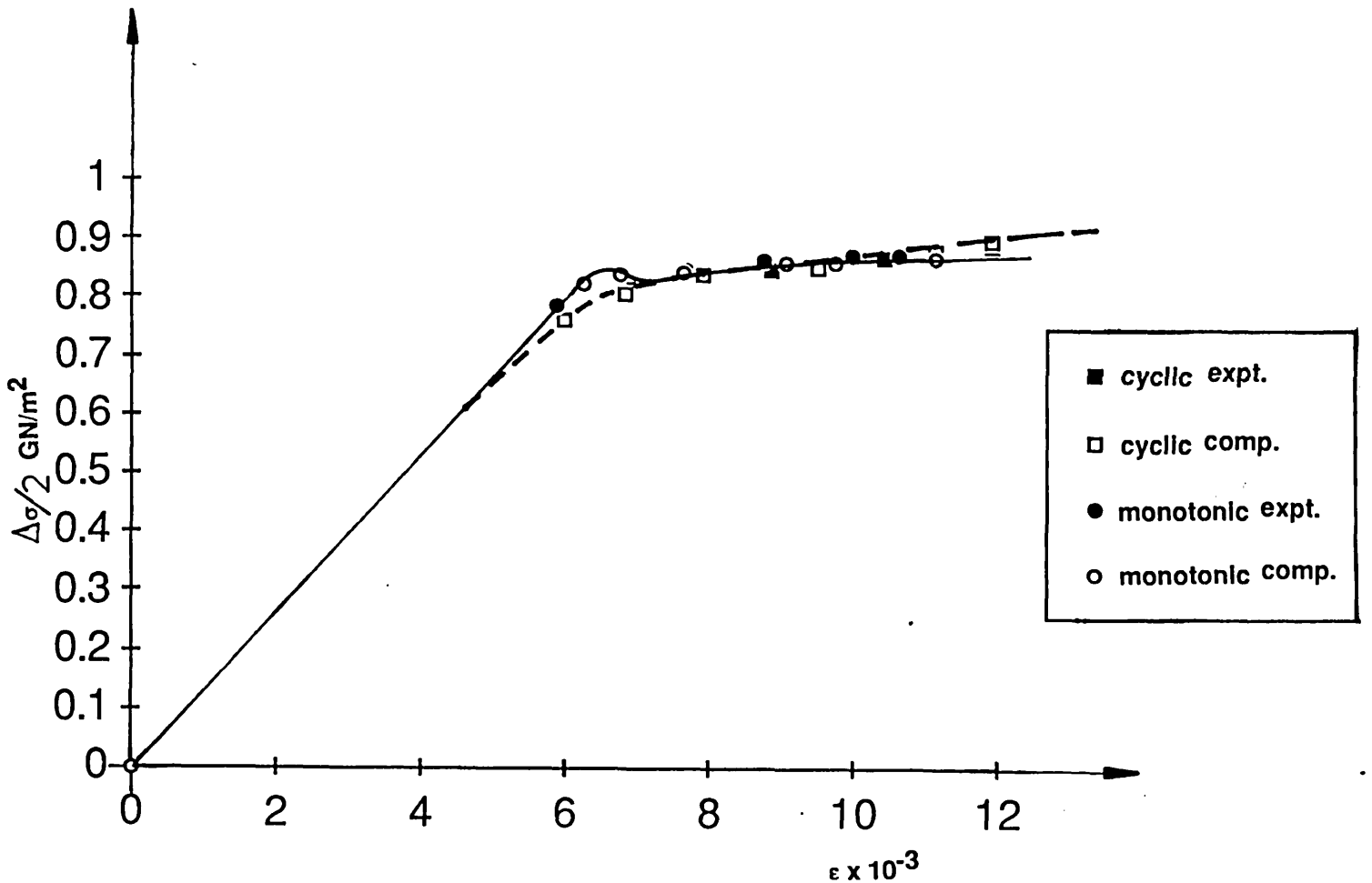


Fig.F.6 Experimental and computed monotonic and cyclic stress-strain curves for Titanium (Ti-6211).

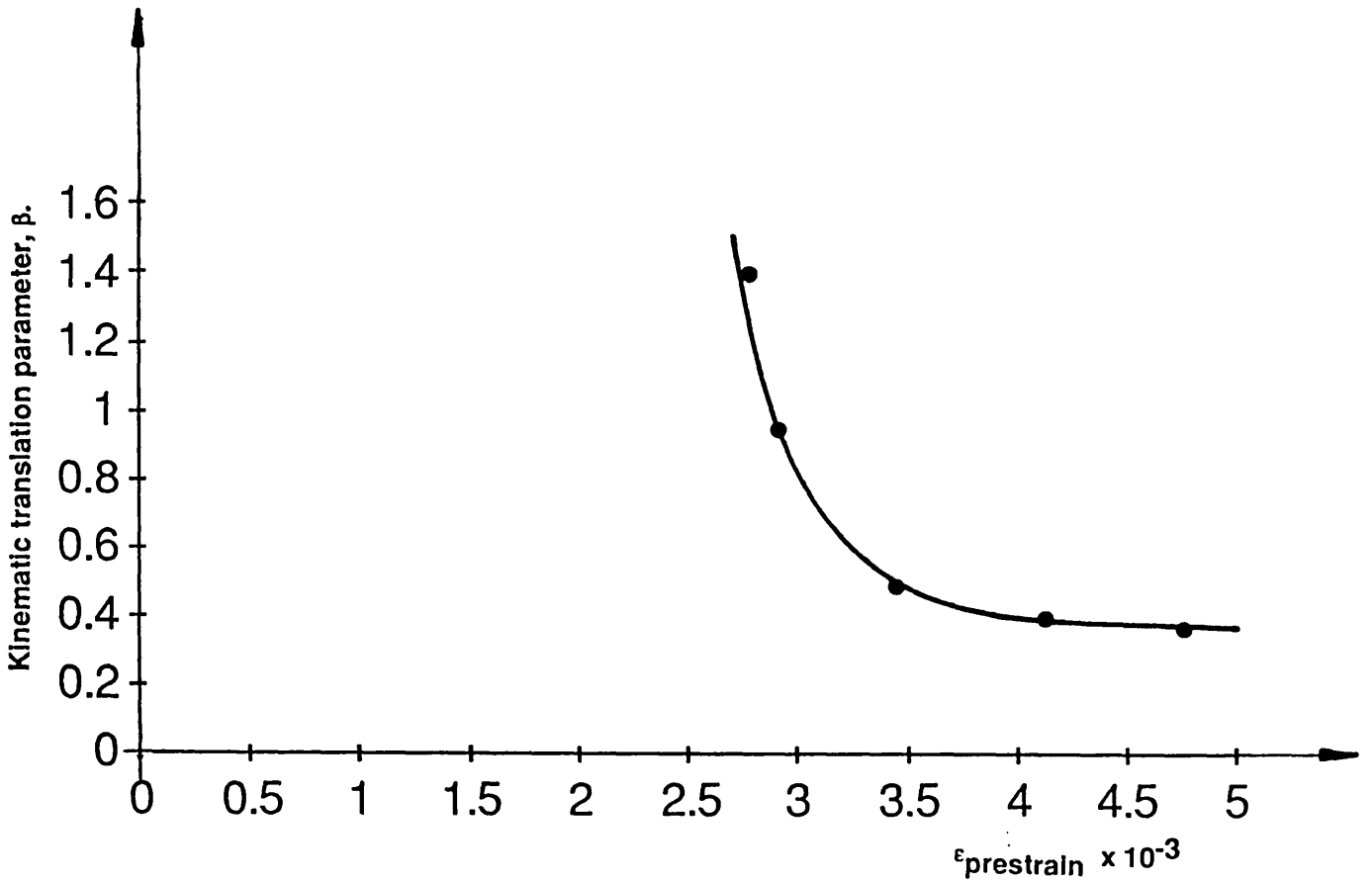


Fig. F.7 Variation of the kinematic translation parameter with initial plastic pre- strain for aluminium H18.

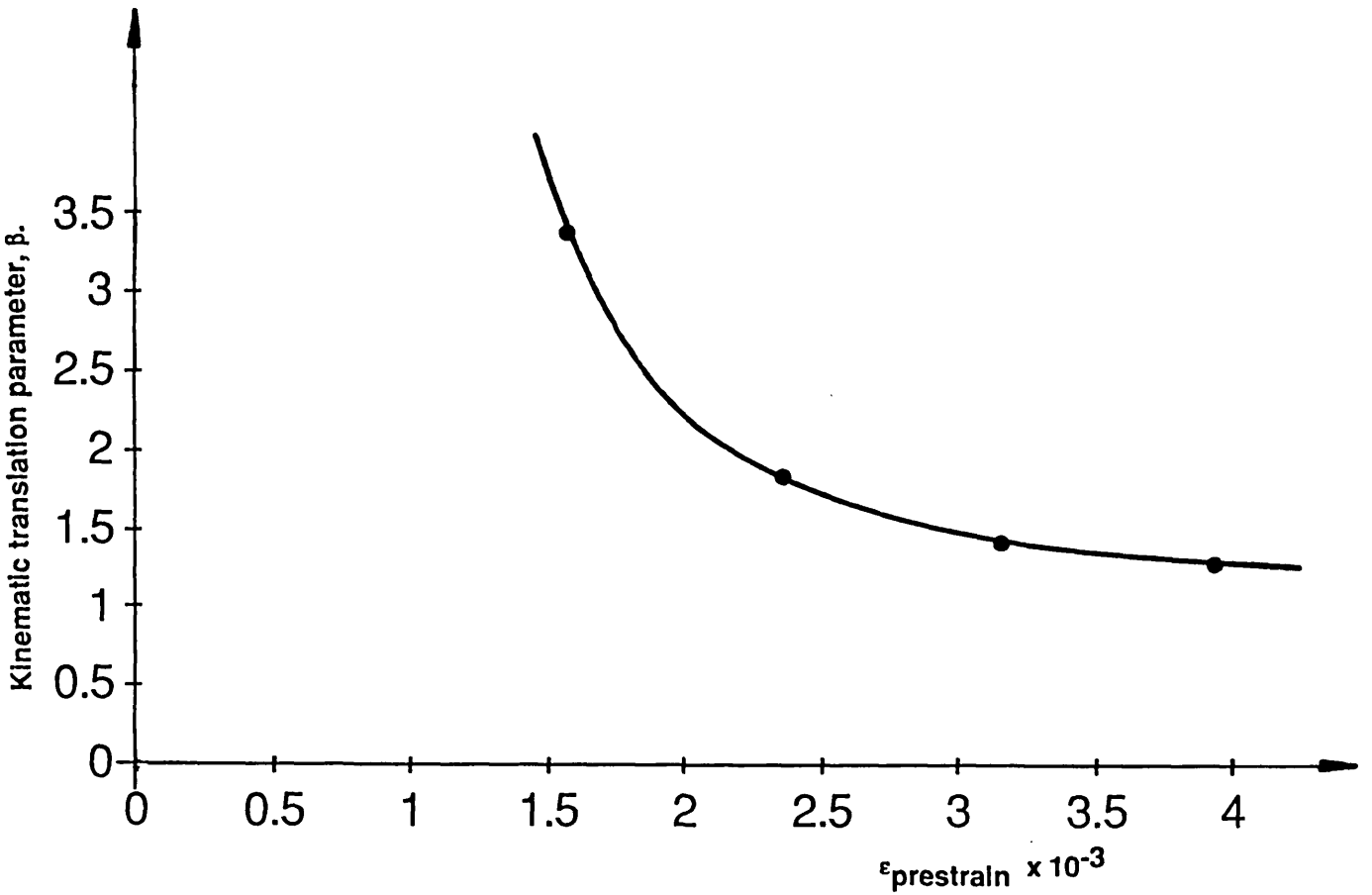


Fig. F.8 Variation of the kinematic translation parameter with initial plastic pre- strain for Titanium (Ti-6211).

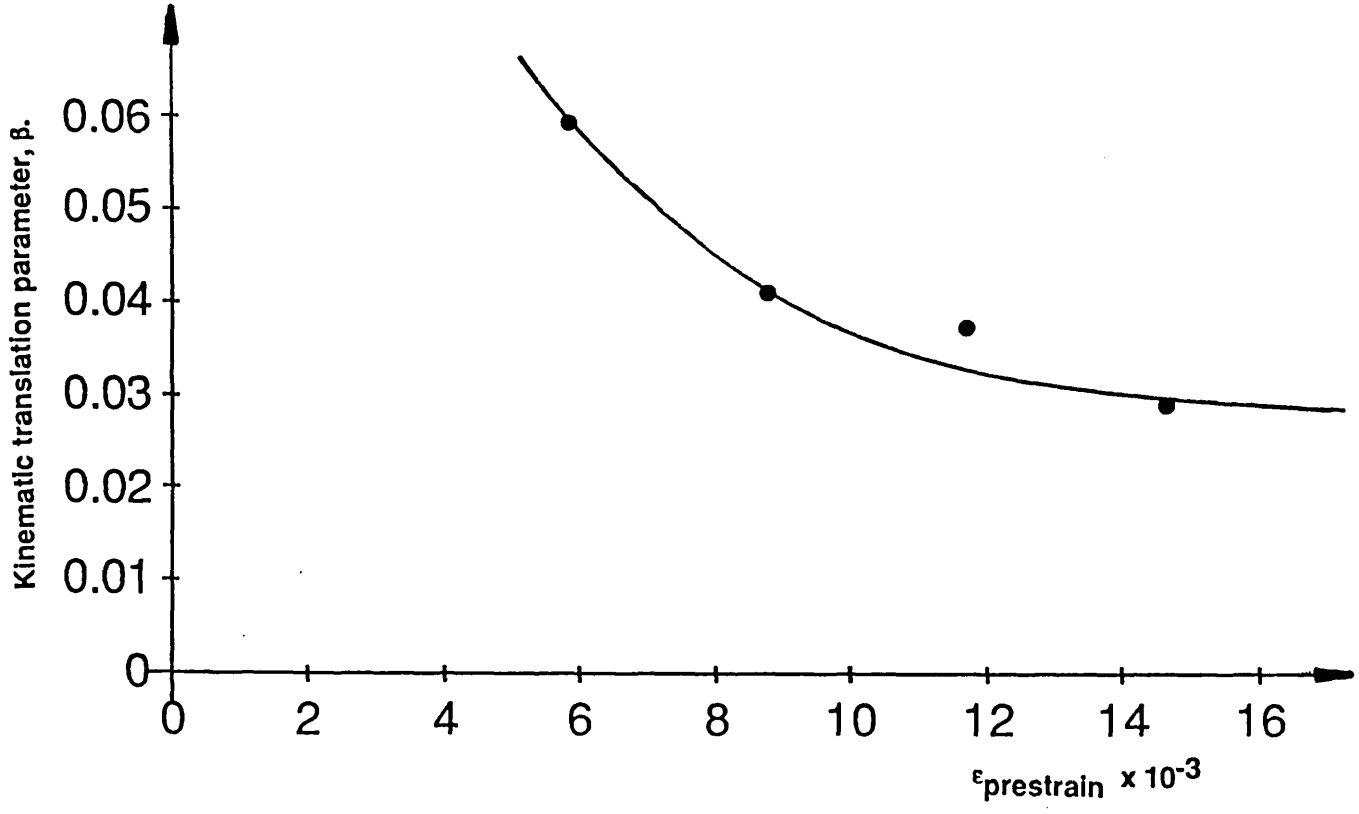


Fig. F.9 Variation of the kinematic translation parameter with initial plastic pre- strain for stainless steel.

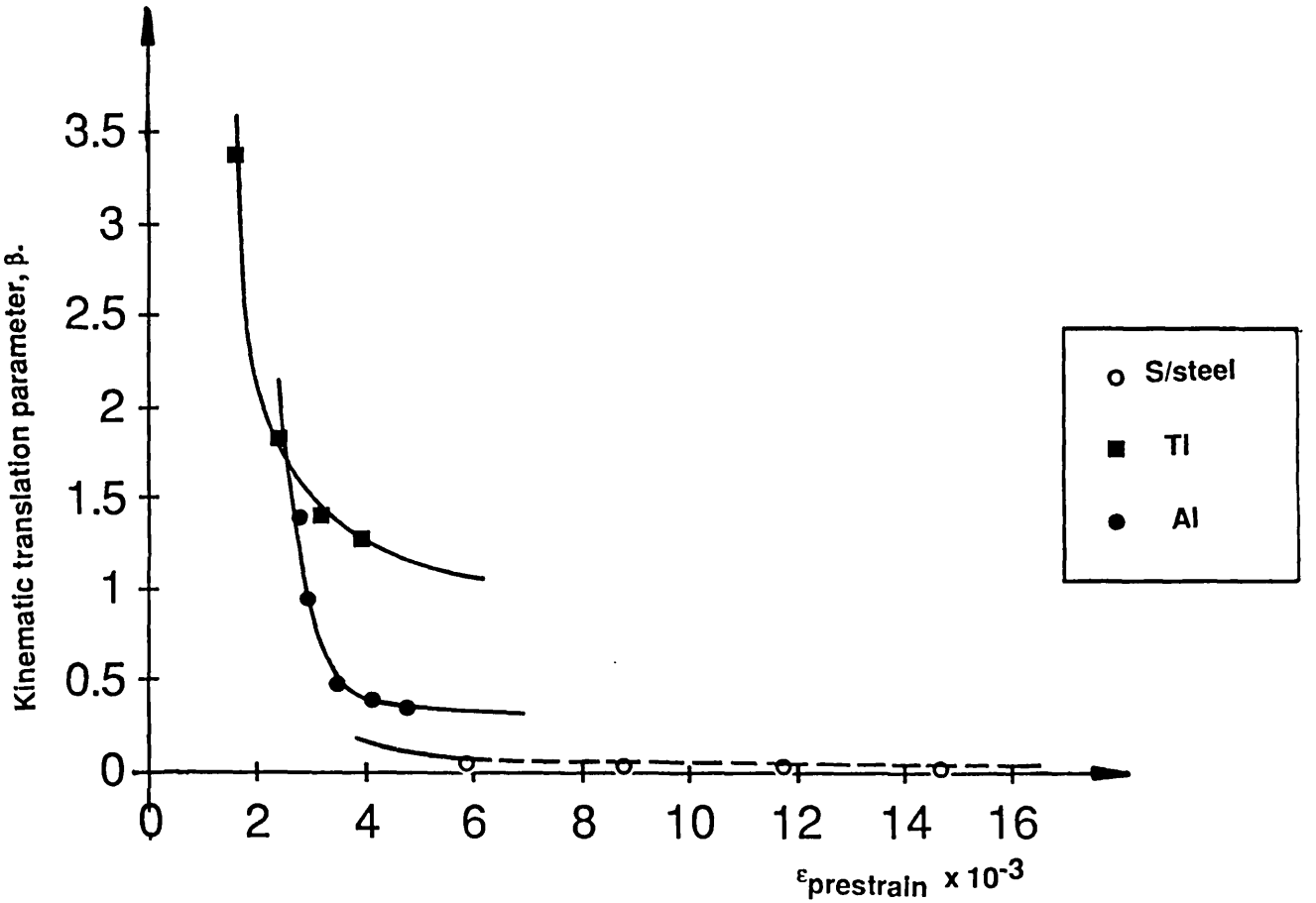


Fig. F.10 Comparison of the variation of β with plastic pre-strain to show material dependence of β.

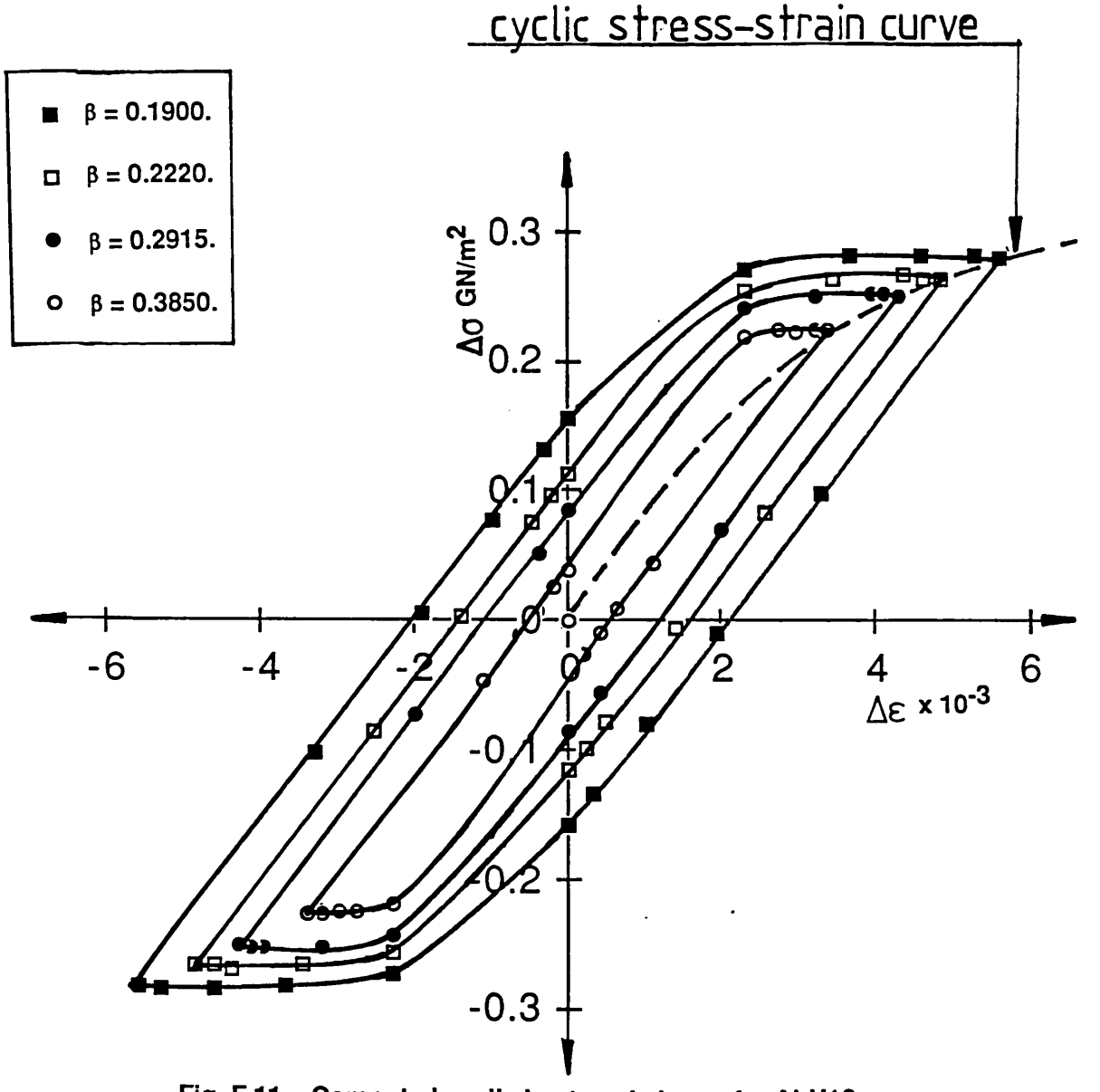


Fig. F.11 Computed cyclic hysteresis loops for Al-H18.